IL NUOVO CIMENTO

1961

IL
NUOVO CIMENTO

PERIODICO ITALIANO DI FISICA

fondato a Pisa nel 1855 da C. Matteucci e R. Piria
dal 1897 Organo della Società Italiana di Fisica
è pubblicato
sotto gli auspici del Consiglio Nazionale delle Ricerche
a cura del Direttore
GIOVANNI POLVANI
Presidente della Società
e
dei Vicedirettori
Giulio Cortini e Nicolò Dallaporta
con la collaborazione di un Comitato di Redazione
i cui membri sono elencati nei N.i 16 e 17 (1960)
del *Bollettino* della Società Italiana di Fisica.

Segretario di Redazione
R. Corbi

Redazione
Bologna, Via Irnerio n. 46
presso l'Istituto di Fisica dell'Università

Direzione
Milano, Via Saldini n. 50
presso l'Istituto di Fisica dell'Università

IL
NUOVO CIMENTO

ORGANO DELLA SOCIETÀ ITALIANA DI FISICA

SOTTO GLI AUSPICI DEL CONSIGLIO NAZIONALE DELLE RICERCHE

VOLUME XXII

Serie decima

Anno centesimosettimo

1961

NICOLA ZANICHELLI EDITORE
BOLOGNA

IL
NUOVO CIMENTO
ORGANO DELLA SOCIETÀ ITALIANA DI FISICA
SOTTO GLI AUSPICI DEL CONSIGLIO NAZIONALE DELLE RICERCHE
E DEL COMITATO NAZIONALE PER L'ENERGIA NUCLEARE

VOL. XXII, N. 1 *Serie decima* 1° Ottobre 1961

On the Multi-Nucleon Capture of K^--mesons.

Y. EISENBERG and M. FRIEDMANN
The Weizmann Institute of Science - Rehovoth

G. ALEXANDER and D. KESSLER
Israel Atomic Energy Establishment - Rehovoth

(ricevuto il 20 Febbraio 1961)

Summary. — In a search for fast ($\geqslant 60$ MeV) Σ-hyperons emitted from multi-nucleon K^--captures at rest, 65 events were found. Using our events, as well as those published before by other groups, we have been able to set an upper limit of $\sim 6\%$ to the reaction $K^-nn \to \Sigma^+n$, relative to the total fast $(2\mathcal{N})\Sigma^-$-production. This was achieved by a detailed study of the distribution of the visible energy associated with K^--stars giving rise to fast identified Σ^+ and Σ^- hyperons. Also, from the visible energy distribution, we have been able to obtain an unbiased estimate for the ratio of the $K^-np \to \Sigma^-p$ and $K^-pp \to \Sigma^+n$ reactions. From the Auger electrons and short prongs associated with the $2\mathcal{N}$-events and with pion-emitting stars we can show that, very probably, the total $2\mathcal{N}$-yield increases significantly with the atomic number of the nucleus in which the K^--capture takes place. A short discussion of the results, in view of several proposed models for the multi-nucleon capture process is also presented.

1. – Introduction.

Recently, it has been demonstrated [1-4], that the multi-nucleon capture mode of K^--mesons at rest in nuclear emulsions plays an important role and

(1) Y. EISENBERG, W. KOCH, M. NIKOLIĆ, M. SCHNEEBERGER and H. WINZELER: *Nuovo Cimento*, **11**, 351 (1959).
(2) K^--Collaboration: *Nuovo Cimento*, **14**, 315 (1959).
(3) M. NIKOLIĆ, Y. EISENBERG, W. KOCH, M. SCHNEEBERGER and H. WINZELER: *Helv. Phys. Acta*, **33**, 221; **33**, 237 (1960).
(4) K^--Collaboration: *Nuovo Cimento*, **19**, 1077 (1961).

that about 30% of all K^--absorptions proceed via this mode. All the possible $2\mathcal{N}$-reactions and also the reaction rates for a self-conjugate nucleus, assuming charge independence, are listed in Table I (for derivation see ref. [1]).

TABLE I.

Reaction	Calculated rate
1. $K^- + n + n \to \Sigma^- + n$	P^2
2. $K^- + n + p \to \Sigma^- + p$	$\frac{2}{9}P^2 + \frac{2}{9}Q^2 + \frac{2}{3}S^2 - \frac{4}{9}PQ\cos\delta$
3. $\to \Sigma^0 + n$	$\frac{4}{9}P^2 + \frac{1}{9}Q^2 + \frac{1}{3}S^2 + \frac{4}{9}PQ\cos\delta$
4. $\to \Lambda^0 + n$	$\frac{1}{3}Q_\Lambda^2 + S_\Lambda^2$
5. $K^- + p + p \to \Sigma^+ + n$	$\frac{1}{9}P^2 + \frac{4}{9}Q^2 + \frac{4}{9}PQ\cos\delta$
6. $\to \Sigma^0 + p$	$\frac{2}{9}P^2 + \frac{2}{9}Q^2 - \frac{4}{9}PQ\cos\delta$
7. $\to \Lambda^0 + p$	$\frac{2}{3}Q_\Lambda^2$

In Table I the following notation is used:

$$\langle T = \tfrac{3}{2} | H_\Sigma^{2\mathcal{N}} | \tfrac{3}{2} \rangle = P \exp[i\alpha],$$

$$\langle \tfrac{1}{2} | H_\Sigma^{2\mathcal{N}} | \tfrac{1}{2} \rangle_{\text{symmetric}} = Q \exp[i\beta],$$

$$\langle \tfrac{1}{2} | H_\Sigma^{2\mathcal{N}} | \tfrac{1}{2} \rangle_{\text{antisymmetric}} = S \exp[i\gamma],$$

$\delta = \alpha - \beta$; Q_Λ and S_Λ are quantities similar to Q and S, for the Λ-hyperon production.

Until now, experiments on two-nucleon capture of K^- at rest were concerned mainly with the total yield of this mode in nuclear emulsions. This was obtained indirectly by determining the yield of one-nucleon interactions from the frequency of charged pions, taking into account the reabsorption probability ($\sim 10\%$), and allowing for neutral pion production (assuming charge independence). By this method, NIKOLIĆ *et al.* [3] obtained $(37 \pm 5)\%$ and the K^- Collaboration [4] $\sim 30\%$ two-nucleon captures. For later discussions we shall adopt the mean value: $(33 \pm 5)\%$ $2\mathcal{N}$-absorptions.

Bubble chamber experiments [5], on the other hand, have shown the $2\mathcal{N}$-absorption of K^- at rest in Deuterium to be very small (about 1%). Recently, in a Helium bubble chamber experiment [6], the value $(17 \pm 4)\%$ $2\mathcal{N}$-absorptions was deduced by using subtraction methods similar to those described above. It should be pointed out, however, that in this case pion reabsorption was assumed to be zero and that even a small probability for pion reabsorption whould reduce the above-mentioned rate (17%) substantially.

---

[5] ALVAREZ Report: *Kiev Conference on High Energy Physics* (1959).

[6] The He Bubble Chamber Group Report, *Rochester Conf. on High Energy Physics* (1960).

Various models [7-9] have been offered for the explanation of the multi-nucleon capture. However, the theoretical situation is still not clear, and more detailed experimental information is required in order to get a better understanding of this process. The rates of the various $2\mathcal{N}$-reactions are known only qualitatively and thus the main purpose of the present work is to obtain a quantitative determination of the $2\mathcal{N}$-reaction rates. Also, since the A-dependence of the total $2\mathcal{N}$-reaction rate may perhaps be a sensitive test of any theory of this process, an attempt to estimate these rates in the light and heavy emulsion nuclei separately will be presented.

2. – Experimental method and general results.

The present results were obtained from a stack of G-5 emulsions, exposed to the 300 MeV/c K^- beam at Berkeley. In a scan along-the-track of this stack, about 6000 K^-_σ stars were found, from which 65 fast Σ's (over 60 MeV), unaccompanied by pions, were observed. These events, including details about the parent stars, are listed in Table II. In column 2, of this table we indicate the Σ-decay mode (*i.e.* $F\Sigma^\pm_\pi$ means an unidentified $\Sigma^\pm \to \pi^\pm$ in flight, $R\Sigma^-_\sigma$ means a negative hyperon coming to rest and producing a capture star, $F\Sigma^+_p$ means $\Sigma^+ \to p$ in flight, etc.). The Σ energy is given in column 3. The energies were determined by the most accurate method appropriate to each case, namely by using the range-energy relation, decay kinematics or grain density. The errors on the energies are between 5% and 10%. In column 4 the ranges of all the accompanying prongs are given. In columns 5 to 7 we give the details about the blobs, Auger electrons and recoils associated with each star.

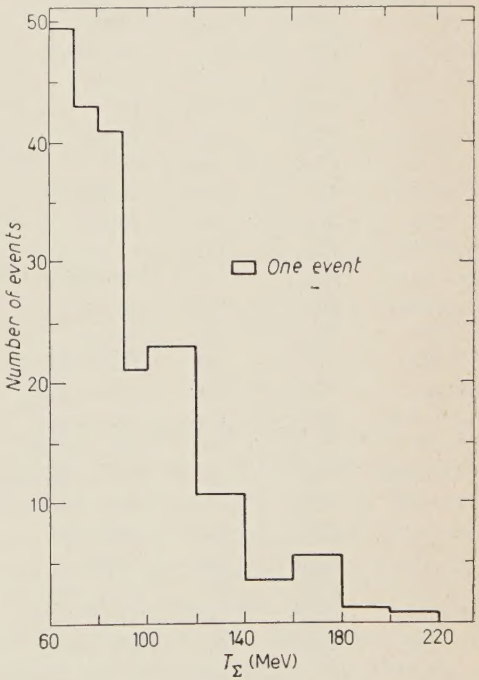

Fig. 1. – Energy spectrum of all fast Σ-hyperons (corrected for loss of Σ^+ stars at rest)

(7) D. H. Wilkinson: *Phil. Mag.*, **4**, 215 (1959).
(8) G. Alexander, Y. Eisenberg and D. Kessler: *Nuovo Cimento*, **15**, 484 (1960).

TABLE II.

Event No.	Hyperon type	T_Σ (MeV) at emission	Ranges of accompanying prongs (μm)	Blob (grains)	Auger electrons (grains)	Recoil (μm)
81/163	$F\Sigma^-_\pi$	99		—	10, 3	—
64/166	$F\Sigma^-_\pi$	96		4	—	—
60/117	$F\Sigma^\pm_\pi$	120		—	4	—
47/6	$F\Sigma^\pm_\pi$	165		—	16, 10	—
54/30	$F\Sigma^\pm_\pi$	74		—	20	—
45/469	$F\Sigma^\pm_\pi$	210		4	8	—
40/1114	$F\Sigma^\pm_\pi$	76		3	18	—
30/660	$F\Sigma^\pm_\pi$	132		—	—	—
15/1942	$F\Sigma^\pm_\pi$	215		5	5, 12	—
57/258	$F\Sigma^\pm_\pi$	120		—	16, 16	—
37/1025	$F\Sigma^+_p$	89		4	19	—
0458	$F\Sigma^+_p$	80		—	—	—
0264	$F\Sigma^+_p$	65		—	—	—
3/1647	$F\Sigma^\pm_\pi$	63	62 000 (*)	5	—	—
16/394	$F\Sigma^\pm_\pi$	110	2 800	—	—	—
31/764	$F\Sigma^\pm_\pi$	114	55 000 (**)	3	—	—
31/190	$F\Sigma^\pm_\pi$	163	9 000	3	6	—
51/160	$F\Sigma^\pm_\pi$	91	13	—	4	—
52/310	$F\Sigma^\pm_\pi$	130	12 500	—	—	—
81/789	$F\Sigma^\pm_\pi$	60	560	—	7	—
70/669	$F\Sigma^\pm_\pi$	110	20 800	—	3	—
41/98	$R\Sigma^-_\sigma$	90	13 000	—	8	—
60/659	$R\Sigma^-_\sigma$	118	1 700	—	3	—
81/410	$R\Sigma^-_\sigma$	70	100 000 (*)	6	—	—
68/842	$F\Sigma^-_\pi$	100	26 700	3	8	—
0159	$F\Sigma^-_\pi$	98	30 000	—	—	—
7/993	$F\Sigma^\pm_\pi$	91	150, 510	3	—	—
9/941	$F\Sigma^\pm_\pi$	110	1 200, 2 000	—	—	—
12/1856	$F\Sigma^\pm_\pi$	110	155, 5 100	8	10	—
19/67	$F\Sigma^\pm_\pi$	105	520, 23 000	—	3	—
18/1043	$F\Sigma^\pm_\pi$	101	3 000, 23 500	—	10	—
23/502	$F\Sigma^\pm_\pi$	110	850, 5 400	10	—	—
44/462	$F\Sigma^\pm_\pi$	105	108, 55	4	—	—
50/356	$F\Sigma^\pm_\pi$	135	1 650, 5	—	—	3
61/622	$F\Sigma^\pm_\pi$	150	570, 800	—	5, 15	—
65/347	$F\Sigma^\pm_\pi$	85	216, 5 600	4	—	—
79/883	$F\Sigma^\pm_\pi$	110	62, 1 200	4	—	3.6
103/1547	$F\Sigma^\pm_\pi$	105	3 700, 11 000	—	—	—
63/688	$F\Sigma^\pm_\pi$	175	600, 5 900	—	5	—
88/490	$F\Sigma^\pm_\pi$	120	12, 4 000	—	—	—
57/564	$F\Sigma^\pm_\pi$	93	8, 320	—	22	—

(*) Interaction in flight, assumed proton, range calculated from g^*.
(**) Leaves stack, assumed proton, range calculated from g^*.

TABLE II (*continued*).

Event No.	Hyperon type	T_Σ (MeV) at emission	Ranges of accompanying prongs (μm)	Blob (grains)	Auger electrons (grains)	Recoil (μm)
38/146	$R\Sigma^-_\sigma$	80	83, 560	—	—	—
26/556	$F\Sigma^-_\pi$	80	100, 16 000	—	—	—
45/1085	$F\Sigma^-_\pi$	94	570, 1 850	9	—	—
16/1805	$F\Sigma^+_p$	135	90, 900	—	23	—
4/1703	$F\Sigma^\pm_\pi$	84	150, 196, 310, 1 310	—	14	4
11/907	$F\Sigma^\pm_\pi$	115	6 100, 5 900	—	—	4.3
14/120	$F\Sigma^\pm_\pi$	76	6, 6, 1 100, 1 700	—	fast	—
19/309	$F\Sigma^\pm_\pi$	92	230, 930, 1 040, 1 650	—	—	—
21/917	$F\Sigma^\pm_\pi$	65	61, 2 300, 23 000	—	—	—
32/100	$F\Sigma^\pm_\pi$	83	7.7, 24, 26, 900, 12 800	—	4	—
39/818	$F\Sigma^\pm_\pi$	80	123, 5 900, 9 000	—	—	—
55/816	$F\Sigma^\pm_\pi$	92	21, 618, 4 600	—	—	1.6
57/595	$F\Sigma^\pm_\pi$	87	29, 130, 4 300, 15 300	—	—	—
71/595	$F\Sigma^\pm_\pi$	163	6, 15, 5 400	—	—	1.6
77/77	$F\Sigma^\pm_\pi$	140	54, 320, 1 410	—	—	—
88/1414	$F\Sigma^\pm_\pi$	78	46, 135, 2 100	—	—	2.4, 4
72/407	$R\Sigma^-_\sigma$	86	90, 270, 1 400	—	—	—
17/1913	$R\Sigma^-_\sigma$	71	63, 380, 460	—	—	3
99/138	$R\Sigma^-_\sigma$	64	19, 51, 140, 1080, 12 5[illegible]0 (**)	—	—	—
32/744	$F\Sigma^+_p$	88	1 050, 2 850, 8 300	—	—	—
54/225	$F\Sigma^+_p$	70	96, 78, 1 200	—	—	—
99/675	$F\Sigma^+_p$	64	115, 760	—	—	1.7
10/973	$F\Sigma^+_p$	78	183, 570, 390, 6 300	8	—	—
59/517	Σ (***)	88	85, 320, 840	—	15	—

(***) Exothermic interaction in flight, energy calculated from q^*.

The energy spectrum of all fast Σ's ($T_\Sigma \geqslant 60$ MeV) is given in Fig. 1. It represents the events obtained in the present work as well as those published by the Bern group ([3]), and the European Collaboration ([4]). The Σ^- correction factor used was 2.8 (*): namely, as a certain Σ^- coming to rest ($R\Sigma^-_\sigma$) we have taken only baryons coming to rest and producing a capture star of 2 prongs, or 1 prong longer than 200 μm; each such event was then taken as corresponding to 2.8 emitted Σ^-'s. Throughout this work, the energy spectra of the Σ^- and Σ^+ hyperons will be assumed to be identical. Since the difference between the two spectra (if any) can not be large, this assumption will not alter any of our conclusions significantly.

([9]) I. E. MCCARTHY and D. J. PROWSE: *Phys. Rev. Lett.*, **4**, 367 (1960).

(*) This correction factor was obtained from a compilation of K^--free-H captures in emulsions. See ref. ([3]) and ([4]).

3. – The multi-nucleon reaction rates.

3·1. *General Remarks.* – Charged hyperons may be emitted in the following multi-nucleon K^- captures:

(1) $$K^- + n + n \to \Sigma^- + n + 237 \text{ MeV}$$

(2) $$K^- + n + p \to \Sigma^- + p + 237 \text{ MeV}$$

(5) $$K^- + p + p \to \Sigma^+ + n + 243 \text{ MeV}$$

namely, reactions (1), (2) and (5) of Table I.

Attempts to determine the relative rates of the above reactions have been, so far, rather qualitative. One could only argue [1-4], that reaction (1), $(\Sigma^- n)$, is quite rare as compared with reaction (2) and (5), $(\Sigma^- p)$ and $(\Sigma^+ n)$, since: i) identified Σ^--hyperons were always seen to be accompanied by other charged prongs, and ii) Σ^+-hyperons quite often ($\sim 30\,\%$) are emitted alone as « clean events ». Thus, all $\Sigma^\pm$ hyperons emitted together with a fast ($\geqslant 30$ MeV) proton were taken as negative, and all $\Sigma^\pm$ « clean » events were assumed to be positive. This method of separation cannot be trusted in a quantitative analysis. Thus, for example, a 30 MeV proton emitted together with a 60 MeV $\Sigma^\pm$-hyperon may very well belong to reactions (1) or (5) above, and not necessarily to reaction (2), since a high energy neutron (~ 180 MeV) could very easily give rise to a 30 MeV secondary proton. On the other hand, a 200 MeV $\Sigma^\pm$ emitted together with a 20 MeV proton will have originated very probably, in reaction (2). Also, in the present work, we have been able to identify 2 $F\Sigma^-_\pi$ « clean » events, and thus statement i) above seems to be no longer absolutely correct.

In the present work a new method (*) for separating the various multi-nucleon primary processes will be described and applied to the data published so far. Since this method uses the visible energy release in each K^--capture star emitting a fast Σ, it enables one to utilize all the events and not only the identified Σ's, as was done in previous experiments.

3·2. *The ε-distribution.* – Let us define the experimental quantity ε as:

$$\varepsilon = \frac{\sum_i (T_i + B_i)}{Q - (T_\Sigma + B_\Sigma)},$$

(*) A brief description of the method and preliminary results were given at the 1960 Rochester Conference.

where T_i is the kinetic energy of the i-th prong and B_i its binding energy (see below). T_Σ and T_Σ are the kinetic energy and binding energy of the Σ-hyperon, and Q was chosen to be 240 MeV, the average Q-value of the $2\mathcal{N}$ reactions. ε is therefore a measure of the fraction of the total energy available to particles other than the Σ itself, which is carried by the charged prongs. Thus, in events produced via reactions (1) or (5), where a neutron is expected to carry a large fraction of the available energy, one should get a small value for ε. Qualitatively, the opposite will happen in the case of (Σ^- p) production: the ε distribution of this reaction should be relatively rich in high ε events. Quantitatively, the (Σ n) and (Σ p) ε-distributions are not expected to be a reflection of each other about $\varepsilon = 0.5$ for the following reason. The formation of the star due to a two-nucleon K^--capture can be roughly divided into two stages: i) the prompt reaction of the resulting two fast baryons with the rest of the nucleus, and ii) the subsequent evaporation of particles due to the excitation produced in the first stage. The first stage—the prompt cascade—is expected to be similar for protons and neutrons ([10]). This means, for example, that the relative numbers of fast neutrons escaping in neutron-produced prompt cascades will equal the relative number of fast protons escaping in proton-produced cascades, etc. Thus, the (Σ^- p) ε-distribution due to the first stage only, should indeed be a mirror image of that of the (Σ n) events. However, the subsequent evaporation will distort this symmetry to some extent, since many more neutrons than charged particles are emitted in the evaporation stage. This will tend to cause a shift of the ε-distribution towards small ε's. Therefore, the (Σ n) ε-distribution will remain peaked at small ε's whereas the (Σ^- p) ε-distribution, originally peaked at high ε's, will be smeared out.

In practice, the following rules have been adopted in calculating ε:

i) All prongs shorter then 5 μm were assumed to be recoils and were not given any binding energy. Since their kinetic energy is negligible, they were not counted at all.

ii) Prongs having a range of $5\ \mu\text{m} \leqslant R \leqslant 110\ \mu\text{m}$ were all assumed to be α-particles ([11]).

iii) Prongs longer then 110 μm were assumed to be protons. This assumption is certainly justified for K^--captures in the heavy emulsion elements, but even in captures in CNO only 6 out of 28 prongs $> 110\ \mu$m turn out to be non-protons ([12]).

([10]) See, for example, the work of METROPOLIS *et al.*: *Phys. Rev.*, **110**, 185 (1958).

([11]) C. GROTE, I. HAUSER, U. KUNDT, U. KRECKER, K. LANIUS K. LEWIN and H. W. MEIER: *Nuovo Cimento*, **14**, 532 (1959).

([12]) D. EVANS, B. D. JONES, B. SANJEEVAIAH, J. ZAKRZEWSKI, M. J. BENISTON, V. A. BULL and D. H. DAVIS: Preprint (1960).

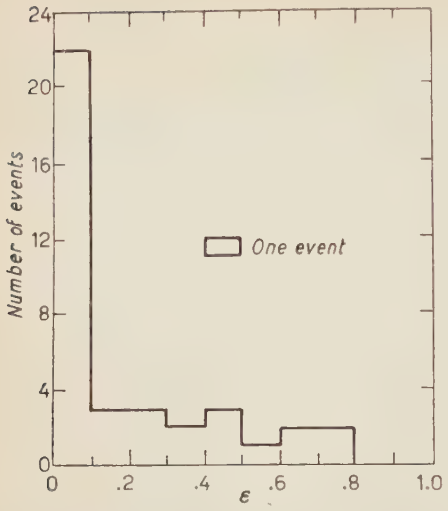

Fig. 2. – ε-distribution of all identified fast ($\geqslant 60$ MeV) Σ^+ events.

iv) The binding energy of each emitted particle (also B_Σ) was assumed to be 8 MeV. This value was calculated from the known isotopic masses and represents rather well the actual situation both for captures in the light and heavy elements.

v) The Q-value was chosen as 240 MeV.

We have checked the above ε-definition against some completely analysable K^--capture events (published recently by EVANS *et al.* [12]). The resulting ε-distribution agreed qualitatively with the description given in this section. It should, however, be clearly understood that a different set of rules, if consistently applied, should lead to the same result, and that the choice of the most realistic convections is important only in order to obtain the best resolution possible.

The experimental ε-distributions for the Σ^+, Σ^- and the $F\Sigma_\pi^\pm$ events are given in Fig. 2, 3 and 4, respectively. The events which we have used in these figures represent as far as possible all the published material on fast Σ's, ($\geqslant 60$ Mev): Bern [3] data, European Collaboration [4], Bruxelles [13] and our own results.

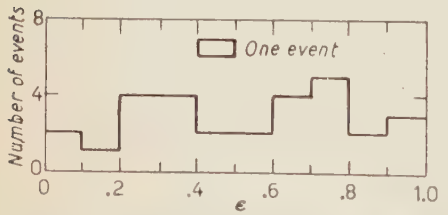

Fig. 3. – ε-distribution of all identified fast ($\geqslant 60$ MeV) Σ^- events.

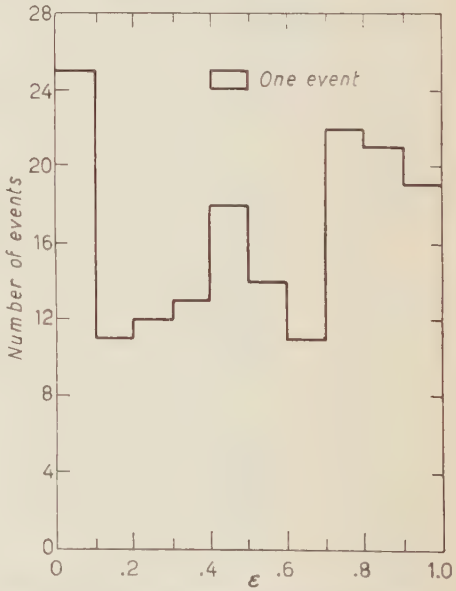

Fig. 4. – ε-distribution of all unidentified fast ($\geqslant 60$ MeV) $\Sigma^\pm \to \pi^\pm$ decays in flight.

[13] G. L. BACCHELLA, A. BERTHELOT, A. BONETTI, O. GOUSSU, F. LÉVY, M. RENÉ, D. REVEL, J. SACTON, L. SCARSI, G. TAGLIAFERRE and G. VANDERHAEGHE: *Nuovo Cimento*, **8**, 215 (1958).

3·3. *The relative rate of the reaction* $K^-nn \to \Sigma^- n$. – By comparing Fig. 2 with Fig. 3 it becomes evident that the ε-distribution of the Σ^+ events is entirely different from that of the Σ^- events. We indeed see, as expected, that more than 50% of all Σ^+ events (22 out of 38) have an ε between 0 and 0.1, whereas the Σ^- hyperon events have a flat ε-distribution, with a slight concentration in the $\varepsilon = 0.5 - 1.0$ interval (16 out of 29 have an ε over 0.5).

Now we are in a position to separate the $(\Sigma^- n)$ from the $(\Sigma^- p)$ events. The $(\Sigma^- n)$ events should have an ε-distribution identical with that of the $(\Sigma^+ n)$ events. However, since a fast 2.$\mathcal{N}$-Σ^+ can be produced only via the $(\Sigma^+ n)$ reaction, it follows that Fig. 2, which is the ε-distribution of all the identified Σ^+ events, must be the general ε-distribution of the reaction (Σn) and in particular it must represent the $(\Sigma^- n)$ ε-distribution. Fig. 3 contains all the identified Σ^- events, and thus represents the ε-distribution of the $(\Sigma^- n)$ events and the $(\Sigma^- p)$ events together. However, since it does not show any peaking at small ε-values and since any substantial contribution of the $(\Sigma^- n)$ reaction to the Σ^- events would cause such a peak (as in Fig. 2), it follows that Fig. 3 represents almost 100% $(\Sigma^- p)$ events only, and that: $(\Sigma^- n)/(\Sigma^- p) < < 2/30 \approx 6\%$. It seems to us that the few events at small ε in Fig. 3 (which include also the 2 $F\Sigma_\pi^-$ « clean » events mentioned earlier) are due to the tail of the $(\Sigma^- p)$ distribution and not to a real contribution of the $(\Sigma^- n)$ reaction, and thus quite possibly the rate of the $(\Sigma^- n)$ reaction is zero.

3·4. *The relative strengths of the* $(\Sigma^- p)$ *and the* $(\Sigma^+ n)$ *reactions.* – We are satisfied that practically all the charged Σ-hyperon events are due either to the $(\Sigma^- p)$ or the $(\Sigma^+ n)$ reactions. The usual methods of estimating the relative strength of these two reactions [1-4] requires an accurate knowledge of the absolute efficiency of identifying a Σ^- and a Σ^+-hyperon. Ideally, if one could identify a large number of $F\Sigma_\pi$ decays, one would obtain an unbiased estimate of the reaction rates. Unfortunately, the number of identified $F\Sigma_\pi$ events is rather small, since it involves following the π-meson to rest: only 14 $F\Sigma_\pi$ events have been so far identified (2 of them are positive).

However, from the ε-distribution we are able to get an unbiased and independent estimate of the Σ^-/Σ^+ ratio using only the $\Sigma^\pm \to \pi^\pm$ in flight, the total Σ energy distribution and the known Σ^+ and Σ^- lifetimes.

The actual separation of $F\Sigma_\pi^\pm$ events is done as follows. Fig. 4 gives the ε-distribution of $\Sigma_\pi^\pm$-decays in flight. These are clearly separated into two main groups: a concentration at small ε which must be due to the $(\Sigma^+ n)$ events, and a general flat area with a slight increase at high ε-values, due to the contribution of the $(\Sigma^- p)$ production. The $(\Sigma^- n)$ reaction, as was shown above, can not give any significant contribution and is thus neglected completely. Using then the actual $(\Sigma^+ n)$ and $(\Sigma^- p)$ ε-distributions (Figs. 2 and 3, respectively), we have calculated the value of $w(\%)$, such that: $w \cdot (\Sigma^+ n) +$

$+(1-w)(\Sigma^- \mathrm{p})$ would give best agreement with the experimental Σ^+ ε-distribution (Fig. 4). It was thus found that $w=(20\pm5)\%$, *i.e.*, that the $F\Sigma_\pi^\pm$ events contain $(20\pm5)\%$ Σ_π^+ hyperons.

In order to get the overall emitted multi-nucleon $(\Sigma^- \mathrm{p})/(\Sigma^+ \mathrm{n})$ ratio, the fraction of Σ^+ and Σ^--hyperons decaying in flight must be determined. This was done by using the known hyperon lifetimes ($\tau_+ = 0.83\cdot10^{-10}$ s and $\tau_- = 1.70\cdot10^{-10}$ s) and the Σ-energy spectrum (Fig. 1). The result is that 94% of the Σ^+ and 78% of the Σ^--hyperons, over 60 MeV, are expected to decay in flight.

The final relative yields of the fast Σ^- and Σ^+ hyperons, for the best value of w, 20%, as well as for $w=15\%$ and 25%, are given in Table III. In

TABLE III. – *Calculated fast Σ^+ and Σ^- yields and expected numbers of Σ_p^+, $R\Sigma_\pi^+$ and $R\Sigma_\sigma^-$ events (for a sample of 166 $F\Sigma_\pi$ events).*

Assumed w (% $F\Sigma_\pi^+$ in $F\Sigma_\pi^\pm$)	No. $F\Sigma_\pi^+$	No. $F\Sigma_\pi^-$	Emitted No. Σ_π^+ ($=\Sigma_p^+$)	No. $R\Sigma_\pi^+$	Emitted No. Σ^-	No. $R\Sigma_\sigma^-$	$R\Sigma_\sigma^-/2.8$	Relative yield (%)	
								Σ^+	Σ^-
20%	33.2	132.8	35.2	2.0	170.3	37.5	13.5	29	71
15%	24.9	141.1	26.4	1.5	181.0	39.8	14.2	23	77
25%	41.5	124.5	44.0	2.5	160.0	35.2	12.6	35	65

this table the expected numbers of Σ_p^+, $R\Sigma_\pi^+$ and $R\Sigma_\sigma^-$ for the sample that we have used, are also presented. The observed numbers in this sample are: 33 Σ_p^+, 3 $R\Sigma_\pi^+$ and 19 $R\Sigma_\sigma^-$ events.

The value $w=20\%$ gives also best agreement with the number of identified $\Sigma^+ \to \mathrm{p}$ events. Since the «true» number of Σ^+-decays can only be greater than the observed one, values of w below 20% may be excluded on these grounds.

As an independent check we have applied the «maximum likelihood» method [14] to our data only. This method makes use of the known Σ-lifetimes and the observed degradation in time of the Σ-beam. We obtained $\Sigma^+=32\%$, in agreement with $(29\pm6)\%$ as given in Table III.

4. – Two-nucleon capture of K$^-$ in the heavy and light elements of nuclear emulsion.

Two method of separating K$^-$-captures in CNO from those in AgBr have been considered hitherto: The first is based on the observation of Auger

[14] M. S. BARTLETT: *Phil. Mag.*, **44**, 249 (1953); C. FRANZINETTI and G. MORPURGO: *Nuovo Cimento Suppl.*, **6**, 577 (1957).

electrons ([3]) associated with the K⁻-capture star, which are expected to be emitted mainly from the heavy emulsion nuclei. The second method makes use of short prongs ($R \leqslant 41$ μm) which have been shown to arise only from light nuclei ([11]), their escape from heavy nuclei being inhibited by the Coulomb barrier. Although the strict validity of both methods may still be open to some doubt, it can be seen from the following tables (IV to VI) that their mutual agreement is very satisfactory: in particular, the number of cases containing both an Auger-electron and a short prong is very small.

Very severe criteria had to be applied to the definition of « short prongs » and « Auger-electrons » in order to exclude all cases which could possibly be interpreted differently by different observers. Therefore, in this analysis short prongs of less than 10 μm, electrons of less than 10 grains and all blobs were not considered.

The method of short prongs will be very difficult to use in this connection, because we have no precise *a priori* knowledge about the dependence of the short prong emission probability on the type of interaction (1.N or 2.N). Therefore, the Auger electron yields will be used for separating light from heavy nuclei captures.

The subsequent analysis will be based on the following three assumptions:

1) All Auger-electrons of 10 grains or more are produced by K⁻-capture in *heavy* atoms (see Tables IV to VI).

2) The emission probability of an Auger-electron from a heavy emulsion nucleus, being an atomic process, is independent of the subsequent nuclear K⁻-capture mode.

3) The certain one-nucleon events, where a $\pi^{\pm}$ is observed, can be regarded as representative samples of the one-nucleon events insofar as the ratio of absorption in heavy and light nuclei is concerned. This assumption is justified since the overall charged pion-reabsorption probability is small (about 10% ([1-3])) and any dependence of this probability on the mass of the nucleus involved will produce only second order effects.

We shall now calculate the two-nucleons capture probability in the heavy emulsion nuclei.

Let n_1, n_2 and $n = n_1 + n_2$ be the number of one-nucleon, two-nucleon and total K⁻-absorptions in all emulsion nuclei, and $p = n_2/n$ the relative rate of two-nucleon absorptions. Similarly, let n_1^H, n_2^H and $n^H = n_1^H + n_2^H$ be the numbers of one-nucleon, two-nucleon and total K⁻-absorptions in the heavy emulsion nuclei. Then, if ϱ is the observed ratio of the yield of Auger-electrons in certain two-nucleon events to that in certain one-nucleon events, we obtain

$$(1) \qquad \varrho = \frac{n_2^H}{n_2} \cdot \frac{n_1^H}{n_1} = \frac{n_2^H}{n_1^H} \cdot \frac{1-p}{p} \qquad \text{or} \qquad \frac{n_2^H}{n_1^H} = \varrho \cdot \frac{n_2}{n_1} .$$

TABLE IV (*). – *Auger-electron and short prong distribution of* K^-*-capture stars from which fast* Σ*'s* ($T_\Sigma \geqslant 60$ MeV) *are emitted.*

Number of events	no short prong	10 μm $\leqslant R_{s.p.} \leqslant$ 41 μm	41 μm $< R_{s.p.} \leqslant$ 110 μm	Total
no electron, or electron of less than 10 grains	28(+1?)+34	7+17	11+7	46(+1?)+58
electrons of 10 grains or more	12(+1?)+ 5	0+ 0	2+0	14(+1?)+ 5
Total	40(+2?)+39	7+17	13+7	62 + 63

(*) The first number refers to the present experiment, the second one to the data of EVANS *et al.* [12].

TABLE V. – *Auger-electron and short prong distribution of* K^-*-capture stars from which charged pions are emitted (present experiment only).*

Number of events	no short prong	10 μm $\leqslant R_{s.p.} \leqslant$ 41 μm	41 μm $< R_{s.p.} \leqslant$ 110 μm	Total
no electron, or electron of less than 10 grains	722	189	140	1 051
electrons of 10 grains or more	51	3	7	61
Total	773	192	147	1 112

TABLE VI. – *Auger-electron and short prong distribution of* K^-*-capture stars from which fast protons* ($T_p \geqslant 60$ MeV) *are emitted.*

Number of events	no short ptong	10 μm $\leqslant R_{s.p.} \leqslant$ 41 μm	41 μm $< R_{s.p.} \leqslant$ 110 μm	Total
No electron, or electron of less that 10 grains	338	93	118	549
Electron of 10 grains or more	50	2	15	67
Total	388	95	133	616

The relative probability of two-nucleon absorption in the heavy elements is then

$$\beta = \frac{n_2^H}{n^H} = \frac{\varrho p}{1 - p + \varrho p} . \tag{2}$$

From the experiment (Tables IV and V) we obtain: $\varrho = 2.9 \pm 0.8$. Thus we immediately see that the $2\mathcal{N}$ reaction is relatively more effective in the heavy emulsion elements than in the light atoms. Further, by using the value of $p = (33 \pm 5)\%$ (see Section **1**), we get $\beta = n_2^H/n^H = (59 \pm 10)\%$.

The preceding analysis is admittedly affected by bad statistics, due to the small number of Auger-electrons observed in the fast Σ-events. Until more data become available we can try to make use of the fast proton events which have been shown [3] to contain about 85% two-nucleon absorptions, instead of the fast Σ-events. Here, the statistics are much better and we get for the ratio of the Auger-electron yield in the fast proton events (Table VI) to that in the certain one-nucleon absorptions (Table V): $\varrho_p = 2.0 \pm 0.4$. The « true » ϱ for a pure sample of two-nucleon absorptions is expected to be somewhat higher because of the 15% one-nucleon absorption included in the fast proton events. We think, therefore, that the final experimental value of ϱ will still lie within the limits of $\varrho = 2.9 \pm 0.8$ on which the analysis is based, although probably rather nearer to the lower limit. Thus, we are convinced that the $2\mathcal{N}$-capture rate in heavy elements is significantly higher than in the average emulsion nucleus (namely $\beta \geqslant 50\%$).

Qualitatively, it is clear from the above discussion that the $2\mathcal{N}$-capture rate in the light emulsion nuclei ($\lambda = n_2^L/n^L$) must be smaller than $(33 \pm 5)\%$. For a more quantitative determination of λ, we note that

$$\lambda = \frac{n_2^L}{n^L} = \frac{p}{1 - q}\left(1 - \frac{\varrho q}{1 - p + \varrho p}\right), \tag{3}$$

where $q = n^H/n$ is the proportion of K⁻-mesons captured in the heavy emulsion nuclei. Unfortunately, q is very poorly known. The value given by GROTE *et al.* [11] ($q \approx 0.75$) is obviously an overestimate, being based on the assumption that all stars without short prongs are due to K⁻-capture in AgBr. The Fermi-Teller « Z-law » predicts $q \approx 0.80$ for nuclear emulsion. However, it was shown experimentally [15], for μ-mesons, that the number of captures in the different components of insulators, is about proportional to the relative abundance of the elements present, in contrast with the « Z-law ». On the other

---

[15] J. C. SENS, R. A. SWANSON, V. L. TELEGDI and D. D. YOVANOVITCH: *Nuovo Cimento*, **7**, 536 (1958).

hand, BELOVITSKII [16] found recently that π^- capture in Uranium-loaded emulsion obeys the « Z-law » fairly well as far as the relative captures in U and the emulsion gelatine is concerned. Obviously, the true value of q must be between the above extremes, namely, the value predicted by the atomic abundance, $q = 0.43$ (obtained by excluding K^- hydrogen captures, since these are known [17] to be rare, about 0.5% only), and the « Z-law » prediction, $q \approx 0.80$. This was demonstrated experimentally by PEVSNER *et al.* [18], using μ^--captures at rest in ordinary emulsion: 58% of the mesons stopped in AgBr and 42% in the gelatine.

It is not evidente that Pevsner's results may be applied to K^--mesons as well. But in any case we consider $q = 0.43$ as a lower limit and this in turn will give an upper limit for λ:

$$\lambda = \frac{n_2^L}{n^L} < (13 \mp 9)\% .$$

This should be compared with the values obtained above for the 2.V-yield in K^--captures by AgBr, $\beta = n_2^H/n^H = (59 \pm 10)\%$.

EVANS *et al.* [12] were able to identify completely 6 events of K^--absorption in light nuclei, out of 63 two-nucleon events. 8 additional events were compatible with capture in light nuclei, if a single neutron is assumed to be emitted. These authors consider therefore 14/63 as a minimum for the fraction of K^- captured in light nuclei and 38/63 as a more realistic estimate. The sample of the above authors seems, however, to have been particulary rich in light nuclei captures, as is evident from Table IV: there are more short prong stars and less energetic Auger-electrons in the experiment of EVANS *et al.* [12] than in the combined data.

From our analysis one can estimate the fraction of light atoms participating in two-nucleon captures:

$$n_2^L/n_2 = 1 - q\beta/p = 1 - \frac{\varrho q}{1 - p + \varrho p} , \tag{4}$$

and this gives $n_2^L/n_2 = (28 \pm 7)\%$ as an upper limit (for $p = 0.38$ and $q = 0.43$).

If we now define η as the ratio of the yield of short prong stars in certain two-nucleon events to that in certain one-nucleon events, one obtains (Table IV

[16] G. E. BELOVITSKII: *Sov. Phys. JETP*, **11**, 473 (1960).

[17] F. C. GILBERT, C. E. VIOLET and R. S. WHITE: *Phys. Rev.*, **107**, 228 (1957).

[18] A. PEVSNER, R. STRAND, L. MADANSKY and T. TOOHIG: *Nuovo Cimento*, **19**, 409 (1961).

and V) $\eta_{exp} = 1.10 \pm .26$. On the other hand

$$\eta = \frac{\lambda}{1-\lambda} \frac{1-p}{p} \cdot \frac{s(2)}{s(1)},$$

where λ has been defined before (eq. (3)) and $s(2)$ and $s(1)$ are the proportions of stars with short prongs among all two- and one-nucleon captures in light elements. The coefficient of $s(2)/s(1)$ is at most $.36 \pm .08$ (again for $p = 0.38$ and $q = 0.43$), therefore, $s(2)/s(1) \approx 3$. Thus the frequency of stars with short prongs is at least 3 times higher in two-nucleon captures by light elements than in one-nucleon captures. This can be qualitatively understood since the two fast baryons resulting from $2\mathcal{N}$-capture are more likely to interact with the rest of the nucleus than the slow hyperon and pion in one-nucleon events. From the above ratio n_2^L/n_2 and from Table IV it can be seen that the fraction of two nucleon captures in light elements having short prongs (with range between 10 μm and 41 μm) is about 70%. This is in agreement with the experiment of EVANS *et al.* ([12]), in which it was observed that in 9 cases out of 14 certain $2\mathcal{N}$ captures in CNO, a short prong of $10\ \mu m \leqslant R \leqslant 41\ \mu m$ was emitted.

5. – Conclusion and discussion.

1) The rate of $\Sigma^- n$ reaction is less than 6% of the rate of the $\Sigma^- p$ reaction and could possibly be zero. This means that the $T = \frac{3}{2}$ transition amplitude P (Table I) is ≈ 0. In this case, the relative rates of the Σ^0 reactions (and thus of all the Σ reactions) are determined completely.

2) The ratio $(\Sigma^- p/\Sigma^+ n)_{emitted}$ is ≈ 2.4. But, since, we have,

$$A_\Sigma = |\langle \Sigma^- p | H | Y^0 n \rangle|^2 = |\langle \Sigma^+ n | H | Y^0 p \rangle|^2 \qquad (Y^0 \text{ stands for } \Lambda^0 \text{ or } \Sigma^0),$$

the following relation exists between the rates of emission and production:

$$(\Sigma^- p/\Sigma^+ n)_{emitted} = (\Sigma^- p/\Sigma^+ n)_{prod.} \cdot \frac{1 - A_\Sigma}{1 - n/p \cdot A_\Sigma}.$$

(The reverse reaction $\Sigma^0 + \mathcal{N} \to \Sigma^\pm + \mathcal{N}'$ can be neglected since i) its rate is smaller than the total absorption of $\Sigma^\pm$, and ii) even when it occurs, it will rarely give a $\Sigma^\pm$ of more than 60 MeV energy). Thus, from the present estimate of $(\Sigma^- p/\Sigma^+ n)_{emitted}$ and by using the value of A_Σ obtained in the $1\mathcal{N}$ study ($A_\Sigma \approx 0.5$ see ref. ([2,3])) we get $(\Sigma^- p/\Sigma^+ n)_{prod.} \approx 1.7$. In order to get a more

reliable value for Σ^-/Σ^+, one needs a larger number of identified $F\Sigma_\pi^\pm$ and a better estimate of A_Σ.

3) One can say the following about the general atomic mass-dependence of the total multi-nucleon K^--capture yield. This rate is very small (1%) in Deuterium ([5]). In He, by neglecting π-reabsorption, the value $(17 \pm 4)\%$ was obtained ([6]). A more realistic estimate of the $2\mathcal{N}$-rate in He is obtained perhaps if we assume a small ($\sim 5\%$) π-reabsorption probability. In this case, the $2\mathcal{N}$-yield in He drops to 13%. Finally, the results of the present experiment (Section **4**) indicate that the total $2\mathcal{N}$-yield for K^--captures in CNO is $\leqslant 22\%$ and in AgBr it is close to 50%. Thus, the $2\mathcal{N}$-yield in K^--captures seems to increase with the atomic number of the nucleus in which the K^--meson is absorbed.

4) Multi-nucleon captures in the light elements of the emulsion (CNO) quite often ($\sim 70\%$) emit a short prong of $10\ \mu m \leqslant R \leqslant 41\ \mu m$. Also, since EVANS *et al.* ([12]) have been able to identify $\sim 20\%$ of all of their $2\mathcal{N}$-events as captures in CNO and since the total $2\mathcal{N}$-yield in CNO is $\leqslant 22\%$, it seems that a large fraction of K^- $2\mathcal{N}$-captures in CNO are analysable. In other words, the K^--capture mechanism in CNO in such that in many cases ($\geqslant 50\%$) only one α-particle is destroyed, and in general, the two or three other α's are emitted as such.

5) The above experimental results are still not accurate enough for deciding between the various multi-nucleon capture models ([7-9]). The direct one-step interaction models ([7-9]) do not predict the reaction rates. The two-step model ([8]), with intermediate state $T=0$, would explain the absence of the Σ^-n reaction in a natural way. This model also predicts $(\Sigma^-p/\Sigma^+n)_{proj.} = n/(p-1) \approx 1.3$ (n and p are the numbers of neutrons and protons of the target nucleus). The present results are not in contradiction with this value, but more precise data are required.

The surprisingly large number of K -captures in light elements in which only one α-particle appears to be destroyed ([12]), seems to support Wilkinson's model ([7]) of K -absorption by peripheral α-particle « clusters ». However, the same result is also expected on the basis of an α-particle structure model of C and O. On the other hand, in the observed two certain K^- nitrogen captures ([12]), the meson is absorbed on the n-p pair and not by an α-structure. (This result is particularly significant because we estimate that in the sample of EVANS *et al.* ([12]) there are no more than 3-4 nitrogen captures.) Similar effects have also been observed in π^--captures ([19]).

The dependence of the total $2\mathcal{N}$-capture yield on the atomic number (see

([19]) See, for example, R. E. MARSHAK: *Meson Physics* (New York, 1952), p. 180 ff.

3 above) could serve as a critical test for any theory of this process. Unfortunately, none of the existing models ([7-9]) makes any definite predictions about this dependence.

* * *

We are very grateful to K. GOTTSTEIN, W. PUESCHEL and J. TIETGE who lent us the stack and their scanning cards, and to the Bevatron crew who performed the exposure. Without their efforts, this experiment would not have been possible. We are also grateful to the K^--Collaboration, particularly to E. H. S. BURHOP and A. BONETTI, for submitting to us many details of their data before publication. One of us (Y.E.) wishes to thank F. G. HOUTERMANS and H. WINZELER for interesting discussions and kind hospitality during his stay at Bern.

The excellent work of our scanning team, particularly Mrs. R. GOTTESMAN, is greatly appreciated.

Note added in proof.

Evidence for strong Y* (the recently discovered hyperon-pion resonance states at about 1400 MeV) effects in K captures by emulsion nuclei has been presented recently ([20]). It is therefore tempting to consider the hypothesis that multi-nucleon K^- captures are due to secondary collisions of Y*: Y*+nucleon$\rightarrow$Y+nucleon. In this case one can understand, qualitatively, the absence of multi-nucleon captures in deuterium and the apparent increase of the $2\mathcal{N}$-yield with A. Our present data are consistent with the assumption that Y_0^* (the $T=0$ isobar) and Y_1^* (the $T=1$ isobar contribute roughly equally to the multi-nucleon reactions.

([20]) Y. EISENBERG, G. YEKUTIELI, P. ABRAHAMSON and D. KESSLER: *Nuovo Cimento*, **21**, 563 (1961). Y. EISENBERG and D. KESSLER: *Proc. of the Aix-en-Provence Conference* (Sept. 1961).

RIASSUNTO (*)

Cercando iperoni Σ veloci ($\geqslant 60$ MeV) emessi in catture di K^- multinucleoniche, abbiamo trovato 65 eventi. Facendo uso di questi eventi e di quelli pubblicati precedentemente da altri gruppi, abbiamo potuto porre un limite superiore del $\sim 6\%$ alla reazione $K^-nn\rightarrow\Sigma^+n$, relativo alla produzione veloce totale $(2\mathcal{N})\Sigma^-$. Siamo giunti a questo risultato con uno studio dettagliato della distribuzione dell'energia visibile associata con le stelle K^-, che originano gli iperoni veloci Σ^+ e Σ^- identificati. Inoltre abbiamo potuto ottenere, dalla distribuzione dell'energia visibile, una stima corretta del rapporto fra le reazioni $K^-np\rightarrow\Sigma^-p$ e $K^-pp\rightarrow\Sigma^+n$. Dagli elettroni Auger e dalle tracce corte associate con gli eventi $2\mathcal{N}$ e con stelle che emettono pioni, possiamo dimostrare che, molto probabilmente, la produzione totale $2\mathcal{N}$ cresce in modo significativo col numero atomico del nucleo in cui ha luogo la cattura del K^-. Inoltre presentiamo una breve discussione di risultati, in vista dei molti modelli prodotti per il processo di cattura multinucleonica.

(*) *Traduzione a cura della Redazione.*

IL NUOVO CIMENTO Vol. XXII, N. 1 1° Ottobre 1961

Donor States and Deformation Around Impurity Atoms in Semiconductors.

S. Shinohara

Department of Physics, Faculty of Science, Hokkaido University - Sapporo

(ricevuto l'11 Agosto 1960; versione revisionata Maggio 1961)

Summary. — Assuming that impurity ions produce only point lattice defects, the change of the ionization energy of the donor state has been estimated semiquantitatively. The value of 0.117 eV has been obtained putting the displacement of the nearest neighbour ion equal to 0.1 of the atom distance. The influence of the self-deformation potential of the trapped electron is negligible.

1. – Introduction.

Koster and Slater (1) investigated impurity states in semiconductors and got the effective-mass Schrödinger equation by expanding the wave function of impurity state using Bloch's wave functions in the energy minimum valley of the lowest conduction band. They proposed a method to calculate the ionization energies of impurity atoms in crystals. Then several authors (2-4) calculated the ionization energies of donor states of Group V atoms in silicon and germanium by this method.

The values obtained by them are independent of doped atoms and smaller than the experimental values by about 30%. Brooks (5), Inui and Mimura (6) and Kaus (7) thought that the effective-mass equation adopted by the pre-

(1) G. F. Koster and J. C. Slater: *Phys. Rev.*, **95**, 1167 (1954).
(2) W. Kohn and J. M. Luttinger: *Phys. Rev.*, **98**, 915 (1955).
(3) C. Kittel annd A. H. Mitchel: *Phys. Rev.*, **96**, 1488 (1954).
(4) M. A. Lampert: *Phys. Rev.*, **97**, 352 (1955).
(5) H. Brooks: *Advance in Electronics and Electron Physics*, **7**, 93 (1955).
(6) T. Inui and H. Mimura: Busseiron-Kenkyu No. **105**, 62 (1957) (in Japanese).
(7) P. E. Kaus: *Phys. Rev.*, **109**, 1944 (1958).

vious methods was inadequate in the vicinity of the atom, center of impurity, because of the large perturbed potential caused by it. They tried to improve this point by using a wave function of the free atom near the impurity atom, but their results were not quite satisfactory.

In the present paper, the differences between the experimental and theoretical ionization energies will be attributed to the strain as done by HERRING ([8]). He did a rough calculation of the contribution of the strain to the ionization energy and obtained 0.03 eV. A more detailed calculation will be done below.

As a simplest model of substitutional atom, let us consider a sphere inserted into a spherical hole in an infinite matrix of elastic material. The size of the hole is assumed to be slightly different from that of the sphere. Then in first order approximation, the volume dilatation becomes zero everywhere in the matrix, so that there is no deformation potential for the trapped electron by the impurity ion.

In the two following cases, however, we can consider that the volume dilatation exists in the mother crystal even if it is a continuous and infinite elastic body:

a) When there is a point defect in the infinite matrix, the deformation has a singularity at the center of the defect, and we can formally think of a volume dilatation of δ-function type at this point.

b) When the lattice is deformed, the energy of the trapped electron varies due to the deformation potential. Therefore, the electron causes a deformation in the matrix around the impurity ion so that it may diminish its own energy. That is the self-deformation potential caused around the impurity atom by the trapped electron cloud.

2. – Deformation potential by a point defect.

Following ESHELBY ([9]), we give briefly the volume dilatation, when a sphere is forced into a spherical hole of slightly different size in an infinite block. The displacement, $\boldsymbol{u}$, of a point in the matrix of which the distance is $\boldsymbol{r}$ from the impurity, becomes

$$\boldsymbol{u} = c\boldsymbol{r}/r^3 = -c\,\mathrm{grad}\,(1/r)\,, \tag{1}$$

where the constant c is a measure of the strength of the defect. Since the

([8]) C. HERRING: *Proc. of Atlantic City Photo-Conductivity Conference*, edited by R. C. BRECKENRIDGE, B. R. RUSSELL and E. E. HAHN (1954), p. 81.

([9]) J. D. ESHELBY: *Solid State Physics*, edited by F. SEITZ and D. TURNBULL, **3**, 75 (1956).

divergence of $\boldsymbol{u}$ is zero, the volume dilatation becomes zero everywhere in the matrix. From a different point of view, however, the dilatation can be proved not to be zero, as described below.

We integrate $\boldsymbol{u}\cdot\boldsymbol{n}\,\mathrm{d}s$, which is the volume swept out by the surface element, $\mathrm{d}S$, with normal $\boldsymbol{n}$, over the closed surface, Σ, surrounding a point defect. The volume enclosed by Σ increases by

$$\Delta V = \int_{\Sigma} \boldsymbol{u}\cdot\boldsymbol{n}\,\mathrm{d}S = c\int_{\Sigma} \frac{\boldsymbol{r}\cdot\boldsymbol{n}}{r^3}\,\mathrm{d}S = 4\pi c\,. \tag{2}$$

Considering that eq. (1) is valid for all $\boldsymbol{r}$, the volume dilatation may be formally

$$(\Delta V/V) = \operatorname{div}\boldsymbol{u} = -\,c\,\nabla^2(1/r) = 4\pi c\;\delta(\boldsymbol{r})\,. \tag{3}$$

We suppose that the strength of the singularity, c, is decided by the displacement of the nearest-neighbour atom of the impurity. This displacement is defined as

$$\boldsymbol{u}_l = \lambda\boldsymbol{L}\,, \tag{4}$$

where $\boldsymbol{L}$ is a position vector from the impurity atom to the nearest neighbour atom ([10]). From (1) and (4), we get

$$c = \lambda L^3\,, \tag{5}$$

where L is the magnitude of the vector $\boldsymbol{L}$. Substituting (5) into (3), the volume dilatation becomes

$$(\Delta V/V) = 4\pi\lambda L^3\;\delta(\boldsymbol{r})\,. \tag{6}$$

According to BARDEEN and SHOCKLEY ([11]), the deformation potential for the trapped electron by the impurity ion is

$$\delta V_p = -\,4\pi E_c\lambda L^3\;\delta(\boldsymbol{r})\,. \tag{7}$$

In eq. (7), we assume that E_c can be defined for the shallow-trapped electron in the same way as for the conduction electron.

Perhaps the deformation around the impurity ion takes place in the following way. For instance, when the impurity ion has a smaller ionic radius than

([10]) T. MORIMOTO, J. TAKAMURA and K. TANI: Busseiron-Kenkyu, No. **30**, 382 (1958) (in Japanese).

([11]) J. BARDEEN and W. SHOCKLEY: *Phys. Rev.*, **80**, 1488 (1954).

the matrix ions, these are displaced in the direction of the impurity (in the case of the larger radius of impurity they are displaced in the opposite direction) because of the weaker repulsive force between the impurity ion and the matrix one, and the crystal becomes smaller in its volume (Fig. 1(*b*)).

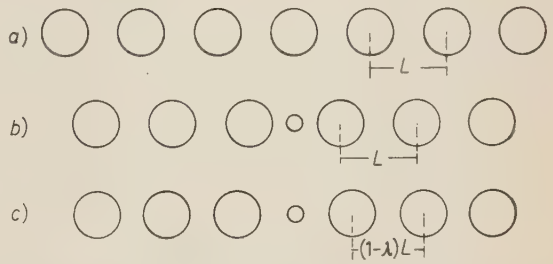

Fig. 1. – The behaviour of the displacement of the matrix ions surrounding the impurity *a*) Perfect crystal. *b*) Crystal containing an impurity with smaller ion radius and the same covalent bond strength. *c*) Crystal containing an impurity with smaller ion radius and weak covalent bond strength.

Furthermore, the s-p hybridized wave functions of the impurity have larger Coulomb interaction in the nucleus than in matrix atoms owing to the ionization of the impurity atom, and the covalent bond strength between the impurity ion and the matrix atom seems to be weaker than between the matrix atoms with each other. Therefore the nearest neighbour atoms are displaced in the opposite direction of the impurity in addition to the above displacement (Fig. 1(*c*)), and the part of the matrix around the impurity is deformed compressively, so that λ in eq. (7) is positive.

In metals, the forces which give rise to the displacements of matrix atoms around a vacancy are mainly the repulsive forces between the metal ions, so that the nearest neighbour atoms are displaced in the inner directions.

In ionic crystals, the ions have strong attractive and repulsive forces and therefore the nearest neighbour ions of a vacancy are displaced in the outer directions in the same way as the semiconductor containing an impurity. As λ is always positive, δV_p reduces the energy of the trapped electron more than when only the Coulomb potential of the impurity ion is adopted.

Since δV_p of eq. (7) contains a δ-function, it does not change the energy of the p-states of Kohn-Luttinger, which coincide with those of the infrared absorption ([12]).

3. – The energy of the ground state.

The potential, δV, for the trapped electron caused by the impurity ion is the summation of the Coulomb part, δV_c, and the deformation part, δV_p;

$$\delta V = \delta V_c + \delta V_p \,. \tag{8}$$

([12]) G. Picus, E. Barstein and B. Henois: *Journ. Phys. Chem. Solids*, **1**, 75 (1956).

Since $\delta \boldsymbol{V}_c$ is a slowly varying potential, the Schrödinger equation can be translated into the effective mass equation, when $\delta \boldsymbol{V}_p$ in eq. (8) is neglected. However, $\delta \boldsymbol{V}_p$ containing the δ-function, the Schrödinger equation of the trapped electron can not be treated in that manner. Therefore, we consider that $\delta \boldsymbol{V}_p$ is the perturbation potential in the Schrödinger equation. For convenience, we do not consider the degeneration of the energy minimum points in the conduction band.

The Hamiltonian of the trapped electron is

$$\boldsymbol{H} = \boldsymbol{H}_0 + \delta \boldsymbol{V}_c + \delta \boldsymbol{V}_p \,, \tag{9}$$

where $\boldsymbol{H}_0$ refers to the perfect lattice. According to Kohn and Luttinger, the approximating wave functions of the Schrödinger equation, which have discrete energy levels under the conduction band, are

$$\Psi_j = F_j(\boldsymbol{r})\, \psi_{\boldsymbol{K}_0}(\boldsymbol{r}) \qquad (j = 0, 1, \ldots), \tag{10}$$

for the unperturbed Hamiltonian, $\boldsymbol{H}_0 + \delta \boldsymbol{V}_c$. In eq. (10), $F_j(\boldsymbol{r})$ is a solution of the effective-mass equation,

$$\left(\sum_i \frac{\hbar^2}{2 m_i^*} \nabla_i^2 + \delta \boldsymbol{V}_c \right) F_j = E_j F_j \,, \qquad (i = x, y, z) \,, \tag{11}$$

where m_i^* is the effective mass of the conduction electron in the i-direction. and $\psi_{\boldsymbol{K}_0}(\boldsymbol{r})$ is a Bloch function of the energy minimum point in the conduction band, of which the wave vector is $\boldsymbol{K}_0$:

$$\psi_{\boldsymbol{K}_0} = \exp\left[i \boldsymbol{K}_0 \boldsymbol{r} \right] u_{\boldsymbol{K}_0}(\boldsymbol{r}) \,. \tag{12}$$

Now, we assume that the unperturbed wave functions in each energy band are the same as the Bloch functions of the perfect crystal even though the unperturbed Hamiltonian is given by $\boldsymbol{H}_0 + \delta \boldsymbol{V}_c$.

Considering the perturbation term, $\delta \boldsymbol{V}_p$, we get the energy of the ground state of the trapped electron as follows:

$$\begin{aligned} E = E_0 + \langle \Psi_0^* \delta \boldsymbol{V}_p \Psi_0 \rangle + \sum_j \frac{|\langle \Psi_0^* \delta \boldsymbol{V}_p \Psi_j \rangle|^2}{E_0 - E_j} + \sum_{l, \boldsymbol{K}} \frac{|\langle \Psi_0^* \delta \boldsymbol{V}_p \Psi_{\boldsymbol{K}}^l \rangle|^2}{E_0 - E_{\boldsymbol{K}}^l} = \\ = E_0 + \int (F_0 u_{K_0})^* \delta \boldsymbol{V}_p (F_0 u_{\boldsymbol{K}_0}) \, \mathrm{d}\boldsymbol{r} + \sum_j \frac{\left| \int (F_0 u_{\boldsymbol{K}_0})^* \delta \boldsymbol{V}_p (F_j u_{\boldsymbol{K}_0}) \, \mathrm{d}\boldsymbol{r} \right|^2}{E_0 - E_j} + \\ + \sum_{l, \boldsymbol{K}} \frac{|\langle \Psi_0^* \delta \boldsymbol{V}_p \Psi_{\boldsymbol{K}}^l \rangle|^2}{E_0 - E_{\boldsymbol{K}}^l} \,, \end{aligned} \tag{13}$$

where Ψ_0 and E_0 are the wave function of the ground state and the energy of the unperturbed system, respectively, $\sum_j$ being the summation over the discrete energy states under the conduction band, and $\sum_{l,\boldsymbol{K}}$ over the states in the energy bands.

Since the perturbation potential, δV_p, is a δ-function, the 3rd term of the right-hand side of eq. (13) has non-zero matrix elements only when F_j is an s-type wave function. Furthermore, if $u_{\boldsymbol{K}}(\boldsymbol{r})$ of the conduction band is the hybridized wave function made by s and p-type wave functions, only the s-type wave function gives non-zero contribution to the matrix element. We define a_s as the amplitude of the s-type function in $u_{\boldsymbol{K}_0}(\boldsymbol{r})$ in the energy minimum point of the conduction band, and rewrite eq. (13) as

$$E = E_0 + a_s^2 \int \delta V_p |F_0|^2 |u^s_{\boldsymbol{K}_0}|^2 \,\mathrm{d}\boldsymbol{r} + \tag{14}$$
$$+ \sum_j \frac{a_s^4 |\int (F_0 u^s_{\boldsymbol{K}_0})^* \delta V_p (F_j u^s_{K_0}) \,\mathrm{d}\boldsymbol{r}|^2}{E_0 - E_j} + \sum_{l,\boldsymbol{K}} \frac{|\langle \Psi_0^* \delta V_p \Psi^l_{\boldsymbol{K}} \rangle|^2}{E_0 - E} .$$

It seems to be reasonable to put F_j equal to what KITTEL and MITCHEL *et al.*, obtained by the variation method:

$$F_0 = \left[\frac{ab^2}{\pi r_0^3}\right]^{\frac{1}{2}} \exp\{-[a^2x^2 + b^2(y^2+z^2)]^{\frac{1}{2}}/r_0\} , \tag{15}$$

where r_0 stands for $\varkappa\hbar^2/mc^2$, and $\varkappa$ is the dielectric constant.

For silicon, F_0 has the energy $E_0 = -0.0286$ eV under the bottom of the conduction band, and a^2 and b^2 are 0.215 and 0.0663, respectively.

As for $u^s_{\boldsymbol{K}_0}(\boldsymbol{r})$, we use approximately the Slater function of the 3s-state for the free silicon atom:

$$u^s_{\boldsymbol{K}_0}(\boldsymbol{r}) = 1.99(\exp[-13.7r] - 2.53r \exp[-4.93r] + \ldots) . \tag{16}$$

The first term of the perturbation, ΔE_1 in (14) becomes by using (7)

$$\Delta E_1 = -4\pi E_c \lambda L^3 a_s^2 |F_0(0)|^2 |u^s_{\boldsymbol{K}_0}(0)|^2 . \tag{17}$$

Inserting; (15) and (16) in (17), ΔE_1 becomes as follows:

$$\Delta E_1 = -15.84 E_c \lambda L^3 a_s^2 ab^2/r_0^3 . \tag{18}$$

For the shallow trapped electron, we can use as E_c the value which was obtained in the calculation of the mobility of the conduction electron. It is 12.80 eV for silicon following BROOKS ([13]). If we assume that the wave function of the conduction band is made by one $3s$- and three $3p$-states in the same proportion, a_s^2 is approximately $\frac{1}{4}$. Therefore, by inserting in eq. (18) the following vales; $L = 2.35 \cdot 10^{-8}$ cm, and $r_0 = 6.37 \cdot 10^{-8}$ cm for Si, ΔE_1 becomes

$$\Delta E_1 = -0.1036\,\lambda \text{ eV}, \tag{19}$$

where λ is a parameter which measures the displacement of the nearest neighbour atom of the impurity.

HUNTINGTON and SEITZ ([14]) showed that λ results equal to 0.2 when a copper ion is inserted at an interstitial position of the lattice in the copper crystal, and 0.02 for the nearest-neighbour atom of the vacancy. If λ has the range from 0.01 to 0.1 for the substitutional impurity in silicon, ΔE_1 has its value in the range from -0.00104 eV to -0.0104 eV. In the first order approximation of the perturbation, for $\lambda = 0.1$ the ionization energy of the donor state of silicon becomes -0.039 eV, which is the summation of E_0 and ΔE_1. For germanium, in the same approximation, it is about -0.0096 eV.

4. – The second order approximation of the perturbation.

The summation, $\sum_j$, in the 3rd-term on the right-hand side of eq. (14) runs over the discrete levels, which lie under the conduction band. Since the perturbation term is of the δ-function type, only the matrix elements between the s-state and the ground states have non-zero values. Following Kohn and Luttinger, the wave function of the $2s$-state and its energy are respectively

$$F_1 = \left(c_1 + c_2 \frac{x^2}{r_0^2} + c_3 \frac{y^2 + z^2}{r_0^2}\right) \exp\left[-2[a^2x^2 + b^2(y^2 + z^2)]^{\frac{1}{2}}/r_0\right], \tag{20}$$

and

$$E_1 = -0.00816 \text{ eV}. \tag{21}$$

Here c_1 is decided by the ortho-normalization:

$$c_1 = c\left(\frac{ab^2}{\pi r_0^3}\right)^{\frac{1}{2}}, \tag{22}$$

([13]) H. BROOKS: *Advances in Electronics and Electron Physics*, **7**, 93 (1955).
([14]) H. B. HUNTINGTON and F. SEITZ: *Phys. Rev.*, **61**, 315 (1942).

where $c = F_1/F_0$ at the origin. The contribution of the $2s$-state to the second order perturbation energy is

$$\Delta E_2' = \frac{a_s^4 (F_0^*(0) u_{\boldsymbol{K}_0}^s(0) 4\pi E_c \lambda L^3 F_1(0) u_{\boldsymbol{K}_0}^s(0))^2}{E_0 - E_1} . \tag{23}$$

Substituting (20), (21) and (22) into (23), we obtain the following relation:

$$\Delta E_2' = -0.526\, c^2 \lambda^2 \text{ eV} . \tag{24}$$

If we put c and λ equal to $\frac{1}{2}$ and 0.1 respectively, $\Delta E_2'$ becomes $-0.00\,13$ eV, which is only ten percent of ΔE_1. Now, we shall estimate the contribution, ΔE_2^c, of the conduction band to the second order perturbation energy in the 4-th terms of eq. (14). Assuming that the state for the electron in the conduction band is free, the state density of the energy E_k in the conduction band becomes

$$\varrho_{E_K} = \frac{1}{4\pi^2} \left(\frac{2m_c}{\hbar^2} \right)^{\frac{3}{2}} (E_K - E_L)^{\frac{1}{2}} , \tag{25}$$

Here E_L is the energy of the bottom of the conduction band, amd m_c is defined as

$$m_c = \delta^{\frac{2}{3}} (m_x^* m_y^* m_z^*)^{\frac{1}{3}} , \tag{26}$$

where δ is the number of the degeneration of the minimum energy of the conduction band, (for example, $\delta = 6$ for Si). Replacing the summation by the integration, ΔE_2^c becomes

$$\Delta E_2^c = \sum_{\boldsymbol{K}} \frac{|\langle \Psi_0^* \delta \boldsymbol{V}_p \Psi_{\boldsymbol{K}}^c \rangle|^2}{E_0 - E_{\boldsymbol{K}}} = \tag{27}$$

$$= (1.99)^4 (4\pi)^2 E_c^2 \lambda^2 L^6 a_s^4 \left(\frac{ab^2}{\pi r_0^3} \right) \int_{E_{\min}}^{E_{\max}} \frac{(1/4\pi^2)(2m_c/\hbar^2)^{\frac{3}{2}} (E_K - E_L)^{\frac{1}{2}}}{E_0 - E_K} \, \mathrm{d}E_K .$$

The upper and lower limits of the integration are the energy at the top of the conduction band and that at the bottom respectively.

Therefore, putting $E_{\min}$ equal to E_L, eq. (27) becomes

$$\Delta E_2^c = -0.297 \cdot 10^{-7} \lambda^2 \left[(E_{\max} - E_L)^{\frac{1}{2}} - (E_L - E_0)^{\frac{1}{2}} \operatorname{tg}^{-1} \frac{(E_{\max} - E_L)^{\frac{1}{2}}}{(E_L - E_0)^{\frac{1}{2}}} \right] \text{eV} . \tag{28}$$

Here $(E_{max} - E_L)$ is the breadth of the conduction band, and $(E_L - E_0)$ is the ionization energy of the unperturbed state. The quantity in square brackets seems to be several electron volts. Therefore, ΔE_2^c is negligible compared to ΔE_1. Similarly, the contribution of the valency band has almost the same magnitude as $|\Delta E_2^c|$ and can be neglected.

By adding ΔE_1 given by eq. (19) and $\Delta E_2'$ given by eq. (24), the ionization energy of the ground state for silicon becomes 0.040 3 eV and 0.029 6 eV for $\lambda = 0.1$ and 0.01, respectively, and for germanium it is 0.009 8 eV for $\lambda = 0.1$ by a similar calculation.

5. – Self-deformation potential.

The trapped electron of the shallow impurity state causes a deformation in the vicinity of the impurity so as to decrease its own energy. The « self-deformation potential » is defined as the potential due to this deformation. Below, the magnitude of the deformation will be obtained by the variation method which was first used by KUBO [15]. The wave function of the trapped electron will be written as ψ and the co-ordinate of the crystal lattice as Q, the energy of the electron can be expressed by

$$H(\psi, Q) = K(\psi) + \delta V_c(\psi) + \delta V_s(\psi, Q) \,, \tag{29}$$

where $K(\psi)$ is the kinetic energy, δV_c the Coulomb energy by the interaction with the impurity ion, and δV_s the deformation potential energy mentioned above.

On the other hand, the energy of the crystal lattice is

$$U(\psi, Q) = U_i(Q) + \delta V_s(\psi, Q) \,, \tag{30}$$

where U_i is the elastic energy by the deformation. If we put the energy of the undistorted lattice equal to zero, the lattice energy $U_i(Q)$ becomes the deformation energy and thus Q can be considered as the volume dilatation. From eqs. (29) and (30), the total energy of the crystal is

$$E = U_i + \delta V_c + \delta V_s + K = H + U_i \,. \tag{31}$$

The variation of (29),

$$(\delta H / \delta \psi)_Q = 0 \,, \tag{32}$$

[15] R. KUBO: *Journ. Phys. Soc. Japan*, **3**, 254 (1946).

gives the Schrödinger's wave equation of the electron,

$$\{\boldsymbol{K}(\boldsymbol{r}) + \delta \boldsymbol{V}_c(\boldsymbol{r}) + \delta \boldsymbol{V}_s(\boldsymbol{r}, Q)\}\psi = H\psi \,. \tag{33}$$

From the variation of the total energy,

$$\delta E = 0 \,, \tag{34}$$

the following relation can be obtained:

$$\frac{\delta E(\psi(Q), Q)}{\delta Q} = \frac{\delta H}{\delta Q} + \frac{\delta U}{\delta Q} = \left(\frac{\delta H}{\delta \psi}\right)_Q \left(\frac{\delta \psi}{\delta Q}\right) + \left(\frac{\delta H}{\delta Q}\right)_\psi + \frac{\delta U}{\delta Q} = 0 \,. \tag{35}$$

With the aid of (30), (31) and (32), eq. (35) turns out to be

$$(\delta U/\delta Q)_\psi = 0 \,. \tag{36}$$

The lattice deformation is determined by eq. (36) for a given wave function ψ of the electron.

Now, if the electron is assumed to have a scalar mass, the density of the trapped electron is spherically symmetric in the ground state. Therefore $\delta \boldsymbol{V}_s$ also seems to be spherically symmetric. If the crystal lattice is assumed to be a continuous, elastic and infinite body, and if the pressures at the distance r and $(r + \Delta r)$ from the center of the impurity ion are denoted as p and $(p + \Delta p)$ respectively, the diagonal elements of the deformation at r are given by the equations,

$$\begin{cases} \alpha = \dfrac{pr^3 - (p + \Delta p)(r + \Delta r)^3}{3k\{(r + \Delta r)^3 - r^3\}} - \dfrac{2}{r^3} \dfrac{\{p - (p + \Delta p)\} r^3 (r + \Delta r)^3}{4n\{(r + \Delta r)^3 - r^3\}} \,, \\ \text{and} \\ \beta = \gamma = \dfrac{pr^3 - (p + \Delta p)(r + \Delta r)^3}{3k\{(r + \Delta r)^3 - r^3\}} + \dfrac{1}{r^3} \dfrac{\{p - (p + \Delta p)\} r^3 (r - \Delta r)^3}{4n\{(r + \Delta r)^3 - r^3\}} \,, \end{cases} \tag{37}$$

where k and n are the bulk modulus and the rigidity of the crystal respectively.

For infinitesimal Δr, (37) turns out to be

$$\begin{cases} \alpha = \left(\dfrac{1}{6n} - \dfrac{1}{9k}\right) r \dfrac{\mathrm{d}p}{\mathrm{d}r} - \dfrac{p}{3k} \,, \\ \text{and} \\ \beta - \gamma = -\left(\dfrac{1}{12n} - \dfrac{1}{9k}\right) r \dfrac{\mathrm{d}p}{\mathrm{d}r} - \dfrac{p}{3k} \,. \end{cases} \tag{38}$$

By definition, the volume dilatation at r is

$$\left(\frac{\Delta V}{V}\right) = \alpha + \beta + \gamma = -\frac{r}{3k}\left(\frac{\mathrm{d}p}{\mathrm{d}r}\right) - \frac{p}{k}. \tag{39}$$

The pressure, p, which the electron exerts on the lattice is

$$p = \mathrm{grad}\,(\delta \boldsymbol{V}_s \cdot \varrho)\,, \tag{40}$$

where ϱ is the electron density. Putting $\delta \boldsymbol{V}_s$ equal to $-E_c(\Delta V/V)$, and substituting (40) into (39), the following equation results:

$$\left(\frac{\Delta V}{V}\right) = \frac{E_c}{3k} r \frac{\mathrm{d}^2}{\mathrm{d}r^2}\left(\frac{\Delta V}{V}\varrho\right) + \frac{E_c}{k}\frac{\mathrm{d}}{\mathrm{d}r}\left(\frac{\Delta V}{V}\cdot\varrho\right). \tag{41}$$

The volume dilatation can be determined by (41) for the given wave function of the trapped electron, so that (36) and (41) are equivalent with each other. If $(\Delta V/V)$ is obtained for a given ψ, ψ is given by

$$\frac{\delta E\{\psi, (\Delta V/V)(\psi)\}}{\delta \psi} = 0\,. \tag{42}$$

Unfortunately, however, eq. (41) can not be solved analytically. In the adiabatic approximation, (33) must be used in place of (42).

Now, we shall estimate the magnitude of the volume dilatation, assuming that ϱ is given by

$$\varrho = (8\pi\zeta^3)^{-1} \exp\left[-r/\zeta\right]. \tag{43}$$

Since the volume dilatation is caused by the interaction between the trapped electron and the lattice, it seems to have almost the same extent as the electron cloud of the trapped state. Suppose that $(\Delta V/V)$ can be written as

$$(\Delta V/V) = A \exp\left[-r/\zeta\right], \tag{44}$$

even though it does not satisfy (41), (36) turns out to be

$$\frac{\partial}{\partial A}\left\{\frac{1}{2}k\int\left(\frac{\Delta V}{V}\right)^2 \mathrm{d}\boldsymbol{r} - E_c\int\frac{\Delta V}{V}\cdot\varrho\,\mathrm{d}\boldsymbol{r}\right\} = 0\,. \tag{45}$$

Substituting (43) and (44) into (45), A is given by

$$A = E_c/8\pi k\zeta^3\,. \tag{46}$$

Therefore, the contribution, ΔE_1^d, of the self-deformation potential to the ionization energy of the impurity state becomes, from eq. (33),

$$\Delta E_1^d = -E_c \int (\Delta V/V) \cdot \varrho \, d\boldsymbol{r} = -E_c^2/64k\zeta^3 . \tag{47}$$

Since the magnitude of ζ is about 10^{-7} cm for silicon, ΔE_1^d, becomes about $-0.000\,4$ eV, which is negligible compared to $-0.028\,6$ eV of E_0. In this calculation use was made of the following values; $E_c = 12.8$ eV and $k = 3 \cdot 10^{12}$ dyne/cm^2.

6. – Discussion.

The ionization energies have been estimated with the aid of the value of E_c which was obtained by calculating the mobility of the conduction electron at room-temperature. If the displacement of the nearest-neighbour ion around the impurity is much larger than the amplitude of the lattice vibration at room-temperature, we can not use the above value of E_c. According to Mott and Johnes' treatments ([16]), the amplitude of the lattice vibration is given by

$$\bar{X} = (\hbar^2 T/kM\Theta^2)^{\frac{1}{2}} , \tag{48}$$

where T is the temperature, M the mass of the matrix ion, and Θ the Debye temperature. For silicon, $\bar{X}$ has the following value at $T = 300$ °K

$$\bar{X}_{300} = 1.10 \cdot 10^{-9} \text{ cm} . \tag{49}$$

Therefore, the ratio of $\bar{X}_{300}$ to the atomic distance is

$$\lambda' = \bar{X}_{300}/L \simeq 0.05 . \tag{50}$$

This is the same order of magnitude as $\lambda = 0.1$ or 0.01 which were assumed in Section 3. This fact justifies our use of the value of E_c which was estimated from the mobility.

Next, to check the limitation of our variational method, let us examine the

([16]) N. F. Mott and H. Johnes: *The Theory of the Properties of Metals and Alloys* (Oxford, London, 1936), p. 244.

first two terms of eq. (14). Using eqs. (11) and (15), these terms become

$$(51) \quad E = \frac{\hbar^2}{6r_0^2}\left(\frac{a^2}{m_x^*} + \frac{b^2}{m_y^*} + \frac{b^2}{m_z^*}\right) - \frac{e^2 ab}{\varkappa r_0 \sqrt{a^2 - b^2}} \sin^{-1}\left(\frac{\sqrt{a^2 - b^2}}{a}\right) - B\lambda ab^2 \ldots .$$

Here it should be noted that the last term in eq. (51) is equal to ΔE_1 given by eq. (18). Fig. 2 shows the E *vs.* a curves in arbitrary scales for constant b and various values of λ. Since the last term in eq. (51) is of third order in a and b, the curves change from I to IV as the parameter λ increases. As far as E has a minimum point, we may use approximately the wave function obtained by the variation method as the unperturbed one. In Fig. 2, E has an inflexion point when $\lambda = 0.1$ in the case of silicon (Curve III). In the case of germanium, however, the value of λ for which E has an inflexion point is much larger than 0.1, because B of the last term in eq. (51) is very small.

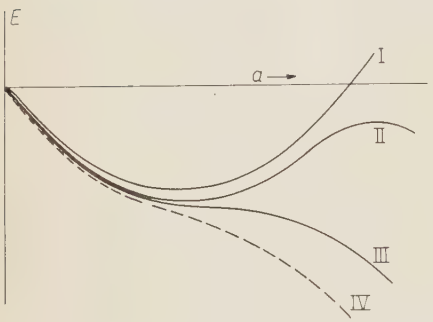

Fig. 2. – Behaviour of E with a (for b = constant). Curve I: $\lambda = 0$. Curve II: $0 < \lambda < 0.1$. Curve III: $\lambda = 0.1$. Curve IV: $\lambda > 0.1$.

In conclusion, even if the ratio of the displacement of the nearest neighbour ion to the atomic distance is assumed as large as 0.1, the contribution of the volume dilatation to the ionization energy of the donor state is only 0.011 7 eV for silicon, and the discrepancy between experimental values and theoretical ones can only partly be explained. These results seem to suggest that the effective mass equation becomes inadequate in the vicinity of impurity atoms.

RIASSUNTO (*)

Supponendo che gli ioni di impurità producano solo difetti puntuali nelle strutture si è calcolata in maniera semiquantitativa la variazione dell'energia di ionizzazione dello stato donatore. Ponendo lo spostamento dello ione più vicino eguale a un decimo della distanza atomica, si è ottenuto il valore di 0.117 eV. L'influenza del potenziale di autodeformazione dell'elettrone catturato è trascurabile.

(*) *Traduzione a cura della Redazione.*

Spins and Parities of Excited Levels in ^{212}Po.

M. Giannini, D. Prosperi and S. Sciuti

Centro di Studi Nucleari della Casaccia - Roma
Scuola di Perfezionamento in Fisica dell'Università - Roma

(ricevuto il 12 Maggio 1961)

Summary. — Spins and parities of excited levels in ^{212}Po are evaluated by the comparison of log *ft* values, conversion coefficients, and transition probability data. Further, spins and parities of the 1513 and 1800 keV levels have been evaluated by angular correlation measurements. All the available data show unambiguously that the first three excited levels are 2^+, 2^+, 1^+. Some uncertainties still remain for the 1680 keV level (0^+, 2^+) and for the 1800 keV level (2^+).

1. – Introduction.

In a previous work [1] on the excited levels of ^{212}Po we proposed a modified decay scheme including 130, 190, 727, 786, 893, 953, 1513, 1620, 1680 keV γ-transitions.

Further, the β-transition percentages were deduced from the measured γ-ray intensities. The lack of accurate data on conversion coefficients did not allow us to introduce the corrections due to conversion.

In the present work we attempt to determine spins and parities of levels and to evaluate the above-mentioned corrections.

Spin and parity assignments of the 727, 1620 and 1800 keV levels were here evaluated by the comparison of log *ft* values, conversion coefficients, and transition probability data. The spin and parity of the 1513 keV level were evaluated by angular correlation measurements between 727 and 786 keV γ-rays, while by angular correlations between 727 and 1073 keV it was possible to confirm the 2^+ assignment to the 1800 keV level.

(1) M. Giannini, D. Prosperi and S. Sciuti: *Nucl. Phys.*, **19**, 380 (1960).

2. – Internal conversion coefficients.

Since the 727 keV transition is well known, we normalized the conversion coefficients α_k deduced from our previous work (1) and from other works (2, 5),

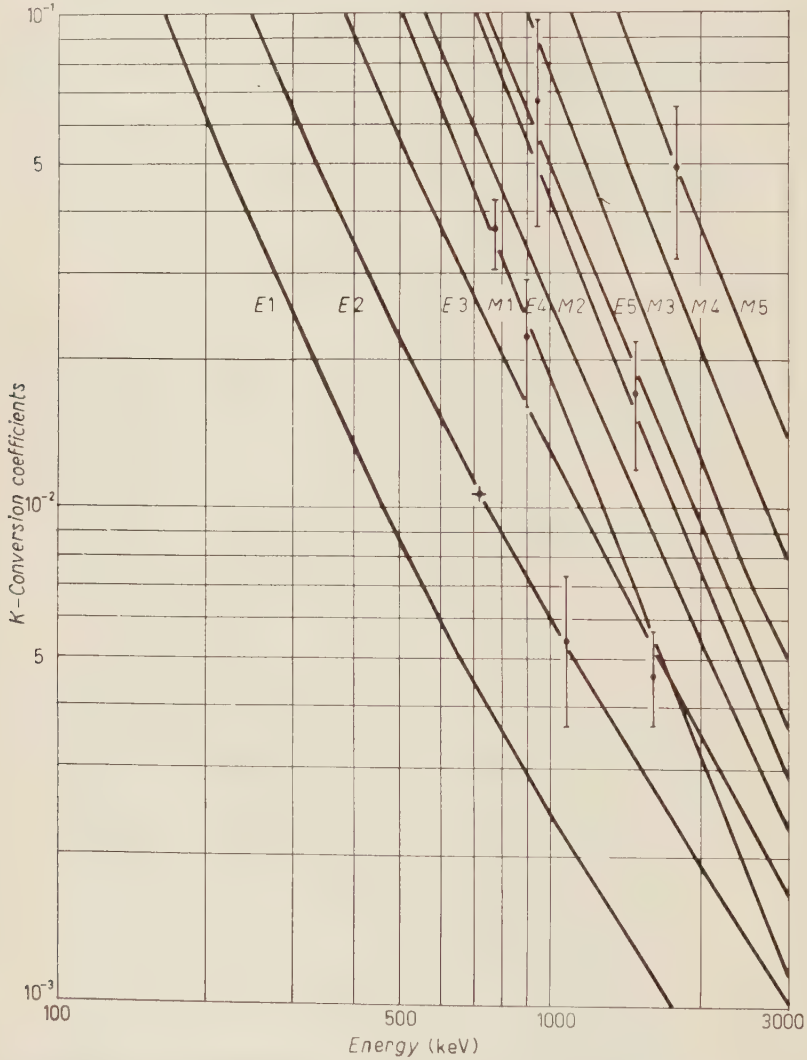

Fig. 1. – k-conversion coefficients for γ-transitions in ^{212}Po. The theoretical curves have been deduced from Rose's tables.

(2) G. T. Emery and W. R. Kane: *Phys. Rev.*, **118**, 755 (1960).
(3) V. Hauser and W. Kerler: *Zeit. f. Phys.*, **158**, 405 (1960).
(4) G. Shupp, H. Daniel, G. W. Eakins and E. N. Jensen: *Phys. Rev.*, **120**,189 (1960).
(5) A. G. Sergeev, E. M. Krisjuk, G. D. Latyshev, In. N. Trofimov and A. S. Remmennyi: *Soviet Physics JETP*, **6(33)**, 878 (1958).

according to the formula:

$$\alpha_k^{(i)} = \alpha_k^{(727)} \frac{I_e^{(i)}}{I_e^{(727)}} \cdot \frac{I_\gamma^{(727)}}{I_\gamma^{(i)}} , \tag{1}$$

where $I_\gamma^{(i)}$ are the experimental γ-ray intensities measured in the above-quoted works and $I_e^{(i)}$ are the electron conversion intensities by KRISJUK *et al.* [5]. We put $\alpha_k^{(727)} = 0.010\,6$.

In Fig. 1 the $\alpha_k^{(i)}$ values deduced from (1) are represented together with the theoretical curves according to ROSE [6].

3. – log *ft* values.

The γ-ray intensities deduced from the above-mentioned works have been employed together with the $\alpha_k^{(i)}$ coefficients (Fig. 1) in order to calculate the log *ft* values reported in Fig. 6.

The intensities are given in transitions per ^{212}Po decay employing the value $0.359 \pm .001$ for the ^{212}Bi branching ratio [7] and the value $5.54 \pm .27$ for the intensity ratio between the 2 614 keV γ-ray of ^{208}Pb and the 727 keV γ-ray [2,4].

In order to get information on the spins, we have compared the calculated log *ft* with all the experimental data available in the lead region (Fig. 10 in ref. [8]).

4. – Transition probabilities.

Further information on γ-transition multipolarities can be obtained from the knowledge of γ-ray and long-range α-particle intensities. We employed the well-known formula

$$\tau_\gamma = \tau_\alpha \frac{I_\alpha}{I_\gamma} , \tag{2}$$

---

[6] M. E. ROSE: *Internal Conversion Coefficients* (Amsterdam, 1958.

[7] F. E. SENFTLE, T. A. FARLEY and N. LAZAR: *Phys. Rev.*, **104**, 1629 (1956); D. PROSPERI and S. SCIUTI: *Nuovo Cimento*, **9**, 734 (1958); P. MARIN, G. R. BISHOP and H. HALBORN: *Proc. Pys. Soc.*, **66**, 607 (1953); P. RICE EVANS and N. J. FREEMAN: *Proc. Phys. Soc.*, **72**, 300 (1958); G. SHUPP, H. DANIEL, G. W. EAKINS and E. N. JENSEN: *Phys. Rev.*, **120**, 189 (1960).

[8] M. GIANNINI, D. PROSPERI and S. SCIUTI: *Nuovo Cimento*, **21**, 430 (1961).

where τ_α and τ_γ are respectively the mean-lives of the γ-rays and long-range α-particles starting from the same level.

In order to evaluate τ_α we employed the Preston formula (9) assuming $R = 9.135$ fermi in agreement with the experimental α-transition probability from the ground state. Furthermore, the dependence of the tunneling effect on the α-particle angular momentum has been taken into account (we assumed L=2 for 9.490, 10.421 and 10.540 MeV α-particles).

The τ_γ values deduced from (2) are plotted in Fig. 2 together with the Weisskopf curves for different multipolarities.

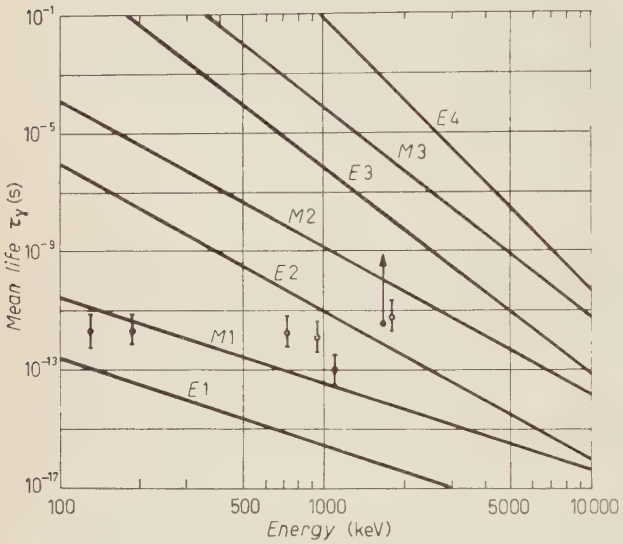

Fig. 2. – τ_γ values concerning γ-transitions in ^{212}Po. The curves represent the Weisskopf estimate.

5. – Angular correlations.

As stated above, we measured the angular correlations between the (727, 786) and (727, 1073) keV γ-rays. The experimental apparatus (8) employed a fast-slow spectrometer ($\tau = 10$ ns for the fast coincidence). The coincidence spectrum was displayed on a 200-channel pulse height analyser. Fig. 3 shows one of the spectra so obtained.

The coincidence rate at various angles for the (727 ; 786) keV cascade was least square fitted to a $1 + a_2 \cos^2\theta$ form neglecting higher order terms (*).

In Fig. 4 are reported the experimental curves together with the attenuated theoretical ones calculated for 2(1)2(2)0 and 1(1)2(2)0 cascades.

The value

$$W(\theta)^{\text{exp}} = 1 + (0.33 \pm .03) \cos^2\theta$$

(9) See G. C. Hanna: *Experimental Nuclear Physics*, vol. III; edited by E. Segrè (New York, London, 1959).

(*) The $a_4 \cos^4\theta$ term can be neglected because the 786 keV transition is essentially $M1$.

is in agreement with the 2(1)2(2)0 cascade to which corresponds an anisotropy of 0.39. From the corrected experimental anisotropy one gets a mixing

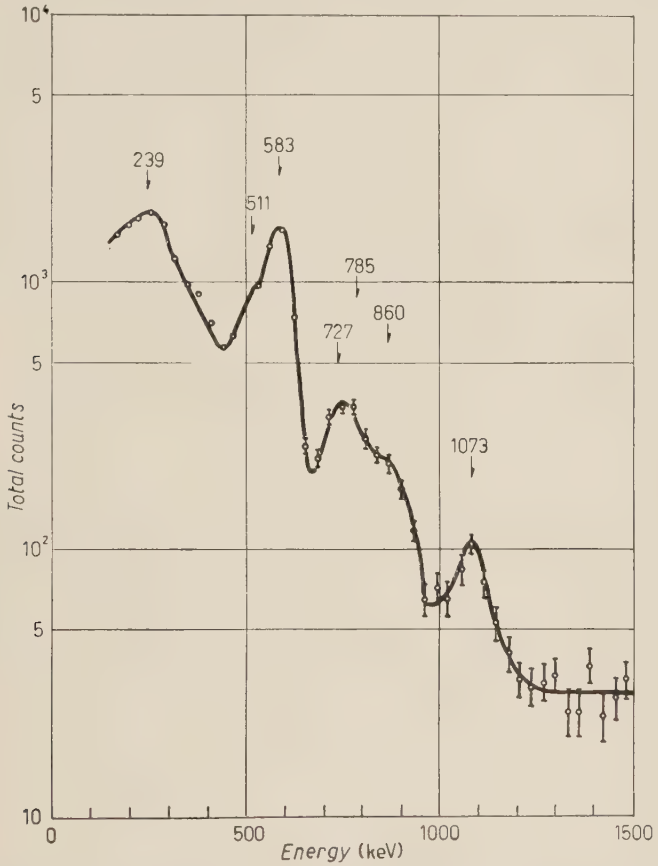

Fig. 3. – γ-spectrum in coincidence with the (720 ; 790) keV region from a RdTh source. Only the 727, 785, 1 073 keV γ-rays belong to the ^{212}Bi $\rightarrow$ ^{212}Po decay.

$\delta^2 \simeq 1.6 \cdot 10^{-3}$ quite close to the value $\delta^2 = 1.8 \cdot 10^{-3}$ deduced from the Weisskopf estimate.

The experimental points due to the

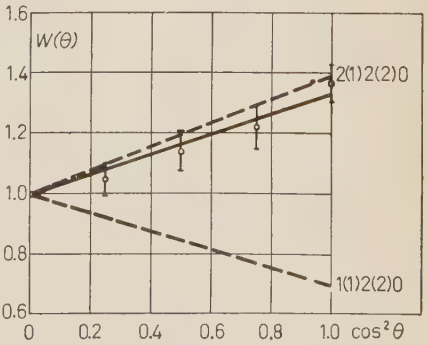

Fig. 4. – Angular correlation between 727, 786 keV γ-rays. The full line is the curve fitted by least-squares. Dashed lines show the theoretical attenuated curves for two different cascades.

(727 : 1073 keV) cascade are shown in Fig. 5. The quoted errors are larger than those in the former measurement due to the low intensity of the 1073 keV γ-rays. Nevertheless the results can be effectively employed for a discussion of the spin assignment. The coincidence rate at various angles was least square fitted to a $1+a_2\cos^2\theta$ form. The theoretical attenuated curves of Fig. 5 refer to the 2(2)2(2)0, 2(1)2(2)0 and 0(2)2(2)0 cascades. The experimental value

$$W(\theta)^{\text{exp}} = \\ = 1 + (0.30 \pm .10)\cos^2\theta$$

is in agreement with the hypothesis that the 1800 keV level is 2^+ and that the 1073 keV transition is essentially $M1$. These results are in disagreement with the conversion coefficient measurements which indicate an $E2$ multipolarity. From our measurement a mixing value of the order of 10^{-2} is obtained.

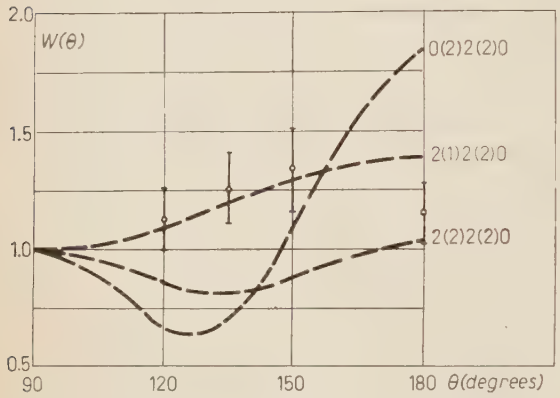

Fig. 5. – Angular correlation between 727, 1073 keV γ-rays. Dashed lines show the theoretical attenuated curves for different cascades.

6. – Conclusions.

In Table I are reported the γ-transition multipolarities deduced from the methods shown in Sections 2, 4, 5, and from the α_k/α_L ratios due to KRISJUK *et al.* (*).

The data concerning 130 and 190 keV transitions, reported by us in (1), will not be considered in the following because their existence has not been confirmed by other authors. Further we admitted the existence of the doubtful 1800 keV γ-transition. 953, 1513 and 1800 keV transitions have weak conversion lines and therefore the corresponding intensities have been measured with large errors. These conversion coefficients give rise to contradictory results. In fact, the experimental values turn out to be larger than the expected ones (in some cases by an order of magnitude).

(*) According to the authors the ratios are affected by quite large errors.

TABLE I.

E_γ (keV)	γ-transition multipolarities deduced from				Final assignments
	α_k coefficients	Transition probabilities	Angular correlations	α_k/α_L ratios	
130	—	$M1$, ($E1$, $E2$)	—	—	$M1$
190	—	$M1$, ($E1$, $E2$)	—	—	$M1$
727	$E2$	$E2$, $M1$	—	$E2$	$E2$
786	$M1(E4)$	—	$M1+(E2)$	$M1+E2$	$M1+(E2)$
893	$M1$	—	—	$(E2+E3)$	$M1$
953	($M2$, $M3$, $E5$)	($M1$, $E2$)	—	—	?
1073	$E2$	$M1$, $E2$	$M1+(E2)$	—	$M1+E2$
1513	($M2$, $E5$)	—	—	—	?
1620	$M1(E4)$	—	—	—	$M1$
1800	($M5$)	$E2$, $M1$	—	—	$E2$, $M1$

Further considerations can be made. The log ft values indicate that ^{212}Po levels can be only 0^+ or 1^+ or 2^+. According to α-particle selection rules, all the levels emitting long range alphas, *i.e.* the 727, 1680, 1800 keV levels, must be 0^+, or 2^+. Therefore the 727 and 1800 keV levels, from which direct transitions to the 0^+ ground state ([10]) start, must be 2^+. The 1513 keV level must be 2^+ according to our angular correlation results. The fact that no long range alphas have been observed, can not be taken as a contrary evidence, because the expected intensity for this α-decay is about 1/30 of the α-intensity from the first excited level. As far as the 1680 keV level is concerned, there is an ambiguity in spin assignment due to the doubtful existence of the 1680 keV direct transition. In fact, its intensity should be about 100 times smaller than the 1620 keV γ-ray intensity. Therefore the 1680 keV γ-rays could not be observed even for a 2^+ level.

In Table II are reported the spin and parity assignments deduced from the analysis of all available data. Accordingly, a tentative decay scheme of ^{212}Bi is reported in Fig. 6. The spin and parity assignments of the first four levels can be considered well established, while the spins and parities of the higher levels are uncertain even though a considerable amount of data is now available.

Further information can be obtained from the relative intensities of different γ-rays starting from a given level. The experimental ratio $I_{1620}/I_{893} \simeq 5$ leads to a $M1$ multipolarity for both the 1620 and 893 keV transitions. The

([10]) F. DE MICHELIS: *Nuovo Cimento*, **19**, 642 (1961).

TABLE II.

Level energy (keV)	Assignements in agreement with Table I	Assignements deduced from log *ft*	Assignements deduced from angular correlations	Final assignment
0	0^+	0^+, 2^+	—	0^+
727	2^+	0^+, 2^+	—	2^+
1 513	1^+, 2^+, 3^+, 4^+	0^+, $2^+(1^+)$	2^+	2^+
1 620	1^+, (2^+, 3^+)	0^+, $2^+(1^+)$	—	1^+
1 680	?	?	—	0^+, 2^+
1 800	2^+, 1^+	0^+, 1^+, 2^+	2^+	2^+

ratio $I_{786}/I_{1513} \simeq 3$ leads to $M1$ and $M2$ multipolarities for 786 and 1513 keV transitions, supporting therefore a 2^+ assignment to the 1513 keV level.

Our proposed decay scheme does not include the 1078.5 keV transition found by KRISJUK *et al.* There are two possible alternatives. In the first, one

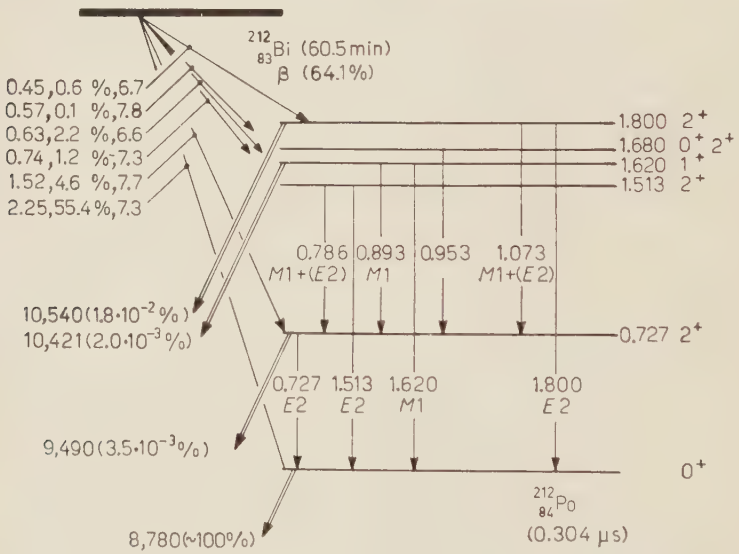

Fig. 6. – Decay scheme of ^{212}Bi (energies in MeV).

must postulate the existence of an additional excited state in ^{212}Po, for which there is no experimental evidence. In the second, one has to claim for the association of the corresponding conversion line to a 1073.4 keV transition in ^{208}Pb from the 3686 keV level to the 2614 keV level. This hypothesis seems to be at present the best because it justifies also the presence of the debated 212 keV transition in the ^{208}Tl decay.

It is of some interest to investigate whether or not the levels of ^{212}Pb exhibit vibrational structures. Some characteristics of the 727 and 1513 keV levels seem to prove their vibrational nature. This is however in disagreement with the $M1$ multipolarity of the 786 keV γ-rays. One can further suppose that also the 1800 keV level could be due to a quadrupole vibrational excitation. This would explain the slowing down of the transition ($2^+ \rightarrow 0^+$ two-phonon transition). However this hypothesis must also be rejected if the 1073 keV γ-rays are $M1$.

The knowledge of ^{212}Po is still uncertain because of the large errors affecting some conversion coefficients and of the ambiguity in the 1073 keV transition multipolarity. Therefore further efforts must be directed towards improving the knowledge of the conversion coefficients.

RIASSUNTO

Sono stati valutati gli spin e parità dei livelli eccitati del ^{212}Po mediante il confronto dei log *ft*, dei coefficienti di conversione e delle probabilità di transizione. Gli spin e le parità dei livelli da 1513 e 1800 keV sono stati inoltre valutati mediante misure di correlazioni angolari. Tutti i dati a disposizione mostrano senza ambiguità che i primi tre livelli eccitati sono 2^+, 2^+, 1^+. Tuttavia permangono ancora alcune incertezze sulle attribuzioni di spin e parità relativi ai livelli da 1680 keV (0^+, 2^+) e 1800 keV (2^+).

3789

On the Experimental Evidence for Pion-Pion Interaction in High-Energy π-$\mathcal{N}$ and $\mathcal{N}$-$\mathcal{N}$ Events.

P. Surányi

Central Research Institute for Physics, Laboratory of Cosmic Rays - Budapest

(ricevuto il 16 Maggio 1961)

Summary. — We assume that the pion cloud plays the most essential role in very high energy π-$\mathcal{N}$ and $\mathcal{N}$-$\mathcal{N}$ interactions. This assumption is checked by comparing some consequences of it with the experimental data in the GeV region.

Introduction.

In recent times the detailed discussions of π-$\mathcal{N}$ interactions have led to the very interesting recognition, that the π-π interaction dominates in the inelastic pion-nucleon interactions ([1,2]). In addition the results of several papers ([3]) indicate that the μ, 2μ, 3μ target masses play a significant role even in the nucleon-nucleus interactions (here μ stands for the pion mass).

According to the experiments ([1,2]) the angular distribution of the pions is strongly collimated in the forward cone and that of the protons in the back-

([1]) G. Maenchen, W. B. Fowler, W. M. Powell and R. W. Wright: *Phys. Rev.*, **108**, 850 (1957).

([2]) V. A. Beliakov, Van-Sho-Fen, V. V. Glagoliev, N. Dalkhazev, P. M. Lebediev, N. N. Melnyikova, V. A. Nikityn, V. Petrzilka, V. A. Sviridov, M. Suk and K. D. Tolstov: *Žurn. Éksp. Teor. Fiz.*, **39**, 937 (1960).

([3]) N. G. Birger and Yu. A. Smorodin: *Žurn. Éksp. Teor. Fiz.*, **36**, 1159 (1959); **37**, 1353 (1969); E. R. T. Awunor-Renner, L. Blaskovitch, B. R. French, G. Ghesquière, I. B. de Minvielle Devaux, W. W. Neale, C. Pellettier, P. Riviet, A. B. Sahiar and I. O. Skillicorn; *Nuovo Cimento*, **17**, 134 (1960); E. M. Friedlander, M. Marcu and M. Spirchez: *Nuovo Cimento*, **18**, 623 (1960).

ward direction. This forward-backward collimation cannot be explained on the basis of statistical and hydrodynamical theories. When the pion angular distribution is transformed into the pion-pion C.M.S. (that is into the system where the target particle is supposed to be a virtual π-meson) it turns out to be partly symmetrical. The asymmetrical part is collimated in the backward cone. BELIAKOV *et al.* [2] separated these two parts of the angular distribution by means of energy discrimination in the L.S. As the C.M.S. of the backward collimated part of the angular distribution in the π-π C.M.S. the π-N system is supposed in Beliakov's paper, however a certain disagreement of this assumption with the experiments is also mentioned there. Another possibility of finding the C.M.S. system in question is to transform the asymmetric part into the π-2π, π-3π, ... systems successively. Our basic assumption is a strong π-π interaction. We shall show the role of the afore-mentioned transformation and discuss some effects of this assumption on multiple meson production.

Several authors tried to solve the problem of multiple meson production making use of models where cloud effects and nucleon core interaction are mixed up [4], using only one-pion exchange diagrams.

1. – Average number of pions in the cloud.

According to our present knowledge one must attribute a certain structure to the nucleon, that is a core in the center, which plays the role of source of a pion field, and a pion cloud which sorrounds the core. Experiments [3] show that the pions of the cloud behave more like « real » pions, for instance their mass is measurable. However, an uncertainty of these pion masses arises because of their finite life time in the cloud which causes among others the well measurable width of the target mass distribution mentioned before [3].

We shall turn now to the problem of the number of pions in the cloud. For the sake of simplicity we shall consider first a π-N collision. According to our assumption the incoming pion begins its interaction with the pions of the cloud. In this interaction several mesons are created. As the π-π interaction is very strong, any pion emitted by the core (« connective » pions) gets into interaction with the pions produced by the primary pion-cloud interaction. The probability of the emission of a free pion by the core is very small. Hence the interaction may be described essentially in terms of the graph shown in Fig. 1. Naturally, the number of « connective » pions may vary. The nucleon-nucleon interaction may be explained in a similar manner with the addition

[4] D. L. BLOKHINTSEV and WANG YUNG: (Unpublished), Dubna D-576; V. S. BARASHENKOV: (Unpublished), Dubna-540.

of a possible pion exchange between the two cores (Fig. 2). Naturally this picture should be used only at energies, where the dissociation time of pions is longer than the collision time.

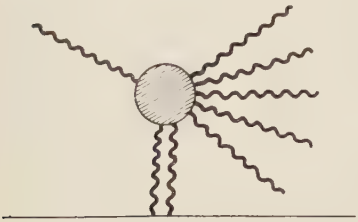

Fig. 1. – Interaction between pion and nucleon according to the proposed model.

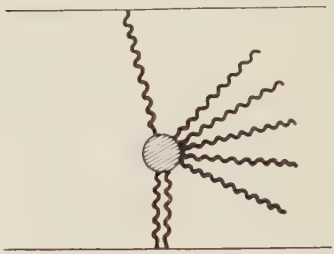

Fig. 2. – Interaction between two nucleons according to the proposed model.

If this picture is valid, the nucleons play no essential role, the mean number of cloud pions determines the total inelastic π-N and N-N cross-sections. Present experimental values show ([5]) that $\sigma_{\text{inel},\pi\text{-N}}$ is equal to, or somewhat smaller than $\sigma_{\text{inel},\text{N-N}}$, which may be understood on the basis of our picture if we suppose the mean number of pions in the cloud ($\langle n \rangle$) to be one or somewhat more.

In the first approximation we may suppose that the number of pions in the cloud shows a Poisson distribution. In a Poisson distribution, having a mean value of 1, the main contribution comes from the values around the zero value. Although the zero meson state contributes to the probability distribution, it has no influence on the inelastic interactions, since, following our supposition, inelastic interaction occurs only when at least one meson is present. Thus to get a proper mean value ($\langle n \rangle'$) of the number of cloud pions one has to drop the zero meson probability from the distribution. If we make a little more precise calculation in the case of $\sigma_{\text{inel, N-N}}/\sigma_{\text{inel, }\pi\text{-N}} = 1$ we obtain $\langle n \rangle = 1.24$ and we get for ($\langle n \rangle'$) a value of about 2 (Appendix I). Fubini and Thirring have shown by a Chew-Low approach that the mean number of pions in the cloud is about 1 ([6]).

2. – Inelasticity coefficients.

The inelasticity coefficient of the nucleon-nucleon interactions may be determined with the help of our model on the basis of the following simple considerations:

([5]) Material of the Kiev Conference (1960).
([6]) S. Fubini and W. E. Thirring: *Phys. Rev.*, **105**, 1382 (1957).

Let us denote the Lorentz-coefficient of the C.M.S. of the two nucleons by γ. In this case the energy of a pion moving together with any of the nucleons is equal to $\mu\gamma$. If we assume that n_a pions from the cloud of nucleon A interact with n_b pions of the cloud of nucleon B, then the total energy of the pions turns out to be $\mu(n_a + n_b)\gamma$. We obtain for the inelasticity coefficient

$$K = \frac{\mu(n_a + n_b)\gamma}{M(2\gamma - 2)},$$

and for the mean value of K

$$\langle K \rangle = \frac{\mu \langle n \rangle'}{M} \frac{\gamma}{\gamma - 1}. \tag{1}$$

Making use of the value $\langle n \rangle' = 2$ and eq. (1), we can calculate the inelasticity coefficient at various energies. The results are summarized in Table I.

TABLE I.

E_{primary}	K_{theor} ($\langle n \rangle' = 2$)	K_{exp}
6.2 GeV	0.58	0.49 ± 0.05 KALBACH *et al.* [7] 0.43 ± 0.06 DANIEL *et al.* [8]
9 GeV	0.51	0.55 ± 0.03 VAN-SHO-FEN *et al.* [9] 0.52 ± 0.03 BOGACHEV *et al.* [10]
∞	0.30	

We may see, that the model gives results in sufficiently good agreement with the experimental values.

---

[7] R. M. KALBACH, J. J. LORD and C. M. TSAO: *Phys. Rev.*, **113**, 330 (1959).

[8] R. R. DANIEL, N. KEMESWARA RAO, P. K. MALHOTRA and Y. TSUZUKI: *Nuovo Cimento*, **16**, 1 (1960).

[9] VAN-SHAO-FEN, T. VISKY, I. M. GRAMINETSKY, V. T. GRISHIN, N. DALKHAZEV, P. M. LEBEDIEV, A. A. NOMOFILOV, M. I. PODGORETSKY and V. N. STRELTSOV: *Žurn. Ėksp. Teor. Fiz.*, **39**, 957 (1960).

[10] N. D. BOGACHEV, S. A. BUNIATOV, I. M. GRAMINETSKY, V. B. LIUBIMOV, YU. P. MEREKOV, M. I. PODGORETSKY, V. M. SIDOROV and D. TUVDENDORZK: *Žurn. Ėsp. Teor. Fiz.*, **37**, 1223 (1959).

3. – Momentum distribution.

In the model discussed above the angular and momentum distribution of the nucleon—playing a rather passive role in the interaction—is essentially independent of the primary energy, and is the same for π-$\mathcal{N}$ and $\mathcal{N}$-$\mathcal{N}$ interactions. In the absence of detailed experimental data we can compare only the average values of longitudinal and transversal momenta in the L.S. The

TABLE II.

Author	p_t (GeV)	p_l (GeV)	Type of primary
BELJAKOV *et al.* [2]	0.37 ± 0.04	0.88 ± 0.06	7 GeV π^-
VAN-SHO-FEN *et al.* [8]	0.37 ± 0.03	0.82 ± 0.16	9 GeV p
DANIEL *et al.* [9]	0.34 ± 0.06	0.52 ± 0.09	6.2 GeV p
BOZÓKI *et al.* [11]	0.29 ± 0.07	0.64 ± 0.16	7 GeV π^-

values given in Table II were obtained by a rough transformation of C.M.S. distributions. As the distribution of protons is symmetrical in the C.M.S., the distribution of forward protons can be obtained by transforming the L.S. to the rest system of the incoming proton. If our assumption is correct and the distribution of nucleons is independent of the primary energy, we have the following connection between the inelasticity and the primary energy:

$$\langle K \rangle = \frac{2\gamma M - 2\gamma(\langle E \rangle - v\langle p_x \rangle)}{2\gamma M - 2M},$$

where $\langle E \rangle$ stands for the mean lab. energy of the backward nucleons, $\langle p_x \rangle$ for their longitudinal momentum, thus $\gamma(\langle E \rangle - v\langle p_x \rangle)$ is the mean C.M.S. energy of nucleons after collision.

Comparing this result with eq. (1), we get

$$\langle n \rangle' = \frac{M - \langle E \rangle + v\langle p_x \rangle}{\mu} \approx \frac{M - \langle E \rangle + \langle p_x \rangle}{\mu},$$

[11] G. BOZÓKI, F. FENYVES, A. FRENKEL, E. GOMBOSI and P. SURÁNYI: (in preparation).

that is

$$\gamma\mu\langle n\rangle' = \gamma M - \langle \bar{E}\rangle \,. \tag{3}$$

The energy loss of the nucleon is equal to the total energy of its interacting pions.

According to the experiments mentioned above we may distinguish experimentally between various target mass states. So there is a possibility to observe in the sense of eq. (3) the discrete values of the inelasticity coefficient in the C.M.S. energy distribution of protons. The C.M.S. distribution of proton momenta measured by the Berkeley group ([7]) can be seen in Fig. 3, the scale of the number n of pions is calculated by means of eq. (3), making use of the consideration that this must hold for individual cases too. Naturally the maxima at the integer values of n are not significant.

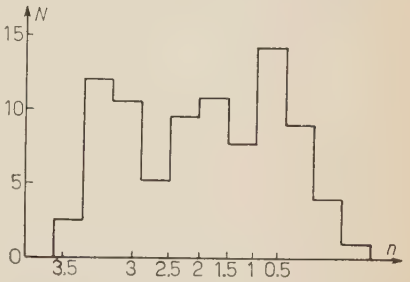

Fig. 3. — Distribution of the number n of target pions according to the experiment of KALBACH *et al.* ([7]).

However, it is clear that a smooth curve cannot be in good agreement with the experimental results. One must mention that from the point of view of the proton distribution clear experimental conditions are very important. In emulsion experiments the proton distribution is strongly influenced by the selection critera; measurements made in bubble chambers offer a poor possibility for distinguishing between positive π-mesons and protons.

From these results it is very easy to deduce the equation of Birger-Smorodin and Awunor-Renner *et al.* ([3]).

From the conservation of energy and momenta we get the following relation

$$M_2 = \sum_i (E_i - p_{xi}) - E_1 + \sqrt{E_1^2 - M_1^2} \,.$$

Here M_2 is the target (nucleon) mass, E_1, M_1 the energy and mass of the moving particle, E_i and p_{xi} the energy and longitudinal momenta of the secondaries. The summation is extended over all secondaries.

BIRGER and SMORODIN have measured the following quantity

$$M_t = \sum{}' (E_i - p_{xi}) - E_1 + \sqrt{E_1^2 - M_1^2} \,,$$

where the sum is extended over all the relativistic particles, that is to say over all particles, save the recoiled proton, and M_t is the effective target mass.

If we take the difference between the two equations we get as result again eq. (3)

$$M_t = M_2 - E_{\text{recoil}} + p_{x\,\text{recoil}} .$$

In the above-mentioned papers [3] the authors have derived the above formula.

Uqing eq. (3) $\langle n \rangle'$ is calculated from several data (see Table III).

TABLE III.

Author	$\langle n \rangle'$	Type of primary
BELJAKOV *et al.* [2]	2.4 ± 0.3	7 GeV π^-
MAENCHEN *et al.* [1]	2.07	5 GeV π^-
DANIEL *et al.* [8]	1.93 ± 0.34	6.2 GeV p
KALBACH *et al.* [7]	2.2 ± 0.2	6.2 GeV p
VAN-SHO-FEN *et al.* [9]	2.6 ± 0.3	9 GeV p
BOZÓKI *et al.* [11]	2.5 ± 0.8	7 GeV π^-

The experimental data are in sufficiently good agreement with a value of $\langle n \rangle'$ of 2.

4. – Charge state ratio.

If we take into account the difference between the probabilities of the emission of charged and neutral pions, respectively, we may get a simple expression for the probabilities of the presence of a proton or a neutron in the final state.

Again using our meson number distribution the probability that a nucleon keeps its charge is (Appendix II)

$$W = \frac{1}{2}\left(1 + \frac{\exp\left[-\frac{4}{3}\langle n \rangle\right](1 - \exp\left[(\langle n \rangle/3)\cdot(\sigma_0/F)\right])}{1 - \exp\left[-\langle n \rangle\,(\sigma_0/F)\right]}\right).$$

If we use $n = 1.24$ then $W = 0.46$.

In p-p and p-n interactions we get for the ratio of the number of forward neutrons and protons in the final state

$$\frac{n \text{ neutron}}{n \text{ proton}} \approx 1.19 .$$

Making use of the results of DANIEL *et al.* [9] and calculating only with particles of « class A »: $n_n/n_p = 1.38 \pm 0.34$. We may get a similar ratio for recoiled nucleons in interactions. According to the experiment of EISBERG *et al.* [12]

$$\frac{n_n}{n_p} = 1.39 \pm 0.28 .$$

Taking into account the conservation of meso-parity one may estimate the probability of the emission of an even and odd number of meson (Appendix III), *e.g.* in π-$\mathcal{N}$ interactions

$$W_{odd} = \frac{1}{2}\left(1 - \exp\left[\langle n\rangle\left(\frac{\sigma_0}{F} - 2\right)\right]\right), \qquad W_{even} = \frac{1}{2}\left(1 + \exp\left[\langle n\rangle\left(\frac{\sigma_0}{F} - 2\right)\right]\right),$$

in $\mathcal{N}$-$\mathcal{N}$ interactions

$$W_{odd} = \frac{1}{2}\left(1 - \exp\left[2\langle n\rangle\left(\frac{\sigma_0}{F} - 2\right)\right]\right), \qquad W_{even} = \frac{1}{2}\left(1 + \exp\left[2\langle n\rangle\left(\frac{\sigma_0}{F} - 2\right)\right]\right).$$

If $\langle n\rangle$ is equal to 1.24 we have

$$W_{even\ \pi\text{-}\mathcal{N}} \approx 0.565 ,$$

$$W_{odd\ \pi\text{-}\mathcal{N}} \approx 0.435 ,$$

$$W_{even\ \mathcal{N}\text{-}\mathcal{N}} \approx 0.509 ,$$

$$W_{odd\ \mathcal{N}\text{-}\mathcal{N}} \approx 0.491 .$$

Naturally, further experimental data and theoretical considerations are needed to verify or reject this model.

In this paper we have discussed only the role of protons in high-energy interactions. Unfortunately it is very difficult to make any consideration

---

[12] L. M. EISBERG, W. B. FOWLER, R. M. LEA, W. D. SHEPHARD, R. P. SHUTT, A. M. THORNDIKE and W. L. WHITTEMORE: *Phys. Rev.*, **97**, 797 (1955).

relating to pions knowing nothing about the nature of π-π interactions. However, it is very likely that statistical theories are not sufficient to explain the inelastic π-π interaction, as the angular distribution of pions is not only strongly anisotropic but even asymmetric (in charge) in the π-π C.M.S.

Further investigations for extending this model to the nucleon-nucleus and pion-nucleus case are in progress.

* * *

Finally, the author is indebted to Dr. E. Fenyves, Mr. G. Domokos, Mr. A. Frenkel and Mr. A. Sebestyén for valuable discussions.

Appendix I

Let σ_0 be the π-π cross-section and F the total geometrical cross-section of the π-field around a nucleon; let us suppose roughly that the emitted pions are in the same state in the cloud. The probability that a pion goes through a surface around a pion without interaction is $1 - \sigma_0/F$. If we have n pions as a target this probability will be $(1 - \sigma_0/F)^n$. The cross-section for a pion will be $\sigma_n = F(1 - (1 - \sigma_0/F)^n)$.

Thus we get for the π-$\mathcal{N}$ cross-section, using the Poisson distribution

$$\sigma_{\pi\text{-}\mathcal{N}} = \sum_n W_n F \left[- 1 \left(1 - \frac{\sigma_0}{F} \right)^n \right] = F \left(1 - \exp \left| - \langle n \rangle \frac{\sigma_0}{F} \right| \right).$$

If we start from the inversed picture, that is from a standing pion and moving nucleon, the cross-section will be naturally the same. In this way we get the nucleon-nucleon cross-section as

$$\sigma_{\mathcal{N}\text{-}\mathcal{N}} = \sum_l W_l F \left(1 - \exp \left| - \langle n \rangle \frac{\sigma_0}{F} l \right| \right) =$$

$$= F \left(1 - \exp \left| - \langle n \rangle \left(1 - \exp \left[- \langle n \rangle \frac{\sigma_0}{F} \right] \right) \right| \right) = F \left(1 - \exp \left[- \langle n \rangle \frac{\sigma_{\pi\text{-}\mathcal{N}}}{F} \right] \right),$$

which gives for $\langle n \rangle$ the formula

$$n = \frac{\log \dfrac{1}{1 - \sigma_{\mathcal{N}\text{-}\mathcal{N}}/F}}{\dfrac{\sigma_{\pi\text{-}\mathcal{N}}}{F}}.$$

The first consequence is

$$\langle n \rangle \geq \frac{\sigma_{\mathcal{N}\text{-}\mathcal{N}}}{\sigma_{\pi\text{-}\mathcal{N}}},$$

3748

using

$$F = (1.4 \text{ fermi})^2 \pi \approx 62 \text{ mb} ,$$

and

$$\frac{\sigma_{\mathcal{N}\text{-}\mathcal{N}}}{F} \approx \frac{\sigma_{\pi\text{-}\mathcal{N}}}{F} \approx 0.36 ,$$

we obtain

$$n\rangle = 1.24 .$$

An other consequence is

$$\sigma_{\pi\text{-}\pi} \approx \sigma_{\mathcal{N}\text{-}\mathcal{N}} (\approx \sigma_{\pi\text{-}\mathcal{N}}) .$$

Now it is very simple to give the distribution of n, taking into account the probability of interaction in case of the presence of n mesons.

We assume, that if one meson interacts with the primary particle, the number of created mesons will be so high, that all the cloud pions will get into interaction with them.

The probability of the presence of n mesons in case of inelastic interaction is

$$W'_n = C \exp [- \langle n \rangle] \frac{\langle n \rangle^n}{n!} \left(1 - \left[1 - \frac{\sigma_0}{F}\right]^n\right) ,$$

where C is a normalisation constant:

$$C = \frac{1}{1 - \exp [- \langle n \rangle (\sigma_0 / F)]} .$$

With this we may caculate $\langle n \rangle'$:

$$\langle n \rangle' = \sum_{n=0}^{\infty} n C \exp [- \langle n \rangle] \frac{\langle n \rangle^n}{n!} \left(1 - \left[1 - \frac{\sigma_0}{F}\right]^n\right) =$$

$$= \langle n \rangle \left(1 + \frac{\sigma_0}{F} \frac{1}{\exp [\langle n \rangle (\sigma_0 / F)] - 1}\right) .$$

Appendix II

The probability of the interaction of k mesons is

$$W'_k = C \exp [- \langle n \rangle] \frac{\langle n \rangle^k}{k!} \left(1 - \left[1 - \frac{\sigma_0}{F}\right]^k\right) .$$

Since the probability of the emission of a charged pion is equal to $\frac{2}{3}$, the probability that a nucleon keeps its charge after the emission of k pions is

$$\frac{1 + (-1)^k (\frac{1}{3})^k}{2},$$

and the probability that a proton remains proton after the inelastic interaction

$$\sum_{k=1}^{\infty} W'_k \frac{1 + (-1)^k (\frac{1}{3})^k}{2} = \frac{1}{2}\left(1 + \frac{\exp\left[-\frac{4}{3}\langle n\rangle\right](1 - \exp\left[(\langle n\rangle/3)(\sigma_0/F)\right])}{1 - \exp\left[-\langle n\rangle(\sigma_0/F)\right]}\right).$$

Appendix III

Because of the mesoparity conservation in π-$\mathcal{N}$ interactions the number of mesons in the final state will be even (Fig. 1), if the number of interacting pions of the cloud is odd.

This probability turns out to be

$$W_{\text{even}}^{\pi\text{-}\mathcal{N}} = \sum_{l=0}^{\infty} W'_{2l+1} = \frac{1}{2}\left(1 + \exp\left[-\langle n\rangle\left(2 - \frac{\sigma_0}{F}\right)\right]\right).$$

It follows that

$$W_{\text{odd}}^{\pi\text{-}\mathcal{N}} = \sum_{l=0}^{\infty} W'_{2l} = \frac{1}{2}\left(1 - \exp\left[-\langle n\rangle\left(2 - \frac{\sigma_0}{F}\right)\right]\right).$$

In the $\mathcal{N}$-$\mathcal{N}$ case, we have two sources, so the number of « connective » pions as well as the number of final state pions is even with a probability of

$$W_{\text{even}}^{\mathcal{N}\text{-}\mathcal{N}} = (W_{\text{odd}}^{\pi\text{-}\mathcal{N}})^2 + (W_{\text{even}}^{\pi\text{-}\mathcal{N}})^2 = \frac{1}{2}\left(1 + \exp\left[-2\langle n\rangle\left(2 - \frac{\sigma_0}{F}\right)\right]\right).$$

The probability of the production of an odd number of pions is

$$W_{\text{odd}}^{\mathcal{N}\text{-}\mathcal{N}} = 2 W_{\text{odd}}^{\pi\text{-}\mathcal{N}} W_{\text{even}}^{\pi\text{-}\mathcal{N}} = \frac{1}{2}\left(1 - \exp\left[-2\langle n\rangle\left(2 - \frac{\sigma_0}{F}\right)\right]\right).$$

Riassunto (*)

Presumiamo che la nuvola pionica abbia il ruolo più importante nelle interazioni π-$\mathcal{N}$ e $\mathcal{N}$-$\mathcal{N}$ alle altissime energie. Si verifica questa ipotesi confrontando alcune delle sue conseguenze con i dati sperimentali nella regione dei GeV.

(*) *Traduzione a cura della Redazione.*

IL NUOVO CIMENTO Vol. XXII, N. 1 1° Ottobre 1961

K-Meson Form Factor in the Bipion Approximation.

PH. SALIN

Faculté des Sciences - Bordeaux (*)

(ricevuto il 15 Giugno 1961)

Résumé. — Le facteur de forme du méson K est calculé en ne considérant que les deux états intermédiaires à deux mésons π et à deux mésons K, et en traitant chaque fois qu'on le rencontre l'état intermédiarie à deux π comme un état résonnant dans l'état $I=J=1$. Les différentes constantes de couplage du problème sont évaluées à partir de formules de Breit et Wigner. Un des résultats numériques obtenus est le rayon de charge moyen que l'on trouve égal à $0.22 \cdot 10^{-13}$ cm.

1. – Introduction.

A large field of work was open to theoretical physicists with the introduction of dispersion relations in modern physics. Two years ago Mandelstam's bidimensional representation was a new way of investigation in elementary particle scattering. Many groups have carried out successful studies: Berkeley, CERN, Bordeaux. etc... From a theoretical point of view this representation was proved in many cases and never failed. Experimentally the results seem to be fitted to a good approximation. Unfortunately those who have dealt with dispersion relations do know the difficulties they met in solving their equations, coupled singular integral equations depending on intermediate processes mostly unknown. Many attempts have been made in order to get solutions: Muskelisvhili-Omnès method [1], N/D Chew and Mandelstam proposal [2], Im T^{-1} method of Feldman, Matthews and Salam [3]. In any case

(*) Postal address: Service de Physique Théorique, 351 Cours de la Libération, Talence (Gironde).

(1) R. OMNÈS: *Nuovo Cimento*, **8**, 316 (1958).

(2) G. F. CHEW and S. MANDELSTAM: *Phys. Rev.*, **119**, 467 (1960).

(3) G. FELDMAN, P. T. MATTHEWS and A. SALAM: *Nuovo Cimento*, **16**, 549 (1960).

it is impossible to get exact solutions, but only approximative forms at low energy, still very complicated and depending on parameters whose necessity is not always obvious, which are interpreted in general as coupling constants Most authors are then satisfied with effective range formulas or try to get out some resonance.

One may think that it is no worth spending such efforts for so few results. Therefore many attempts are made at the present time to introduce in the usual dispersion technics some models, which keeping the general feature of the results would bring real simplifications in the calculations.

On another hand, the study of intermediate states is of principal interest in the dispersion relation formulation. States with one single particle are interpreted as poles in the scattering matrix, and states with two particles induced an energy continuum and then a cut. One is naturally tempted to consider a resonant intermediate state with two particles as a bound state, and to deal with it as if it were a single particle state with mass equal to the energy of resonance. In the calculations the cuts are then replaced by poles.

The last point we should like to notice in this introductory part is that it is a general fact that high mass states do not contribute as much as low mass state. See for example ([4]).

All these reasons explain why the bipion model wasf ully successful, as it is the lowest mass state in strong interactions and the simplest one. It was introduced by M. Gourdin, D. Lurié and A. Martin ([5,6]) exactly to exhibit the two-pion contribution in the Mandelstam representation. Explicit calculations have been given by M. Gourdin, Y. Noirot and Ph. Salin ([7]) in the pion-kaon scattering. This model has been applied to many interesting problems: nucleon-nucleon scattering ([8]), pion-nucleon scattering and nucleon form factor ([9]). Recently Stanghellini ([10]) has shown that the bipion model could be very simply derived from symmetry considerations in particle scattering.

So one must not exclude that these investigations, which were *a priori* considered only as useful means to simplify equations, leaving their general behaviour unchanged, become a deeper translation of what occurs in elementary particle interactions, while clearing up the theory.

Of course, what has been done for the two pion state could be extended

([4]) M. Baker and F. Zachariasen: *Phys. Rev.*, **119**, 438 (1960).
([5]) M. Gourdin: Seminar given in the Corsica Summer School (1960).
([6]) M. Gourdin, D. Lurié and A. Martin: *Nuovo Cimento*, **18**, 933 (1960).
([7]) M. Gourdin, Y. Noirot and Ph. Salin: *Nuovo Cimento*, **18**, 651 (1960).
([8]) D. Amati, E. Leader and B. Vitale: *Nuovo Cimento*, **18**, 409 (1960).
([9]) J. Bowcock, W. N. Cottingham and D. Lurié: *Nuovo Cimento*, **16**, 918 (1960).
([10]) A. Stanghellini: *Nuovo Cimento*, **18**, 1258 (1960).

to more complicated states as the three-pion state « tripion » ([6]), meson $K' = K + \pi$ ([11,12]), etc.

In this paper we have applied the bipion model to the study of the kaon form factor. Dealing as in ref. ([6]) we could write at once

$$F_K(q^2) = e\left(1 + \frac{\alpha q^2}{q_r^2 + q^2}\right) = e[1 + \beta q^2 F_\pi(q^2)] , \tag{1}$$

where F_K is the kaon form factor and F_π the pion one.

But we have tried to go forward, taking in account the two-kaon intermediate state, the kaon mass being not so large compared to the pion mass. We have supposed that the $K\bar{K}$ phase shift was dominated by the bipion scattering, and in these approximations we have obtained an exact solution whose principal behaviours are the following:

1) $F_K(q^2)$ goes to zero at infinity, following Drell and Zachariasen theorem ([13]);

2) $F_K(q^2)$ reduces to formula (1) in first approximation;

3) $F_K(0) = e$;

4) $F_K(t)$ is non singular at the threshold $t = 4\varkappa^2$, $\varkappa$ being the K-meson mass.

2. – Matrix element.

We are interested with the following graph:

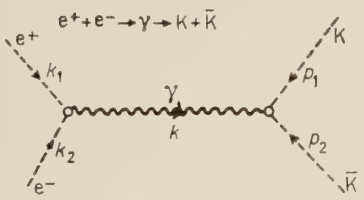

Fig. 1.

We call k_1 and k_2 the momentum of e^+ and e^-, k the momentum of the virtual photon, p_1 and p_2 the momentum of the two K-mesons, and we take all these energy-momentum four-vectors ingoing.

([11]) J. Bernstein and S. Weinberg: *Phys. Rev. Let.*, **5**, 481 (1960).
([12]) M. Gourdin: Bordeaux PTB-6 and PTB-7, to be published.
([13]) S. D. Drell and F. Zachariasen: *Phys. Rev.*, **119**, 463 (1960).

t will be the energy in the center-of-mass system

$$t = -(p_1 + p_2)^2 = -k^2 .$$

We define as usual the S matrix element by

$$S_{fi} = (2\pi)^4 \delta_4(p_1 + p_2 + k_1 + k_2) \frac{1}{(2\pi)^6} \frac{e^2}{2\sqrt{p_1^0 p_2^0 k_1^0 k_2^0}} T_{fi} . \tag{2}$$

and we chose the two couplings electrons-photon and photon-K-mesons to be

$$H_{e^+e^-\gamma} = e\bar{\psi}_{e^+}\gamma_\mu \psi_{e^-} A_\mu . \tag{3}$$

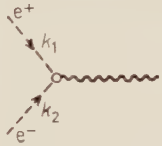

Fig. 2.

$$H_{\gamma K\bar{K}} = eA_\mu(\Phi_K \partial_\mu \Phi^*_{\bar{K}} - \partial_\mu \Phi_K \Phi^*_{\bar{K}}) . \tag{4}$$

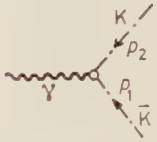

Fig. 3.

In the first Born approximation it is not difficult to evaluate the graph of Fig. 1; we readily write

$$T_{fi} = \bar{v}_{e^+}(-k_1)\gamma_\mu v_{e^-}(k_2) \frac{\delta_{\mu\nu}}{k^2}(p_2 - p_1)_\nu = \frac{1}{k^2} \bar{v}_{e^+}(-k_1)(p_2 - p_1) v_{e^-}(k_2) , \tag{5}$$

where v_{e^+} and v_{e^-} are the electron field spinors. Then our form factor $M(t)$ is given by

$$T_{fi} = \frac{1}{k^2} \bar{v}_{e^+}(-k_1)(p_2 - p_1) v_{e^-}(k_2) M(t) , \tag{6}$$

with the requirement

$$M(0) = 1 . \tag{7}$$

3. – Dispersion relation.

The isospin of the K-meson is $\frac{1}{2}$. We are exactly in the same situation as for the nucleon form factor [14]. The total isospin is then either 1, isovector

[14] C. F. Chew, R. Karplus, S. Gasiorowicz and F. Zachariasen: *Phys. Rev.*, **110**, 265 (1958).

case, or 0, isoscalar case, and we suppose a dispersion relation on our form factor $M_{V,S}(t)$

$$M_{V,S}(t) = \frac{1}{\pi}\int_{(2\mu)^2}^{+\infty} \frac{g_{V,S}(t')\,\mathrm{d}t'}{t' - t - i\varepsilon}, \tag{8}$$

where the subscript V or S refers to isovector or isoscalar and $g_{V,S}(t)$ are spectral functions which will be determined later.

We obviously have

$$\begin{cases} \langle K^+K^- | T | \gamma \rangle \propto M_V(t) + M_S(t)\,, \\ \langle K^0 \bar{K}^0 | T | \gamma \rangle \propto M_V(t) - M_S(t)\,, \end{cases} \tag{9}$$

with the normalization of $M_{V,S}(t)$ for $t = 0$

$$M_{V,S}(0) = \frac{1}{2} = \frac{1}{\pi}\int_{(2\mu)^2}^{\infty} \frac{g_{V,S}(t')\,\mathrm{d}t'}{t'}\,.$$

As in the nucleon case the total angular momentum of the reaction $\gamma \to K + \bar{K}$ is one. We are in a P-wave state. So the state must be odd either on space inversion or in charge conjugation.

We now focus our attention on the spectral functions $g_{V,S}(t)$. They are related to a sum over all possible intermediate states. Because of G-invariance only intermediate states with an odd (resp. even) number of pions will contribute in the g_S (resp. g_V) function.

We write

$$\begin{cases} g_V = g(2\pi) + g(4\pi) + \ldots + g_V(K\bar{K}) + \ldots + g_V(N\bar{N}) + \ldots\,, \\ g_S = g(3\pi) + g(5\pi) + \ldots + g_S(K\bar{K}) + \ldots + g_S(N\bar{N}) + \ldots\,. \end{cases} \tag{10}$$

In this work we shall only keep the two functions $g(2\pi)$ and $g_V(K\bar{K})$ by summing the three diagrams below:

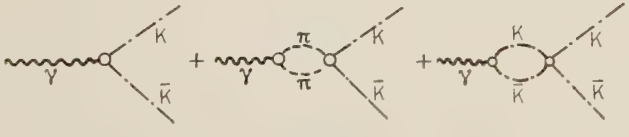

Fig. 4.

4. – Evaluation of the three graphs.

a) The first graph is the first Born approximation and as it is easy to see from eq. (2) to (7) we could take it into account in our representation with a subtracted dispersion relation in $t=0$. We write

$$M_{V,S}(t) = \frac{1}{2} + \frac{t}{\pi}\int_{(2\mu)^2}^{+\infty} \frac{g_{V,S}(t')\,dt}{t'(t'-t-i\varepsilon)}. \tag{11}$$

The two other graphs induce cuts in the t complex plane. One cut from $(2\mu)^2$ to $+\infty$ and another one from $(2\varkappa)^2$ to $+\infty$. We call μ the π-meson mass and $\varkappa$ the K-meson mass.

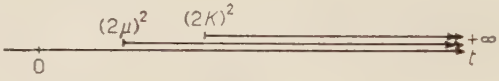

Fig. 5.

b) We consider the two pion intermediate state of graph (2) Fig. 4 as a bipion, that is to say we replace the cut running from $(2\mu)^2$ to $+\infty$ by a pole in $M_V(t)$.

This term is written

$$\frac{\lambda}{t_r - t}, \tag{12}$$

where λ is a real constant proportional to the $\gamma\pi\pi$ and $\pi\pi K\bar{K}$ coupling constants (the symbol $\pi\pi$ designates the bipion state); t_r is the energy of resonance of the two pions in the $I=1$, $J=1$ state.

Many theoretical [9,15] and experimental works give evidence for $t_r \simeq 22.4\mu^2$. We shall adopt this value in our calculations.

As we shall be interested by negative values of t, *i.e.* for values of t far from t_r, we may consider that our approximation of taking a pole for describing a resonance is in fact fairly good.

By summing these two contributions we already find formula (1):

$$M_V = \frac{1}{2} + \frac{\lambda t}{(t_r - t)t_r}, \qquad M_S = \frac{1}{2}.$$

[15] J. Bowcock, W. N. Cottingham and D. Lurié: *Phys. Rev. Lett.*, **5**, 388 (1960). See also ref. [14] of this paper.

But in this approach we precisely intend to go forward and to evaluate the intermediate state with two K-mesons.

c) The third graph depends on the $K\bar{K}$ elastic scattering. Because till now we know nothing on this, we shall suppose that it occurs mainly through the two-pion state.

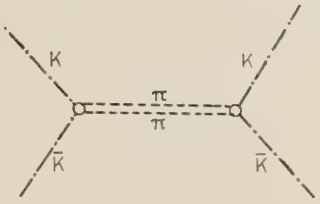

Fig. 6.

Bowcock, Cottingham and Lurié [9] have supposed a resonating form for the $\pi\pi$ scattering amplitude in the $I=1$, $J=1$ state,

$$\exp[i\delta]\sin\delta = \frac{\gamma q^3}{t - t_r - i\gamma q^3}, \tag{13}$$

which satisfies the requirements of unitarity and correct lowen-ergy behaviour, and has a pole in $t=t_r$.

In our approximation we assume that the $K\bar{K}$ scattering is dominated by this $\pi\pi$ resonance, and so that there exists a pole in the $K\bar{K}$ matrix element for $t=t_r$. If we adopt the bipion model we then obtain for the $K\bar{K}$ scattering a Breit and Wigner form:

$$T_{K\bar{K}} = \exp[i\bar{\delta}]\sin\bar{\delta} = \frac{g^2 k^3}{t - t_r - i g^2 k^3}, \tag{14}$$

where g is a coupling constant proportional to the $\pi K\bar{K}$ coupling constant and k is the K-meson momentum

$$k = \tfrac{1}{2}\sqrt{t - 4\varkappa^2}\,.$$

5. – Evaluation of the coupling constants.

The bipion is an isovector of spin 1. So it will be represented by the vectorial field B_μ^x satisfying the Klein-Gordon equation:

$$(\Box - B^2)\,B_\mu^x = 0\,,$$

with the complementary condition $\partial_\mu B_\mu^x = 0$.

Then, its propagator is given by [5]

$$\frac{\delta_{\mu\nu} + P_\mu P_\nu / B^2}{P^2 + B^2} .$$

It is not difficult to evaluate the different possible graphs:

1) *Annihilation* $\mathrm{K} + \overline{\mathrm{K}} \to \mathrm{B}$.

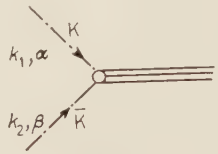

Fig. 7.

$$H_{\mathrm{K}\overline{\mathrm{K}}\mathrm{B}} = G \Phi_{\mathrm{K}}^{\wedge} \overleftrightarrow{\partial}_\mu \tau^\nu \Phi_{\mathrm{K}}^{*\beta} B_\mu^\nu , \tag{15}$$

and in the momentum space we write the vertex:

$$T_{\mathrm{K}\overline{\mathrm{K}}\mathrm{B}} = G(k_2 - k_1)_\mu \tau^\nu .$$

For the $\mathrm{K}\overline{\mathrm{K}}$ elastic scattering we get

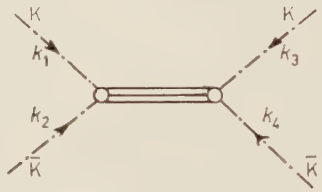

Fig. 8.

$$T_{\mathrm{K}\overline{\mathrm{K}} \to \mathrm{K}\overline{\mathrm{K}}} = G^2 (k_2 - k_1)_\mu \tau^\nu \frac{\delta_{\mu\nu} + P_\mu P_\nu / B^2}{t_r - t} (k_3 - k_4)_\nu \tau^\nu = - G^2 \frac{4k^2 \cos\theta}{t_r - t} , \tag{16}$$

$k = |\boldsymbol{k}|$ is the K-meson momentum.

We now want to connect the constant g of eq. (14) with G, the coupling constant K-meson-bipion and Γ the width of the two-pion resonance.

As in reference [7] the P-wave scattering amplitude for $\mathrm{K}\overline{\mathrm{K}}$ is given by

$$T = \frac{8\pi W}{k} 3 \cos\theta \exp[i\bar{\delta}] \sin\bar{\delta} .$$

From eq. (14) and eq. (16) we get

$$-\frac{4G^2k^2}{t_r-t}=\frac{24\pi W}{k}\frac{g^2\varkappa^3}{t-t_r},$$

$$G^2=6\pi W_r g^2 . \tag{17}$$

The width of the resonance Γ is related to the phase shift $\bar{\delta}$ by the formula:

$$\exp[i\bar{\delta}]\sin\bar{\delta}=\frac{\Gamma}{W-W_r-i\Gamma},$$

so that

$$\Gamma=\frac{g^2k_r^3}{2W_r},$$

and

$$g^2=\frac{2W_r}{k_r^3}\Gamma=\frac{G^2}{6\pi W_r} . \tag{18}$$

If we call λ_1 the bipion-$\pi\pi$ coupling constant we see from formulas (13) and (18) that

$$\lambda_1^2=6\pi W_r\gamma ,$$

$\gamma=0.376\mu^{-1}$ is the value given by reference (9), so

$$\lambda_1=5.8 , \tag{19}$$

then

$$\frac{G^2}{\lambda_1^2}=\frac{g^2}{\gamma}=\frac{q_r^3}{k_r^3},$$

$$G=\pm 3.9 , \qquad g^2=0.17\mu^{-1} . \tag{20}$$

2) K-*meson form factor.*

Photon-bipion interaction. This term has been studied by M. Gourdin (5)

$$T_{\gamma B}=\frac{t_r}{\lambda_1}e\mu , \tag{21}$$

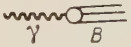

Fig. 9.

where λ_1 is the bipion-$\pi\pi$ coupling constant.

Photon-bipion-$K\bar{K}$

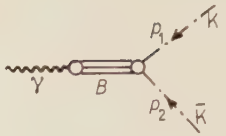

Fig. 10.

$$T_{\gamma K\bar{K}} = \frac{t_r}{\lambda_1} e_\mu \frac{\delta_{\mu\nu} + P_\mu P_\nu / B^2}{t_r - t} G(p_1 - p_2)_\nu \tau^\gamma = \frac{G t_r}{\lambda_1} \frac{e_\mu (p_1 - p_2)_\mu}{t_r - t} \tau^\gamma . \tag{22}$$

So we get the value of λ in eq. (12)

$$\lambda = \frac{G t_r}{\lambda_1} = \pm 15 \mu^2 . \tag{23}$$

6. – Integral equation.

We now come back to the dispersion relation problem. First we took a subtracted relation in $t = 0$ with $M_r(0) = \frac{1}{2}$. Then we replaced the first cut from $(2\mu)^2$ to $+\infty$ by a pole in $t = t_r$.

At last, neglecting all other states, the discontinuity of function $M_r(t)$ on the second cut $[(2\varkappa)^2, +\infty]$ is given by the unitarity relation:

$$\operatorname{Im} M_r(t) = g_r(t) = T_{K\bar{K}} M_r^*(t) . \tag{24}$$

We then obtain the following integral equation:

$$M_r(t) = \frac{1}{2} + \frac{\lambda t}{(t_r - t) t_r} + \frac{t}{\pi} \int_{(2\varkappa)^2}^{+\infty} \frac{g_r(t')\, \mathrm{d}t'}{t'(t' - t - i\varepsilon)} , \tag{25}$$

which is of the Omnès form:

$$\varphi(z) = f(z) + \frac{1}{\pi} \int_{4\varkappa^2}^{\infty} \frac{\varphi(x' + i\varepsilon)\, T_{K\bar{K}}^*(x')\, \mathrm{d}x'}{x' - z} , \tag{26}$$

with

$$\varphi(z) = \frac{M_r(z)}{z} ,$$

$$f(z) = \frac{1}{2z} + \frac{\lambda}{(t_r - z) t_r} ,$$

$$T_{K\bar{K}} = \exp[i\bar{\delta}] \sin \bar{\delta} .$$

It is easy to find an Omnès solution $q(z)$ of this equation having the analytic properties:

a) a pole in $z = 0$ of residue $\frac{1}{2}$;

b) a pole in $z = t_r$ of residue $-\lambda/t_r$;

c) a cut from $4\varkappa^2$ to $+\infty$ on the real axis.

Operating as in references ([16]) and ([17]) a solution arising from these analytical properties is

$$M_r(t) = \frac{1}{2} \exp\left[i\bar{\delta}(t)\theta(t-4\varkappa^2) + \tau^1(t)\right] \left\{1 + \frac{2\lambda t}{(t-t_r)t_r} \exp\left[-\tau^1(t_r)\right]\right\}, \tag{27}$$

where

$$\tau^1(t) = \frac{P}{\pi} t \int_{4\varkappa^2}^{+\infty} \frac{\bar{\delta}(x)}{x(x-t)} \, \mathrm{d}x \,, \tag{28}$$

and $\theta(t-4\varkappa^2)$ is the step function.

The last point of our calculation is $\tau^1(t)$, with the phase shift given by

$$\exp\left[i\bar{\delta}(t)\right] \sin \bar{\delta}(t) = h(t) = \frac{g^2 k^3}{t - t_r - i g^2 k^3} \,,$$

$$\operatorname{tg} \bar{\delta}(t) = \frac{g^2 k^3}{t - t_r} \,,$$

so that

$$\tau^1(t) = \frac{P}{\pi} t \int_{4\varkappa^2}^{\infty} \frac{1}{x(x-t)} \operatorname{arc\,tg} \frac{g^2 k'^3}{x - t_r} \mathrm{d}x = \frac{P}{\pi} t \int_{4\varkappa^2}^{\infty} \frac{\operatorname{arctg} a(x)}{x(x-t)} \mathrm{d}x \,; \tag{29}$$

$a(x)$ goes to zero as $x \to 4\varkappa^2$ and to infinity as x goes to infinity. So $\operatorname{arctg} a(x)$ goes from zero to $\pi/2$ when x varies from $4\varkappa^2$ to $+\infty$.

To expedite this last integral it is easy to show by simple computation thet $\operatorname{arctg} a(x)$ may be approximated by the function

$$\frac{\pi}{2} \left(\frac{x - 4\varkappa^2}{x - \alpha} \right)^{\frac{3}{2}},$$

([16]) J. G. Rushbrooke and D. Radojicie: *Phys. Rev. Lett.*, **5**, 567 (1960).

([17]) N. Cabibbo and R. Gatto: *Nuovo Cimento*, **10**, 1086 (1958).

for $4\varkappa^2 \leqslant x \leqslant +\infty$ which has the same behaviour in $x = 4\varkappa^2$ and at infinity. $\varkappa$ is a parameter which may be fitted to a very good approximation ($\varkappa < 4\varkappa^2$).

We give the value of α for some values of $g^2/2\sqrt{2}$

$\frac{g^2}{2\sqrt{2}}$	0.01	0.05	0.1	0.2	0.5	0.8	1	1.5	2	4	10
α	-418	-70	-17	14	39	43.7	45	46.8	47.9	48.9	49.6 .

There is no difficulty is evaluating the integral

$$\tau^1(t) = P\frac{t}{2}\int_{4\varkappa^2}^{+\infty}\left(\frac{x-4\varkappa^2}{x-\alpha}\right)^{\frac{3}{2}}\frac{\mathrm{d}x}{x(x-t)},$$

$$\tau^1(t) = a_1\frac{t}{t-\alpha} + a_2 + \left(\frac{t-4\varkappa^2}{t-\alpha}\right)^{\frac{3}{2}}\log\frac{\sqrt{4\varkappa^2-\alpha}}{\sqrt{|t-\alpha|}+\sqrt{|t-4\varkappa^2|}},$$

$$a_1 = -\frac{4\varkappa^2-\alpha}{\alpha}, \qquad a_2 = -\left(\frac{4\varkappa^2}{\alpha}\right)^{\frac{3}{2}}\log\frac{4\varkappa^2-\alpha}{\sqrt{\alpha}+2\varkappa},$$

$\tau^1(t)$ has the good following behaviour $\begin{cases} \tau^1(0) = 0, \\ \tau^1(4\varkappa^2) = cte, \\ \lim\limits_{t\to\infty}\tau^1(t) = -\infty, \end{cases}$

Finally we put

$$\exp|\tau^1(t)| = \left(\frac{\sqrt{\alpha}+2\varkappa}{\sqrt{t-4\varkappa^2}+\sqrt{t-\alpha}}\right)^2,$$

and we get the final solution for $t \geqslant 4\varkappa^2$

$$M_r(t) = \frac{1}{2}\left[\frac{t-t_r-ig^2k^3}{\sqrt{(t-t_r)^2+g^4k^6}}\right]\left[\frac{\sqrt{\alpha}+2\varkappa}{\sqrt{|t-4\varkappa^2|}+\sqrt{|t-\alpha|}}\right]\cdot$$

$$\cdot\left[1+\frac{2\lambda t}{(t-t_r)t_r}\,\frac{\sqrt{|t_r-4\varkappa^2|}+\sqrt{|t_r-\alpha|}}{\sqrt{\alpha}+2\varkappa}\right],$$

$$q = \tfrac{1}{2}\sqrt{t-4\varkappa^2}, \qquad 4\varkappa^2 = 50, \qquad t_r = 25.$$

7. – Numerical results.

We define the mean square radius by the usual formula:

$$\langle r^2 \rangle = -6 \left[\frac{\mathrm{d}}{\mathrm{d}t} \log M(t) \right]_{t=0},$$

$$\langle r^2 \rangle = 3 \left[\frac{1}{4\varkappa\sqrt{\bar{\alpha}}} - \frac{2\lambda}{t_r^2} \frac{\sqrt{|t_r - 4\varkappa^2|} + \sqrt{|t_r - \alpha|}}{\sqrt{\bar{\alpha}} + 2\varkappa} \right],$$

with the value of the parameters given above we find for $\lambda < 0$

$$\langle r^2 \rangle = 0.22 \cdot 10^{-13} \text{ cm} .$$

If now we neglect the two-K-meson intermediate state we get for the r.m.s. radius a very closed value

$$\langle r^2 \rangle = 0.20 \cdot 10^{-13} \text{ cm} .$$

Then we have computed the form factor for some value of t on the following graph:

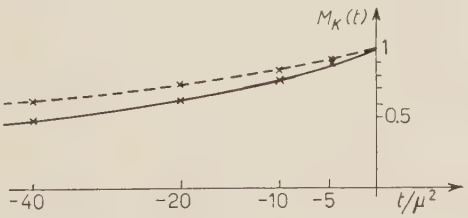

Fig. 11. – Form facter $M(t)$ *vs.* t the energy. The dashed line is the K-meson form factor without two-K-meson intermediate state.

Conclusion.

It is quite difficult to give effective conclusions from our calculations, essentially because our parameters have a very rude determination. Some improvements in their knowledge by other means would be of great interest and we may hope it will be soon.

Nevertheless our results are of the order of value one could rightly hope. For the mean square radius our value is not far from those obtained by

K. TANAKA ([18]) from mass difference of neutral and charged meson $\langle r^2 \rangle = 0.48 \cdot 10^{-13}$ cm and by D. J. HALL ([19]) $\langle r^2 \rangle = (0.5 \div 0.2) 10^{-13}$ cm.

An interesting point one should notice is that the two-K-meson intermediate state gives a very small contribution to the form factor. Its effect is to increase the magnitude of $\langle r^2 \rangle$ and to decrease the form factor. But the behaviour at infinity is different. In the two-pion approximation, $M(t)$ goes to a constant at infinity, while the solution of our integral goes to zero as $t^{-\frac{1}{2}}$.

Another point is that $\langle K^0 \bar{K}^0 | T | \gamma \rangle$ is not equal to zero as could be predicted by perturbation theory. This interaction of neutral K-meson with electromagnetic field has already been noticed by G. FEINBERG ([20]). In our calculations this last contribution is rather small because we took $M_s(t) = \frac{1}{2}$. But we could take into account other intermediate states as for instance the three pions which could contribute in $M_s(t)$.

At last, it would be interesting to evaluate the contribution of K-meson form factor in such a problem as electromagnetic structure of nucleon.

FEDERBUSH, GOLDBERGER and TREIMAN ([21]) have shown that the K-meson pair intermediate state was of no importance in nucleon form factor. This fact is not in desagreement with our results if the K-nucleon coupling constant is very small.

* * *

I acknowledge very sincerily Professor R. GATTO who suggested me this study and followed his development, and Doctor N. CABIBBO who provided me the Omnès solution of eq. (25). I am very grateful to Professor M. GOURDIN who read the manuscript and proposed me many improvements.

([18]) K. TANAKA: *Phys. Rev.*, **117**, 1402 (1960).
([19]) D. J. HALL: *Phys. Rev. Lett.*, **6**, 31 (1961).
([20]) G. FEINBERG: *Phys. Rev.*, **109**, 1381 (1958).
([21]) P. FEDERBUSH, M. L. GOLDBERGER and S. B. TREIMAN: *Phys. Rev.*, **112**, 642 (1959).

Note added in proof.

The last experimental data on the bipion resonance give $t\bar{l} = 30\mu^2$ and half width $\Gamma = 100$ MeV.

With these values we get

for the bipion-$\pi\pi$	coupling constant	$\lambda_1 = \pm\ 4.94$,
for the bipion-KK	coupling constant	$G = \pm\ 4.31$,
for the photon-KK	coupling constant	$\lambda = \pm\ 26.17$.

The r.m.s. radius is slightly larger, $\langle r^2 \rangle = 0.27 \cdot 10^{-13}$ cm with the two-kaon intermediate state and $\langle r^2 \rangle = 0.25 \cdot 10^{-13}$ cm without this contribution.

RIASSUNTO (*)

Calcolo il fattore di forma del mesone K non tenendo conto che dei due stati intermedi a due mesoni π ed a due mesoni K, e trattando lo stato intermedio a due π, ogni volta che lo si incontra, come uno stato risonante con $I = J = 1$. Valuto le diverse costanti di accoppiamento del problema a partire dalle formule di Breit e Wigner. Uno dei risultati numerici ottenuti è il raggio di carica medio, che trovo uguale a $0.22 \cdot 10^{-13}$ cm.

(*) *Traduzione a cura della Redazione.*

IL NUOVO CIMENTO Vol. XXII, N. 1 16 Ottobre 1961

Transfer of Negative Muons to Gases Dissolved in a Hydrogen Bubble Chamber (*) (**).

M. Schiff (***)

The Enrico Fermi Institute for Nuclear Studies
The Department of Physics, The University of Chicago - Chicago, Ill.

(ricevuto il 19 Giugno 1961)

Summary. — The transfer reactions $(\mu^- H)+X \to (\mu^- X)+H$, where H = p or d and X = Ne or He, were studied by observing variations in the fractions of μ^- undergoing nuclear capture or catalyzing the fusion process $p+d \to {}^3He$. In deuterium-free hydrogen with a neon contamination of $(105^{+50}_{-25})\cdot 10^{-6}$, half of the muons are transferred to neon. Transfer to neon is 3 times more frequent if the hydrogen contains enough deuterium to saturate the reaction $(\mu^- p)+d \to (\mu^- d)+p$. Transfer to helium is at least two orders of magnitude slower than to neon. Stars induced by μ^- and π^- were analysed. No transfer of π^- was detected. The effect of the transfer reactions on the measurement of μ^- capture by hydrogen is discussed. It is shown that the transfer reactions can be used for experiments on μ^- capture by separated neon isotopes and possibly by ^3He.

Introduction.

When negative mesons come to rest in matter, various atomic and molecular processes precede the ultimate decay or nuclear interaction. An understanding of these intermediate reactions is important for the interpretation of experiments on the interaction of mesons with nuclei. Atomic and molecular

(*) This work was supported in part by the U.S. Atomic Energy Commission and in part by a joint program of the Office of Naval Research and the U.S. Atomic Energy Commission.

(**) A thesis submitted to the Department of Physics, the University of Chicago, in partial fulfilment of the requirements for the Ph. D. degree.

(***) Present address: 7 bis Rue Alexandre Parodi, Paris 10.

effects are most important for muons because of their long lifetime and weak nuclear interaction. In particular, the transfer of μ^- from hydrogen to foreign elements has a bearing on some μ^- capture experiments.

This paper describes an experimental study of the transfer of μ^- from a hydrogen mesic atom to a foreign element X of atomic number >1:

$$(\mu^-\mathrm{p})+\mathrm{X} \rightarrow (\mu^-\mathrm{X})+\mathrm{p}\,,$$

$$(\mu^-\mathrm{d})+\mathrm{X} \rightarrow (\mu^-\mathrm{X})+\mathrm{d}\,.$$

Our incentive for studying these reactions was twofold:

1) The partial transfer of μ^- to impurities may raise the frequency of μ^- nuclear capture in liquid hydrogen by a significant amount. Unless it is accounted for, this possibility makes the interpretation of the measured frequency meaningless or at least ambiguous.

2) By deliberately adding noble gases to a hydrogen bubble chamber, it might be possible to make use of the transfer reactions to perform some interesting experiments. In particular, a measurement of the rate of nuclear capture of μ^- by ^{3}He and a study of the capture by separated neon isotopes might be possible.

Except for one observation by SARGENT ([1]), previous experimental ([2-4]) and theoretical ([5-9]) work gives information only on the transfer to deuterium.

([1]) C. P. SARGENT: *A diffusion cloud chamber study of very slow mesons*, thesis (Columbia University, unpublished), p. 10-14.

([2]) L. W. ALVAREZ, H. BRADNER, F. S. CRAWFORD, Jr., J. A. CRAWFORD, P. FALK-VAIRANT, M. L. GOOD, J. D. GOW, A. H. ROSENFELD, F. SOLMITZ, M. L. STEVENSON, H. K. TICHO and R. D. TRIPP: *Phys. Rev.*, **105**, 1127 (1957); M. CRESTI, K. GOTTSTEIN, A. H. ROSENFELD and H. K. TICHO: *Atomic Energy Commission Report U.C.R.L.* 3782, p. 8 (1957) (unpublished).

([3]) A. ASHMORE, R. NORDHAGEN, K. STRAUCH and B. M. TOWNES: *Proc. Phys. Soc. (London)*, **71**, 161 (1958).

([4]) J. G. FETKOVICH, T. H. FIELDS, G. B. YODH and M. DERRICK: *Phys. Rev. Lett.*, **4**, 570 (1960).

([5]) F. C. FRANK: *Nature*, **160**, 525 (1947).

([6]) J. D. JACKSON: *Phys. Rev.*, **106**, 330 (1957).

([7]) T. H. R. SKYRME: *Phil. Mag.*, **2**, 910 (1957).

([8]) S. COHEN, D. JUDD and R. J. RIDDELL, Jr.: *Atomic Energy Commission Report U.C.R.L.*, 8391 (1959).

([9]) Y. B. ZELDOVICH and S. S. GERSHTEIN: *Žurn. Èxp. Teor. Fiz. (U.S.S.R.)*, **35**, 649 (1958), [translation: *Soviet Physics J.E.T.P.*, **8**, 453 (1959)]; and *Usp. Fiz. Nauk.*, **71**, 581 (1960), [translation: *Soviet Physics-Uspekhi*, **3**, 593 (1961)].

The work of ALVAREZ *et al.* [2] showed that the reaction

$$(\mu^- p) + d \rightarrow (\mu^- d) + p + 135 \text{ eV},$$

is very fast. For very small deuterium concentrations, the ratio — fraction of μ^- transferred to deuterons/number of deuterons per proton — is $> 10^3$. In the present experiment, we studied the transfer of μ^- from hydrogen to neon and helium. We also studied the stars produced by the capture of μ^- by Ne and the stars following the capture of π^- by ^{4}He and Ne. In the following sections, we discuss 1) the principle of the experiment, 2) the experimental procedure, 3) the analysis of μ^- events, 4) pion stars, 5) results and 6) conclusions.

1. – Principle of the experiment.

In this Section we describe the atomic and molecular processes which occur when μ^- come to rest in hydrogen contaminated with deuterium and with elements of $Z > 1$. We consider the reactions leading to observable events. These reactions are shown in Fig. 1.

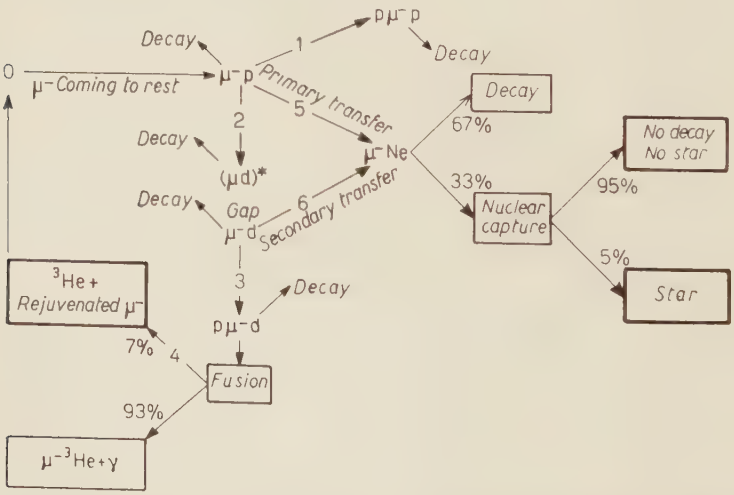

Fig. 1. – Reactions of μ that come to rest in hydrogen contaminated with deuterium and neon. The reactions are identified by numbers corresponding to those in Fig. 2, in Sections 1 and 5, and in the Appendix. The branching ratios were obtained from references [3,12].

1·1. *Pure hydrogen.* – The formation of a mesic atom (μ^-p) occurs in a time ($\sim 10^{-9}$ s) ([10]) which is short compared to the mean life of a muon. The ultimate decay or nuclear capture may be preceded by the formation of a mesic molecule:

$$(\mu^-p)+p \rightarrow (p\mu^-p)\,. \tag{1}$$

This reaction gives no observable effect.

1·2. *Transfer to deuterium.* – If deuterium is added, a new reaction may occur ([2-9]):

$$(\mu^-p)+d \rightarrow (\mu^-d)^*+p+135\ \text{eV}\,. \tag{2}$$

We use an asterisk to emphasize that the (μ^-d) atom is initially far above thermal velocity. The long mean free path of the fast neutral $(\mu^-d)^*$ system can lead to a visible gap between the end of the muon track where the $(\mu^-d)^*$ was formed and the point where a new process occurs. The next observable process is usually the decay of the muon. Sometimes it is preceded by the following sequence of reactions:

$$(\mu^-d)+p \rightarrow (p\mu^-d)\,, \tag{3}$$

$$(p\mu^-d) \rightarrow {}^3\text{He}+\mu^-+5.4\ \text{MeV}\,. \tag{4}$$

For low deuterium concentrations we may neglect the formation of $(d\mu^-d)$ ([4]). In reaction (4) the muon receives most of the energy release of the nuclear fusion it has catalyzed. This « rejuvenated » muon has a range of 17 mm in liquid hydrogen.

The occurence of a rejuvenated muon indicates two things: the μ^- has been transferred to deuterium *and* it has undergone no further transfer. The presence of a gap indicates a transfer to deuterium but does not exclude further transfer. Since they are difficult to measure, we have used gaps only to differentiate between secondary and primary transfers to Ne (reactions 6 and 5 of Fig. 1 and of Section 1·3).

1·3. *Transfer to neon.* – If neon is added to deuterated hydrogen, the following reactions may occur:

$$(\mu^-p)+\text{Ne} \rightarrow (\mu^-\text{Ne})+p\,, \tag{5}$$

$$(\mu^-d)+\text{Ne} \rightarrow (\mu^-\text{Ne})+d\,. \tag{6}$$

([10]) A. S. WIGHTMAN: *Phys. Rev.*, **77**, 521 (1950).

At low deuterium concentrations, most of the (μ^-d) atoms come from the reaction $(\mu^- p) + d \rightarrow (\mu^- d)^* + p$; in that case we call (6) a secondary transfer to neon.

The expected frequencies of μ^- nuclear capture in hydrogen and in neon are respectively $\sim 1/1000$ ([11]) and $\frac{1}{3}$ ([12]). Therefore, the absence of a decay electron indicates a transfer to neon. A further indication of transfer is sometimes obtained since the excited neon nucleus may emit one or more heavily ionizing particles (a star).

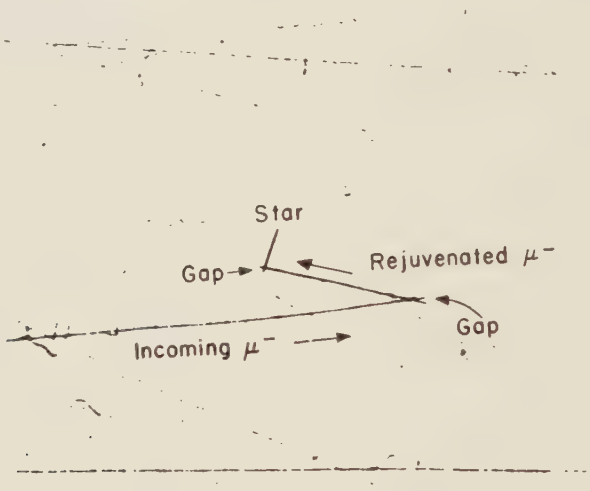

Fig. 2. – Photograph showing an unusual event. A μ^- comes to rest in hydrogen (reaction 0), is transferred to a deuteron (2), a pd mesic molecule is formed (3), and undergoes a nuclear fusion whose energy « rejuvenates » the μ^- (4); the muon comes to rest a second time (0), is transferred to a deuteron (2) and from there to a neon atom (6). The nuclear capture of μ^- by Ne is followed by the emission of a charged particle (star). The numbering of the reactions is that of Fig. 1. The gaps are clearly visible in the original negative. The photograph has been retouched to make the gaps more visible.

The formation of (μ^-Ne) can also be observed indirectly since the neon transfer reactions (5) and (6) compete with the reactions (2) and (3) which lead to rejuvenated muons (4).

In conclusion, the transfer of muons to neon can be observed through two

([11]) H. PRIMAKOFF: *Rev. Mod. Phys.*, **31**, 802 (1959). For the capture rate in liquid hydrogen, see also S. WEINBERG: *Phys. Rev. Lett.*, **4**, 575 (1960).

([12]) J. C. SENS: *Phys. Rev.*, **113**, 679 (1959). The measurements of SENS are interpolated to obtain the value for Ne.

independent effects: the frequency of μ^- nuclear capture rises and the frequency of rejuvenated μ^- drops.

An unusual event is shown in Fig. 2. to serve as an illustration of the effects described in the last two Sections.

1·4. *Transfer to helium.* – The probability of nuclear capture of μ^- by ^{4}He is very small $\sim 10^{-3}$ ([11]). But transfer to helium can give rise to two effects:

a) competition with the transfer to deuterium will decrease the frequency of rejuvenated μ^-, and

b) competition with transfer to neon will decrease the frequency of μ^- nuclear captures since the nuclear capture rate is much smaller in He than in Ne.

1·5. *The experiment.* – Negative muons were brought to rest in a liquid hydrogen bubble chamber containing various small amounts of deuterium, neon and helium. The frequency of μ^- nuclear capture and of rejuvenated μ^- was measured in each mixture. The results were analysed in terms of the various transfers involved.

Negative pions were also brought to rest in each mixture. A study of the pion induced stars provided important additional evidence for the presence of helium and neon. This evidence removes most of the uncertainties which might otherwise exist concerning the solution of He and Ne in the chamber.

2. – Experimental procedure.

2·1. *The beam.* – A 99% pure μ^- beam was obtained with an average of two μ^- stops per picture. The π^- beam was obtained simply by reducing the absorber thickness. We thus obtained reproducible μ^- and π^- beams throughout the run, even with frequent switching from one to the other.

2·2. *The introduction of gases.* – Deuterium, hydrogen contaminated with neon, and pure helium were added to the natural hydrogen. The mixtures obtained are described in Table I. The volume of the bubble chamber system was 9.6 liters. The quantities of impurities introduced were measured by recording a pressure drop in a cylinder of known volume and temperature. No change in the operating conditions of the chamber could be correlated with the introduction of contaminants. The temperature of the bubble chamber was about 27 °K.

TABLE I. - *Mixtures of hydrogen, deuterium, helium, and neon used in the experiment.*

Nominal mixture (*a*)	*Operation performed*	Concentration of added gases in atoms per million protons (*b*)		
		Deuterium	Neon	Helium
Hydrogen A	Filled chamber with uncontaminated natural hydrogen	0	0	0
Ne 15	Emptied 20% of the chamber. Refilled with natural hydrogen contaminated with 80 ppm of neon.	0	15.5±2	0
Ne 15+D 400	Added deuterium.	406±30	15.5±2	0
Ne 260	Emptied 30% of the chamber. Refilled with natural hydrogen contaminated with 900 ppm of neon	245±45	260 ±25	0
Ne 260+He 930	Added 11 liters of helium (S.T.P.)	245±45	260 ±25	930±230
	Emptied the chamber completely			
Hydrogen B	Refilled with uncontaminated natural hydrogen.	0	0	0
D 650	Added deuterium.	653±45	0	0
He 1600+D 650	Added 20 liters of helium.	653±45	0	1600±250

(*a*) Numbers indicate approximate concentrations in parts per million.
(*b*) Here, we only indicate the impurities that were deliberately introduced ([15]).

2·2.1. Deuterium and helium. – Deuterium and helium were introduced into the chamber after it was full and operating.

Once it had been contaminated with helium, the bubble chamber remained a close system, *i. e.* no hydrogen was released to adjust the amount of liquid in the chamber. All the helium introduced therefore remained within the bubble-chamber system. In the experiment, the maximum amount of helium used was 20 liters. In order to exclude the possibility that most of the helium remained within the small vapor phase, a solubility test was later made with increased sensitivity: we used three times more helium (about 1 He atom per 200 H atoms). The absence of significant rise in the operating pressure showed that most of the 60 liters of helium had gone into the condensed phase.

2·2.2. Neon. – The filling line leading to the bubble chamber went through a charcoal purifying trap maintained at liquid nitrogen temperature and then through a condensing line at 20 °K. To prevent the neon from freezing (its melting point is 24 °K), it was greatly diluted with hydrogen before being put in the chamber.

2·2.3. An attempt with argon. – An attempt was made to obtain a large transfer of μ^- to argon. The argon contaminated hydrogen was not passed through the purifier and precipitation occurred on the windows before the chamber was completely filled. The chamber could still be operated but track quality was poor. Scanning indicated that little or no transfer of μ^- had been achieved; the fraction of μ^- nuclear capture was only about 5 %.

3. – Analysis of μ^- events.

The pictures were taken with three 35 mm cameras. The projected view used in scanning was approximately twice full scale. Forty thousand pictures were scanned.

3·1. *Rejuvenated* μ^-. – Rejuvenated muons appear as kinks (cf. Fig. 2). Scanning was done on a single view. The other two views were used to check the appearance of the events and for measurements. All films were scanned at least twice. The efficiency of a single scan was 97 %.

The angular selection criteria were:

a) angle between the incoming μ^- and the rejuvenated $\mu^- \geqslant 50°$ on the view used for scanning;

b) dip angle of the rejuvenated $\mu^- \leqslant 53°$.

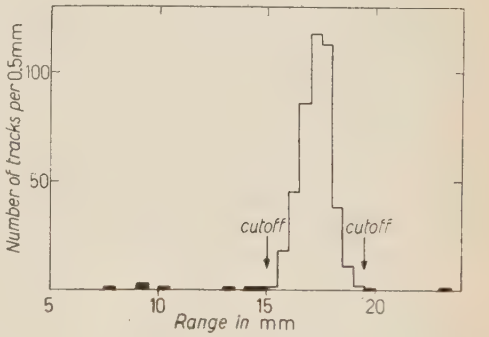

Fig. 3. – Identification of rejuvenated μ^- by range. The graph shows the distribution of the 442 events fulfilling the angular selection criteria adopted for rejuvenated μ^- (cf. Section 3·1). The background of spurious events is seen to be negligible.

In order to ascertain that these criteria eliminated the effect of the scanning bias against forward angles and short projected lengths, we checked the isotropy of the events fulfilling the selection criteria, particularly of those which had been missed once. Ten events were rejected by using cut-offs in length (cf. Fig. 3). The average track length of the remaining 432 events is (17.3 ± 0.5) mm; the

corresponding energy value, (5.3 ± 0.1) MeV, is that expected for μ^- rejuvenated through reaction (4). The events found are listed in Table II.

TABLE II. – *Rejuvenated μ^- and μ^--induced stars (a).*

Nominal mixture (*b*)	Decays	Rejuvenated μ^-		μ^- induced stars				
				Single-prong stars		Two-prong stars	Total	Stars per 10^3 μ^-
		Decaying	Captured	without gap	with gap			
Hydrogen A	10134	34	0	0	0	0	0	0
Hydrogen B	10271	50	0	0	1	0	1	0.1
D 650	9580	131	0	0	0	0	0	0
He 1600 + D 650	9720	106	0	0	0	0	0	0
All neon-free hydrogen	39705	321	0	0	1	0	1	0.03
Ne 15	10300	32	4	12	9	1	22	2.0 ± 0.5
Ne 15 + D 400	8500	52	5	7	13	2	22	2.4 ± 0.5
Ne 260	9268	9	3	49	43	7	99	8.1 ± 0.8
Ne 260 + He 930	2825	4	2	17	11	1	29	7.8 ± 1.5

(*a*) See Sections 3·1 and 3·3 of text.
(*b*) See Table I for detailed description.

To compute the frequency of rejuvenated μ^- as plotted in Fig. 6, we applied two corrections to the fractions obtained from Table II: a 3 % correction for the finite size of the chamber and a geometric factor of 1.73 for the selection criteria. The combined factor is 1.68.

3·2. *Nuclear capture of μ^-.* – Any event consisting of a heavy track, ending

TABLE III. – *Nuclear capture of μ^- (a). In the absence of neon, the background is seen to be small. It is due primarily to π^- capture.*

Nominal mixture (*b*)	Decays	Captures	% captures
Hydrogen A	5300	86	1.6 ± 0.2
Hydrogen B	1070	17	1.6 ± 0.4
D 650	3124	26	0.8 ± 0.2
He 1600 + D 650	3167	21	0.7 ± 0.2
All neon-free hydrogen	12661	150	1.17 ± 0.1
Ne 15	5215	378	6.76 ± 0.35
Ne 15 + D 400	3899	424	9.80 ± 0.5
Ne 260	775	264	25.4 ± 1.7
Ne 260 + He 930	474	170	26.4 ± 2.0

(*a*) See Section 3·2 of text.
(*b*) See Table I for detailed description.

within a well-defined central region of the chamber, with no visible decay electron, was called a capture. The events found are listed in Table III. Most of the scanning for capture was done by two independent observers. The overall scanning efficiency was taken as unity.

3·2.1. Background. – Two types of events can simulate a μ^- nuclear capture:

a) decays in which the electron is missed;

b) π^- captures and proton stops.

a) The introduction of neon could conceivably have made the chamber partly insensitive to minimum ionizing tracks. No change in the track quality could be correlated with the introduction of neon and only a few doubtful events were found, *i.e.* events listed as questionable by one observer or classified differently by two observers. Further, if the chamber had been partly insensitive, one would have missed more decays near the windows since the minimum track length is shorter in that region. No difference in the depth distributions of μ^- endings for captures and decays was detected in any of the mixtures containing neon. It thus seems unlikely that a significant number of decays was missed because of a partial insensitivity of the chamber.

b) Since no magnetic field was used, π^- captures and proton stops could usually not be distinguished from μ captures. The apparent frequency of captures in neon-free hydrogen shows that π^- and protons caused a background of the order of 1% (cf. Table III).

3·3. *μ^- induced stars and rejuvenated μ^- undergoing nuclear capture.* – The capture of μ^- by a nucleus of $Z > 1$ can be followed by the emission of one or several heavily ionizing particles (p, d, ...) forming a star.

3·3.1. Selection criteria. – A one-prong star is defined as follows:

a) the track is heavy (*i.e.* not an electron);

b) it starts within 5 mm of the end of a meson which stops without decaying;

c) its projected length is $\geqslant 4$ mm;

d) its angle with the meson track is $\geqslant 60°$;

e) it stops within the chamber.

The lengths and angle indicated here refer to the projected view (twice full scale). No geometrical limitations were used for two-prong stars.

3·3.2. Gaps. – A gap between the end of the meson track and the beginning of the prong appeared in a large fraction of the stars. An example of such an event can be seen in Fig. 2. The observer making the measurement of the prong lengths grouped all stars into three categories: star without gap, star with gap and two-prong star. The result of this classification appears in Table II. The stars found in the two mixtures containing 260 parts per million (ppm) of Ne were also studied by two other observers. They made an independent classification and in addition measured each gap to $\frac{1}{2}$ mm in the view where it was most apparent. The agreement between the three independent classifications of one-prong stars is shown in Fig. 4.

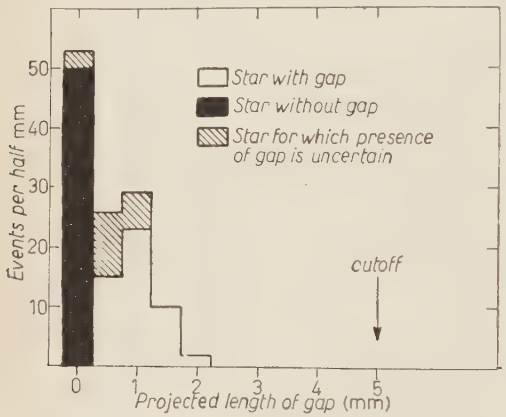

Fig. 4. – Distribution of gaps associated with stars. Stars with a gap provide a direct evidence for the two-step transfer: $(\mu^- p) + d \rightarrow (\mu^- d)^* + p$, $(\mu^- d)^* + Ne \rightarrow \rightarrow (\mu^- Ne) + d$. Stars were classified by 3 independent observers. The shaded areas indicate events for which one scanner disagreed with the others on the presence of a gap. The agreement is adequate for present purposes. The distribution of gap lengths shows that stars with a gap cannot be due to accidental coincidences between μ^- endings and prongs. The magnification due to reprojection was about 2.

3·3.3. Background. – In the absence of neon, one star was found in $4 \cdot 10^4$ stops. For hydrogen contaminated with neon, the possible sources of background are:

a) a μ^- undergoing nuclear capture might have its end point in accidental coincidence with a proton arising from another cause;

b) stars might be due to the pion contamination of the μ^- beam (large angle π-p scattering or π^--induced star on neon);

c) a μ^- undergoing nuclear capture might undergo large angle scattering.

These possibilities were examined experimentally and were found to have a negligible effect.

3·3.4. Events found. – The events are listed in Table II. Eleven two-prong stars and 162 one-prong stars were found in neon-contaminated hydrogen. The longest prong found among the two-prong stars has the range of an 11.6 MeV proton. The longest one-prong star has the range of a 29 MeV proton and a visible gap. The range distribution of 136 one-prong stars is shown in Fig. 5, for stars with and without visible gap.

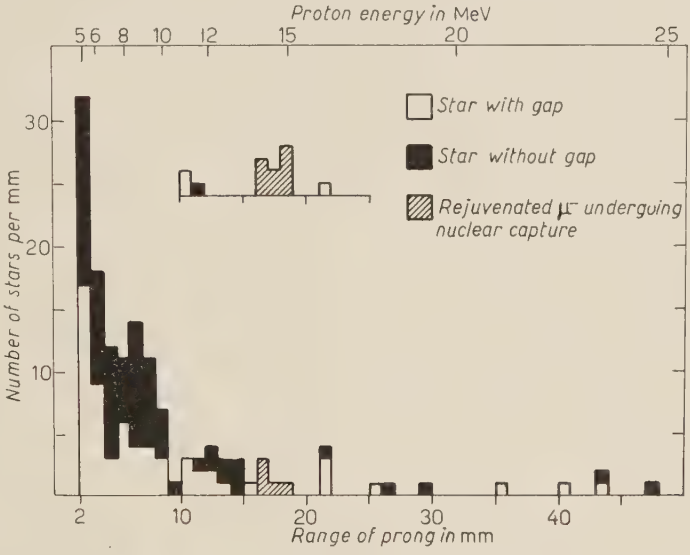

Fig. 5. – Range distribution of 136 stars induced by the capture of μ^- by Ne nuclei. The upper scale gives the energy of the prongs if they are assumed to be protons. The cut-off introduces a bias against short prongs; this bias becomes negligible for a 7 MeV proton. The longest star is off the scale. The auxiliary histogram shows the prongs of range 10 to 25 mm, found in the mixtures containing 15 ppm of Ne. The 9 events of the shaded area must be rejuvenated μ^- having undergone nuclear capture. They have been omitted from the main histogram. One of the events in the shaded area of the main histogram (at 17 mm) is a rejuvenated μ^- inducing a star. The identification of the 4 other events of this area is uncertain.

Events initially classified as stars and having a range between 15.6 and 18.3 mm were later classified as rejuvenated μ^- undergoing nuclear capture. In the mixtures containing 15 ppm of neon, 9 out of 41 events were in this range; the auxiliary histogram of Fig. 5 shows that the identification of these 9 events as rejuvenated μ^- is fairly unambiguous. In the more concentrated solutions, the frequency of rejuvenated μ^- decreased while the frequency of μ^--induced stars increased. As a result, the identification of the five events represented by the shaded area of the main histogram is ambiguous, except for one event produced by a rejuvenated μ^- inducing a star.

3·4. *Indirect methods of measuring the frequency of μ^- nuclear capture.* – In Section 3·2 we described the direct method, « method 1 », for determining the nuclear capture rate (*i.e.* observation of non-decaying μ^-). μ^- nuclear capture gives rise to two other effects which may be used to determine the capture rate indirectly: rejuvenated μ^- and μ^--induced stars.

3·4.1. μ^--induced stars (Method 2). – With 260 ppm of Ne, the frequencies of μ^- captures and of stars are respectively $(24.2\pm1.7)\%$ and $(0.81\pm0.08)\%$. Hence, the fraction of μ^- nuclear captures that are followed by the emission of a star fulfilling the selection criteria listed in Section 3·3.1 is $(3.2\pm0.5)\%$. Using this percentage, one can derive the frequency of μ^- nuclear capture in Ne solutions from the measured frequency of stars. This method may also be used to test for other impurities of $Z\approx10$ (*e.g.* C, N and O) if we assume that they behave as neon does.

3·4.2. Rejuvenated μ^- (Method 3). – Table II lists the rejuvenated μ^-'s with and without decay electrons. Using these events, one obtains the frequency of μ^- nuclear capture appearing in the last column of Table V. This method is particularly useful for neon-free hydrogen. From the absence of rejuvenated μ^- undergoing nuclear capture we obtain the following *upper limit* to the fraction of μ^- transferred to impurities of $Z>2$ in neon-free hydrogen (hydrogen A not included): 3% to carbon, less to higher Z elements. Note that the absence of μ^- captures does not exclude transfer to helium. Note also that in hydrogen A the statistics on rejuvenated μ are too poor to exclude a sizeable transfer to impurities; however, the absence of significant transfer to impurities of $Z>2$ appears probable since we find no induced stars.

Table V shows that the agreement between the three ways of measuring the frequency of μ^- nuclear capture is satisfactory.

4. – Pion stars: check of the presence of neon and helium.

Eleven thousand pictures, containing $1.6\cdot10^5$ stops, were scanned for π^--induced stars. The selection criteria for one-prong stars were as follows:

a) range $\geqslant50$ mm (50 mm is the range of a 25 MeV proton in liquid hydrogen);

b) projected angle with the meson track $\geqslant80°$.

One-prong stars fulfilling these criteria were distinguished from π-p scattering by the absence of a recoil proton. Two-prong stars were distinguished from π-p and p-p scattering by momentum balance. Thirty-four stars were found to satisfy the criteria. They are classified in Table IV.

4·1. *Check on the neon contamination.* – Since helium was found to be present in all the mixtures used (see next section) and since π^- capture in He can produce only zero or one-prong stars, the presence of neon is best studied by using only multiple-prong stars. It will be seen in Table IV that the number of multiple-prong stars per π^- stop increases from 0/38 000 to 12/64 000 when the neon concentration is increased from 15 ppm to 260 ppm. The increase in the amount of neon dissolved is also demonstrated by the large increase in the fraction of μ^- transferred to neon (in particular, see Section 5·1.1*d* below). From these observations, we conclude that:

TABLE IV. – *Stars induced by π^- capture.*

Nominal mixtures (*a*)	Stops	Stars		
		One-prong $\geqslant 80°$ $\geqslant 50°$ mm	Two and three-prong	Stars/per stop (*b*)
All neon-free hydrogen	62 000	11	0	$320 \cdot 10^{-6}$
Ne 15 Ne 15 + D 400	38 000	1	0	$50 \cdot 10^{-6}$
Ne 260 Ne 260 + He 930	64 000	10	12	$470 \cdot 10^{-6}$

(*a*) See Table I for detailed description.
(*b*) The number of one-prong stars was multiplied by 1.8 to take into account the exclusion of forward angles.

a) the mixtures containing « 15 ppm » of Ne were not saturated in Ne. Hence, unless a fraction of the Ne was lost before entering the bubble-chamber system, the concentration of Ne in solution was equal to the nominal value.

b) the amount of Ne dissolved in the « 260 ppm » mixtures of Ne is equal to the nominal amount, at least in order of magnitude.

From the last column of Table IV, we see that the ratio — number of stars per stop/number of Ne atoms per proton — is of order unity. This shows that little or no transfer of π^- occurred. (Even if we allow for the possibility that a large fraction of Ne was lost before entering the bubble-chamber system, we can still conclude that, in a given Ne solution, the probability of transfer is at least four orders of magnitude smaller for pions than for muons.)

4·2. *Check on the helium contamination.* – The transfer to helium was found to be unexpectedly slow. Poor solubility of helium was a possible explanation, but this hypothesis had to be discarded after a solubility test was performed (cf. Section 2·2.1). In order to also exclude the possibility of an error during the introduction of the helium, we searched for internal evidence of the presence of helium in the mixture with the highest nominal He concentration —

« 1630 ppm He+650 ppm D ». A comparison of the frequency of stars before and after the introduction of helium seemed to demonstrate the presence of helium, but this remained unconvincing due to the presence of stars in hydrogen not deliberately contaminated with elements of $Z>1$. To eliminate this ambiguity, scanning of additional π^- stops in pictures taken during an earlier part of the run was undertaken [13]. The « uncontaminated » hydrogen was not helium free. The presence of helium was unambiguously detected through the stars of unique range coming from the reaction

$$(7) \qquad {}^4\mathrm{He}+\pi^- \rightarrow \mathrm{t}+\mathrm{n}\,.$$

Triton tracks from (7) were found both in the « uncontaminated » hydrogen and in the « 1630 ppm He+650 ppm D » mixture. The tritons indicated concentrations of 10^{-3} and $2\cdot10^{-3}$ of helium respectively [13]. (The He+D sample is discussed further in reference [13], Table I). Mass-spectrometric analysis of a sample of hydrogen from the same source as our « uncontaminated » hydrogen showed a concentration of $0.2\cdot10^{-3}$ of helium [15]. Additional helium may have entered the chamber while it was being filled since He was passed through the charcoal trap in an earlier experiment.

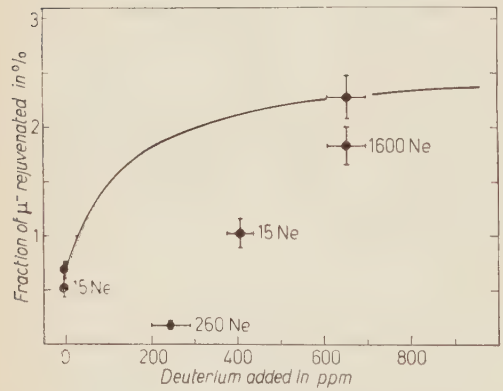

Fig. 6. – Percentage of rejuvenated μ^- in the various mixtures. The curve shows the percentage expected in the absence of impurities other than deuterium. The amount of noble gas added is indicated in ppm for each experimental point. The results show that transfer to neon is high and transfer to helium is low.

5. – Experimental results and discussion.

5·1. *Qualitative results on transfer reactions.* – Table V and Fig. 6 show the frequency of μ^- nuclear

[13] M. SCHIFF, R. H. HILDEBRAND and C. GIESE: *Phys. Rev.*, **122**, 265 (1961). In this study it was found that about $\frac{1}{3}$ of the stars had ranges corresponding to the ${}^4\mathrm{He}+\pi^-\rightarrow \mathrm{t}+\mathrm{n}$ reaction. The total number of 5 to 110 mm stars per stopping pion was approximately equal to the fraction of He atoms in the solution.

[14] D. STOMINGER J. M. HOLLANDER and G. T. SEABORG: *Rev. Mod. Phys.*, **30**, 585 (1958).

[15] C. GIESE: (private communication). A mass-spectrometric analysis of a sample of our commercial hydrogen showed $(40\pm14)10^{-6}$ of deuterium and $2\cdot10^{-4}$ of helium.

TABLE V. – *Nuclear captures per μ^- stop.*

Nominal mixture (*a*)	Concentration of added gases in atoms per million protons (*b*)			Number of nuclear captures per μ^- stop		
	Deuterium	Neon	Helium	Method 1 (*c*) using ordinary non-decaying μ^-	Method 2 (*d*) using stars	Method 3 (*d*) using rejuvenated μ^-
Hydrogen A	0	0	0	$< 1.2\%$	$\leqslant 0.3\%$ (no star in 10^4 stops)	$\leqslant 3\%$ (34 decaying, none captured)
Ne15	0	15.5 ± 2	0	$(5.6 \pm 0.4)\%$	$(6.1 \pm 1.4)\%$	$\frac{4}{36} = 11\%$
Ne 15+D 400	406 ± 30	15.5 ± 2	0	$(8.6 \pm 0.5)\%$	$(7.0 \pm 1.4)\%$	$\frac{5}{57} = 9\%$
Ne 260	245 ± 45	260 ± 25	0	$(24.2 \pm 1.7)\%$ (*d*)		$\frac{3}{12} = 25\%$
Ne260–He930	245 ± 45	260 ± 25	930 ± 230	$(25.2 \pm 2.0)\%$	$(24 \pm 5)\%$	$\frac{2}{6} = 33\%$
Hydrogen B	0	0	0	$< 1.3\%$	$\sim 0.1\%$ (one star found in $3 \cdot 10^4$ stops)	$\leqslant 0.4\%$ (287 decaying none captured)
D 650	653 ± 45	0	0	$< 0.7\%$		
He1600+D650	653 ± 45	0	$1\,600 \pm 250$	$< 0.5\%$		

(*a*) Numbers indicate approximate concentrations in parts per million.
(*b*) We only indicate the impurities that were deliberately introduced ([15]).
(*c*) These numbers obtained from Table III, after correcting for background.
(*d*) See Section 3·4 of text.

capture and the frequency of rejuvenated μ^- in the various mixtures. Both show that transfer to neon is fast and transfer to helium is slow.

We now list our conclusions for neon and helium, referring in each case to the relevant figures and tables.

5·1.1. Neon:

a) Transfer to neon is already appreciable for neon concentrations of order 10^{-5}: cf. in Table V the frequency of μ^- nuclear capture, measured by methods 1, 2 and 3 in (Ne 15) and in (Ne 15+D 400); also, cf. in Fig. 6 the frequency of rejuvenated μ^- when $C_D = 446$ ppm and $C_{Ne} = 15$ ppm.

b) The reaction

$$(\mu^-\mathrm{d})^* + \mathrm{Ne} \rightarrow (\mu^-\mathrm{Ne}) + \mathrm{d}\,, \tag{6}$$

contributes appreciably to the transfer to neon: cf. in Table II stars with a gap in all mixtures containing deuterium and neon.

c) The addition of deuterium increases transfer to neon: cf. in Table V the rise in the frequency of μ^- nuclear capture, as measured by method 1, when deuterium was added to the 15 ppm Ne mixture.

d) It is possible to obtain conditions in a hydrogen bubble chamber, where most of the μ^- are eventually transferred to neon: cf. in Fig. 6 the frequency of rejuvenated μ^- in the more concentrated neon solution; also, cf. in Table V the frequency of nuclear capture, as measured by method 1, and compare it to the frequency expected in pure neon (0.33) ([12]).

Transfer to neon can be increased by the addition of deuterium. We estimate that if we had added a large amount of deuterium (say 5%) to the more concentrated neon solution, the fraction of μ transferred to neon would have been 88%.

In addition, the procedure used to introduce the neon suggests that it is possible to dissolve at least 3 times more neon (*). The fraction of μ^- transferred to neon would then be $\geqslant 96\%$.

5·1.2. Helium. – *Transfer to helium is much slower than to neon*: compare in Fig. 6 the effect of adding 1600 ppm of He, to the effect of adding 260 ppm of Ne; cf. also in Table V the frequencies of μ^- nuclear capture, as measured by methods 1 and 2, before and after the addition of 930 ppm of He to the neon mixture.

5·2. *Quantitative results on transfer reactions.* – The measurements described in this paper give us information on the competition between various processes. We thus get ratios of reaction rates and not the rates themselves. When the ratios involve the transfer processes, we call them transfer ratios. Because of the many reaction channels involved, even a simplified quantitative analysis requires a cumbersome formalism which we leave to the Appendix. An outline of the analysis is as follows.

(*) The more concentrated neon mixture was obtained by refilling 30% of the chamber with hydrogen containing 900 ppm of neon. By completely emptying and refilling with the 900 ppm mixture, we would probably have been able to obtain a solution 3 times more concentrated in neon.

The transfer ratio has the following physical meaning: if X_{pNe} is the primary transfer ratio to neon, then $C_{pNe} = 1/X_{pNe}$ is the concentration of neon in deuterium-free hydrogen such that the frequency of

(5) $$(\mu^- p) + Ne \to (\mu^- Ne) + p \,,$$

is 50%. Analogously, $C_{dNe} = 1/X_{dNe}$ is the concentration of neon in deuterated hydrogen such that the reaction

(2) $$(\mu^- p) + d \to (\mu^- d)^* + p \,,$$

has a 50% chance of being followed by the reaction

(6) $$(\mu^- d)^* + Ne \to (\mu^- Ne) + d \,.$$

With this notation, the statement *c*) of Section 5˙1.1 means:

$$X_{dNe} > X_{pNe} \qquad \text{or} \qquad C_{dNe} < C_{pNe} \,.$$

5˙2.1. Transfer to deuterium. – From the values of the frequency of rejuvenated μ^- measured for two deuterium concentrations C_0 and C_1, the transfer ratio to deuterium and the saturation frequency were derived:

$$X_{pd} = (8.9^{+6.2}_{-3.6}) \cdot 10^3 \quad \text{and} \quad \beta = (2.64 \pm 0.35) \cdot 10^{-2} \,.$$

β is the probability that a transferred μ^- will be rejuvenated. The values found for the frequency of rejuvenated μ^-, in « natural » hydrogen and at saturation, agree with the values $r_0 = (0.7 \pm 0.2) \cdot 10^{-2}$ and $\beta = (2.5 \pm 0.4) \cdot 10^{-2}$ found by ALVAREZ *et al.* [2]. Our estimated error on X_{pd} comes largely from the error on the deuterium concentration C_0 of the « natural » hydrogen used. C. GIESE [15] measured $C_0 = (40 \pm 14) \cdot 10^{-6}$.

The normal isotopic abundance [14] is $C_0 = 150 \cdot 10^{-6}$, but in manufacturing hydrogen gas the isotopic composition may be altered considerably from that of water.

5˙2.2. Transfer to neon. – The fraction Q of μ^- undergoing nuclear capture is proportional to the fraction f_{Ne} of μ^- transferred to neon:

(14) $$Q(C_D, C_{Ne}) = Q_{Ne} f_{Ne}(C_D, C_{Ne})$$

where Q_{Ne} is the probability of nuclear capture in pure neon. Interpolation of the extensive measurements of SENS ([12]) yields $Q_{Ne} = 0.33$. Assuming $Q_{Ne} = 0.33 \pm 0.05$, and using the frequencies of nuclear capture measured in the neon samples containing 15 ppm of Ne, we find:

$$X_{pNe} = (9.5 \pm 3.0) \cdot 10^3 \quad \text{and} \quad X_{dNe} = (2.7 \pm 0.9) \cdot 10^4 .$$

Note that the values of Q in the 15 ppm neon mixtures were far below Q_{Ne}, *i.e.* transfer to neon in these two mixtures war far from complete. Hence, the results are not too sensitive to the value of Q_{Ne} used; this is particularly true of the ratio $y_{Ne} = X_{dNe}/X_{pNe}$. On the other hand, the value found for y_{Ne} depends sensitively on the value of the transfer ratio to deuterium, which itself depends on the value of the deuterium concentration in uncontaminated hydrogen. Finally, note that possible errors on the value of the concentration of neon dissolved in the neon mixtures affect the two transfer ratios in the same way and, hence, leave y_{Ne} unaffected.

5'2.3. Transfer to helium. – By adding 930 ppm of helium to the 260 ppm Ne mixture, we hoped to observe the competition between helium and neon, but transfer to helium was at least one order of magnitude below the value for which the experiment was planned so that no effect was observed. A more sensitive test was obtained by observing the effect of the competition between helium and deuterium. A small drop was observed in the frequency of rejuvenated μ^- indicating that $X_{dHe} \sim 10^2$, although $X_{dHe} = 0$ is not excluded.

5'3. *Conclusions concerning μ^- capture experiments.*

5'3.1. Capture by hydrogen. – One might expect that the large transfer to deuterium found by ALVAREZ *et al.* ([2]) was due to some anomaly and that appreciable transfer to other elements would not occur. In view of the large transfer to neon, it would now be unreasonable to dismiss the possibility of appreciable transfer to impurities like carbon, nitrogen and oxygen. The presently available data give no hint of a simple Z dependence of the transfer ratios. If we assume that transfer to nitrogen ($Z = 7$) is half as large as that to neon ($Z = 10$), then the effect of one ppm of nitrogen would be to multiply the frequency of μ^- nuclear capture in pure hydrogen by a factor 3. There is no way of knowing whether a small transfer to impurities has occurred or not; therefore, an experiment relying on the absence of decay electrons to identify a nuclear capture by hydrogen can only yield an upper limit. To measure the rate of the reaction $\mu^- + p \to n + \bar{\nu}$, one will have to identify the capturing nucleus by detecting the emitted neutron.

5'3.2. Capture by ^{3}He. – Recently, detailed calculations of the total capture of μ^- by ^{3}He have been made ([11,16,17]). A measurement of this capture rate might be a substitute for the very difficult measurement of the capture rate by hydrogen. We now show that if our estimate of the transfer ratio from deuterium to helium is confirmed by further experiments, it will be possible to use the transfer to helium to achieve a measurement of the rate of nuclear capture of μ^- by ^{3}He. The transfer to helium need not be complete; a 50% transfer is sufficient. If $C_{d\mathrm{He}} \sim 10^{-2}$, one would need to dissolve about 1% of ^{3}He. The work of DERRICK, PEWITT and YODH ([13]) and the test described in Section 2'2.1 show that this is possible.

One needs to know accurately the fraction of μ^- transferred to helium. This is achieved by using a « large » amount of deuterium (say 5%), and measuring the frequencies of rejuvenated μ, r_b and r_a, before and after the introduction of helium. Additional advantages of this procedure are: 1) the effect of primary transfer to impurities is reduced by a large factor $C_{\mathrm{D}}N_{\mathrm{D}}$, 2) the effect of secondary transfer to impurities cancels out (cf. Appendix 4).

The frequency of μ^- nuclear capture by ^{3}He is given by

$$Q_{\mathrm{He}} = \frac{r_b}{r_b - r_a}\left| Q_a - \frac{r_a}{r_b} Q_b \right|, \tag{19a}$$

Q_b and Q_a are the measured frequencies of μ^- nuclear capture, before and after the introduction of ^{3}He.

5'3.3. Capture by neon isotopes. – Transfer to neon can be made almost complete. The technique outlined in the last section can be used to make a precision measurement of the capture rate of μ^- by separated neon isotopes. A study of μ^--induced stars is also made possible by the transfer to neon.

We wish to emphasize that the above conclusions concerning μ^- capture experiments do not depend on the exact numerical values of the transfer ratios involved; rather, they come from the qualitative results on transfer reactions summarized in Section 5'1.

6. – Conclusions.

In this experiment, we studied the transfer of μ to impurities deliberately introduced into a hydrogen bubble chamber: deuterium, neon and helium. Stars induced by π^- were also studied in order to check the presence of helium

([16]) C. WERNTZ: *Nucl. Phys.*, **16**, 59 (1960).
([17]) A. FUJII: *Phys. Rev.*, **118**, 870 (1960).

and neon. Our main purpose was to examine the possible bearing of transfer reactions on some μ^- capture experiments in hydrogen bubble chambers.

6·1. *Transfers.*

6·1.1. Neon. – A large transfer was observed, both through an increase in the frequency of μ^- nuclear capture and through a decrease in the frequency of pd fusions. Stars were observed, where a gap between the muon ending and the prong provided direct evidence for the transfer from deuterium to neon. In fact, $(\mu^-\mathrm{d})$ atoms that come from a transfer to deuterium will lose their μ^- to neon even more readily than $(\mu^-\mathrm{p})$ atoms. We found

$$C_{\mathrm{pNe}} = (105^{+50}_{-25})\cdot 10^{-6} \quad \text{and} \quad C_{\mathrm{dNe}} = (37^{+18}_{-9})\cdot 10^{-6},$$

where C_{pNe} and C_{dNe} are the neon concentrations in pure hydrogen and in highly deuterated hydrogen which will cause a 50% transfer.

6·1.2. Helium. – Transfer is very slow: the decrease in the frequency of pd fusions that followed the addition of 0.16% of helium to deuterated hydrogen was small; it showed that C_{dHe}, the concentration of He in deuterated hydrogen for 50% transfer, is at least of the order of 1%.

6·2. *Stars.*

6·2.1. Muons. – From the study of the stars following the nuclear capture of μ^- by Ne, we conclude:

a) The probability of emission of a charged particle of range larger than that of a 4.4 MeV proton is $(5\pm1.5)\%$.

b) Among the stars that could be detected, the frequency of two-prong stars was about 5%.

6·2.2. Pions. – From the study of pion stars, we conclude:

a) Triton emission occurs in about $\frac{1}{3}$ of the stars induced by the capture of π^- by ^{4}He for prongs in the range 0.029 to 0.64 g/cm^2 of hydrogen ([13]).

b) The number of pion stars per pion stop is of the same order of magnitude as the number of He atoms per proton, *i.e.* little or no transfer of π^- to He occurs ([13]).

c) If it occurs at all, transfer of π^- to neon is at least four orders of magnitude smaller than μ^- transfer.

6·3. μ^- *capture experiments.* – From our results on the transfer reactions, we draw the following conclusions:

a) In order to measure the rate of nuclear capture by pure hydrogen, it will be necessary to establish the identity of the capturing nucleus.

b) One can dissolve enough neon into a hydrogen bubble chamber to make the transfer to neon practically complete. Possible applications are: a measurement of the rates of nuclear capture and a study of μ^- induced stars for separated neon isotopes.

c) Transfer to helium is low, yet it might be sufficient to allow a measurement of the rate of nuclear capture by ^{3}He.

* * *

I wish to express my thanks and gratitude to Professor R. H. Hildebrand for his guidance and constant encouragement throughout this work. He suggested this experiment and pointed out the use of rejuvenated muons as an independent method of studying μ transfers. This experiment would have been impossible without the cooperation and help of each member of the Chicago bubble chamber group: E. Denton, R. Handler, R. H. Hildebrand, P. Kloeppel, H. Kobrak, S. Lucero, M. Pyka, and S. C. Wright. The bubble chamber was designed by R. H. Hildebrand. R. Bizzarri made substantial contributions during early stages of its construction. E. Denton and M. Pyka were particularly helpful during experimental work directly associated with this paper. I am grateful to J. H. Hildebrand for his help in problems of solubility and to R. H. Dalitz for encouragement and helpful discussions. I wish to thank C. Giese for analysing samples of deuterium and helium. The measuring table used was designed by S. D. Warshaw The scanning was skillfully done by A. Georgoulakis and T. Belden.

Appendix

We shall put on a quantitative basis the analysis presented in Section 5. In order to do so, it is necessary to establish a convenient notation.

A1. *Notation.*

A1·1. Rates of reactions. We have tried to use a notation consistent with that of Fetkovitch *et al.* [4].

C_D, C_{Ne}, C_{He} = number of deuterons, neon atoms, helium atoms per proton; usually expressed in parts per million (ppm),

(A-2) $C_D\lambda_{pd}$ = rate of $(\mu^-p)+d \rightarrow (\mu^-d)^*+p$,

(A-5) $C_{Ne}\lambda_{pNe}$ = rate of $(\mu^-p)+Ne \rightarrow (\mu^-Ne)+p$,

(A-6) $C_{Ne}\lambda_{dNe}$ = rate of $(\mu^-d)^*+Ne \rightarrow (\mu^-Ne)+d$,

$C_{He}\lambda_{pHe}$ = rate of $(\mu^-p)+He \rightarrow (\mu^-He)+p$,

$C_{He}\lambda_{dHe}$ = rate of $(\mu^-d)^*+He \rightarrow (\mu^-He)+d$,

λ_0 = rate of $\mu^- \rightarrow e^-+\nu+\bar{\nu}$,

(A-1) λ_{HH} = rate of $(\mu^-p)+p \rightarrow (p\mu^-p)$,

(A-3) λ_{DH} = rate of $(\mu^-d)+p \rightarrow (p\mu^-d)$.

A1'2. Ratios of reaction rates. In a bubble chamber experiment, one does not determine rates of reactions but only ratios of reaction rates. For instance, one cannot measure the rate of (2) but only the ratio $X_{pd} = \lambda_{pd}/(\lambda_0+\lambda_{HH})$ which we call the transfer ratio to deuterium. Analogously we have:

$X_{pNe} = \lambda_{pNe}/(\lambda_0 + \lambda_{HH})$ = primary transfer ratio to neon,

$X_{dNe} = \lambda_{dNe}/(\lambda_0 + \lambda_{DH})$ = secondary transfer ratio to neon,

$X_{pHe} = \lambda_{pHe}/(\lambda_0 + \lambda_{HH})$ = primary transfer ratio to helium,

$X_{dHe} = \lambda_{dHe}/(\lambda_0 + \lambda_{DH})$ = secondary transfer ratio to helium.

A2. *Transfer to deuterium.* – The probability of transfer to deuterium is:

$$f_D(C_D) = C_D\lambda_{pd}/(\lambda_0 + \lambda_{HH} + C_D\lambda_{pd}) = C_D X_{pd}/(1 + C_D X_{pd}).$$

When $C_D = 1/X_{pd}$, this probability is 50 %.

Call β the probability that a transferred μ will be rejuvenated. The probability that any μ^- stopping in the chamber should be rejuvenated is

(A-8) $$r = \beta f_D.$$

A measurement of r for two values of C_D will yield X_{pd} and β. Using

$$r_0 = (0.69 \pm 0.08)10^{-2}, \quad \text{for} \quad C_0 = (40 \pm 14)10^{-6}\ (^{15}),$$

and

$$r_1 = (2.27 \pm 0.20)10^{-2}, \quad \text{for} \quad C_1 = C_0 + (653 \pm 45)10^{-6},$$

we obtain:

$$X_{pd} = (8.9^{+6.2}_{-3.6})10^3, \quad \text{and} \quad \beta = (2.64 \pm 0.35)10^{-2}.$$

3-784

A3. *Transfer to neon.* – In hydrogen containing neon and deuterium in low concentrations C_{Ne} and C_D, we have the following probabilities of reaction:

(A-9) *primary transfer to* Ne $p_{Ne}(C_D, C_{Ne}) = C_{Ne}X_{pNe}/(1+C_DX_{pd}+C_{Ne}X_{pNe})$,

(A-10) *transfer to deuterium* $p_D(C_D, C_{Ne}) = C_DX_{pd}/(1+C_DX_{pd}+C_{Ne}X_{pNe})$,

(A-11) *secondary transfer to* Ne $s_{Ne}(C_D, C_{Ne}) = p_D(C_D, C_{Ne}) \times C_{Ne}X_{dNe}/(1+C_{Ne}X_{dNe})$,

(A-12) *total transfer to* Ne $f_{Ne}(C_D, C_{Ne}) = p_{Ne}(C_D, C_{Ne}) + s_{Ne}(C_D, C_{Ne})$,

(A-13) μ^- *staying on deuterium* $f_D(C_D, C_{Ne}) = p_D(C_D, C_{Ne}) - s_{Ne}(C_D, C_{Ne})$.

Call Q_{Ne} the probability of nuclear capture in pure Ne. In the various mixtures, we measured the probability of μ^- nuclear capture

(A-14) $$Q(C_D, C_{Ne}) = Q_{Ne}f_{Ne}(C_D, C_{Ne}) .$$

A value of X_{pd} was derived from our data in the previous section. SENS [12] made extensive measurements of capture rates, both below and above $Z = 10$; interpolation of his results yields $Q_{Ne} = 0.33$. If we now substitute equations (9) to (12) into equation (14), our measurements of $Q(C_D, C_{Ne})$ in the 15 ppm Ne mixtures yield:

$$X_{pNe} = 1/C_{pNe} = (9.5 \pm 3.0)10^3 , \qquad \text{and} \qquad X_{dNe} = 1/C_{dNe} = (2.7 \pm 0.9)10^4 .$$

Using the values found for X_{pd}, X_{pNe}, X_{dNe} and β and using eq. (8) to (14), we can compute the expected values of the experimental quantities not yet used; the comparison between measured and derived quantities is shown in Table VI. Note that the large fractions of stars showing a gap give an independent confirmation of the fact that $X_{dNe} > X_{pNe}$. The overall agreement shows that the values of the transfer ratios derived from our measurements can serve as good guides in planning experiments involving the transfer of μ^- from protons and deuterons to neon atoms.

TABLE VI. – *Test of internal consistency (cf. Appendix III). The probability of nuclear capture in neon was taken to be* $Q_{Ne} = 0.33$.

Nominal mixture (*a*)	Percentage of nuclear capture		Percentage of rejuvenated μ^-		Percentage of transfers occurring from deuterium	
	Computed	Measured	Computed	Measured	Computed	Measured (*b*)
Ne 15			0.44	0.52 ± 0.09	42	$> (43 \pm 13)$
Ne 15 + D 400			1.44	1.02 ± 0.14	89	$> (65 \pm 23)$
Ne 260	26.1	24.2 ± 1.7	0.14	0.18 ± 0.05	47	$> (45 \pm 9)$

(*a*) See Table I for detailed description.

(*b*) We used the fraction of μ^--induced stars showing a gap (cf. Fig. 4). Since not all gaps are visible, the fraction of secondary transfers is larger than the fraction of stars showing a gap.

A4. *Transfer to helium.* – Before and after the addition of 1 600 ppm of He to deuterated hydrogen, the fractions of rejuvenated μ were respectively:

$$r_b = (2.27 \pm 0.20)10^{-2}\,, \qquad \text{and} \qquad r_a = (1.82 \pm 0.18)10^{-2}\,.$$

The relative drop in the fraction of μ^- ending up on deuterium is

$$\text{(A-15)} \qquad \frac{r_b - r_a}{r_a} = C_{\mathrm{He}} X_{\mathrm{dHe}} \left[1 + \frac{1 + C_{\mathrm{He}} X_{\mathrm{dHe}}}{y_{\mathrm{He}}(1 + C_{\mathrm{D}} X_{\mathrm{pd}})} \right],$$

where $y_{\mathrm{He}} = X_{\mathrm{dHe}}/X_{\mathrm{pHe}}$. Equation (15) is derived from equations (8), (10), (11) and (13) with Ne replaced by He. Equating (15) to the experimental value (0.25 ± 0.17), and using the numerical values of $C_{\mathrm{D}} X_{\mathrm{pd}}$ and C_{He}, we find:

$$\text{(A-15}a\text{)} \qquad X_{\mathrm{dHe}} = \frac{(1.5 \pm 1.0)10^2}{1 + 0.14/y_{\mathrm{He}}}\,.$$

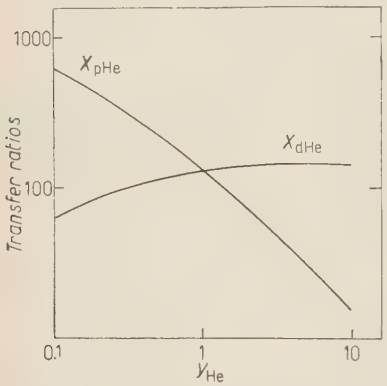

Fig. 7. Transfer ratios for He (cf. eq. (15*a*) of Appendix).

We have made the approximation $C_{\mathrm{He}} X_{\mathrm{dHe}} \ll 1$ which is sufficient for our purpose. Fig. 7 shows X_{dHe} and X_{pHe} as a function of their ratio y_{He}. It shows that, *provided the observed drop in rejuvenated μ^- is not due to a statistical fluctuation*, at least one of the transfer ratios to helium is $\sim 10^2$. The possibility that $X_{\mathrm{dHe}} \sim 10^2$ is of particular interest: transfer from deuterium to helium could then be used to achieve a measurement of the rate of nuclear capture of μ^- by ^{3}He (cf. Section 5·3.1).

We now derive eq. (19*a*) of Section 5·3.2. Fig. 8 shows the transfer reactions occurring in deuterated hydrogen. As above, the subscripts *b* and *a* refer to

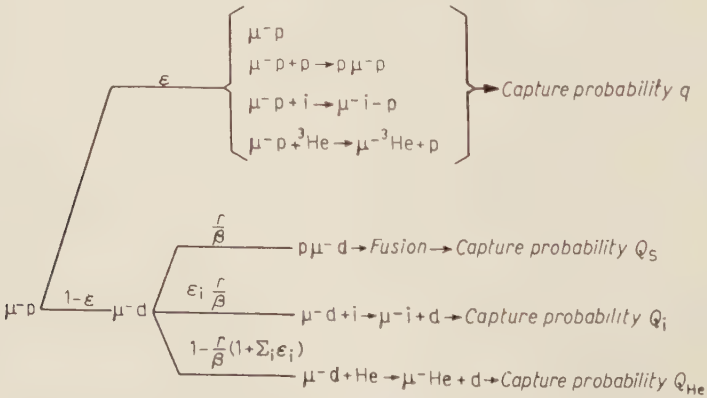

Fig. 8. – Processes related to capture probabilities (cf. eqs. (16-18) of the Appendix). Impurities other than ^{3}He are designated by « *i* ».

the hydrogen before and after the introduction of helium, but now we consider ^{3}He in concentration C_{He}: Referring to Fig. 8, we see that the following equations hold:

$$(\text{A-16}) \quad r_b = (1 - \varepsilon_b)\beta(1 + \sum_i \varepsilon_i)^{-1} ,$$

$$(\text{A-17}) \quad Q_b = (1 - \varepsilon_b) r_b \beta^{-1} [Q_s + \sum_i \varepsilon_i Q_i] + \varepsilon_b q_b ,$$

$$(\text{A-18}) \quad Q_a = (1 - \varepsilon_a) \{ r_a \beta^{-1} [Q_s + \sum_i \varepsilon_i Q_i] + [1 - r_a \beta^{-1} (1 + \sum_i \varepsilon_i)] Q_{\mathrm{He}} \} + \varepsilon_a q_a .$$

Straigtforward substitutions yield:

$$(\text{A-19}) \quad Q_{\mathrm{He}} = \frac{r_b}{r_b - r_a(1 - \varepsilon_b)} \left| Q_a - \frac{r_a}{r_b} Q_b + \varepsilon_a (Q_a - q_a) - \varepsilon_b \frac{r_a}{r_b} (Q_b - q_b) \right| .$$

This is identical with eq. (19*a*) except for correction terms of order

$$\varepsilon_b = (C_{\mathrm{D}} X_{\mathrm{pD}})^{-1} , \qquad \text{and} \qquad \varepsilon_a = (1 + C_{\mathrm{He}} X_{\mathrm{pHe}}) \varepsilon_b ;$$

remembering that q is the fraction of captures in the absence of deuterium, one sees that, unless primary transfer to impurities is large, the correction terms inside the bracket amount roughly to $\varepsilon_a Q_{\mathrm{He}}$.

Note the following points:

1) The form of the dependence of f_{D} on C_{D} is used only to estimate ε_b and ε_a, not to determine the main term of Q_{He}.

2) The effect of secondary transfer to impurities is completely eliminated: eq. (19) holds for all values of ε_i. Of course, the background due to secondary transfer to impurities must not be so high that $\sum_i \varepsilon_i Q_i \gg Q_{\mathrm{He}}$. HILDEBRAND has shown that it is possible, with conventional techniques, to fill a bubble chamber with hydrogen which is pure enough for this purpose ([18]).

([18]) R. H. HILDEBRAND: (private communication).

RIASSUNTO (*)

Si sono studiate le reazioni di trasferimento $(\mu^- \mathrm{H}) + \mathrm{X} \to (\mu^- \mathrm{X}) + \mathrm{H}$, dove H = p o d e X = Ne o He, osservando le variazioni delle frazioni dei μ^- soggetti a cattura nucleare o che catalizzano il processo di fusione $\mathrm{p} + \mathrm{d} \to {}^3\mathrm{He}$. In idrogeno privo di deuterio con combinazione di neon di $(105^{+50}_{-25}) \cdot 10^{-6}$, metà dei muoni passano al neon. Il trasferimento al neon ha frequenza tripla se l'idrogeno contiene abbastanza deuterio da saturare la reazione $(\mu^- \mathrm{p}) + \mathrm{d} \to (\mu^- \mathrm{d}) + \mathrm{p}$. Il trasferimento all'elio è almeno per due ordini di grandezze più lento di quello al neon. Si sono analizzate le stelle prodotte da μ^- e π^-. Non si è rivelato alcun trasferimento di π^-. Si discute l'effetto delle reazioni di trasferimento sulla misura della cattura di μ^- da parte dell'idrogeno. Si mostra come le reazioni di trasferimento si possono usare negli esperimenti di cattura dei μ^- da parte di isotopi separati del neon e forse anche del ^{3}He.

(*) *Traduzione a cura della Redazione.*

IL NUOVO CIMENTO Vol. XXII, N. 1 1° Ottobre 1961

Analyticity and Crossing for Partial Waves.

J. G. Taylor (*)

Rias - Baltimore, Md.

(ricevuto il 26 Giugno 1961)

Summary. — We prove that the use of crossing symmetry, analyticity, and unitarity, to determine partial wave amplitudes is valid for every order in perturbation theory. This is shown for the equal mass case. An approximation scheme is developed for evaluating the left-hand cut contribution to a partial wave dispersion relation, which should be more reliable then a Legendre polynomial expansion.

1. – Introduction.

It has been hoped (1) that the Mandelstam representation, together with crossing symmetry and unitarity, give a complete dynamical specification of all scattering processes. This hope will not be realizable when the Mandelstam representation is invalid. It has been shown (2) to be invalid in fourth order in perturbation theory for the « superanomalous » threshold case, in particular for π-d and Σ-Σ scattering. It has also been shown (3) to be invalid in sixth order due to the presence of acnodes, as in pΛ and π-Σ scattering. It may still be possible to write a two-dimensional representation which will be valid in such cases, but this does not seem easy. There is still the possibility that the Mandelstam representation is invalid for all processes, even for the equal mass case. Thus it is interesting to investigate what can be done, at

(*) On leave of absence from Christs College, Cambridge.

(1) S. Mandelstam: *Phys. Rev.*, **112**, 1344 (1958); G. F. Chew and S. Mandelstam: *Phys. Rev.*, **119**, 467 (1960).

(2) S. Mandelstam: *Phys. Rev.*, **115**, 1741 (1959).

(3) R. J. Eden, P. Landshoff, J. C.Polkinghorne and J. G. Taylor: Cambridge University preprint (March, 1961).

present, to replace the property of analyticity given by the Mandelstam representation in the complete dynamical programme by something with more possibility of validity for all scattering processes.

Pion-pion scattering is the only process for which the CAU programme (the use of crossing, analyticity and unitarity to determine the scattering amplitude) has been pursued with any hope of obtaining the low energy phase shifts in terms of a small number of arbitrary parameters; it is certainly the most fundamental in the CAU programme. As a part of our more complete investigation we would like to consider the validity in perturbation theory of the use of crossing, analyticity and unitarity made to obtain ([1]) the $I=J=1$ pion-pion resonance which has recently been unambiguously observed ([5]) at 760 MeV. We will be able to do this if we can show that the properties used to obtain this resonance were weaker than the Mandelstam representation. This was indeed the case, where the analyticity assumed was only that each partial wave is analytic in a cut energy plane. It is of interest to discuss the analyticity of partial wave amplitudes in perturbation theory, and to see if such analyticity will be strong enough to give a complete dynamical specification of a scattering process when combined with analyticity and unitarity. We wish to investigate briefly, then, in this paper the following three questions:

i) Are the partial wave amplitudes analytic in a cut plane to every order in perturbation theory?

ii) Is the derivation of the $I=J=1$ resonance by BRANSDEN and MOFFAT ([4]) justifiable?

iii) Do the properties of crossing, reduced analyticity (of partial wave amplitudes) and unitarity give a complete dynamical specification of scattering processes (the reduced CAU or CRAU programme)?

Our answer to the first question is yes, at least for the equal mass case, as discussed in Section 2. It does not seem possible to extend the simple method we use there to the unequal mass case. However, we expect the property to be more universal than the Mandelstam representation, since in the super-anomalous threshold case the partial wave amplitudes are still ([6]) analytic in a cut plane in the fourth order box diagram in perturbation theory, whereas this diagram has complex singularities invalidating the Mandelstam representation. Further the sixth order diagram which has an acnode has analytic partial wave amplitudes ([3]). Thus we conjecture that all partial wave

([4]) B. BRANSDEN and J. MOFFAT: *Phys. Rev. Lett.*, **6**, 708 (1961).

([5]) A. R. ERWIN, R. MARCH, W.D. WALKER and E. WEST: *Phys. Rev. Lett.*, **6**, 628 (1961).

([6]) J. G. TAYLOR and A. E. WARBURTON: *Phys. Rev.*, **120**, 1506 (1960).

amplitudes are analytic for all processes, and we are certain that our conjecture has a larger range of validity in the low energy region than the Mandelstam representation. In other words the complex singularities causing trouble in the partial waves will be farther away from the low energy region than in the complete scattering amplitude.

In order to answer the second question it is necessary to show that crossing symmetry can be used independently of the Mandelstam representation. This we show in Section 3. Thus we obtain a justification of the coupled S and P wave pion-pion equations to every order in perturbation theory, and also of their use by BRANSDEN and MOFFAT [4] to obtain the $I=J=1$ pion-pion resonance.

In order to answer our third question, we have to obtain a method of continuing the absorptive part of the complete scattering amplitude to values of the cosine of the scattering angle less than -1. This problem is evidently not easy since it would require an infinite number of partial waves to achieve this continuation correctly. We discuss in Section 4, an approximate method for achieving this continuation which may be reasonable in the energy region expected to be covered by a given set of partial waves. We discuss the method explicitly for the equal mass case, leaving more detailed applications to other publications. Our discussion indicates that the solution of the CRAU programme should be a reasonably accurate representation of the phase shifts of a given set of angular momentum states. This will be true in the energy range for which the two-particle approximation to the unitarity condition is good. The extension of the CRAU programme to take into account inelastic processes in the unitarity condition is not discussed here.

2. – Analyticity of partial wave amplitudes.

To prove that each partial wave is analytic in a cut plane we use the notation and results of reference [7]. The n-th order term in perturbation theory may be written as an integral over Feynman parameters in the form

$$M(s_1, s_2) = \int \mathrm{d}\alpha_1 \ldots \mathrm{d}\alpha_n \, \delta\Big(1 - \sum_{ii} \alpha\Big) D^{-m}, \tag{1}$$

where the denominator function D is a linear function of the energy s_1 and the momentum transfer s_2

$$D(s_1, s_2, \alpha) = s_1 \cdot f_1(\alpha) + s_2 \cdot f_2(\alpha) - K_{12}(\alpha), \tag{2}$$

[7] R. J. EDEN: *Phys. Rev.*, **119**, 1763 (1960).

where f_1, f_2 and K_{12} are functions of the parameters $\alpha_1, \ldots, \alpha_n$. We will use the property that D is negative for any values of $\alpha_1 \ldots \alpha_n$ in the region of integration of (1) when (s_1, s_2) belongs to the region Δ: $0 < s_1 < 4m^2$, $0 < s_2 < 4m^2$, $s_1 + s_2 < 4m^2$, and also that $D(4m^2, 0, \alpha) < 0$.

In the center of mass system for channel 1, with energy s_1 and scattering angle θ we have

$$s_2 = \tfrac{1}{2}(\cos\theta - 1)(s_1 - 4m^2) \tag{3}$$

so

$$D(s_1, \cos\theta, \alpha) = s_1[f_1 + \tfrac{1}{2}(\cos\theta - 1)f_2] + 2m^2(1 - \cos\theta) f_2 - K_{12} . \tag{4}$$

We consider the l-th partial wave amplitude

$$M_l(s_1) = \int_{-1}^{+1} p_l(\cos\theta)\, M(s_1, \cos\theta) . \tag{5}$$

We wish to show that $M_l(s_1)$ is analytic in a cut plane with cut from $-\infty$ to 0 and from $4m^2$ to ∞. We will do this in three stages:

a) We first show that $M_l(z)$ is analytic in z when $\operatorname{Im} z \neq 0$. This will be so if $D(z, \cos\theta, \alpha) \neq 0$ for $-1 \leqslant \cos\theta \leqslant +1$ and all α in the range of integration. Suppose that $D(z, \cos\theta, \alpha) = 0$ for some $\cos\theta$ and α in the interesting range. Then

$$\operatorname{Im} D(z, \cos\theta, \alpha) = \operatorname{Im} z[f_1 + \tfrac{1}{2}(\cos\theta - 1) f_2] = 0$$

so

$$f_1 + \tfrac{1}{2}(\cos\theta - 1) f_2 = 0 . \tag{6}$$

Then

$$\operatorname{Re} D(z, \cos\theta, \alpha) = 2m^2(1 - \cos\theta) f_2 - K_{12} . \tag{7}$$

If $\cos\theta \neq \pm 1$ then we use eq. (6) in (7) to obtain

$$\operatorname{Re} D(z, \cos\theta, \alpha) = m^2(1 - \cos\theta) f_2 + 2m^2 f_1 - K_{12} < 0$$

since the point $s_1 = 2m^2$, $s_2 = m^2(1 - \cos\theta)$ belongs to Δ. If $\cos\theta = +1$ then from (6), $f_1 = 0$ and $\operatorname{Re} D = -K_{12} < 0$. If $\cos\theta = -1$ then $f_1 = f_2$ and $\operatorname{Re} D = 4m^2 f_1 - K_{12} < 0$. Hence $M_l(z)$ is analytic for $\operatorname{Im} z \neq 0$.

b) We next show that $\lim_{\varepsilon \to 0_+} M_l(s_1 + i\varepsilon) = M_l(s_1)$ if $s_1 > 4m^2$, where $M_l(s_1)$ is defined by eq. (1) and (5), and in (1) the denominator $D(s_1 s_2 \alpha)$ is furnished

with $+i\varepsilon$ by the Feynman prescription. We let $g(\alpha, \cos\theta) = f_1(\alpha) + \frac{1}{2}(\cos\theta - 1) f_2(\alpha)$. That part of $M_l(s_1 + i\varepsilon)$ for which the range of variables α and $\cos\theta$ have $g \geqslant 0$ will have the same boundary value as $\varepsilon \to 0$ as for the physical partial wave amplitude $M_l(s_1)$, so it will be necessary to discuss only the case $g \leqslant 0$. For this case, since $(s_1 - 4m^2) \geqslant 0$, then

$$D = (s_1 - 4m^2)g + 4m^2 f_1 - K_{12} \leqslant 4m^2 f_1 - K_{12} < 0 .$$

Hence the function $M_l(z)$ obtained by the result *a*) has the correct boundary value on the upper side of the line $s_1 > 4m^2$. We also have $M_l(s_1 - i\varepsilon) = M_l(s_1)$ if $s_1 < 0$, since this limit is valid for the region of $\cos(\theta, \alpha)$ with $g < 0$, and for $g \geqslant 0$ we have $D = s_1 g + 2m^2(1 - \cos\theta) f_2 - K_{12} \leqslant m^2(1 - \cos\theta) f_2 - K_{12} < 0$ for $-1 \leqslant \cos\theta \leqslant +1$.

c) Finally we show that the cut along the real axis is from $-\infty$ to 0 amd $4m^2$ to ∞ for $M_l(s_1)$. We know that the cut is at least along these intervals since $M_l(s_1)$ has a non-zero absorptive partt here (unless special selection rules hold). For $0 < s_1 < 4m^2$ we wish to show that D is negative, so that $M_l(s_1)$ is analytic in this region. The point s_1, $s_2 = \frac{1}{2}(\cos\theta - 1)(s_1 - 4m^2)$ belongs to D if $-1 < \cos\theta \leqslant +1$, so D is negative. Also if $\cos\theta = -1$, then $s_3 = 4m^2 - s_1 - s_2 = 0$, since we may write

$$D = s_1 f_1 + s_3 f_3 - K_{13} , \quad \text{then} \quad D(s_1 = s,\ s_3 = 0,\ \alpha) = s f_1 - K_{13} < 0 ,$$

by eq. (8-40) of reference (7).

Hence $M_l(s)$ is analytic for $0 < s < 4m^2$.

Thus we have proved that in every order of perturbation theory each partial wave amplitude is analytic in the cut energy plane. We would like to extend the above proof to the general mass case. One of the main difficulties involved in doing this is of an algebraic nature in the relations between the kinematical variables. This complicated relationship gives rise to singularities in the complex energy plane for partial wave amplitudes, usually on a circle determined from the kinematics of the theory, so that the energy no longer seems a suitable variable to use. In any case the singularities of $M_l(s)$ are given from the general perturbation diagram by either *a*) $\cos\theta = \pm 1$, and the integral over the Feynman parameters has a singularity in energy, or *b*) there is a singularity in the α integration whose position (which may be complex) depends only on the energy (which also may be complex). It is known that for several physical processes the forward scattering amplitude is analytic in a cut plane independently of perturbation theory. However, it has not been possible to derive the same analyticity for the backward scattering amplitude.

We will not discuss this situation in general any further here, except to remark that analyticity of partial waves will be more general than the Mandelstam representation. This has been shown for the 4-th order superanomalous case of π-d and Σ-Σ scattering and 6-th order p-Λ and π-Σ scattering, for both of which the Mandelstam representation is invalid, though the partial waves are analytic. Thus our conjecture of analytic partial waves has no known counter-examples.

3. – Crossing symmetry.

The coupled S and P waves of the CAU programme used by BRANSDEN and MOFFAT [4] to obtain the $I=J=1$ $\pi\pi$ resonance were derived assuming analyticity of the partial waves, unitarity, and crossing symmetry. We have shown in the last section that the partial waves are analytic in a cut plane, at least in perturbation theory, independently of the validity of the Mandelstam representation. Unitarity is a property independent of the Mandelstam representation. Thus in order to ensure that the coupled $\pi\pi$ equations are above suspicion, we must determine whether or not we may use crossing symmetry without the Mandelstam representation. The crossing equation takes the form

$$M(s_1, s_2) = M(s_2, s_1)\,, \tag{8}$$

where we are considering neutral mesons for simplicity (the other two crossing equations for charged pions only give restrictions on the partial waves entering the various isotopic spin amplitudes). To give meaning to eq. (8) we must ensure that M is defined for the relevant values of s_1 and s_2. This is so to all orders in perturbation theory in the Euclidean region Δ of the last section, since M is analytic in both variables there. In particular crossing will have meaning in a neighborhood of the symmetry point $s_1 = s_2 = s_3 = +\frac{4}{3}$, so justifying the use of derivative conditions at the symmetry point derived from eq. (8) to reduce the number of free parameters entering the solutions of the coupled S and P wave equations.

We also need to use (8) outside the Euclidean region, and in particular for $s_1 = 4(\nu+1)$, $s_2 = -2\nu(1-\cos\theta)$ with $\nu = q^2 < -1$ and $|\cos\theta| < 1$, where q and θ are the momentum and scattering angle in the centre of mass. We will assume here that it is possible to continue M by some means out of Δ to such values of the variables. The exact form of continuation necessary for the π-π problem is as follows. For $\nu > 0$ we may write the imaginary part of M as a sum of contributions from the channels with s_2, s_3 as energy, then use crossing symmetry, and write finally $\mathrm{Im}\, M(\nu, \cos\theta) = 2\,\mathrm{Im}\, M^{(1)}(\nu_c, \cos\theta_c)$. $\mathrm{Im}\, M^{(1)}(\nu_c, \cos\theta_c)$ is the continuation of the absorptive part of channel 1 to

the relevant values of its variables, and

$$(9) \qquad \nu_c = \frac{\nu}{2}(1+\cos\theta) - (\nu+1)\,, \qquad \nu_c \cos\theta_c = \frac{\nu}{2}(1+\cos\theta) + (\nu+1)\,.$$

We project out the l-th partial wave, and writing the integration variable as ν', we obtain

$$(10) \quad \mathrm{Im}\, M_l(\nu) = -\frac{4}{\nu}\int_0^{-\nu-1} \mathrm{d}\nu'\, \mathrm{Im}\, M\left(\nu', 1+2\left(\frac{\nu+1}{\nu'}\right)\right) P_l\left(1+2\left(\frac{\nu'+1}{\nu}\right)\right).$$

We use this equation for $\nu < 0$.

This is the other use of crossing in the π-π problem, determining the discontinuity on the left hand cut for each partial amplitude as an integral over physical energies of the scattering amplitude. In order to be able to use (10) we need to be able to define a continuation in $\cos\theta$ of $M(\nu, \cos\theta)$ for each $\nu > 0$, from the physical $\cos\theta$ region to $\cos\theta \leqslant -1$. In general we need that $\mathrm{Im}\, M(\nu', \cos\theta)$ is analytic in $\cos\theta$ when $\cos\theta = 1 - 2\big((\nu+1)/\nu'\big)$, when ν is fixed less than -1, $0 \leqslant \nu' \leqslant -\nu-1$. The region of analyticity is a strip along the negative real axis with a branch point at

$$\cos\theta = +\left\{1 + 4(\nu+1)/\left[1-\nu+\sqrt{(\nu+1)(\nu+9)}\right]\right\}$$

and including the physical region. This will then allow sense to be made of eq. (10), at least in principle. Under the assumption that only a finite number of partial waves are important, as was made in the $\pi\pi$ problem keeping only S and P waves, the continuation is easily made by a Legendre expansion in $\cos\theta$. Thus we have completely justified the use of crossing symmetry made in deriving the $\pi\pi$ solutions in this way.

We only expect the continuation made in this manner to be reasonable for low energies, $\nu \leqslant 10$, say, since for $\nu < -9$ the Legendre expansion used on the right hand side of (10) diverges. There is evidently an important practical problem to overcome if one attempts to use (10) without using the double spectral functions to do the continuation of M in $\cos\theta$. We discuss this in the next section, where a possible approach to this problem is given which avoids explicit use of the double spectral functions.

4. – Continuation in $\cos\theta$.

To achieve an approximate continuation in $\cos\theta$, we will first consider the region of analyticity in $\cos\theta$ required for $\mathrm{Im}\, M(\nu', \cos\theta)$ entering on the right-hand side of (10). We have $\cos\theta = 1 + 2\big((\nu+1)/\nu'\big)$, and we may con-

sider $\mathrm{Im}\, M(\nu', \cos\theta)$ as a function of the single variable ν' or $\cos\theta$ when ν is fixed. The invariant variables are $s_1 = 4(\nu'+1)$, $s_2 = 4(\nu+1)$, $s_3 = -4\nu - s_1$. We will use the boundary of the region of non-vanishing of the double spectral functions to obtain the expected region of singularity. We note that this region can be arrived at from perturbation diagrams. Then the first singularity in $\cos\theta$ as it becomes more negative than -1 is a branch point at $\cos\theta = -a(\nu) = +\left\{1+4(\nu+1)/\left[1-\sqrt{(\nu+1)(\nu+9)}\right]\right\}$, with a cut away from the physical region $|\cos\theta| \leqslant 1$. To make sense of the right hand side of (10) we will need that $\mathrm{Im}\, M(\nu', \cos\theta)$ for each fixed $\nu < -1$ and with $\cos\theta = 1 + 2((\nu+1)/\nu')$, is analytic in a strip in the $\cos\theta$ plane which includes the physical region, which extends from this region along the negative real axis, surrounds the branch cut starting at $\cos\theta = -a(\nu)$. Such analyticity will certainly be much weaker than the Mandelstam representation, which requires analyticity in a cut plane in $\cos\theta$. We will assume that this « strip » analyticity is valid, so making sense of crossing, as we saw in the last section.

In order to achieve this continuation approximately, we consider the mapping $\omega = [(\cos\theta + a(\nu))^{\frac{1}{2}} - b]^{-1}$. The cut $\cos\theta \leqslant -a(\nu)$ maps into the circle $|\omega + (1/2b)| = 1/b$ in the ω-plane. We then replace the function on the circle by a pole at an internal point of the circle whose position we will fix later. The pole approximation will be best when the circle is as far away from the physical region as possible. For then the circle of singularities will have the best chance of being well approximated by a pole, as viewed from the physical region. We choose $b = \sqrt{a(\nu) - 1}$, since then the physical region $-1 \leqslant \cos\theta \leqslant +1$ is mapped into $\left[\sqrt{a(\nu)+1} - \sqrt{a(\nu)-1}\right]^{-1} \leqslant \omega \leqslant +\infty$, with $\cos\theta = -1$ going into $\omega = +\infty$. Evidently the backward region is farthest away from the circle, so our pole approximation should be most satisfactory there.

We do not attempt to use this pole approximation for all partial waves. Let us suppose we wish to obtain a solution of the CRAU programme for a range of ν up to some maximum energy. We suppose that only partial waves up to the L-th are important in this energy range. Then we may write down a set of dispersion relations for, say, the inverse partial wave amplitudes, expressing each inverse amplitude as an integral over a right-hand cut with known discontinuity (by unitarity), and over a left-hand cut. The discontinuity on the left-hand cut is determined by eq. (10). To evaluate the right-hand side of (10) we expand $\mathrm{Im}\, M(\nu', \cos\theta)$ as a sum of the first L partial waves plus a remainder. The remainder is taken to be given by the pole $\Gamma/(\omega - \lambda)$, after the first L partial waves have been projected out. Thus we take, for a given $\nu < -1$,

$$\mathrm{Im}\, M(\nu', \cos\theta) = \sum_{l=0}^{L-1} \mathrm{Im}\, M_l(\nu') P_l(\cos\theta) + N(\nu'; \cos\theta)\,,$$

with

$$N(\nu', \cos\theta) = \frac{\Gamma}{[\omega(\cos\theta) - \lambda]} - \sum_{l=0}^{L-1} \int_{-1}^{+1} \mathrm{d}x P_l(x) \frac{\Gamma}{\omega(x) - \lambda},$$

where $\omega(x) = \left[(x + a(\nu))^{\frac{1}{2}} - b\right]^{-1}$. Thus we obtain a set of coupled integral equations for the functions $M_l(\nu)$, for $0 < l < L$, with solutions which depend on Γ and λ.

We expect that the pole replacement takes account of the effect of the partial waves with $l \geqslant L$ more accurately than if they were neglected. These higher partial waves have been taken account of, though at the expense of introducing two further parameters, Γ and λ. We don't expect to be able to obtain these parameters from crossing conditions applied to the first L partial waves, since we expect that Γ and λ will not depend very sensitively on them. We may obtain all the partial waves with $l \geqslant L$ in terms of crossing, analyticity and unitarity, since now the left-hand cut discontinuity for each partial wave with $l \geqslant L$ is given uniquely in terms of the lower partial waves, Γ and λ. We may now apply crossing to the $(L+1)$-st partial wave (in terms of derivative conditions at the symmetry point), and hope to obtain values for Γ and λ which will not generate important values of phase shifts δ_l in the region $\nu \leqslant \nu_0$, if $l \geqslant L$.

We can at most hope that this method of continuation is a reasonably effective phenomenological method to obtain phase shifts for the first few partial wave amplitudes. It is of interest to see if the method when applied to the $\pi\pi$ problem, will give a result similar to that obtained by neglecting all except the S and P waves in the expansion in (11).

To check the goodness of the pole replacement it may be necessary to see if the use of two poles (with further derivative conditions at the symmetry point) alters appreciably the results obtained with a single pole. It is to be expected that if values of the energy above $\nu \sim 30$ are to be considered then more than one pole will be required to replace the circle contribution. This is due to the fact that the value of the radius $(1/b)$ of the circle in the ω-plane tends to infinity as the value of ν entering the crossing eq. (10) tends negatively to infinity.

Thus our answer to question iii) of the introduction is that the CRAU programme is soluble, in principle, by the pole approximation method. That this method will prove of value can only be decided by further work.

* * *

The author would like to thank J. Moffat for interesting discussions and W. W. Bender, Director of RIAS, for the hospitality of the Institute while this work was carried out.

RIASSUNTO (*)

Proviamo che l'uso della simmetria incrociata, dell'analiticità e dell'unitarietà, per determinare le ampiezze d'onda parziali è valida in ogni ordine nella teoria della perturbazione. Questo viene dimostrato per il caso di masse eguali. Sviluppiamo uno schema di approssimazioni per valutare il contributo del taglio a sinistra alle relazioni di dispersione dell'onda parziale, che dovrebbe essere più attendibile di uno sviluppo in polinomi di Legendre.

(*) *Traduzione a cura della Redazione.*

IL NUOVO CIMENTO Vol. XXII, N. 1 1° Ottobre 1961

On the Existence of Solutions of the Pion-Pion Dispersion Equations – II.

C. Lovelace

Department of Physics, Imperial College - London

(ricevuto il 28 Giugno 1961)

Summary. — The Shirkov equations are shown to be consistent without a cut-off, unlike the Chew-Mandelstam equations. Their asymptotic behaviour at high energies can be determined exactly. This can be used to make predictions about the signs of the various partial waves, and in some cases about the existence of resonances. The behaviour at infinity is always of Gribov type, even with a P-wave resonance.

1. – Introduction.

In previous work (1) we showed that the Chew-Mandelstam equations for pion-pion scattering have no exact solutions (except, possibly, solutions oscillating at infinity) unless the imaginary part of the P-wave is taken to vanish. This result arose as follows: By unitarity, $\mathrm{Re}\, A_l^I(+\infty)$ and $\mathrm{Im}\, A_l^I(+\infty)$ must be finite. We make the physically reasonable assumption that they go to constants at infinity, and do not oscillate. The partial wave dispersion relation then implies that $\mathrm{Re}\, A_l^I(+\infty)$ cannot be finite unless

$$\mathrm{Im}\, A_l^I(-\infty) = \mathrm{Im}\, A_l^I(+\infty)\,. \tag{1.1}$$

This also follows from a general theorem given recently by Sugawara and Kanazawa (2). Now $\mathrm{Im}\, A_l^I(-\infty)$ can be calculated in terms of $\mathrm{Im}\, A_l^I(\nu)$ in

(1) C. Lovelace: *Nuovo Cimento*, **21**, 305 (1961).

(2) M. Sugawara and A. Kanazawa: *Subtractions in Dispersion Relations*, Purdue preprint (1961).

the physical region by the Chew-Mandelstam crossing relations and a theorem on Cesáro limits. We found that (1) could not be satisfied, unless the imaginary part of the P-wave vanished throughout the physical region.

In the Chew-Mandelstam equations, only the S and P waves are assumed to have imaginary parts, but the real parts of all the higher partial waves are included. Another set of equations has been proposed by SHIRKOV and others ([3,4]), in which the real parts of all but a finite number of partial waves are also neglected. For these equations, (1.1) merely implies that

$$\text{Im}\, A_l^I(\infty) = 0 \,. \tag{1.2}$$

and does not lead to any inconsistency. The same happens for the Chew-Mandelstam equations, when only the S-waves are assumed to have imaginary parts.

In these cases, the points $= \infty$ can be shown to form a closed system, independent of what happens elsewhere. Because of this, the asymptotic behaviour is determined by algebraic equations of a quite simple kind, which can be solved exactly. A typical result is

$$\left.\begin{aligned} &\sqrt{\frac{\nu}{\nu+1}}\,\text{ctg}\,\delta_0^0(\nu) \approx 1.4730\,(\ln \nu/\pi)\,, \\ &\sqrt{\frac{\nu}{\nu+1}}\,\text{ctg}\,\delta_1^1(\nu) \approx -\,22.837\,3(\ln \nu/\pi)\,, \\ &\sqrt{\frac{\nu}{\nu+1}}\,\text{ctg}\,\delta_0^2(\nu) \approx 4.810\,2(\ln \nu/\pi)\,, \end{aligned}\right\} \quad \text{as } \nu \to \infty\,. \tag{1.3}$$

This is the asymptotic behaviour of the equations given by HO, HSIEN and ZOELLNER ([4]), including the imaginary parts of the S and P waves and the real parts of the S, P, D and F waves.

The exact asymptotic behaviour (1.3) shows by its existence that the Shirkov equations do not require a cut-off. One might suppose that, apart from this, it would be rather useless, since the Shirkov equations are not accurate at high energies. However, this is not so, for we can use our knowledge of their high-energy behaviour to make low-energy predictions.

We see from (1.3) that the P-wave is negative at high energies. Therefore it must either be repulsive at all energies or else resonant, according to the

([3]) A. V. EFREMOV, M. G. MESHCHERYAKOV, D. V. SHIRKOV and H. Y. TZU: *Nucl. Phys.*, **22**, 202 (1961).

([4]) HSIEN DING-CHANG, HO TSO-HSIU and W. ZÖLLNER: *Žurn. Èksp. Teor. Fiz.*, **39**, 1668 (1960).

Shirkov equations. For the S-waves we can say still more, for we can use the coupling constant to determine the signs at threshold. The Chew-Mandelstam equations give

$$A_0^0(-\tfrac{2}{3}) \approx -5\lambda\,, \qquad A_2^0(-\tfrac{2}{3}) \approx -2\lambda\,, \tag{1.4}$$

neglecting all but S and P waves. At these low energies the Shirkov equations will differ little from the Chew-Mandelstam ones, so that (1.4) should at least have the same sign. Now the S-waves will only change sign between $\nu = -\frac{2}{3}$ and threshold if there is a bound state, or a Castillejo-Dalitz-Dyson (CDD) zero [5] below threshold. The former does not occur, and we can assume that the latter does not. Both S-wave scattering lengths will then have the opposite sign to λ. Also, by (13), both S-waves are positive at high energies. Therefore if λ is positive both S-waves will be resonant. Two resonances in the same partial wave seem rather unlikely, so we can conclude that, if λ is negative, a bound state or CDD zero will be needed to make either S-wave resonant. Both these conclusions about the S-waves are realized in the S-dominant solutions of Chew, Mandelstam and Noyes [6]. The behaviour of the P-wave, however, is quite different in the latter.

It is well known that

$$A_l^I(\nu) \sim \nu^l\,, \qquad \text{as } \nu \to 0. \tag{1.5}$$

The Shirkov crossing relations, (2.5), therefore give

$$A_1^1(-1) = (-2a_0 + 5a_2)/18\,, \tag{1.6}$$

where $a_{0,2}$ are the S-wave scattering lengths. By (1.5), A_1^1 must have a simple zero at $\nu = 0$. If there are no bound states or CDD zeros below threshold, the sign of the P-wave just above threshold will therefore be opposite to (1.6). Thus we have the conclusion: If the S-wave scattering lengths satisfy

$$2a_0 > 5a_2\,, \tag{1.7}$$

there will be a P-wave resonance, if

$$2a_0 < 5a_2\,, \tag{1.8}$$

the P-wave will be repulsive unless there is a CDD zero.

[5] L. Castillejo, R. H. Dalitz and F. J. Dyson: *Phys. Rev.*, **101**, 453 (1956).
[6] G. F. Chew, S. Mandelstam and H. P. Noyes: *Phys. Rev.*, **119**, 478 (1960).

Some other conclusions may be drawn from (1.3). We see that the high energy behaviour is independent of the coupling constant, except when the latter vanishes. The limits $\lambda \to 0$ and $\nu \to \infty$ are not interchangeable. If one expands in a perturbation series, the terms behave asymptotically like $\lambda(\lambda \ln \nu)^n$, so that the coupling always becomes strong at high energies. This is in general agreement with what had been predicted by the methods of the renormalization group. In each order of the perturbation expansion, one subtraction will be necessary. However, the dispersion integrals for the exact solution will converge without subtractions. Thus we have the opposite situation from the Chew-Mandelstam equations [1]—the exact solution behaves better than any order of perturbation theory.

The asymptotic behaviour (1.3) is also independent of the presence of CDD zeros [5]. Therefore, if the « normal » solution of the Shirkov equations was unable to give a P-wave resonance, it should be possible to introduce one as a new elementary particle. The corresponding CDD zero in the P-wave would not give rise to any subtraction difficulties. We have seen that the P-wave will be repulsive at high energies. Now a Castillejo-Dalitz-Dyson zero against a repulsive background would result in a resonance of a very peculiar shape. It could not be fitted by a normal resonance formula. This might, perhaps, explain some of the conflicting evidence about the pion-pion interaction.

The asymptotic behaviour (1.3) will no longer hold if there are CDD zeros at infinity, corresponding to the addition of terms like $\alpha_l \nu$ or $\beta_l \nu^2$ to $1/A_l^l$. Very recently Efremov, Tzu and Shirkov [7] have indicated a connection between these and unrenormalizable interactions in perturbation theory. However solutions of this type suffer from one grave disadvantage—they vanish at infinity at least as fast as ν^{-2}. (The example considered by Efremov, Tzu and Shirkov goes like ν^{-4}.) This seems in plain contradiction with experiment. For this reason we don't consider such solutions to be promising as far as strong interactions are concerned, though they may be very important for weak interactions.

If one neglects the crossing term, the asymptotic behaviour is

$$\sqrt{\frac{\nu}{\nu+1}} \operatorname{ctg} \delta^1(\nu) \approx (\ln \nu/\pi) , \qquad \text{as} \qquad \nu \to \infty , \tag{1.9}$$

in all cases. Eq. (1.3) thus shows that the contribution of the crossing term to $1/A_1^1(\nu)$ at high energies is nearly 24 times larger than the contribution of the direct term. The validity of the pole approximation for the P-wave therefore

---

[7] A. V. Efremov, H. Y. Tzu and D. V. Shirkov: *The neutral model for the investigation of the pion-pion scattering*, Dubna preprint (1961).

seems doubtful. Also, when solving the Shirkov equations by an iterative method, it will be necessary to put the correct asymptotic behaviour of the P-wave into the trial solution. Starting from the solution without crossing term, one could not expect convergence.

If the crossing term is omitted in the Chew-Low equations, the cut-off must be increased by a factor of 2.5 to maintain the correct position of the (3, 3) resonance. We have seen that for relativistic equations of the Shirkov type, the P-wave is even more sensitive to the crossing term. Preliminary investigations indicate that this may be a general feature for all processes. Now it is known ([8]) that, if the crossing term is omitted in the relativistic $\pi.N$ theory, a (3, 3) resonance is obtained at 10 MeV, instead of the experimental 195 MeV. There is therefore some hope that the Shirkov equations may improve this.

In Section **2** we give some formulae relating to the Shirkov equations which we shall need. In Section **3** we investigate the asymptotic behaviour of the Shirkov equations. Our main results are that consistent equations can be obtained without introducing either the double spectral functions or a cut-off, and that these equations show no connection between the existence of a P-wave resonance and the behaviour at infinity. In the light of these two papers, certain lines of work look more promising than before, and others less. In Section **4** we discuss this.

2. – The Shirkov equation.

For forward scattering, the crossing relations take a particularly simple form. For pion-pion scattering they are

$$\text{(2.1)} \qquad \begin{cases} A^0(-\nu-1,\,1) = [\tfrac{1}{3}A^0(\nu,1) - A^1(\nu,1) + \tfrac{5}{3}A^2(\nu,1)]^*\,, \\ A^1(-\nu-1,\,1) = [-\tfrac{1}{3}A^0(\nu,1) + \tfrac{1}{2}A^1(\nu,1) + \tfrac{5}{6}A^2(\nu,1)]^*\,, \\ A^2(-\nu-1,\,1) = [\tfrac{1}{3}A^0(\nu,1) + \tfrac{1}{2}\,A^1(\nu,1) + \tfrac{1}{6}A^2(\nu,1)]^* \end{cases}$$

Here A^I is the amplitude with isotopic spin $I = 0$, 1 or 2, and ν is the square of the centre-of-mass momentum of either pion. The other variable is $\cos\vartheta$, the cosine of the centre-of-mass scattering angle.

([8]) S. Frautschi and J. Walecka: *Phys. Rev.*, **120**, 1486 (1960).

The expansion in partial waves is given by

$$A^I(\nu, \cos\vartheta) = \sum_{l=0}^{\infty} (2l+1) P_l(\cos\vartheta) A_l^I(\nu) . \tag{2.2}$$

For I even, only even values of l contribute, for I odd l must also be odd. These partial waves satisfy the unitarity condition

$$\mathrm{Im}\,[1/A_l^I(\nu)] = -\sqrt{\frac{\nu}{\nu+1}}, \qquad \nu \geqslant 0 . \tag{2.3}$$

Now suppose that all except the S and P waves are so small that we may neglect them entirely. (2.2) then gives for forward scattering

$$A^0(\nu, 1) \approx A_0^0(\nu) , \quad A^1(\nu, 1) \approx 3A_1^1(\nu) , \quad A^2(\nu, 1) \approx A_2^0(\nu) . \tag{2.4}$$

Substituting this into (2.1), we have the Shirkov crossing relations [3]

$$A_{0,1}^I(-\nu-1) = \sum_{I'} A_{II'}[A_{0,1}^{I'}(\nu)]^* , \tag{2.5}$$

where

$$A_{II'} = \begin{pmatrix} \frac{1}{3} & -3 & \frac{5}{3} \\ -\frac{1}{9} & \frac{1}{2} & \frac{5}{18} \\ \frac{1}{3} & \frac{3}{2} & \frac{1}{6} \end{pmatrix} . \tag{2.6}$$

These enable the imaginary parts on the left hand cut to be determined, and thus complete the dynamical scheme of dispersion relations and unitarity.

We find from (2.5) that two independent combinations of the A's,

$$A_0^0 - 6A_1^1 , \qquad \text{and} \qquad 3A_1^1 + A_2^2 , \tag{2.7}$$

are even under the interchange $\nu \to -1-\nu^*$, and one,

$$2A_0^0 + 9A_1^1 - 5A_0^2 , \tag{2.8}$$

is odd under this interchange.

In the Shirkov equations both the real and imaginary parts of the higher partial waves are neglected, as against the Chew-Mandelstam equations where only the imaginary parts are neglected. We can, however, include the real parts of a finite number of higher partial waves within the Shirkov scheme. This is done by considering the crossing relations for derivative forward scat-

tering, as well as those for forward scattering itself. Including the real parts of the D and F waves gives the crossing relations [4]

$$
\left\{
\begin{aligned}
&\operatorname{Im} A_0^0(-\nu-1) = -\frac{1}{3}\left[\operatorname{Im} A_0^0(\nu) - \left(12 - \frac{3}{\nu}\right)\operatorname{Im} A_1^1(\nu) + 5 \operatorname{Im} A_0^2(\nu)\right] + \\
&\qquad + \left(\frac{\nu+1}{18}\right)\frac{\mathrm{d}}{\mathrm{d}\nu}\left[\operatorname{Im} A_0^0(\nu) - 9 \operatorname{Im} A_1^1(\nu) + 5 \operatorname{Im} A_2^0(\nu)\right], \\
&\operatorname{Im} A_1^1(-\nu-1) = -\frac{1}{15}\left[-2 \operatorname{Im} A_0^0(\nu) + \frac{1}{2}\left(21 + \frac{3}{\nu}\right)\operatorname{Im} A_1^1(\nu) + 5 \operatorname{Im} A_0^2(\nu)\right] + \\
&\qquad + \left(\frac{\nu+1}{180}\right)\frac{\mathrm{d}}{\mathrm{d}\nu}\left[-2 \operatorname{Im} A_0^0(\nu) + 9 \operatorname{Im} A_1^1(\nu) + 5 \operatorname{Im} A_0^2(\nu)\right], \\
&\operatorname{Im} A_0^2(-\nu-1) = -\frac{1}{6}\left[2 \operatorname{Im} A_0^0(\nu) + \left(12 + \frac{3}{\nu}\right)\operatorname{Im} A_1^1(\nu) + \operatorname{Im} A_0^2(\nu)\right] + \\
&\qquad + \left(\frac{\nu+1}{36}\right)\frac{\mathrm{d}}{\mathrm{d}\nu}\left[2 \operatorname{Im} A_0^0(\nu) + 9 \operatorname{Im} A_1^1(\nu) + \operatorname{Im} A_0^2(\nu)\right], \\
&\qquad\qquad \text{for} \quad \nu \geqslant 0 .
\end{aligned}
\right. \tag{2.9}
$$

For the Shirkov equations with S and P waves only, the real parts, as well as the imaginary parts, satisfy simple crossing relations (2.5). This is no longer so if the real parts of the D and F waves are included, nor if the P-wave is left out. Having crossing relations for the real parts also, makes the equations much easier to solve [9]. Thus it would probably be advantageous to solve them first with S and P waves only, and then to use the result as a trial solution in the equations with D and F waves.

3. – Asymptotic behaviour of the Sirkov equations.

In this section we investigate the asymptotic behaviour of the following types of Shirkov equations: S-waves only, and S and P waves only, S and P waves with real parts of D and F waves. We also investigate the asymptotic behaviour of the Chew-Mandelstam equations with S-waves only. If our results are to be trusted, it is important that they shall not be sensitive to the precise number of partial waves included. Therefore we must investigate several different types of equations, even if we only want to apply one.

[9] G. Salzman and F. Salzman: *Phys. Rev.*, **108**, 1619 (1957).

Consider the Shirkov equations with S and P waves only. First we prove that the imaginary parts must vanish at infinity. The equality of the imaginary parts at $\nu = \pm\infty$, (1.1), was proved in a previous paper [1], and also by SUGAWARA and KANAZAWA [2]. Now the expressions (2.7) must be even under $\nu \to -1-\nu^*$, so that their imaginary parts must be odd under $\nu \to -1-\nu$. Since by unitarity $\operatorname{Im} A_l^I(+\infty) \geqslant 0$, (1.1) therefore implies (1.2).

The unitarity condition (2.3) gives

$$\operatorname{Im}[1/A_l^I(+\infty)] = -1\,. \tag{3.1}$$

Now suppose

$$\operatorname{Im}[1/A_l^I(-\infty)] = c_I - 1\,. \tag{3.2}$$

We assume that $c_I \neq 0$, and $c_I \neq \pm\infty$. If there are no CDD zeros at infinity [5,7], we can write dispersion relations for $1/A_l^I$ with one subtraction

$$\operatorname{Re} 1/A_l^I(\nu) = \frac{1}{a_I} + \sum_{n=1}^{N} \frac{\Gamma_n^I}{z_n - \nu} + \frac{\nu - \nu_0}{\pi} \int_{-\infty}^{\infty} \frac{\mathrm{d}\nu' \operatorname{Im}[1/A_l^I(\nu')]}{(\nu' - \nu_0)(\nu' - \nu)}\,, \tag{3.3}$$

where the pole terms correspond to CDD zeros in the finite region [5]. Since they represent unstable elementary particles, we can assume that there are only a finite number of them. (3.1) and (3.2) then give asymptotically

$$\sqrt{\frac{\nu}{\nu+1}}\, \operatorname{ctg} \delta_l^I(\nu) = \operatorname{Re}[1/A_l^I(\nu)] \approx c_I(\ln \nu/\pi) \approx \tag{3.4}$$

$$\approx \operatorname{Re}[1/A_l^I(-\nu)]\,, \qquad \text{as } \nu \to \infty.$$

With $b_I = 1/c_I$ we get for A_l^I asymptotically,

$$\operatorname{Im} A_l^I(\nu) \approx [\pi b_I/\ln \nu]^2\,, \qquad \text{as } \nu \to \infty, \tag{3.5}$$

$$\operatorname{Im} A_l^I(-\nu) \approx (1 - 1/b_I)[\pi b_I/\ln \nu]^2\,, \qquad \text{as } \nu \to \infty. \tag{3.6}$$

$$\operatorname{Re} A_l^I(\nu) \approx \pi b_I/\ln \nu \approx \operatorname{Re} A_l^I(-\nu)\,, \qquad \text{as } \nu \to \infty. \tag{3.7}$$

The Shirkov crossing relations (2.5) then give

$$b_I - (b_I)^2 = \sum_{I'} A_{II'}(b_{I'})^2 , \tag{3.8}$$

$$b_I = \sum_{I'} A_{II'} b_{I'} , \tag{3.9}$$

as the requirements for consistent asymptotic behaviour. (3.9) can be shown to be a consequence of (3.8), using the fact that the eigenvalues of $A_{II'}$ are ± 1. The algebraic eq. (3.8) can be solved numerically. There are two sets of real solutions—the one given in Table I, and also all $b_I = 0$. The latter corresponds to non-logarithmic behaviour at infinity, for which the above argument breaks down.

If one leaves out the P-wave in the Shirkov equations, (3.8) become

$$\begin{cases} 3b_0 = 4(b_0)^2 + 5(b_2)^2 , \\ 6b_2 = 2(b_0)^2 + 7(b_2)^2 , \end{cases} \tag{3.10}$$

whose non-zero solution is also given in Table I. There is now no equation corresponding to (3.9), since the real parts don't satisfy crossing relations in this case.

If one includes the real parts of the D and F waves, the crossing relations are (2.9). Now if $\operatorname{Im} A_l^I \sim (\ln \nu)^{-2}$, then $\nu[\mathrm{d} \operatorname{Im} A_l^I/\mathrm{d}\nu) \sim (\ln \nu)^{-3}$, so that (2.9) becomes asymptotically

$$\operatorname{Im} A_{0,1}^I(-\nu - 1) = -\sum_{I'} \sigma_{II'} \operatorname{Im} A_{0,1}^{I'}(\nu) , \qquad \nu \geqslant 0 , \tag{3.11}$$

where

$$\sigma_{II'} = \begin{pmatrix} \frac{1}{3} & -4 & \frac{5}{3} \\ -\frac{2}{15} & \frac{7}{10} & \frac{1}{3} \\ \frac{1}{3} & 2 & \frac{1}{6} \end{pmatrix} . \tag{3.12}$$

This gives

$$b_I - (b_I)^2 = \sum_{I'} \sigma_{II'}(b_{I'})^2 , \tag{3.13}$$

which can also be solved numerically.

The Chew-Mandelstam equations, when both the S and P waves have

imaginary parts, were previously shown to be inconsistent [1]. However, if only the imaginary parts of the S-waves are included, they are consistent. The crossing relations are then

$$(3.14)\quad \begin{cases} \operatorname{Im} A_0^0(-\nu-1) = -\dfrac{1}{\nu+1}\displaystyle\int_0^\nu d\nu' \left[\frac{2}{3}\operatorname{Im} A_0^0(\nu') + \frac{10}{3}\operatorname{Im} A_0^2(\nu')\right], \\ \operatorname{Im} A_0^2(-\nu-1) = -\dfrac{1}{\nu+1}\displaystyle\int_0^\nu d\nu' \left[\frac{2}{3}\operatorname{Im} A_0^0(\nu') + \frac{1}{3}\operatorname{Im} A_0^2(\nu')\right], \\ \qquad\qquad\qquad\qquad\qquad\qquad\qquad\qquad \nu \geqslant 0\,. \end{cases}$$

Inserting (3.5) gives by a straightforward calculation,

$$(3.15)\quad \begin{cases} \operatorname{Im} A_0^0(-\nu) \approx -(\pi/\ln\nu)^2\left[\frac{2}{3}(b_0)^2 + \frac{10}{3}(b_2)^2\right], \\ \operatorname{Im} A_0^2(-\nu) \approx -(\pi/\ln\nu)^2\left[\frac{2}{3}(b_0)^2 + \frac{1}{3}(b_2)^2\right], \end{cases} \qquad \text{as } \nu \to +\infty\,.$$

Combining this with (3.6), we get

$$(3.16)\quad \begin{cases} 3b_0 = 5(b_0)^2 + 10(b_2)^2\,, \\ 3b_2 = 2(b_0)^2 + 4(b_2)^2\,, \end{cases}$$

which can similarly be solved.

The asymptotic behaviour for these various types of equations are given in Table I. The first column shows which partial waves have imaginary parts,

TABLE I. – *Asymptotic behaviour of various equations for pion-pion scattering.*

$$c_I = \pi \lim_{\nu\to\infty} [\operatorname{ctg} \delta^1_{0,1}(\nu)/\ln\nu]\,.$$

Imaginary parts	Real parts	c_0	c_1	c_2
S	S	1.477 2	—	5.027 4
S	∞	2.2	—	5.5
S, P	S, P	1.474 8	— 26.708 2	4.906 1
S, P	S, P, D, F	1.473 0	— 22.837 3	4.810 2

the second shows which partial waves real have parts. The other three columns list the $c_I = 1/b_I$ obtained by solving eq. (3.10), (3.16), (3.8) and (3.11), respectively. The asymptotic behaviours are got by substituting these into (3.4).

The above arguments prove that these are the only asymptotic behaviours with $\cot \delta_l^I \sim \ln \nu$. It is easily seen that they will correspond to the perturbation solutions. In addition to these, there are the solutions with CDD zeros at infinity, which have asymptotic behaviour $\cot \delta_l^I \sim \nu^n$, but, as mentioned in Section 1, these to not seem satisfactory for strong interactions. One may enquire whether any other asymptotic behaviours, for example $\cot \delta_l^I \sim \ln \ln \nu$, are possible. Investigations thus far have not disclosed any, but we cannot yet exclude them completely.

4. – Conclusions.

Our main conclusions are that the Shirkov equations are consistent without a cut-off, and that their asymptotic behaviour is completely independent of what happens elsewhere. This asymptotic behaviour is determined by algebraic equations which can be solved exactly. From it one can make predictions about the signs of various partial waves and, in favourable cases, about the existence of resonances.

In their recent work on the calculation of the double spectral functions [10] CHEW and FRAUTSCHI have proposed a connection between a large P-wave, and the behaviouv of the total cross-section at infinity. They seem to have two reasons for suggesting this. The first was based on the Chew-Mandelstam equations, which they thought had this behaviour if the P-wave was included but was not too large. This can now be seen to be erroneous. The Chew-Mandelstam equations, in fact, have no consistent behaviour at infinity at all. The trouble starts as soon as there is any P-wave, not merely when it gets large [1]. The Shirkov equations are consistent, but for them there is not connection between the high-energy behaviour and the size of the P-wave. They always have GRIBOV behaviour [11] ($\sim [\ln \nu]^{-2}$ at infinity), even with a CDD zero in the P-wave. Chew and Frautschi's second reason was Regge's work on potential scattering [12]. He found a connection between the behaviour of

[10] G. F. CHEW and S. FRAUTSCHI: *Phys. Rev. Lett.*, **5**, 580 (1960); *A dynamical theory for strong interactions at low momentum transfers but arbitrary energies*, Berkeley preprint UCRL-9510 (1960).

[11] V. GRIBOV: *Nucl. Phys.*, **22**, 249 (1961).

[12] T. REGGE: *Nuovo Cimento*, **14**, 951 (1959); **18**, 947 (1960).

the double spectral functions for large momentum transfer and the existence of a P-wave resonance. As to this, two remarks may be made. Firstly, Regge's method depends quite essentially on the existence of a *single* potential, linking all the partial waves. It is only because of this that the extension to complex angular momenta can be made. Secondly, as we have seen, crossing symmetry plays a crucial role in determining the asymptotic behaviour, and this must inevitably be lacking in any potential model. Thus, although Regge's work is very interesting, there is at present no evidence that his result carries over into field theory.(*)

The main attraction of Chew and Frautschi's work is that it explains why the peripheral model should have succeeded so much better than expected. This is quite independent of whether the asymptotic behaviour postulated by them is correct. The latter does, however, affect the usefulness of their techniques at low energies. Otherwise there seems to be no reason to suppose that the calculation of the double spectral functions will offer much improvement on the Shirkov equations, so far as low energies are concerned.

In the meantime the following position seems at least tenable: *a*) The behaviour at infinity is independent of what happens elsewhere and in particular of P-wave resonances. We cannot expect the detailed asymptotic behaviour of the Shirkov equations, as determined above, to survive the introduction of the double spectral functions, but it does not seem too unreasonable to hope that this feature will survive. *b*) Quantitative results at low energies can be obtained by including only a finite number of partial waves. Predicting the pion-nucleon (3, 3) resonance would be the crucial test for this.

We have seen that the real parts of the D and F waves can be included in the Shirkov equations without giving any inconsistency. The reason for this was that if

$$\text{Im}\, A_l^I \sim (\ln \nu)^{-2}\,, \qquad \text{as } \nu \to \infty \tag{4.1}$$

then

$$\nu \left[\frac{\mathrm{d}\ \text{Im}\, A_l^I}{\mathrm{d}\nu}\right] \sim (\ln \nu)^{-3}\,, \qquad \text{as } \nu \to \infty\,, \tag{4.2}$$

so that terms of the latter type don't affect the asymptotic behaviour. It seems reasonable to conclude that the same will happen if one includes the

(*) *Note added in proof.* – From an analysis of the experimental $\pi\mathcal{N}$ diffraction scattering, we have recently found strong evidence that Regge's asymptotic behaviour is physically correct, contrary to our above statement.

real parts of any *finite* number of partial waves, though this has not been checked in detail. However, if one includes the real parts of an infinite number of partial waves, then terms like (4.2) may add up to something with quite different asymptotic behaviour, thus leading to the inconsistency of the Chew-Mandelstam equations.

Now in the Chew-Mandelstam equations the real parts of all the higher partial waves are included, whereas in the Shirkov equations one only keeps the real parts of a finite number. Therefore, at least in principle, the Chew-Mandelstam equations ought to be more accurate than those of SHIRKOV ([13]). The fact that the Chew-Mandelstam equations don't possess solutions, while the less accurate Shirkov equations do, might then lead one to question whether the solutions of the Shirkov equations could be believed. This could only be fully resolved by a study of the double spectral functions. We do have two pointers, however: The results are insensitive to the precise number of real parts, at least if this is small (Table I). Actual inconsistencies only seem to arise when the number of real parts is infinite. This suggests that the trouble in the Chew-Mandelstam equations is mathematical—if one includes many more real than imaginary parts, the approximation scheme becomes unbalanced and inconsistencies result. In this case, the Shirkov equations can be believed.

In subsequent work we intend to investigate conditions for the absence of ghost states and complex poles in the solutions of the Shirkov equations, and the related question of the conditions under which Castillejo-Dalitz-Dyson zeros can be present. The results of the present work can then be used to construct approximate solutions. We also want to determine the asymptotic behaviour for other systems, particularly pion-nucleon scattering, so as to predict signs and resonances. Finally, improved numerical methods are being worked out, for use in solving the Shirkov equations exactly.

* * *

I am grateful to Prof. A. SALAM, Dr. P. T. MATTHEWS and Dr. T. KIBBLE for their interest and encouragement.

([13]) A. Q. SARKER: *Integral equations for the low energy pion-pion scattering*, Birmingham preprint (1961).

Note added in proof.

In our previous paper ([1]) we pointed out that the solutions of Bransden and Moffat are not solutions of the Chew-Mandelstam equations. Of course this does not neces-

sarily mean that they are physically wrong, as the CM equations are themselves only approximate. They can, in fact, be shown to be solutions of equations lightly different from those of Chew and Mandelstam (BRANSDEN and MOFFAT: unpublished).

RIASSUNTO (*)

Dimostro che, a differenza delle equazioni di Chew-Mandelstam, le equazioni di Shirkov sono coerenti senza alcun cut-off. Il loro comportamento asintotico ad alta energia puo esser determinato esattamente. Si puo utilizzare questo fatto per fare delle predizioni sui segni delle varie onde parziali, ed in alcuni casi sull'esistenza di risonanze. Il comportamento all'infinito è sempre del tipo di Gribov, anche con una risonanza d'onda P.

(*) *Traduzione a cura della Redazione.*

Differential Cross-Section for the D(d, n) Reaction.

C. Milone and R. Ricamo

Istituto di Fisica dell'Università - Catania
Centro Siciliano di Fisica Nucleare - Catania
Istituto Nazionale di Fisica Nucleare - Sezione Siciliana

(ricevuto il 12 Luglio 1961)

Summary. — The differential cross-section for the D(d, n) reaction was measured at $E_d = 1.6$ and 0.6 MeV. Neutrons emitted at different angles where detected by recoil protons in nuclear emulsions. In the laboratory system the ratio $\sigma(0°)/\sigma(90°)$ is 8.2 ± 0.8 at $E_d = 1.6$ MeV and 4.2 ± 0.4 at $E_d = 0.6$ MeV, according to the average known values.

1. – Introduction.

In many laboratories monoenergetic neutrons of some MeV are produced with the D(d, n)^{3}He reaction. If the accelerating voltage is lower than (1 ÷ 2) MV, neutrons of different energies are more easily obtained by changing the direction of the neutron beam instead of changing the accelerating voltage.

The neutron flux is deduced from the known differential cross-section $\sigma(\vartheta)$ for the d-d reaction rather than measured directly in every experiment, due to the difficulty of such measurements at various neutron energies.

However some differences can be observed in the experimental differential cross-section. In Table I we report the ratios of this cross-section at $\vartheta = 0°$ and 90° for $E_d = 0.6$ MeV as deduced from the data of different authors [1-5] and, where necessary, interpolated.

(1) G. T. Hunter and H. T. Richards: *Phys. Rev.*, **76**, 1445 (1949).
(2) P. S. Preston, P. F. Show and S. A. Young: *Proc. Roy. Soc.*, A **226**, 206 (1954); elaborated by J. D. Seagrave, Los Alamos Report 2162 (1958).
(3) P. R. Cagnon and G. E. Owen: *Phys. Rev.*, **101**, 1798 (1956).
(4) J. C. Fuller, W. E. Danco and D. C. Ralf: *Phys. Rev.*, **108**, 91 (1957).
(5) L. Gonzáles, J. Rapaport and J. J. Van Loef: *Phys. Rev.*, **120**, 1319 (1960).

The possibility that the average accepted behaviour of the $\sigma(\vartheta)$ could be not correct was suggested to us by the study of the $^{31}P(n, p)^{31}Si$ reaction ([6]).

TABLE I.

D(d, n) $E_d = 0.6$ MeV	
$(\sigma(0°)/\sigma(90°))_{Lab}$	References
3.9 (*)	HUNTER, 1949 ([1])
5.3	PRESTON, 1954 ([2])
3.2	CAGNON, 1956 ([3])
3.4	FULLER, 1957 ([4])
3.7	GONZÁLES, 1960 ([5])

(*) Interpolated.

Indeed, the average behaviour of the cross-section for this reaction, as obtained in our laboratory, is the same as that found by other authors ([7,8]) in the region $E_n = (2.7 \div 5)$ MeV. In the region around $E_n = 2.2$ MeV a discrepancy by a factor about 2 is seen between the cross-section found by ([7]) and that found by ([8]), while at $E_n = 2$ MeV the cross-sections agree together.

A similar discrepancy may be observed for the $^{32}S(n, p)^{32}P$ reaction in the region around $E_n = 2.2$ MeV ([9-11]).

In the experiments ([6,7,9,10]) the neutrons were obtained from the D(d, n) reaction and the neutron flux at different ϑ angles was deduced from the known behaviour of the differential cross-section $\sigma(\vartheta)$ for the D(d, n) reaction.

In the experiments ([8,11]) the neutron flux was measured by means of ^{238}U fission chambers using the known fission cross-section ([12]) of ^{238}U.

In order to conciliate the results obtained in the two groups of experiments we decided to start measuring carefully the differential cross-section for the D(d, n) reaction at $E_d = 0.6$ MeV and, to check our results, we experimented also at $E_d = 1.6$ MeV.

([6]) P. CUZZOCREA, G. PAPPALARDO and R. RICAMO: *Nuovo Cimento*, **16**, 450 (1960).

([7]) R. RICAMO: *Nuovo Cimento*, **8**, 383 (1951).

([8]) J. A. GROUND, R. L. HENKEL and B. L. PERKIN: *Phys. Rev.*, **109**, 425 (1958).

([9]) E. LUSCHER, R. RICAMO, P. SCHERRER and W. ZUNTI: *Helv. Phys. Acta*, **23**, 561 (1950).

([10]) P. HUBER and T. HURLIMANN: *Helv. Phys. Acta*, **28**, 23 (1955).

([11]) L. ALLEN jr., W. A. BIGGERS, R. J. PRESTWOOD and R. K. SMITH: *Phys. Rev.*, **107**, 1363 (1957).

([12]) D. J. HUGHES and J. A. HARVEY: *Neutron Cross Section*, BNL 325.

At both deuteron energies, the neutron energy region around 2.2 MeV is obtained around $\vartheta_n = 120°$, in the laboratory system.

In the center-of-mass system, the differential cross-section is symmetrical respect to $\vartheta_{cm} = 90°$, being [4]

$$\sigma(\vartheta)_{cm} = \sigma(90°)_{cm}\,(1 + A\cos^2\vartheta + B\cos^4\vartheta)\,. \tag{1}$$

This gives a mean of testing the reliability of the experimental results on the $\sigma(\vartheta)$.

2. – Experimental procedure.

Neutrons were produced bombarding a D_2O ice target with 5 μA of deuterons in our 2 MeV HVEC Van de Graaff as in P(n, p)Si experiment [6].

Neutrons were detected by recoil protons in nuclear plates (Fig. 1).

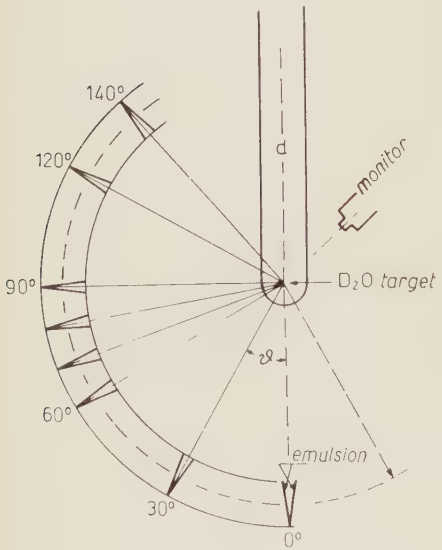

Fig. 1. – Experimental arrangement.

At each ϑ angle two plates have been exposed; the plane of each plate made an angle of 3° with the direction of the neutrons.

Two experiments have been made, the first at $E_d = 1.6$ with a D^+ beam, the other at $E_{(2D)} = 1.2$ MeV with a $(2D)^+$ beam, so that in the second experiment we really have had $E_d = 0.6$ MeV. With our 2 MeV Van de Graaff this technique is preferable since at 0.6 MV the voltage stability is poor.

Ilford C-2 plates have been employed in the experiment at 1.6 MV and L-4 plates in the experiment at 1.2 MV. All plates were 1 in. × 3 in. × 200 μm thick.

The plates, developed with the two temperatures technique generally used in this laboratory, have been scanned with binocular microscopes (generally 105× objective and 8× ocular).

As the differential $\sigma(\vartheta)$ cross-section depends on the ϑ angle, different areas have been scanned in the plates exposed at different angles ϑ in order to have for each θ about the same number of scanned tracks. For each plate the scanned area was < 1 cm²; the mean distance between the scanned area and the center of the D_2O target was 30 cm.

Only tracks contained in a square pyramid having the known direction of the incoming neutron as axis and a semiaperture of 15° have been accepted.

Under these conditions, if ϑ is the angle between the incoming neutron and the recoil proton, the relation

$$E_p = E_n \cos^2 \vartheta \qquad (2)$$

may be approximated with $E_p \approx E_n$.

For each angle ϑ and for both E_d values we built the neutron spectrum to control the experimental dispersion and to compare the measured value of the mean neutron energy with that expected.

Typical neutron spectra are shown in Fig. 2 for $\vartheta = 0°$ and 90° at $E_d = 0.6$ MeV. For $\vartheta > 10°$ neutron energies were corrected according to (2).

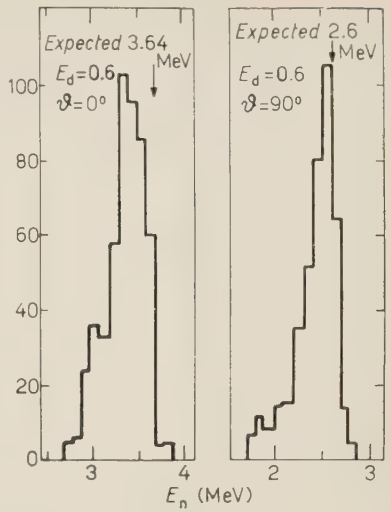

Fig. 2. – Experimental neutron distribution from D(d, n) reaction for $E_d = 0.6$ MeV at $\vartheta_{lab} = 0°$ and 90°.

The relative dispersions are (10÷15) %. The mean difference between the expected and the measured neutron energy is (100÷200) keV.

The background was negligible.

The differential D(d, n) cross-sections reported in Fig. 3 and Fig. 4 have been obtained from the number of tracks/mm² at various angles ϑ, divided by the values of the cross-section for the n-p elastic scattering at the corresponding neutron energies.

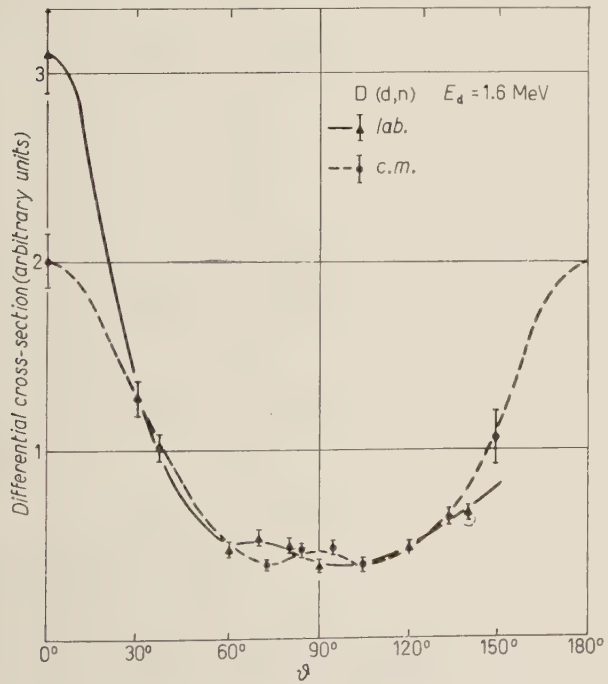

Fig. 3. – Differential cross-section $\sigma(\theta)$ for D(d, n) reaction at $E_d = 1.6$ MeV (arbitrary units).

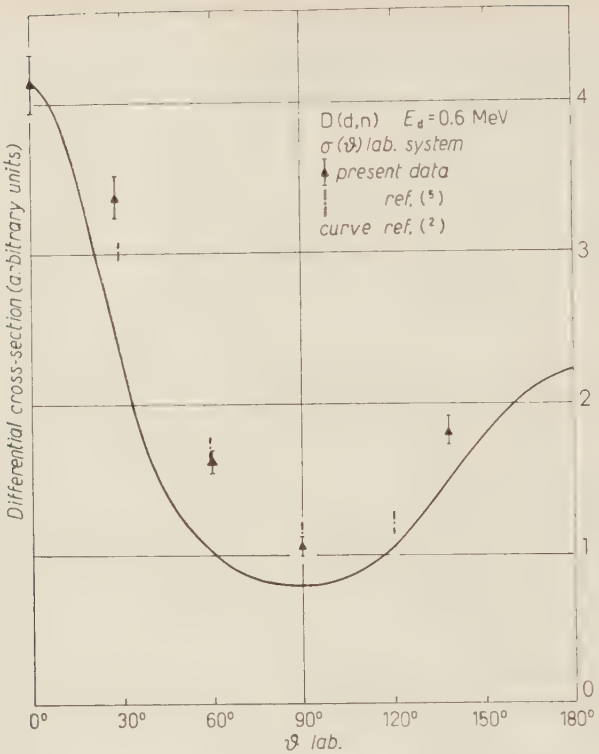

Fig. 4. – Differential cross-section for D(d, n) reaction at E_d=0.6 MeV. The points of Gonzáles (5) and curve of Preston (2) are also reported (arbitrary units).

3. – Discussion.

At every angle ϑ a monoenergetic neutron beam is expected if a very thin ice target is bombarded with a monoenergetic deuteron beam.

In our case the energy spread of the deuteron beam was ± 2 keV at 1.2 and 1.6 MeV. The thickness of the ice target was about 150 keV at 1.6 MeV and 115 keV at 1.2 MeV. The useful target area was about 5×5 mm^2 and taking into account the scanned area on the photoplates this gives an uncertainty of the order of few degrees in the direction of the neutron incoming on the plates.

Experimentally we measure the projection l of the track in the plane of the emulsion, the dip z and the angle φ between the direction of the incoming neutron and the projection of the initial direction of the proton recoil track on the plane of the emulsion.

For protons of several MeV, Δl may be only a few per cent. $\Delta\varphi$ is of the order of $\pm 2°$. If β is the dip angle, $\Delta\beta$ is of the order of many degrees.

This, for $\beta < 15°$ and $\varphi < 15°$ does not give any serious uncertainty in the neutron energy determination but gives an uncertainty of the order of $(10 \div 15)\%$ [13] in the determination of the number of the proton recoil tracks contained inside the « square pyramid » we have considered, and consequently gives a limitation in the precision of the absolute flux determination.

In the case of relative flux determinations (as in our case) the systematic errors in β may be partially compensated.

The differential D(d, n) cross-section obtained at $E_d = 1.6$ MeV is shown in Fig. 3 in the laboratory system and in the c.m. system. Only statistical errors are reported.

After normalization to $\theta = 0°$ the experimental points agree with the distribution to be expected according to the results obtained by other authors [14,1,15].

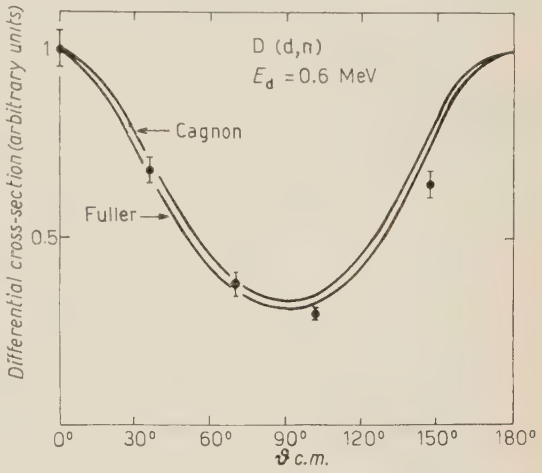

Fig. 5. – Differential D(d, n) cross-section at $E_d = 0.6$ MeV in the c.m. system. Points: present data. Curves: are due to CAGNON [3] and FULLER [1].

In Fig. 4 the experimental points refer to the differential D(d, n) cross-section at $E_d = 0.6$ MeV in the laboratory system.

The points of GONZÁLES [5] and the curve [2] are also reported; all values are normalized to $\theta = 0°$.

From our experiment at $E_d = 0.6$ MeV we deduce for the ratio $\left(\sigma(0°)/\sigma(90°)\right)_{lab}$ a value of 4.2 ± 0.4.

In Fig. 5 the experimental points obtained at $E_d = 0.6$ MeV are reported in the center-of-mass system. The curve refers to the differential cross-section given by CAGNON [3] and FULLER [1]. From our experiment we have $\left(\sigma(0°)/\sigma(90°)\right)_{cm} = 3.6 \pm 0.4$.

The behaviour of σ for D(d, n) we have obtained at $E_d = 0.6$ MeV agrees with the average value deduced from the measurements made in other laboratories.

[13] See for instance: J. B. MARION and J. L. FOWLER: *Fast Neutron Physics*, Vol. IV, part. I (New York, 1960), p. 328.

[14] J. M. BLAIR, G. FREIER, E. LAMPI, W. SLEATER and J. M. WILLIAMS: *Phys. Rev.*, **74**, 11 (1948).

[15] J. L. FOWLER and J. E. BROLLEY: *Rev. Mod. Phys.*, **28**, 103 (1956).

RIASSUNTO

Viene misurata la sezione d'urto differenziale della reazione

$$D + D = {}^3He + n + 3.27\ MeV\ .$$

per deutoni incidenti di 1.6 e 0.6 MeV essendosi rilevate a 0.6 MeV discrepanze superiori al 10% tra i valori della letteratura. I neutroni emessi a diversi angoli sono rivelati mediante i protoni di rinculo in emulsioni nucleari. Nel sistema del laboratorio si trova $\sigma(0^\circ)/\sigma(90^\circ)=8.2+0.8$ per $E_d=1.6$ MeV e 4.2 ± 0.4 per $E_d=0.6$ MeV in accordo con la media dei valori dei vari autori.

IL NUOVO CIMENTO Vol. XXII, N. 1 1° Ottobre 1961

Single Pion Production in Proton-Proton Collisions According to the One-Particle Exchange Model.

G. Da Prato

Laboratori Nazionali del C.N.E.N. - Frascati

(ricevuto il 16 Luglio 1961)

Summary. — Single pion production in nucleon-nucleon collisions is calculated in the one-pion exchange approximation. All the possible diagrams of this kind are calculated in the « pole » approximation discussed in the text: also the interferences between them are taken into account. The lab. energy spectra of the final nucleons are calculated and compared with the experimental data at 2.85 GeV. This comparison shows a remarkably good agreement for small values of the squared 4-momentum of the virtual pion. For higher values the qualitative behaviour is still reproduced, but the theoretical absolute values are larger than the experimental ones.

1. – Introduction.

We want to study the processes of single pion production in proton-proton collisions, namely the reactions:

$$p+p \to p+n+\pi^+ \tag{1}$$

$$p+p \to p+p+\pi^0 \tag{2}$$

by using the model which describes the processes as occurring through the exchange of a single pion (Fig. 1).

This approach has been suggested by the fact that, in the last years, experimental evidence has been produced that in high energy inelastic processes small momentum transfers of the recoiling target particle are strongly favoured [1].

[1] J. G. Rushbrooke and D. Radojicic: *Phys. Rev. Lett.*, **5**, 567 (1950); A. P. Batson, B. B. Culwick, J. G. Hill and L. Riddiford: *Proc. Roy. Soc. (London)*, **251**, 218 (1959).

This situation can be qualitatively explained through a mechanism of interaction due to the exchange of a single pion (2), and for some particular reactions detailed calculations have been performed (3). The situation, however, is not yet completely clear, because in the quoted papers (3) drastic simplifications have been made, *e.g.* by neglecting some of the possible one-pion exchange (OPE) diagrams and the various mutual interference terms. New detailed experimental data on single pion production in proton-proton collision have recently been obtained at 2.85 GeV of the incident proton in the lab. system (4).

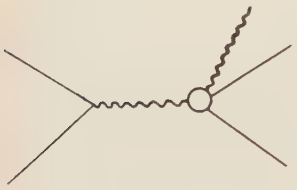

Fig. 1. OPE diagram for the description of process (1) or (2). Full lines represent nucleons, dashed lines represent pions.

In the laboratory energy spectra of the final nucleons one finds again strong peaks corresponding to very small momentum transfers. This indicates again that the one-particle exchange plays an important role in the particular processes (1) and (2). We think it useful to calculate the spectra predicted by this model in the whole physical region by taking into account all the possible OPE effects. By comparing the prediction of the model with the experiment, we expect to find a sensibly good agreement in the region of small momentum transfers, where the further approximations made in order to obtain quantitative numerical results (5) can be well justified. These approximations consist in neglecting the influence of the « pion form factors » of the upper vertex in Fig. 1 and of the propagator of the virtual pion; and in considering as Δ^2-independent (6) the partial wave amplitudes for the « off shell » pion-nucleon scattering. (The scattering angle which enters in the description of the lower vertex (5) is not taken on shell, but its dependence on Δ^2 is taken into account.) For the region of higher momentum

(2) See for instance: F. Salzman and G. Salzman: *Phys. Rev.*, **120**, 599 (1960).

(3) E. Ferrari: *Nuovo Cimento*, **15**, 652 (1960) and *Phys. Rev.*, **120**, 988 (1960); S. D. Drell: *Phys. Rev. Lett.*, **5**, 278, 342 (1960); F. Salzman and G. Salzman: *Phys. Rev. Lett.*, **5**, 377 (1960); J. Iizuka and A. Klein: *Phys. Rev.* **123**, 669 (1961); F. Selleri: *Phys. Rev. Lett.*, **6**, 64 (1961). In the last two papers an error of normalization is contained. In both cases the theoretical predictions would be correct if multiplied by two.

(4) G. A. Smith, H. Courant, E. C. Fowler, H. Kraybill, J. Sandweiss and H. Taft: Yale University, preprint. The experimental lab. energy spectra used in this paper are a private communication of the above authors. We thank Dr. G. A. Smith and Prof. H. Taft for having sent us these data.

(5) E. Ferrari and F. Selleri: *Peripheral model for inelastic processes* (to be published as internal CERN report).

(6) Here we denote by Δ^2 the square of the 4-momentum of the intermediate particle. We use the metric $p^2 = |\boldsymbol{p}|^2 - p_0^2$:

transfers we know a priori that these approximations are not good, but the comparison of the theory with the experiment can always give us a suggestion for approaching the problem of the OPE contribution when the intermediate particle is very virtual. We expect in this region to obtain an overestimate of the OPE contribution, which in all probability is mainly due to the neglected effects of the «pionic form factor» in the upper vertex of Fig. 1. Also the calculation of the interference effects generally involves at least one of the interfering terms considerably off shell. In this paper, however, it will be seen that these effects are not so important, and, in some cases, they turn out to be negligible.

Section 2 will be dedicated to notations and kinematics, Section 3 to the study of the lower vertex, Section 4 to the calculation of the differential cross-sections and finally Section 5 to the discussion of the obtained results.

2. – Notations, kinematics, Feynman graphs.

We denote by p_1, k_1, p_2, k_2, q_2 the energy-momentum 4-vectors of the incoming proton, target proton, outgoing proton, outgoing neutron (proton) for the first (second) reaction and outgoing pion respectively. We call μ the pion mass and M the nucleon mass. Furthermore, we define the kinematical invariants

$$(3) \qquad W^2 = -(p_1 + k_1)^2, \qquad l^2 = -(k_2 - q_2)^2, \qquad u^2 = -(p_2 + q_2)^2,$$

$$\Delta^2 = (k_2 - k_1)^2, \qquad r^2 = (k_2 - p_1)^2, \qquad s^2 = (p_2 - k_1)^2, \qquad t^2 = (p_2 - p_1)^2$$

Among them the following relations hold

$$(4) \qquad \Delta^2 + r^2 + u^2 = s^2 + t^2 + l^2 = W^2 - 3M^2$$

W, l, u, are respectively: the total c.m. energy, the energy of k_2 and q_2 in their c.m. system and the energy of p_2 and q_2 in their c.m. system. Δ^2, r^2, s^2, t^2 are nucleon momentum transfers.

Five of the invariants (3) are sufficient to obtain a complete description of the kinematics.

We will use also the following quantities:

a) In the c.m. system of p_2 and q_2 χ' is the 3-momentum of p_2 and q_2, p'_{10}, k'_{10}, p'_{20}, k'_{20}, q'_{20} are the energies of p_1, k_1, p_2, k_2, q_2 respectively, ε' is the angle between p_2 and p_1, β' the angle between p_2 and k_1, α' the angle between p_1 and k_1, φ' is the p_2 azimuthal angle in a frame of reference with the z axis directed along p_1.

b) In the c.m. system of p_2 and k_2 the same quantities will be denoted by χ'', p''_{10}, k''_{10}, p''_{20}, k''_{20}, q''_{20}, ε'', β'', α'', η'' respectively. Finally $T_L(p_2)$ and $T_L(k_2)$ will be the lab. kinetic energies of particles p_2 and k_2 respectively and K the 3-momentum of p_1 and k_1 in the c.m. system. We have

$$T_L(k_2) = \frac{\Delta^2}{2M}, \qquad T_L(p_2) = \frac{s^2}{2M}. \tag{5}$$

The expression of the other kinematical quantities as functions of the invariants are given in [5].

The T matrix is defined by

$$S_{fi} = \delta_{fi} + \frac{iM^2\delta^4(p_2 + k_2 + q_2 - p_1 - k_1)}{\sqrt{2}(2\pi)^{\frac{7}{2}}(p_{10}k_{10}p_{20}k_{20}q_{20})^{\frac{1}{2}}} T_{fi}, \tag{6}$$

p_{10}, k_{10}, p_{20}, k_{20}, q_{20} are the energies in an arbitrary frame of reference. The differential cross-section $\mathrm{d}\sigma$ is given by

$$\mathrm{d}\sigma = \frac{M^4}{2(2\pi)^5 KW} \overline{\sum_{\text{spin}}} |T_{fi}|^2 \delta^4(p_2 + k_2 + q_2 - p_1 - k_1) \frac{\mathrm{d}^3p_2\, \mathrm{d}^3k_2\, \mathrm{d}^3q_2}{p_{20}k_{20}q_{20}}. \tag{7}$$

The bar over the summation symbol indicates the average over initial spins. Formula (7) is equivalent to:

$$\mathrm{d}\sigma = \frac{M^4}{8(2\pi)^4 K^2 W^2} \overline{\sum_{\text{spin}}} |T_{fi}|^2 \frac{\chi'}{u} \mathrm{d}\cos\varepsilon' \mathrm{d}\varphi' \mathrm{d}u^2 \mathrm{d}\Delta^2, \tag{8}$$

and also equivalent to

$$\mathrm{d}\sigma = \frac{M^4}{8(2\pi)^4 K^2 W^2} \overline{\sum_{\text{spin}}} |T_{fi}|^2 \frac{\chi''}{l} \mathrm{d}\cos\varepsilon'' \mathrm{d}\varphi'' \mathrm{d}l^2 \mathrm{d}s^2. \tag{9}$$

We shall use (8) for the k_2 particle spectrum and (9) for the p_2 particle spectrum.

The allowed physical region is determined from the following relations

$$0 \leqslant \varphi' \leqslant 2\pi \tag{10}$$

$$0 \leqslant \varepsilon' \leqslant \pi \tag{11}$$

$$(M + \mu)^2 \leqslant u^2 \leqslant \{M^2 + (W^2/2M^2)[2K(\Delta^4 + 4M^2\Delta^2)^{\frac{1}{2}} - \Delta^2 W]\} \tag{12}$$

$$\left\{\begin{array}{l} \frac{1}{2}\{W^2 - \mu^2 - 2M\mu - 4M^2 - (K/W)[(W^2 - \mu^2 - 2M\mu)^2 - 4M^2W^2]^{\frac{1}{2}}\} \leqslant \Delta^2 \\ \leqslant \frac{1}{2}\{W^2 - \mu^2 - 2M\mu - 4M^2 + (K/W)[(W^2 - \mu^2 - 2M\mu)^2 - 4M^2W^2]^{\frac{1}{2}}\} \end{array}\right. \tag{13}$$

for the case (8), and by the relation which we obtain by exchanging $\varphi' \to \varphi''$, $\varepsilon' \to \varepsilon''$, $u^2 \to l^2$, $\Delta^2 \to s^2$ for the case (9).

The four possibile Feynman graphs are given in Fig. 2.

Let T_i^u and T_i^l be the T matrix elements relative to upper and lower vertices of the i-th graph. We have [7]

$$(14) \quad T_{fi} = \left[\frac{\langle T_1^u \rangle \langle T_1^l \rangle}{\Delta^2 + \mu^2} + \frac{\langle T_3^u \rangle \langle T_3^l}{s^2 + \mu^2} - \right. \\ \left. - \frac{\langle T_2^u \rangle \langle T_2^l \rangle}{r^2 + \mu^2} - \frac{\langle T_4^u \rangle \langle T_4^l \rangle}{t^2 + \mu^2} \right],$$

for reaction (1) and

$$(15) \quad T_{fi} = \left[\frac{\langle T_1^u \rangle \langle T_1^l \rangle}{\Delta^2 + \mu^2} + \frac{\langle T_4^u \rangle \langle T_4^l \rangle}{t + \mu^2} - \right. \\ \left. - \frac{\langle T_2^u \rangle \langle T_2^l \rangle}{r^2 + \mu^2} - \frac{\langle T_3^u \rangle \langle T_3^l \rangle}{s^2 + \mu^2} \right],$$

for reaction (2). The minus signs are due to the Pauli principle.

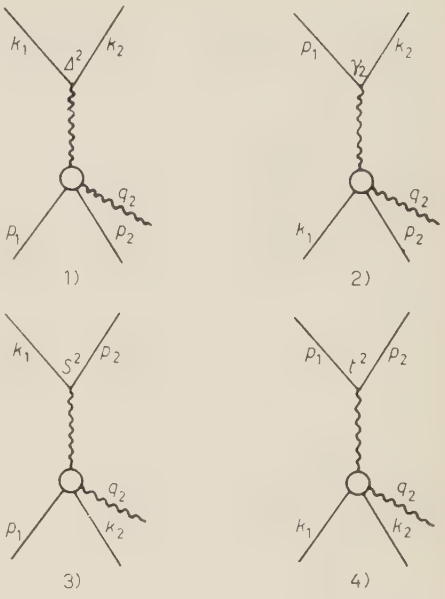

Fig. 2. – The possible OPE Feynman graphs for the process (1) or (2). In the upper vertices are written the relative momentum transfers.

3. – Pion-nucleon scattering amplitude.

Let p_1 and p_2 be the energy-momentum 4-vectors of the nucleons, and q_1 and q_2 those of the pions. We consider first the physical process; then $q_1^2 = -\mu^2$. The T matrix elements are of the following form [8]

$$(16) \quad \langle T^l \rangle = \bar{u}(p_2)(-A + iB\gamma \cdot q_2)\, u(p_1)$$

$u(p_2)$ and $u(p_1)$ are the nucleon spinors and A and B are given by

$$(17) \quad \begin{cases} A = 4\pi \left(f_1 \dfrac{u + M}{p'_{20} + M} - f_2 \dfrac{u - M}{p'_{20} - M} \right), \\ B = 4\pi \left(f_1 \dfrac{1}{p'_{20} + M} + f_2 \dfrac{1}{p'_{20} - M} \right), \end{cases}$$

---

[7] Brackets stand for indices fi.

[8] G. F. CHEW, M. L. GOLDBERGER, F. E. LOW and Y. NAMBU: *Phys. Rev.*, **106**, 1337 (1957).

with

$$(18)\qquad \begin{cases} f_1 = \sum_{l=0}^{\infty} f_{l+} P'_{l+1}(\cos\varepsilon') - \sum_{l=2}^{\infty} f_{l-} P'_{l-1}(\cos\varepsilon') \\ f_2 = \sum_{l=1}^{\infty} (f_{l-} - f_{l+}) P'_l(\cos\varepsilon') \,, \end{cases}$$

u is the total c.m. energy, p'_{20} is the nucleon energy and ε' the scattering angle in the c.m. system P'_l are derivatives of Legendre polinomials. When q_1 goes off shell ($q_1^2 = \Delta^2$) formula (17) is modified in the following way [10]

$$(19)\qquad \begin{cases} A(u^2, \Delta^2) = 4\pi \left| f_1(u^2, \Delta^2, t^2) \dfrac{u + M}{\sqrt{(p'_{10} + M)(p'_{20} + M)}} - \right. \\ \qquad\qquad \left. - f_2(u^2, \Delta^2, t^2) \dfrac{u - M}{\sqrt{(p'_{10} - M)(p'_{20} - M)}} \right| , \\ B(u^2, \Delta^2) = 4\pi \left| f_1(u^2, \Delta^2, t^2) \dfrac{1}{\sqrt{(p'_{10} + M)(p'_{20} + M)}} + \right. \\ \qquad\qquad \left. + f_2(u^2, \Delta^2, t^2) \dfrac{1}{\sqrt{(p'_{10} - M)(p'_{20} - M)}} \right| . \end{cases}$$

This definition leaves unchanged the bidimensional representation of the T matrix elements [8] where the only Δ^2-dependence is contained in f_1 and f_2 [*]. In the expression (18) the whole t^2-dependence is contained in $\cos\varepsilon'$, which can be easily « extrapolated » off shell by means of its definition

$$(20)\qquad \cos\varepsilon' = \frac{2p'_{10}p'_{20} - 2M^2 - t^2}{2|\boldsymbol{p}'_1||\boldsymbol{p}'_2|} .$$

while the amplitudes f_l are considered as t^2-independent. This procedure can be trusted only at low Δ^2: but it is at present the simplest one and gives the extension of Chew and Low's formula [9] to the whole physical region.

Quantities (19) will be used in the calculation of graph 1. In graphs 2, 3, 4. we have as arguments of A and B u^2r^2, l^2s^2, l^2t^2 respectively.

The reactions occurring in the lower vertex are:

$$(21)\qquad \pi^+ + \mathrm{p} \to \pi^+ + \mathrm{p}$$

$$(22)\qquad \pi^0 + \mathrm{p} \to \pi^+ + \mathrm{n}$$

(*) See also [5] for a discussion of this subject.

[9] G. F. Chew and F. E. Low: *Phys. Rev.*, **113**, 1640 (1959).

[10] In the following, we shall write $A(u^2, \Delta^2)$ instead of (u^2, Δ^2, t^2) and so on: the obvious momentum transfer-dependence is dropped for simplicity.

for reaction (1) and

$$\pi^0+\mathrm{p}\to\pi^0+\mathrm{p} \tag{23}$$

for reaction (2).

Reaction (21) is in a pure $\frac{3}{2}$ isotopic state and the only important wave is the $p_{\frac{3}{2}}$ wave. For this reason for the calculations of $\langle T'\rangle$ relative to (21) we have considered only f_{1+} different from 0; we use for it the one-resonance level formula ([11])

$$\begin{cases} f_{1+}(u)=\dfrac{1}{2\chi'}\dfrac{\Gamma_1}{(u_1-u)-i(\Gamma_1/2)}\,, \\ \Gamma_1=\dfrac{2(\chi a)^3}{1+(\chi a)^2}\gamma_\lambda^2\,, \end{cases} \tag{24}$$

with $a=5.91$, $\gamma_\lambda^2=0.062\,5$, $u_1=1.314$ in units of proton mass ([12]). Reaction (22) contains a mixture of $\frac{3}{2}$ and $\frac{1}{2}$ isotopic spin states. With increasing energy $p_{\frac{3}{2}}^{\frac{3}{2}}$, $d_{\frac{3}{2}}^{\frac{1}{2}}$, $f_{\frac{5}{2}}^{\frac{1}{2}}$ waves become, in turn, dominant. In this case we have considered different from 0 only

$$f_{1+}^{\frac{3}{2}} \quad \text{for} \quad u\leqslant 1.51 \tag{25}$$

$$f_{2-}^{\frac{1}{2}} \quad \text{for} \quad 1.51\leqslant u\leqslant 1.69 \tag{26}$$

$$f_{3-}^{\frac{1}{2}} \quad \text{for} \quad u\geqslant 1.69 \tag{27}$$

f_{2-} and f_{3-} have been calculated by empirical one-resonance level formulas (valid only in the above-mentioned intervals) from the latest experimental data ([13]). We obtain

$$f_{2-}(u)=\frac{1}{2.288\chi'}\frac{\Gamma_2}{(u_2-u)-i\Gamma_2/2}\,, \tag{28}$$

$$\begin{cases} \Gamma_2=68.23\,u^3-315.30\,u^2+485.21\,u-248.47 \\ u_2=1.619\,, \end{cases} \tag{29}$$

$$f_{3-}(u)=\frac{1}{2\chi'}\frac{\Gamma_3}{(u_3-u)-i\Gamma_3/2}\,, \tag{30}$$

$$\begin{cases} \Gamma_3=-7.96\,u^3+48.33\,u^2-96.27\,u+63.27 \\ u_3=1.800\,. \end{cases} \tag{31}$$

([11]) M. Gell-Mann and K. Watson: *Ann. Rev. Nucl. Sci.*, **4**, 219 (1954).

([12]) We will express in the following all numerical results in units of proton mass. unless otherwise stated.

([13]) P. Falk-Vairant and G. Valladas: Centre d'Etudes Nucléaires de Saclay, rapport à la conférence de Rochester (1960).

Reaction (23) contains also a mixture of isotopic spin states. $p^{\frac{3}{2}}$ waves are dominant in interval (25), $d^{\frac{3}{2}}$ and $f^{\frac{5}{2}}$ waves in intervals (26) and (27), but in the latter cases the $p^{\frac{3}{2}}$ wave is not negligible with respect to $d^{\frac{3}{2}}$ and $f^{\frac{5}{2}}$ waves, because it enters multiplied by a factor of 4 (when squared). For this reason the calculations relative to reaction (2) are somewhat more complicated than those relative to reaction (1). In the next section we will first consider reaction (1) and on this basis we will obtain a good approximation for the calculations of reaction (2).

4. – Spin summations.

By substituting in (14) the $\langle T_i^u \rangle$ calculated with the usual Feynman rules and the $\langle T_i^l \rangle$ obtained from (16) and (20), and finally by averaging over initial and summing over final spins we obtain for the first reaction

$$(32)\qquad |T|^2 = F_1(u^2, l^2, \Delta^2, s^2) + F_1(u^2, l^2, r^2, t^2) + \tfrac{1}{9}F_1(l^2, u^2, s^2, \Delta^2) + \\ + \tfrac{1}{9}F_1(l^2, u^2, t^2, r^2) + F_2(u^2, l^2, \Delta^2, s^2) + \tfrac{1}{9}F_2(l^2, u^2, s^2, \Delta^2) + \\ + \tfrac{1}{3}F_3(u^2, l^2, \Delta^2, s^2) + \tfrac{1}{3}F_3(u^2, l^2, r^2, t^2)$$

with

$$(33)\qquad F_1(u^2, l^2, \Delta^2, s^2) = \\ = \frac{2g^2u^2(2\pi)^2}{M^4}\,\frac{\Delta^2}{(\Delta^2+\mu^2)^2}\,\mathrm{Re}[f_1f_1^* + f_1f_2^*\cos\varepsilon' + f_2f_1^*\cos\varepsilon' + f_2f_2^*]\,,$$

$$(34)\qquad F_2(u^2, l^2, \Delta^2, s^2) = \frac{2(2\pi)^2 g^2}{M^4}\,\frac{u^2}{(\Delta^2+\mu^2)(r^2+\mu^2)}\,\mathrm{Re}\{[(p'_{10}-M)(k'_{10}-M)]^{\frac{1}{2}}\cdot \\ \cdot[f_1f_1^*\cos\alpha' + f_2f_2^* + f_1f_2^*\cos\varepsilon' + f_2f_1^*\cos\beta'](u+M) + [(p'_{10}+M)(k'_{10}+M)]^{\frac{1}{2}}\cdot \\ \cdot[f_2f_2^*\cos\alpha' + f_1f_1^* + f_2f_1^*\cos\varepsilon' + f_1f_2^*\cos\beta'](u-M)\}\,,$$

$$(35)\qquad F_3(u^2, l^2, \Delta^2, s^2) = -\frac{g^2}{4M^4}\,\frac{1}{(\Delta^2+\mu^2)(s^2+\mu^2)}\,\mathrm{Re}\{L[AA^* - \mu^2BB^*] - \\ - N[MBA^* + MAB^* + 2BB^*]\chi'(|\boldsymbol{p}'_1|\cos\varepsilon' + p'_{10}q'_{20}) + P[BA^* - AB^*] + \\ + Q[2BA^*(\chi'|\boldsymbol{p}'_1|\cos\varepsilon' + p'_{10}q'_{10}) + MAA^* + \mu^2BB^*]\}\,.$$

Here the f_i are functions of u^2 and Δ^2; f_i^* are functions of u^2 and Δ^2 in (33), of u^2 and r^2 in (34), of l^2 and s^2 in (35). We have

$$(36)\qquad L = up'_{20}(|\boldsymbol{p}'_1||\boldsymbol{k}'_1|\cos\alpha' + p'_{10}k'_{10}) - u\chi'k'_{10}|\boldsymbol{p}'_1|\cos\varepsilon' - \chi'|\boldsymbol{k}'_1|\cos\beta'\cdot \\ \cdot(up'_{10} - M^2) + M^2(M^2 - up'_{10} - k'_{10}p'_{20})$$

$$N = \chi' |\boldsymbol{p}_1'| (u k_{10}' - M^2) + \chi' |\boldsymbol{k}_1'| \cos\beta' u(u - p_{10}') + M^2(\mu^2 - p_{10}' q_{20}') + \tag{37}$$
$$+ \tfrac{1}{2}(\Delta^2 + 2M^2)(\chi'^2 + p_{20}' q_{20}')$$

$$P = M\{\chi' |\boldsymbol{p}_1'| \cos\varepsilon'[W^2 - 3M^2 + \mu^2 + u k_{10}' + 2p_{10}'(q_{20}' - p_{20}' - k_{10}')] + \tag{38}$$
$$+ \chi' |\boldsymbol{k}_1'| \cos\beta'(u p_{10}' - M^2) + |\boldsymbol{k}_1'| |\boldsymbol{p}_1'| \cos\alpha'(2k_{10}' - u)M - q_{20}' p_{10}' k_{10}'(k_{20}' - p_{10}' - k_{10}') +$$
$$+ M^2 q_{20}'(p_{10}' - k_{10}') + p_{10}' q_{20}'(\mu^2 - p_{10}' p_{20}') + M^2(\chi'^2 + p_{20}' q_{20}')\}$$

$$Q = M\{|\boldsymbol{k}_1'| |\boldsymbol{p}_1'| \cos\alpha' - \chi' |p_1'| \cos\varepsilon' + k_{10}'(u - p_{10}') + p_{20}'(k_{20}' - k_{10}')\} \tag{39}$$

g is the renormalized pion-nucleon coupling constant

$$g^2 = \frac{16\pi M^2 f^2}{\mu^2}, \tag{40}$$

$$f^2 = 0.08\,. \tag{41}$$

The f_1 terms come from square moduli of the single graphs, the F_2 terms from interferences between graphs which differ for the exchange of the initial nucleons, and the F_3 terms from interferences between graphs which differ for the exchange of the final nucleons. The interference terms between graphs which differ for the exchange of both initial and final nucleons vanish. The factors $\frac{1}{3}$ and $\frac{1}{9}$ are due to isotopic spin.

By putting (32) into (8) and (9) we get the spectra of outgoing nucleons. In case (8) the integrals of the first, the second and the fourth term can be easily reduced to single integrals because the integrands are φ'-independent ([5]). We can get a similar reduction also in case (9).

The main contributions to the cross-section are due to the F_1 terms. At 2.85 GeV, the F_2 terms give a contribution about five times as small as the F_1 terms the F_3 terms give a negligible contribution. We note also that the F_2 terms are the smaller the larger is the number of waves occurring.

Consider reaction (2). In this case we neglect the interference terms F_3, because they are the same as in the previous case, apart from isotopic spin factors. For the other terms we use formula (33) (without the F_3 terms) with the following additional modifications:

a) the numerical coefficient in front of all the F_1 and F_2 terms is $\frac{1}{18}$;

b) for F_1 terms we have assumed the following expressions in intervals (25), (26) and (27) for f_1 and f_2

$$\begin{cases} f_1 = 6f_{1+} \cos\varepsilon' \\ f_2 = -2f_{1+} \end{cases}, \tag{41'}$$

$$\begin{cases} f_1 = 6f_{1+} \cos\varepsilon' - f_{2-} \\ f_2 = -2f_{1+} + 3f_{2-} \cos\varepsilon' \end{cases} \tag{42}$$

and

$$\left\{ \begin{array}{l} f_1 = 6f_{1+}\cos\varepsilon' - 3f_{3-}\cos\varepsilon' \\ f_2 = -2f_{1+} + f_{3-}\,\frac{3}{2}(5\cos^2\varepsilon' - 1) \end{array} \right. \tag{43}$$

respectively.

5. – Concluding remarks.

Numerical results at 2.85 GeV for reactions (1) and (2) are shown and compared with experimental data in Figs. 3, 4 and 5. The agreement is very good when the squared four-momentum of the virtual pion is small (of the order of few times the squared π-meson mass). Not only the presence and the exact position of the low and high energy peaks are correctly predicted, but also their absolute normalization is reproduced within the experimental errors. This, to our opinion, definitely suggests that the one-pion exchange contribution plays an important role in the description of processes (1) and (2). Let us analyse the general behaviour of Figs. 3 and 4 referring to reaction (1).

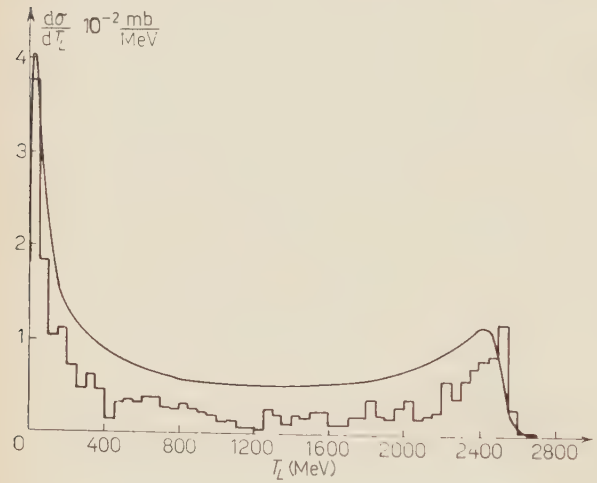

Fig. 3. – Theoretical and experimental spectrum of outgoing neutrons in the lab. system for the $p + p \to p + n + \pi^+$ reaction at 2.85 GeV of kinetic energy in the lab. system of the incoming protons.

As we said already in the text, all the interferences between the diagrams in Fig. 2 turn out to be small. Therefore, we can discuss, in a first approximation, the four diagrams separately. The largest contribution is always given from the graphs 1 and 2 of Fig. 2, where the π^+ comes out with the proton and allows the formation of the pure $T = J = \frac{3}{2}$ resonance. The squared matrix element of graph 1 contains the factor $\Delta^2(\Delta^2 + \mu^2)^{-2}$ which would give alone a steep maximum at $\Delta^2 \simeq \mu^2$. The further Δ^2-dependence of the cross-section, given from the phase space limitations on the integration over the other dynamical variables, shifts this maximum to $\Delta^2 \simeq 2\mu^2$. Due to the proportionality of Δ^2 to the lab. neutron energy, this gives the low

energy peak in Fig. 3. The high energy peak, which exists again for low values of the squared four-momentum of the virtual pion (r^2 this time), is contributed from graph 2. Its existence can be understood as follows. Graph 1 gives a strong backward peak of the neutrons in the c.m. angular distribution. Graph 2 gives a symmetric c.m. forward peak. The fact that these diagrams give a symmetric contribution is simply an effect of the Pauli principle, stating that all the final particles in a reaction in which the initial ones are identical, must have a c.m. angular distribution symmetric around 90°. The forward neutrons in the c.m. will then give rise to the high energy peak in the lab. system, while the backward ones give rise to the low energy peak. This effect is enhanced by the presence of the 33 resonance in the lower vertices. For the proton spectrum the argument is similar, though a little more complicated. The protons from graphs 1 and 2 are coming out together with a π^+. Tendency of formation of the 33 isobar will be shown. It should be clear that since the c.m. angular distribution of the « isobar » is the same as that of the neutron and since the proton is much heavier than the pion (the kinetic relative energy being small), its angular distribution will again be peaked forward and backward, though less markedly than for the neutron. Therefore, again, we should expect high and low energy peaks in the proton lab. spectra, of course broader than in the neutron case. Practically for the high energy peak the

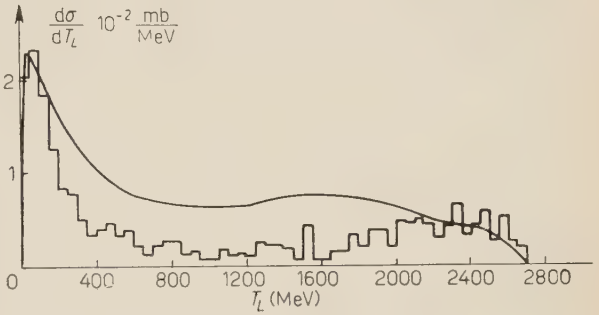

Fig. 4. Theoretical and experimental spectrum of outgoing protons in the lab. system for the reaction $p+p \rightarrow p+n+\pi^+$ at 2.85 GeV of kinetic energy in the lab. system of the incoming protons.

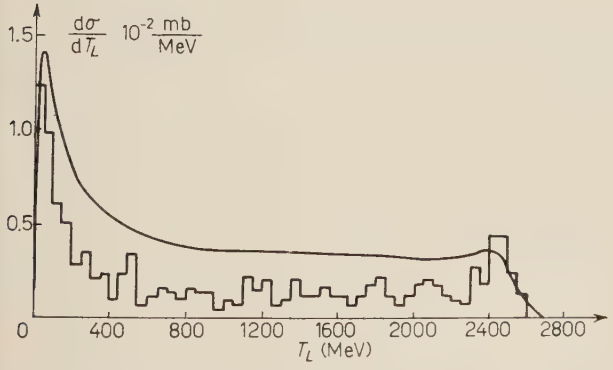

Fig. 5. – Theoretical and experimental spectrum of outgoing protons in the lab. system for the reaction $p+p \rightarrow p+p+\pi^0$ at 2.85 GeV of kinetic energy in the lab. system of the incoming protons.

broadening is so large that the peak disappears, but in any case we have a concentration of events at high energy.

Similar considerations hold also for reaction (2): in this case, further complications arise from the fact that all the 4 diagrams have the same weight and that in all of them d and f waves are present. The qualitative features discussed above can be, however, easily extended also to this case.

* * *

We thank Professor L. Van Hove for kind hospitality in the theoretical group at CERN, where an important part of this work has been carried out. We thank also the CERN Ferranti computer staff for invaluable help in the numerical calculations. We thank Drs. E. Ferrari and F. Selleri for very useful suggestions and for continuous advice. We are indebted also to Professors M. Cini and R. Gatto for their interest in this work.

RIASSUNTO

La produzione singola di pioni nell'urto nucleone-nucleone è calcolata nell'approssimazione di un solo pione scambiato. Sono stati calcolati tutti i possibili diagrammi di questo tipo nella « pole approximation » discussa nel testo; si è tenuto conto anche dei termini di interferenza fra essi. Sono stati calcolati gli spettri nell'energia nel laboratorio dei nucleoni finali e sono stati confrontati con i dati sperimentali a 2.85 GeV. Questo confronto mostra un notevole buon accordo per piccoli valori del quadrato del quadri-impulso del pione virtuale. Per valori più alti il comportamento qualitativo è ancora riprodotto, ma i valori teorici sono più grandi di quelli sperimentali.

Energy Spectrum of Photoneutrons from Cobalt.

V. Emma, C. Milone and A. Rubbino

Istituto di Fisica dell'Università - Catania
Centro Siciliano di Fisica Nucleare - Catania
Istituto Nazionale di Fisica Nucleare - Catania

S. Jannelli and F. Mezzanares

Istituto di Fisica dell'Università - Messina
Istituto Nazionale di Fisica Nucleare - Messina

(ricevuto il 16 Luglio 1961)

Summary. — The energy spectrum of the photoneutrons emitted at 90° from cobalt irradiated by a collimated 30 MeV bremsstrahlung beam is studied by recording the protons recoil tracks in L-4 Ilford photoemulsions 400 μm thick. The neutron spectrum is analysed in neutron energy steps of 0.5 MeV, starting from $E_{n\,min}=2$ MeV. A maximum around $E_n=(4\div5)$ MeV in the experimental spectrum gives evidence of a contribution of other processes besides the evaporation. The interpretation of the experimental results is discussed.

1. – Introduction.

Many experiments on the photoneutron spectra from several elements have shown that for heavy nuclei ($A>180$) [1-9] the photoneutron emission proceeds predominantly by evaporation processes.

(1) P. R. Byerly jr. and W. E. Stephens: *Phys. Rev.*, **81**, 473 (1951).
(2) G. A. Price: *Phys. Rev.*, **93**, 1279 (1954).
(3) M. E. Toms and W. E. Stephens: *Phys. Rev.*, **108**, 77 (1957).
(4) G. M. Zatsepina, L. E. Lazareva and A. N. Pospelov: *Sov. Phys. JEPT*, 5, 21 (1957).
(5) G. Cortini, C. Milone, A. Rubbino and F. Ferrero: *Nuovo Cimento*, **9**, 85 (1958).
(6) S. Cavallaro, V. Emma, C. Milone and A. Rubbino: *Nuovo Cimento*, **9**, 736 (1958).
(7) V. Emma, C. Milone, A. Rubbino and R. Malvano: *Nuovo Cimento*, **17**, 365 (1960).
(8) R. F. Askev and A. P. Baston: *Nucl. Phys.*, **20**, 408 (1960).
(9) H. N. Kornblum and S. C. Freden: Private communication.

On the contrary the photoneutrons from light ($A < 16$) nuclei ([10-11]) occur mainly by transition to the ground state or to the first excited states of residual nuclei. The statistical theory cannot be applied in this case, but as the mass number A of the irradiated elements increases, the evaporation contribution becomes more and more important.

For medium elements ([12-13]) both processes compete and a clear separation between the contributions of the two processes in the experimental spectrum is not easy.

In most investigations on the spectra the photoneutrons are recorded by means of the proton recoil tracks in photonuclear emulsions. In this case for $E_n < (1 \div 2)$ MeV the uncertainty in the relative neutron flux becomes relevant.

But $E_n < (1 \div 2)$ MeV is also the region where the maximum of neutron emission is expected for evaporation ([5-6]).

For this reason a comparison between the experimental and the calculated spectra is made in the region beyond the expected maximum of the energy spectra according to the evaporation theory.

In the present paper the results of an investigation on the photoneutrons from $^{59}_{27}$Co, a medium and deformed element, are reported.

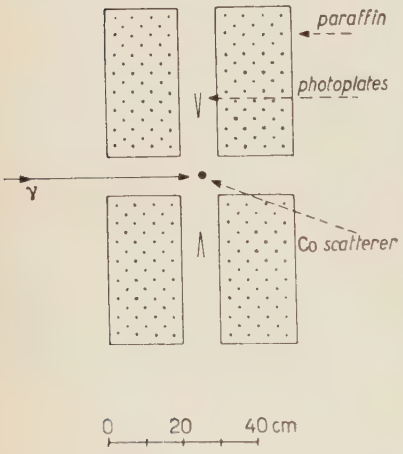

Fig. 1. – Experimental arrangement.

2. – Experimental procedure.

A 68.5 g cobalt target has been irradiated by a collimated γ-ray beam from the B.B.C. Betatron of Torino « Molinette ».

The distance between the betatron target and the cobalt was 1 m.

The photoneutrons were recorded by means of L-4 Ilford plates, 400 μm thick with the emulsion layers at a mean distance of 15 cm from the cobalt. Paraffin 20 cm thick screened the plates against the neutrons from the betatron (Fig. 1).

The exposure was of 2000 roentgen at $E_{\gamma\max} = 30$ MeV.

([10]) C. MILONE and A. RUBBINO: *Nuovo Cimento*, **13**, 1035 (1959).

([11]) V. EMMA, C. MILONE and A. RUBBINO: *Phys. Rev.*, **118**, 1297 (1960).

([12]) G. CORTINI, C. MILONE, T. PAPA and R. RINZIVILLO: *Nuovo Cimento*, **14**, 54 (1959).

([13]) V. EMMA, C. MILONE and R. RINZIVILLO: *Nuovo Cimento*, **14**, 1149 (1959).

The conventional method used to analyze the proton recoil tracks is described in previous works [5-10].

Some correction factors to obtain the neutron spectra by the experimental proton spectra are reported in Fig. 2. The correction factor is $[T_{Co} \cdot T_{Pb} \cdot \sigma \cdot P(l)]^{-1}$.

The tracks utilized were only those whose original direction fell into a pyramid centered on the neutron beam and having semiaperture $\beta = \varphi = 15°$.

The relation $E_n = E_p/\cos^2 \vartheta$ (where $\cos \vartheta = \cos \beta \cos \varphi$) was used only for $\vartheta \geqslant 5°$.

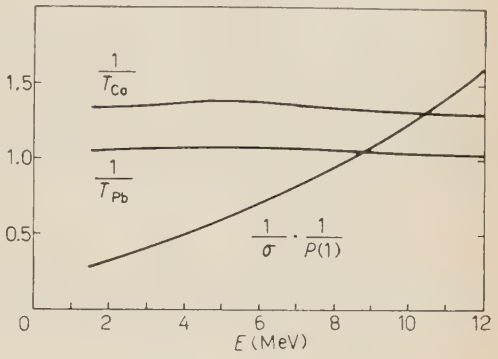

Fig. 2. – $T_{Co}(E_n)$ = probability that a neutron does not collide in the Co target. $T_{Pb}(E_n)$ = probability that a neutron does not collide in the lead screen. $P_l(E_p)$ = probability that a proton track ends its range in the emulsion of 400 μm thick for maximum accepted dip angle $\beta = 15°$. $\sigma(E_n)$ = = cross-section for the neutron-proton collision (barns).

3. – Results.

3·1. *Low energy neutrons.* ($E_n < 4$ MeV). – In Fig. 3 the points represent the experimental energy distribution of the photoneutrons. The curves represent the evaporation spectra calculated by means of the expression [6-14]

$$(1) \qquad F(E_n) = K E_n \sigma(E_n) \int_{B_0 + E_n}^{E_\beta} \frac{\omega(E_R)\sigma_{\gamma n}(E_\gamma) I(E_\gamma, E_\beta)\, dE_\gamma}{\int_0^{E_\gamma - E_n} E_n \sigma(E_n)\omega(E_R)\, dE_n},$$

where: E_n = neutron energy;

$\sigma(E_n)$ = reaction cross-section for neutrons of energy E_n on residual nucleus [15];

B_0 = binding energy;

$\omega(E_R)$ = energy level density in residual nucleus with excitation energy $E_R = E_\gamma - B_0 - E_n$;

[14] V. F. Weisskopf and D. H. Ewing: *Phys. Rev.*, **57**, 472 (1940).

[15] H. Feshbach and V. F. Weisskopf: *Phys. Rev.*, **76**, 1550 (1949).

$\sigma(\gamma, n)$ = cross-section for the (γ, n) process ([16,17]);
$I(E_\gamma, E_\beta)$ = bremsstrahlung spectrum with maximum energy E_β ([18,19]).

The $F(E_n)$ distribution (1) is not sensitive to small variation in the $\sigma(\gamma, n)$ adopted values ([16,17]).

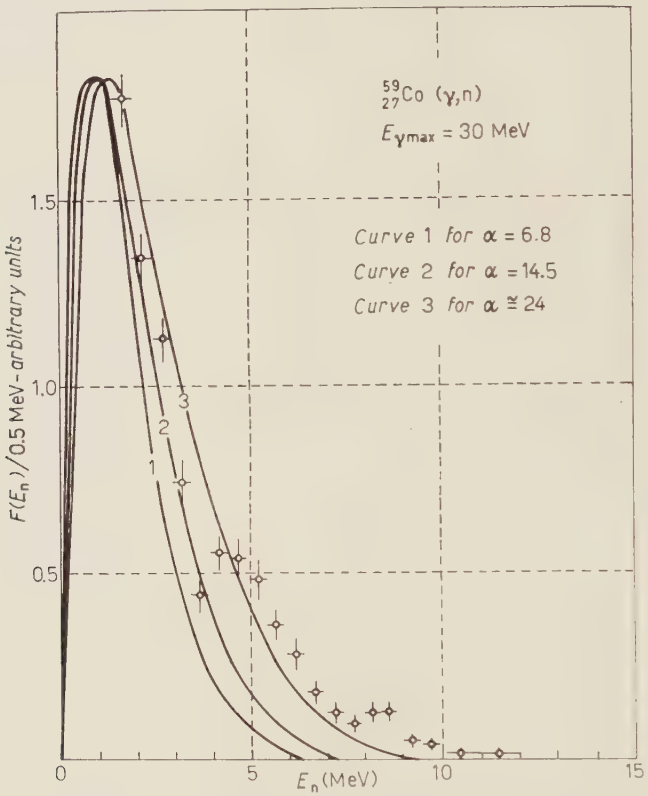

Fig. 3. – Points: experimental photoneutron spectrum from cobalt. The curves represent evaporation spectra calculated according to expression (1). For $\omega(E_R)$ given by (2): curve (1) for $\alpha=6.8$; curve (2) for $\alpha=14.5$; curve (3) for $\alpha=24$ using $\omega(E_R)$ given by (3).

According to different authors the level density can be represented by

$$\omega(E_R) = C \exp[\alpha E_R]^{\frac{1}{2}} ; \tag{2}$$

([16]) R. M. MONTALBETTI, L. KATZ and J. GOLDEMBERG: *Phys. Rev.*, **91**, 659 (1953).
([17]) P. A. FLUORNOY, R. S. TICKLE and W. D. WHITEHEAD: *Phys. Rev.*, **120**, 1424 (1960).
([18]) J. H. CARVER and K. H. LOKAN: *Austral. Journ. Phys.*, **30**, 312 (1957).
([19]) C. MILONE, S. MILONE TAMBURINO, R. RINZIVILLO, A. RUBBINO and C. TRIBUNO: *Nuovo Cimento*, **7**, 729 (1958).

in our case the parameter α assumes the values 6.8, 11.6, and 14.5 according to references ([20,14,21]), respectively. In Fig. 3 the curves (1) and (2) are obtained for $\alpha = 6.8$ and 14.5 MeV^{-1}.

The curve (3) is obtained using the expression

$$\omega(E_R) = C(\exp[\alpha E_R])^{\frac{1}{2}}/E_R^2 , \tag{3}$$

with $\alpha = 24$ ([22]).

The curve (2) seems to give a best fit with experimental points in the low energy region.

Generally some caution is required about this type of assertion since a not negligible contribution to the low energy part of the spectrum may be given by (γ, 2n) and (γ, pn) processes. In our case this contribution seems to be very small for neutron energy higher than 2 MeV, but the deficiency of experimental data below $E_n = 1.5$ MeV does not consent exact assertions (see Section **4**).

3·2. *High energy neutrons.* ($E_n > 4$ MeV). – The experimental spectrum shown in Fig. 3 gives evidence of an high energy tail and of a clear peak around $E_n = (4 \div 5)$ MeV.

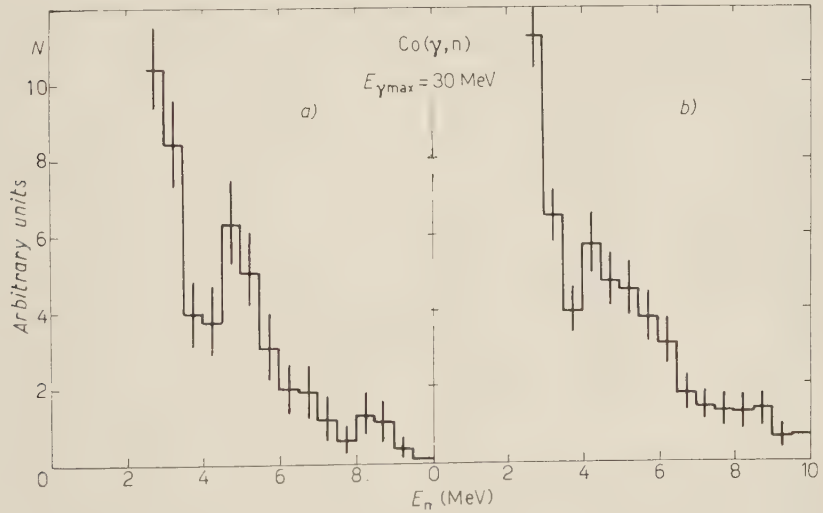

Fig. 4. – Partial photoneutron spectra from Co as measured independently at Catania (*a*) and Messina (*b*) laboratories.

(*) Quite similar results have been obtained by W. R. Dixon: *Canadian Journ. Phys.*, **33**, 785 (1955), by irradiation of Cu and Pb targets with 70 MeV bremsstrahlung.

([20]) B. C. Diven and G. M. Almy: *Phys. Rev.*, **80**, 407 (1950).

([21]) S. A. Moszkowsky: *Handb. d. Phys.*, **39**, 437 (1957).

([22]) V. Facchini *et al.*: Private communication.

A similar situation has been found for other medium and heavy elements: tails and peaks more or less pronounced have been found in the photoneutron spectra from Al [12], Ca [13], K [13], Cr [5], Rh [23], Cu [1], Pb [3], Ta [5], Au [6,8], U [9] (*).

The high energy tail of the spectra out of the calculated evaporation curves is usually interpreted in terms of a neutron emission with a very low energy excitation of the residual nucleus.

In the present photoneutron spectrum from cobalt the peak around $E_n = (4 \div 5)$ MeV is well marked and has been found in Catania (Fig. 4*a*) as well as in the Messina (Fig. 4*b*) laboratories.

The good agreement between the two partial results (normalyzed to the same total flux) confirms clearly the existence of this peak and its position.

4. – Discussion.

4·1. *Evaporation spectra.* – The spectra calculated by means of the expression (1) for $\alpha = 6.8$ MeV^{-1} and $\alpha = 14.5$ MeV^{-1}, respectively, (see Fig. 3) are also reported in Fig. 5 and compared with the spectra calculated according to the simplified and commonly used expression [12,13,7]

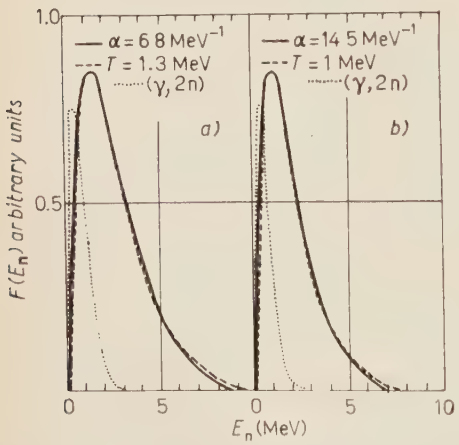

Fig. 5. – Calculated evaporation spectra: full line by expression (1). Broken line by expression (4). Dotted lines refer to the estimated contribution of (γ, 2n) see text Section 4·2.

$$(4) \qquad F(E_n) = \text{const}\, E_n \sigma(E_n) \exp[-E_n/T],$$

T being the « nuclear temperature ».

As Fig. 5*a* shows, the spectrum calculated according to expression (1) for $\alpha = 6.8$ MeV^{-1} agrees with that calculated according to expression (4) for $T = 1.3$ MeV. A similar agreement is shown in Fig. 5*b* between the correspondent curves obtained for $\alpha = 14.5$ MeV^{-1} and $T = 1.0$ MeV respectively.

(23) A. AGODI, S. CAVALLARO, G. CORTINI, V. EMMA, C. MILONE, R. RINZIVILLO, A. RUBBINO and F. FERRERO: *Compt. Rend. Congrès International de Physique Nucléare* Paris, 7-12 Julliet 1958 (Paris, 1959), p. 625.

The expression (4) refers to the case of a defined excitation energy of the compound nucleus (experiments with monoenergetic photons); in this case the residual nucleus after the neutron emission is left in a defined average energy $\bar{E}_R \simeq E_{R\max}$.

As the $\sigma(E_n)$ cross-section varies very slowly for neutron energies above $(1 \div 2)$ MeV, the expression (4) may be written in the form:

$$F(E_n) = KE_n \exp[-E_n/T], \tag{4'}$$

where T is a function that increases slowly with E_R and is generally interpreted as a « nuclear temperature » determined by $[T(E_R)]^{-1} = [\mathrm{d} \ln \omega(E_R)]/\mathrm{d}E_R$.

According to expression (4') the maximum of $F(E_n)$ lies at $E_n = T$.

For irradiation with monoenergetic γ-rays, according to expression (1) the $F(E^n)$ distribution depends on $E_n\omega(E_R)$. For $\omega(E_R)=\exp[\alpha(E_\gamma - E_{th} - E_n)]^{\frac{1}{2}}$, (2), the maximum of $F(E_n)$ lies at

$$E_n^* = \frac{2}{\alpha}([1 + \alpha(E_\gamma - E_{th})]^{\frac{1}{2}} - 1). \tag{5}$$

This shows that for irradiation with monoenergetic γ-rays of energy E_γ, the average energy of the residual nucleus and the correspondent nuclear temperature $E_n^* = f(E_\gamma)$ increases slowly as the energy E_γ increases.

In Fig. 6*a* is reported the function $E_n^* = f(E_\gamma) = T(E_\gamma)$ calculated according to expression (5).

In conclusion if monochromatic γ-rays are used, the expression (4) or (4') may represent the $F(E_n)$ distribution, if appropriate values of $T = f(E_\gamma)$, are used.

This conclusion shows also that in the case of irradiation with a bremsstrahlung beam it should be incorrect to use for $F(E_n)$ the expression (4). Indeed

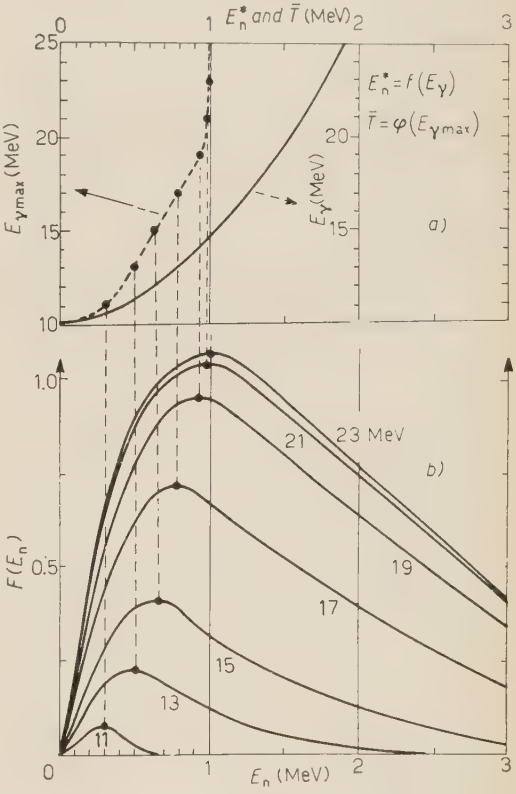

Fig. 6. – Co(γ, n). *a*) Full line: $E_n = f(E_\gamma)$ calculated according to expression (5) for monoenergetic γ-rays. Dotted line $\bar{T} = f(E_{\gamma max})$. *b*) Distribution $F(E_n)$ calculated according to expression (1) for the values of $E_{\gamma max}$ indicated in the curves and for $\alpha = 14.5$ MeV [1].

$\bar{E}_{\mathrm{Rmax}}$ varies between zero and $(E_{\gamma\max} - E_{\mathrm{threshold}})$, and so different temperatures $T = T(E_\gamma)$ are contemporarely present.

The expression (4) may represent also the $F(E_n)$ distribution by the introduction of a « mean temperature $\bar{T}$ » in the following way.

When for irradiation with a bremsstrahlung spectrum at a given $E_{\gamma\max}$ according to expression (1) the maximum of $F(E_n)$ lies at $E_n^*(E_{\gamma\max})$, we can assume $\bar{T} = E_n^*(E_{\gamma\max})$ in the expression (4'). Under this assumption the distribution (1) and (4) are similar.

In the case of cobalt we have calculated according to expression (1) the distributions $F[E_n(E_{\gamma\max})]$ for several values of $E_{\gamma\max}$ (Fig. 6*b*).

The behaviour of $\bar{T} = E_n^*(E_{\gamma\max})$ is shown in Fig. 6*a*.

As Fig. 6 shows, $E_n^*(E_{\gamma\max})$ increases with $E_{\gamma\max}$, but more slowly than $E_n^*(E_{\gamma\max})$ and reaches a maximum (1 MeV in our case) for $E_{\gamma\max} > 20$ MeV.

This trend of T is due to the behaviour of the factor $\sigma(\gamma, \mathrm{n}) \cdot I(E_\gamma, E_\beta)$.

4·2. *Other contributions to the photoneutron emission.* – The total photoneutron cross-section has been measured up to 24 MeV ([16-17]) by other authors.

According to the recent measurements of the $\sigma(\gamma, \mathrm{n})$ ([17]) the giant resonance seems to be splitted into two resonances as expected ([24-25]) for strongly deformed nuclei.

In paper ([17]) the total cross-section is obtained from the yield curves after having corrected the experimental data for the neutron multiplicity above the $(\gamma, 2\mathrm{n})$ threshold (~ 18.6 MeV), using the statistical theory of nuclear reactions ([17,7]) in order to obtain the $(\gamma, 2\mathrm{n})$ cross-section.

At the excitation energies used, the (γ, np) process is negligible respect to the $(\gamma, 2\mathrm{n})$ because the emission of charged particles is strongly inhibited by the Coulomb barrier.

In Fig. 7*a* the factor $\sigma(\gamma, \mathrm{n}) \cdot I(E_\gamma, E_\beta)$ as a function of $(E_\gamma - E_{\mathrm{th}}(\gamma, \mathrm{n}))$ is reported: curves I and II are obtained using respectively the $\sigma(\gamma, \mathrm{n})$ cross-section given in ref ([16-17]).

In the same Fig. 7 is reported the factor $2 \cdot \sigma(\gamma, 2\mathrm{n}) \cdot I(E_\gamma, E_\beta)$ as function of $\frac{1}{2}[E_\gamma - E_{\mathrm{th}}(\gamma, 2\mathrm{n})]$. Namely in this case we make the roughly simplified assumption that the two neutrons are emitted with same energy in the single reaction. Making the same hypothesis we have calculated by means of eq. (1) the evaporation spectra due to the $(\gamma, 2\mathrm{n})$ process. The spectra obtained using for the parameter α the values 6.8 and 14.5, respectively, are reported in dotted lines in Fig. 5*a* and 5*b*. The results show that the neutron contribution is quite negligible for $E_n \cdot 2$ MeV. In Fig. 7*b* we have reported the

([24]) R. OKAMOTO: *Phys. Rev.*, **110**, 143 (1958).
([25]) M. DANOS: *Nucl. Phys.*, **5**, 23 (1958).

$D(E_n)$ difference between the experimental photoneutron spectrum (Fig. 3) and the evaporation curve calculated using for α the value 14.5 MeV^{-1}.

At $E_n > 4$ MeV the difference is attributed to the contribution of processes different from evaporation. This contribution should be $\sigma(\gamma, n) \cdot I(E_\gamma, E_\beta)$ — see Fig. 7*a* — if the residual nucleus was left in the ground state.

The ratio between this difference and the total spectrum gives an estimate of the fractional contribution of neutrons emitted by other process than the evaporation. This ratio is ~ 0.35 for $E_n > 2$ MeV.

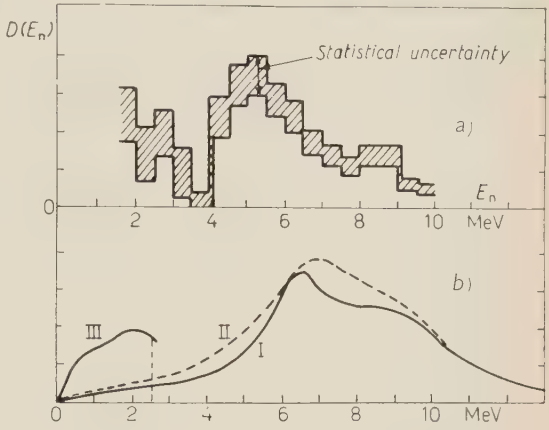

Fig. 7. – *a*) Expected photoneutron distribution for transition to the ground state for the (γ, n) process, curves I and II and for the (γ, 2n) process, curve III (see text). Abscissae: $E_\gamma - E_{th}$ (d, n) for curves I and II; $\frac{1}{2}[E_\gamma - E_{th}(\gamma, 2n)]$ for curve III. Ordinates: $\sigma(\gamma, n) \cdot I(E_\gamma, E_\beta)$ for curves I and II; $2\sigma(\gamma, 2n) \cdot I(E_\gamma, E_\beta)$ for curve III. *b*) $D(E_n)$ = difference between the experimental spectrum and the evaporation curve 2 of Fig. 3.

At $E_n < 3.5$ MeV we have also a positive difference between the experimental spectrum and the $\sigma(\gamma, n) \cdot I(E_\gamma, E_\beta)$. In this energy region the difference may be attributed to the contribution of (γ, 2n) processes.

The trend of the expected contribution of (γ, 2n) reaction for processes different than evaporation is shown in Fig. 7*b* curve III for E_n up to 2.5 MeV, say for E_γ up to 24 MeV, that is the maximum value of the known $\sigma_T(\gamma, n)$ cross-section. The experimental uncertainty being too large it is not possible to obtain more detailed information.

5. – Conclusion.

For $E_n > 2$ MeV the photoneutron emission from $^{59}_{27}$Co at 90° and under 30 MeV bremsstrahlung may be attributed—see Fig. 3—for about 65 % to evaporation and for ~ 35 % to other processes.

The high energy tail and the peak generally more or less evident in the medium and heavy nuclei (see Section 3·2) are well evident at 90° in the photoneutron spectrum from cobalt.

The contribution of processes different than evaporation is quite similar to the distribution $\sigma(\gamma, n) \cdot I(E_n, E_\beta)$, with a low shift that could indicate an average excitation of the residual nucleus of about 1 MeV.

* * *

This work has been supported in part by contribution of the C.R.R.N.

RIASSUNTO

Si studia lo spettro energetico dei fotoneutroni emessi a 90° dal cobalto irradiato con bremsstrahlung di 30 MeV. I neutroni sono rilevati mediante i protoni di rinculo in emulsioni Ilford L-4 di 400 μm. Lo spettro energetico è stato analizzato in intervalli di 0.5 MeV a partire da $E_n = 2$ MeV. Si mette in evidenza nello spettro una « coda » di alta energia ed un massimo intorno ad $E_n = (4 \div 5)$ MeV che indicano, per l'emissione di neutroni, un contributo di altri processi oltre a quello di evaporazione. Si discutono i risultati sperimentali.

IL NUOVO CIMENTO Vol. XXII, N. 1 1° Ottobre 1961

Comparison of Three Equations for the Spacing of Nuclear Levels.

Y. P. VARSHNI (*)

Division of Pure Physics, National Research Council - Ottawa

(ricevuto il 17 Luglio 1961)

Summary. — The equations of Bethe, Weisskopf and of Lang and Le Couteur for the spacing of nuclear levels have been compared using the experimental data for 40 nuclei. The average errors obtained by the three equations are not very different. Bethe's equation has been found to give the best results. Odd-even effects on the pre-exponential constants in the three equations have been discussed.

1. – Introduction.

In recent years, a good deal of experimental information on nuclear energy levels has been accumulated. These data have proved valuable in determining the dependence of the density of energy levels on the excitation energy and in analysing the theoretical postulates underlying the statistical model of the nucleus and the statistical theory of nuclear reactions.

Since BETHE's [1] original work in 1936 quite a few attempts have been made to calculate the level density on different models of the nucleus. A concise review of some of these has been given by MORRISON [2] and by TER HAAR [3]. Recently, a detailed esposition of the various theoretical attempts

(*) National Research Council Postdoctorate Fellow.

(1) H. A. BETHE: *Phys. Rev.*, **50**, 332 (1936); *Rev. Mod. Phys.*, **9**, 79 (1937).

(2) P. MORRISON: *Experimental Nuclear Physics* (Editor: E. SEGRÈ), vol. **2** (New York, 1953), p. 31.

(3) D. TER HAAR: *Elements of Statistical Mechanics* (New York, 1954), p. 296.

has been given by ERICSON (4). References (5-13) provide some of the recent investigations in this field.

However, the overall picture as regards the validity of the theoretical postulates as well as the applicability of the various mathematical expressions for the level density is not clear. Considerable discrepancies have been found by a number of workers. We shall refer to these with the individual equations. Also very few comparative studies of the various equations have been carried out.

In the present paper we have attempted to compare three of the simple equations suggested for the level density ω or the average level spacing D.

2. – The three equations.

Bethe's treatment of the problem was based on a gas-like model. The individual nuclear particles are supposed to move in a simple potential hole, and the energy of the complete nucleus is supposed to be the sum of the energies of the individual particles. This amounts to assuming the interaction between the particles to be small; the nucleus would then be comparable to a gas. The problem then reduces itself to the calculation of the « entropy » of a Fermi gas containing a given number of particles A and having a given excitation energy U above the zero point energy of the Fermi gas.

With this picture, Bethe obtained the following equation for the mean spacing D of nuclear levels of some definite angular momentum J:

$$D = P(AU)^{-2} \exp\left[-2(\mu A U)^{\frac{1}{2}}\right], \tag{1}$$

where A is the mass number and P and μ are constants, μ is equal to $\frac{1}{11}$ (after correcting (14) to $r_0 = 1.3 \cdot 10^{-13}$ cm) when U is in MeV.

A similar but more sophisticated model was proposed by BARDEEN (15) which is often referred to as the « free particle model with correlations ».

(4) T. ERICSON: *Adv. in Phys.*, **9**, 425 (1960).
(5) J. M. B. LANG and K. J. LE COUTEUR: *Proc. Phys. Soc.*, A **67**, 586 (1954).
(6) P. FONG: *Phys. Rev.*, **102**, 434 (1956).
(7) T. D. NEWTON: *Can. Journ. Phys.*, **34**, 804 (1956); *Errata*, **35**, 1400 (1957).
(8) N. ROSENZWEIG: *Phys. Rev.*, **105**, 950 (1957); **108**, 817 (1957).
(9) M. EL-NADI and M. WAFIK: *Nucl. Phys.*, **9**, 22 (1958).
(10) A. G. W. CAMERON: *Can. Journ. Phys.*, **36**, 1040 (1958); **37**, 244 (1959).
(11) T. ERICSON: *Nucl. Phys.*, **6**, 62 (1958); **8**, 265 (1958); **11**, 481 (1959).
(12) D. B. BEARD: *Phys. Rev. Lett.*, **3**, 432 (1959).
(13) D. W. LANG and K. J. LE COUTEUR: *Nucl. Phys.*, **13**, 32 (1959); **14**, 21 (1959-60).
(14) I. DOSTROVSKY, P. RABINOWITZ and R. BIVINS: *Phys. Rev.*, **111**, 1659 (1958).
(15) J. BARDEEN: *Phys. Rev.*, **51**, 799 (1937).

The energy dependence of the result is given by an equation similar to (1) but with $\mu = \frac{1}{2}$ (corrected to $r_0 = 1.3 \cdot 10^{-13}$ cm).

While formulating the statistical theory of nuclear reactions, WEISSKOPF [16] required an expression for the level density. « On account of the extreme inaccuracy of any nuclear model » he was led to develop an approximate expression for ω by other methods which were less exact but perhaps more general than Bethe's method. His expression may be put as

$$1/D = \omega = C \exp\left[2\sqrt{aU}\right], \tag{2}$$

where C and a are parameters. The parameters, which vary with atomic weight, are determined (BLATT and WEISSKOPF [17]) from experimental values of D for levels excited by neutrons slightly above thermal energy ($U \sim$ binding energy of neutron in the compound nucleus) and for levels near the ground level ($U \sim 1$ MeV).

Eq. (2) is a simplification of the Bethe's equation (1) in that the energy dependence of the non-exponential factor has been neglected.

Weisskopf's eq. (2) is the simplest and perhaps the most widely used by experimentalists. However, as emphasized by ERICSON [18] recently, it is unsatisfactory on theoretical grounds. According to Blatt and Weisskopf it « may (only) serve as a first extremely rough approximate orientation to the general features of the density of nuclear levels ».

BLATT and WEISSKOPF [17] have given values of the constants C and a for some typical values of the mass number A. These have been reproduced in Table I. The constant a is usually taken to be proportional to A (FONG [6], EL-NADI and WAFIK [9]). But it may be noted that the values of a obtained from the analysis of a certain class of experiments are almost independent of A. This anomaly has been discussed by IGO and WEGNER [19].

TABLE I. – *Values of C and a in Weisskopf's eq.* (2).

A	C (MeV^{-1})	a (MeV^{-1})	CA^2	a/A
27	0.5	0.45	364.5	.1667
63	0.3	2	1190.7	.0317
115	0.02	8	264.5	.0696
181	0.01	10	325.8	.0552
231	0.005	12	266.8	.0519

[16] V. F. WEISSKOPF: *Phys. Rev.*, **52**, 295 (1937).

[17] J. M. BLATT and V. F. WEISSKOPF: *Theoretical Nuclear Physics* (New York, 1952), p. 368.

[18] T. ERICSON: *Proc. Intern. Conf. Nuclear Structure* (Kingston, 1960), p. 697.

[19] G. IGO and H. E. WEGNER: *Phys. Rev.*, **102**, 1364 (1956).

Nuclear energy level densities depend not only on the total number of nucleons in a nucleus but also on whether the neutron and proton numbers are odd or even ([7,10,20]). Two recipes have been advanced to take into account this effect. WEISSKOPF and EWING ([21]) suggested that the odd-even effects be taken into account in the pre-exponential constant C by setting

$$C_{\text{odd}} = 2C_{\text{even-odd}} = 2C_{\text{odd-even}} = 4C_{\text{even-even}} . \tag{3}$$

HURWITZ and BETHE ([22]) pointed out that it is more nearly correct to consider the odd-even effects on level densities as arising from the displacements of ground state energies caused by nucleon pairing. On this basis they suggest that, for all but odd-odd nuclei, the excitation energy appearing in the level density formula be counted from a corrected ground state or characteristic level, displaced upward from the true ground state.

With Hurwitz-Bethe's assumption, eq. (2) becomes

$$\frac{1}{D} = \omega = C \exp\left[2\sqrt{a(U-\varepsilon)}\right] , \tag{4}$$

in which ε defines the characteristic level. The mass dependence of the constant C in eq. (4) was found by FONG ([6]) to be given by

$$C = 0.38\, C^{-0.005A} \tag{5}$$

and an improved equation has been suggested by EL-NADI and WAFIK ([9]):

$$C = 0.82 \exp\left[0.071\, A - 0.000\,26\, A^2\right] . \tag{6}$$

A more rigorous treatment of the gas-like model was carried out by LANG and LE COUTEUR ([5]) who showed that the application of the thermodynamic properties of a Fermi gas to the nucleons of a nucleus yields the following equation for the spacing of nuclear levels of zero spin:

$$D = 0.11 A^2 (U+t)^2 \exp\left[-\left(2\left(\frac{AU}{11}\right)^{\frac{1}{2}} + \frac{3}{32}(11U)^{\frac{2}{3}}\right)\right] , \tag{7}$$

where

$$t = \left(\frac{10.5\, U}{A}\right)^{\frac{1}{2}} - \frac{7.9}{A} .$$

([20]) J. W. MEADOWS: *Phys. Rev.*, **91**, 885 (1953).
([21]) V. F. WEISSKOPF and D. H. EWING: *Phys. Rev.*, **57**, 472 (1940).
([22]) H. HURWITZ and H. A. BETHE: *Phys. Rev.*, **81**, 898 (1951).

This equation has been recently examined by BROWN and MUIRHEAD [23] on 41 nuclei and has been found to give satisfactory results. They made use of the experimental data from a variety of sources. An average quantum number of spin was assigned tentatively to each group of levels, the assignment being made either from information obtained in the individual experiments, or from reasonable assumptions concerning the magnitude of the spin of the initial and product nuclei involved in the individual reactions and the energy of the incident particles. The spacing of nuclear levels of spin I, D_I, was assumed to be given by

$$(2I+1)D_I = D \tag{8}$$

whence eq. (7) could be applied. For the sake of brevity we shall refer to eq. (7) as the L-L equation.

3. – Comparison of the three equations.

In most of the cases the nuclear level spacing is available only at one energy for a particular nucleus. Weisskopf's eq. (2) involves C and a which are functions of A. As we shall be employing data pertaining to different nuclei for evaluating these parameters, we need to express them in terms of A. In line with Bethe's equation and the findings of some of the earlier workers we put

$$a = \nu A \ , \tag{9}$$

where ν is a constant.

Table I shows the product CA^2 for the C values given by BLATT and WEISSKOPF [17]. It will be noticed that except for $A = 63$, the product CA^2 appears to be roughly a constant. In any case the values of C given in Table I are highly approximate and can only give a crude representation of the variation of C with A, and we shall not be very wrong in assuming

$$C = \frac{1}{RA^2} \ , \tag{10}$$

where R is a constant.

Such an assumption will also be in harmony with eq. (1).

Thus the eq. (2) may be put as

$$D = RA^2 \exp\left[-2(\nu A U)^{\frac{1}{2}}\right] . \tag{11}$$

[23] G. BROWN and H. MUIRHEAD: *Phil. Mag.*, **2**, 473 (1957).

The equations of Bethe and of Lang and Le Couteur can be used directly. Bethe's equation, as originally given has definite numerical values for the constants P and μ. However, here we have treated them as flexible parameters to be determined from the experimental data.

For taking into account the odd-even effects, we have followed the practice of WEISSKOPF and EWING [21] and have assumed different values of C for odd mass, even and odd nuclei.

For eqs. (1) and (11) we have determined the parameters from the experimental data, but in the case of eq. (7) we have utilized the results of

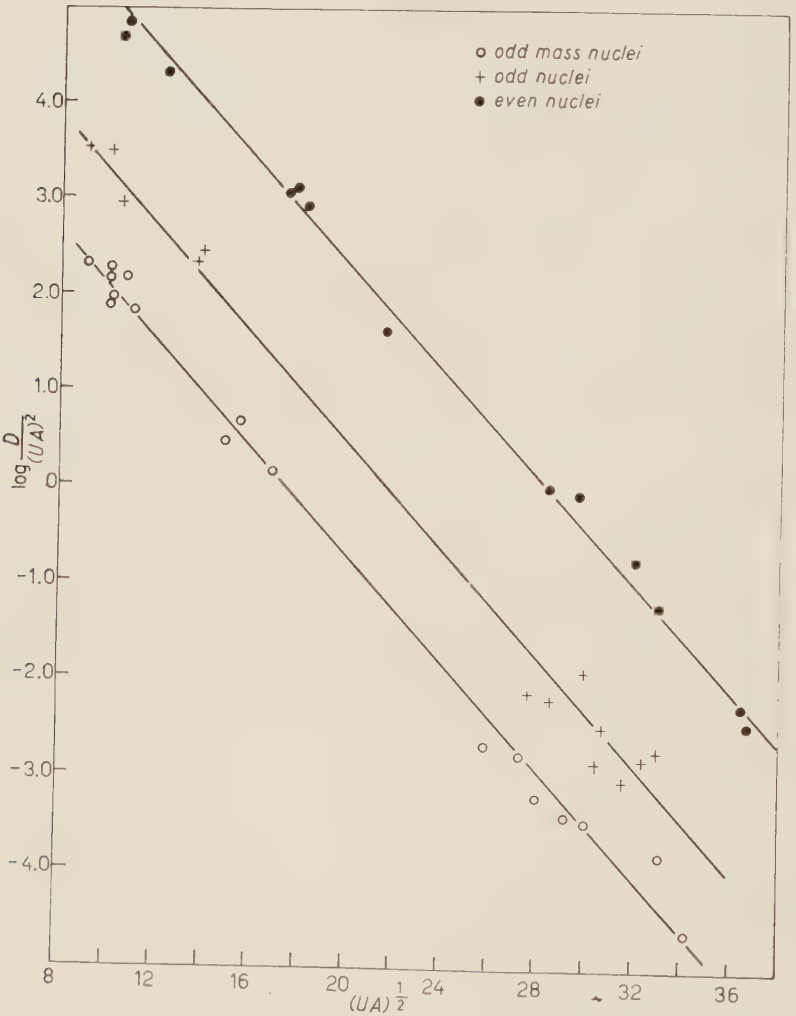

Fig. 1. $\log |D/(UA)^2|$ *vs.* $(UA)^{\frac{1}{2}}$. To avoid overlapping, the points for odd nuclei have been displaced upwards by 1.5, and those for even nuclei by 2.5.

Brown and Muirhead. The L-L equation does not exhibit odd-even effects. To incorporate these we have introduced a factor λ in the equation:

$$D = \lambda(0.11)A^2(U+t)^2 \exp\left[-\left[2\left(\frac{AU}{11}\right)^{\frac{1}{2}} + \frac{3}{32}(11U)^{\frac{2}{3}}\right]\right]. \tag{12}$$

The determination of λ will be discussed below.

Brown and Muirhead ([23]) have collected together data on nuclear level spacings and these were utilized for comparing the eqs. (1), (11) and (12).

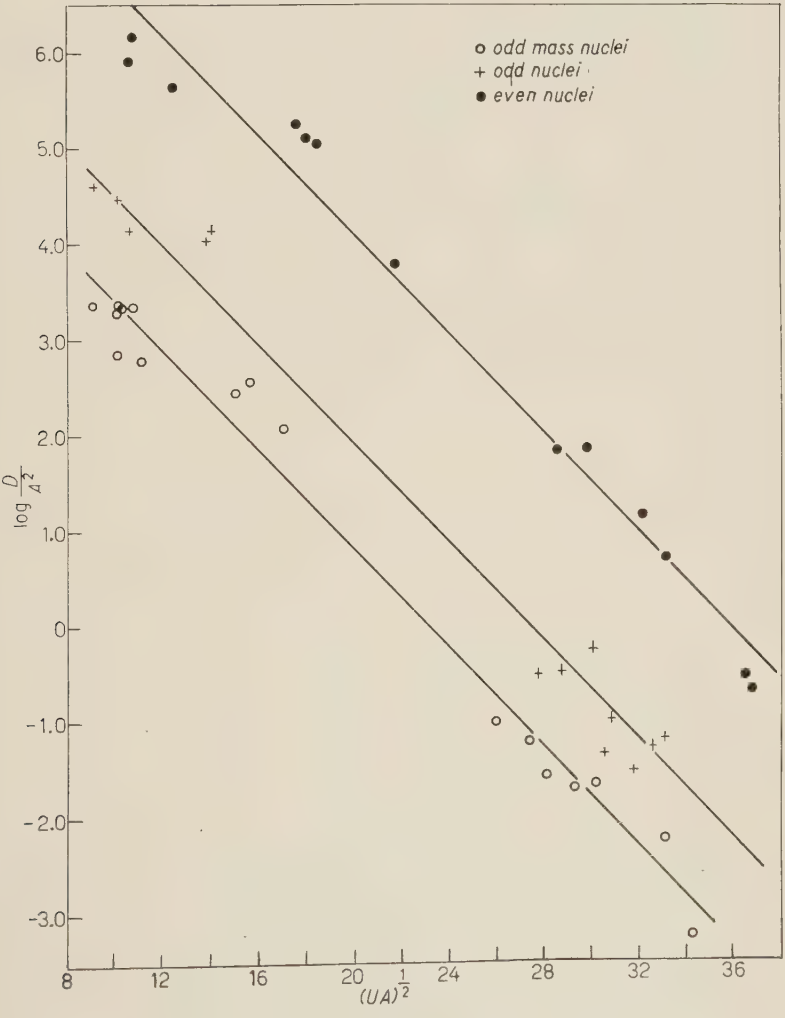

Fig. 2. – $\log [D/A^2]$ *vs.* $(UA)^{\frac{1}{2}}$. To avoid overlapping, the points for odd nuclei have been displaced upwards by 1.5, and those for even nuclei by 2.5.

We have omitted ^{152}Eu from consideration as all the three equations gave very large errors in this case.

Eqs. (1) and (11) may be put as

$$\log_{10}\frac{D}{(AU)^2} = m - n(AU)^{\frac{1}{3}}, \tag{13}$$

and

$$\log_{10}\frac{D}{A^2} = f - g(AU)^{\frac{1}{3}}, \tag{14}$$

where m, n, f and g are constants.

Fig. 1 shows $\log[D/(AU)^2]$ *vs.* $(AU)^{\frac{1}{3}}$ and Fig. 2 shows $\log[D/A^2]$ *vs.* $(AU)^{\frac{1}{3}}$ for the various nuclei under consideration. To avoid overlapping, the points for odd and even nuclei have been displaced upwards by certain amounts noted below the figures.

The constants in eq. (13) for odd-mass nuclei were evaluated by the method of least squares. The value of μ found for odd-mass nuclei was also assumed to hold for even and odd nuclei, and the constant P was adjusted by the available data. A similar procedure was followed for eq. (14). The constants so determined have been recorded in Table II.

TABLE II. – *Values of the constants in eq.* (1) *and* (11).

Bethe's eq. (1)	m	n	P	μ
odd nuclei	4.5542	0.2778	$3.583\cdot10^4$	0.1023
odd-mass nuclei	4.8825	0.2778	$7.630\cdot10^4$	
even nuclei	5.4137	0.2778	$25.92\cdot10^4$	
Weisskopf's eq. (11)	f	g	R	ν
odd nuclei	5.6060	0.2588	$4.036\cdot10^5$	.0888
odd-mass nuclei	5.9911	0.2588	$9.797\cdot10^5$	
even nuclei	6.7834	0.2588	$60.73\cdot10^5$	

BROWN and MUIRHEAD ([23]) have given the « error factor » D_{exp}/D_{theor} for these nuclei by the L-L equation. To take into account the odd-even effects these were « normalized » in the following way. For example, for odd-mass nuclei the average of the various error factors was taken. This average defines λ in eq. (12), and the error factors given by Brown and Muirhead were modified accordingly. An identical procedure was followed for even and odd nuclei. The values of λ for odd, odd-mass and even nuclei were found to be 0.685, 1.253 and 6.97 respectively.

TABLE III. – *Odd nuclei.*

Nucleus	U in MeV	Measured average level spacing in eV	Average I	$D=(2I+1)\ D_I$	B. eq. (1) D_{exp}/D_{theor}	W. eq. (11) D_{exp}/D_{theor}	L.-L. eq. (12) $\lambda=0.685$ D_{exp}/D_{theor}
$^{24}_{11}$Na	3.5	$1.5\cdot10^5$	2	$7.5\cdot10^5$	1.04	0.76	0.6
$^{26}_{13}$Al	7.3	$4\ \cdot10^4$	5/2	$2.4\cdot10^5$	1.25	3.23	1.5
$^{28}_{13}$Al	4.0	$7\ \cdot10^4$	2	$3.5\cdot10^5$	0.68	0.61	.4
$^{28}_{13}$Al	7.0	$5\ \cdot10^4$	3	$3.5\cdot10^5$	1.97	4.64	2.2
$^{32}_{15}$P	3.2	$2\ \cdot10^5$	2	$1.0\cdot10^6$	1.72	1.01	1.0
$^{114}_{49}$In	7.2	14 ± 2	9/2	$(1.4\pm0.2)\cdot10^2$	0.53	0.69	0.4
$^{116}_{49}$In	6.6	14 ± 2	9/2	$(1.4\pm0.2)\cdot10^2$	0.32	0.37	0.3
$^{134}_{55}$Cs	6.7	42 ± 5	7/2	$(3.4\pm0.4)\cdot10^2$	2.48	2.66	1.6
$^{160}_{65}$Tb	5.8	10 ± 1.0	3/2	40 ± 4	0.38	0.30	0.2
$^{166}_{67}$Ho	5.7	12 ± 1.3	7/2	96 ± 10	1.05	0.79	0.6
$^{170}_{69}$Tm	5.9	15 ± 2	1/2	$30\pm\ 4$	0.52	0.40	0.3
$^{176}_{71}$Lu	6.0	7 ± 2	7/2	56 ± 16	1.49	1.15	0.9
$^{182}_{73}$Ta	6.0	9 ± 1	7/2	$72\pm\ 8$	2.55	1.92	1.3

The experimental data and the values of the error factor, D_{exp}/D_{theor}, as calculated by the three equations have been tabulated in Tables III, IV

TABLE IV. – *Odd-mass nuclei.*

Nucleus	U in MeV	Measured average level spacing in eV	Average I	$D=(2I+1)D_I$	B. eq. (1) D_{exp}/D_{theor}	W. eq. (11) D_{exp}/D_{theor}	L.-L. eq. (12) $\lambda=1.253$ D_{exp}/D_{theor}
$^{21}_{11}$Na	5	$2.5\cdot10^5$	3/2	$1.0\cdot10^6$	0.83	1.04	0.8
$^{23}_{11}$Na	9.8	$5\ \cdot10^4$	1	$1.5\cdot10^5$	0.57	2.22	1.1
$^{25}_{12}$Mg	3.3	$3\ \cdot10^5$	2	$1.5\cdot10^6$	0.96	0.55	0.6
$^{25}_{13}$Al	4.1	$3\ \cdot10^5$	2	$1.5\cdot10^6$	1.22	1.02	1.0
$^{27}_{13}$Al	9.0	$7\ \cdot10^4$	3/2	$2.8\cdot10^5$	1.33	4.24	2.2
$^{29}_{14}$Si	4.0	$4\ \cdot10^5$	2	$2.0\cdot10^6$	1.91	1.49	1.5
$^{31}_{14}$Si	3.3	$4\ \cdot10^5$	2	$2.0\cdot10^6$	1.62	0.88	1.1
$^{31}_{15}$P	9.3	$2.5\cdot10^4$	2	$1.2\cdot10^5$	0.98	3.16	1.6
$^{33}_{16}$S	3.1	$2\ \cdot10^5$	3/2	$8\ \cdot10^5$	0.65	0.31	0.5
$^{41}_{20}$Ca	3.0	$2.5\cdot10^5$	3/2	$1.0\cdot10^6$	1.04	0.48	0.6
$^{93,95,97,99,101}_{42}$Mo	6.9	$(5\ \pm1.5)\cdot10^2$	1/2	$(10\pm3)\ \cdot10^2$	0.45	0.54	0.4
$^{113}_{50}$Sn	8.0	$(1.5\pm0.8)\cdot10^2$	1/2	$(3\pm1.6)\cdot10^2$	1.08	1.45	1.0
$^{117}_{50}$Sn	7.3	$(1.5\pm0.7)\cdot10^2$	1/2	$(3\pm1.4)\cdot10^2$	0.71	0.82	0.6
$^{119}_{50}$Sn	6.6	$(2\ \pm1)\ \cdot10^2$	1/2	$(4\pm2)\ \cdot10^2$	0.52	0.52	0.4
$^{121,123,125}_{50}$Sn	6.1	$(5\ \pm2)\ \cdot10^2$	1/2	$(10\pm4)\ \cdot10^2$	0.95	0.83	0.7
$^{179,181}_{72}$Hf	6.1	$(1\ \pm0.5)\cdot10^2$	1/2	$(2\pm1)\ \cdot10^2$	3.49	2.37	2.2
$^{239}_{92}$U	4.9	18 ± 2	1/2	36 ± 4	1.10	0.46	0.6

and V. The sources of the experimental data are given in the paper of BROWN and MUIRHEAD [23].

TABLE V. – *Even nuclei.*

Nucleus	U in MeV	Measured average level spacing in eV	Average I	$D=(2I+1)D_I$	B. eq. (1) D_{exp}/D_{theor}	W. eq. (11) D_{exp}/D_{theor}	L.-L. eq. (12) $\lambda=6.97$ D_{exp}/D_{theor}
$^{24}_{12}$Mg	4.8	$4 \cdot 10^5$	3	$2.8 \cdot 10^6$	0.78	0.48	0.4
$^{24}_{12}$Mg	12.8	$7 \cdot 10^4$	2	$3.5 \cdot 10^5$	1.06	3.44	1.7
$^{26}_{12}$Mg	4.3	$3 \cdot 10^5$	5/2	$1.8 \cdot 10^6$	0.48	0.24	0.3
$^{28}_{14}$Si	12.0	$5 \cdot 10^4$	5/2	$3 \cdot 10^5$	1.27	3.49	1.9
$^{32}_{16}$Si	4.8	$3 \cdot 10^5$	2	$1.5 \cdot 10^6$	0.68	0.39	0.4
$^{32}_{16}$Si	10.0	$1.1 \cdot 10^4$	3/2	$4.5 \cdot 10^5$	1.58	3.08	3.0
$^{38}_{18}$A	12.3	$5 \cdot 10^3$	5/2	$3 \cdot 10^4$	0.54	1.35	0.8
$^{96}_{42}$Mo	9.2	$(3.7 \pm 1.2) \cdot 10^2$	5/2	$(22 \pm 7) \cdot 10^2$	1.96	1.93	1.2
$^{98}_{42}$Mo	8.3	$(3.7 \pm 1.2) \cdot 10^2$	5/2	$(22 \pm 7) \cdot 10^2$	1.07	0.91	0.6
$^{118}_{50}$Sn	9.3	$(1.2 \pm 0.3) \cdot 10^2$	1/2	$(2.4 \pm 0.6) \cdot 10^2$	1.22	1.06	0.8
$^{120}_{50}$Sn	8.6	$(3 \pm 1.4) \cdot 10^2$	1/2	$(6 \pm 2.8) \cdot 10^2$	1.82	1.41	1.1
$^{178}_{72}$Hf	7.6	5.6 ± 0.6	$\leqslant 3/2$	22 ± 2.4	0.77	0.38	0.3
$^{180}_{72}$Hf	7.4	8 ± 2	$\leqslant 3/2$	32 ± 8	0.96	0.45	0.4

4. – Discussion.

In a situation like this, where the calculated and observed values may differ by a factor of 3 or so, the customary method of using percentage error as a measure of the comparison is no longer useful. Instead the quantity

TABLE VI. – *Average values of* $|\log D_{exp}/D_{theor}|$.

Nuclei	Bethe's eq. (1)	Weisskopf's eq. (11)	L.-L. eq. (12)
odd	0.253	0.300	0.297
odd-mass	0.157	0.260	0.199
even	0.153	0.332	0.289
for all nuclei	0.185	0.294	0.256
error factor (for all)	1.53	1.97	1.8

$|\log D_{exp}/D_{theor}|$ can be used as a measure of the difference between the two sets of values (NEWTON [7], CAMERON [10]). Table VI shows the average

values of

$$\log (\text{error factor}) = \left| \log \frac{D_{\text{exp}}}{D_{\text{theor}}} \right| ,$$

for the three equations.

It will be noted that the average values of log (error factor) for the three equations are not very different. We would like to emphasize that the experimental data used here are not very accurate and some of the values of D may be in error by a factor of 2 or more. With this important reservation we may discuss the results obtained by different equations. Bethe's equation is seen to give the smallest average error factor. The Lang-Le Couteur's equation is an extension of Bethe's equation and it may appear surprising that the error by the L-L equation is larger than that by Bethe's equation. The cause of this discrepancy lies in the fact that we have not tried to adjust the parameters in the L-L equation for the best fit. The Weisskopf's eq. (11) is seen to give a larger error factor than the Bethe's equation, thus giving an « experimental » support to the opinion (Ericson [18]) that Bethe's equation is more satisfactory.

Most of the nuclei considered in the present study are non-magic; the exceptions are $^{41}_{20}$Ca, isotopes of $_{50}$Sn, and $^{38}_{18}$A. In view of the fact that the error factors for these nuclei are not very large, it appears that the magic number effects in the spacing of nuclear levels are not very pronounced for these nuclei.

The constants μ and ν have similar significance, and it is reasonable that their values have come out to be quite close to each other. As may be qualitatively expected, μ is slightly larger than ν. Our value of μ is very close to the theoretical value predicted by Bethe, viz., 0.091. Different workers have reported widely differing values of ν. We are quoting some of them below. It may be pointed out that sometimes slightly different equations have been used by different workers and the values of ν given below do not necessarily signify exactly the same parameter.

(i) Le Couteur [24] (1950): $\nu = 0.081$;

(ii) Heidmann and Bethe [25] (1951) : for eq. (2) in the range $15 < A < 70$ $a = 0.035\,(A - 12)$ or $\nu = 0.035\ \ (1 - 12/A)$;

(ii) Blatt and Weisskopf [17] (1952): eq. (2), see Table I, $\nu \sim 0.05$;

(iv) Fong [6] (1956): eq. (4), $\nu = 0.05$;

[24] K. J. Le Couteur: *Proc. Phys. Soc.*, A **63**, 259 (1950).
[25] J. Heidmann and H. A. Bethe: *Phys. Rev.*, **84**, 274 (1951).

(v) Ross ([26]) (1957) found a to increase with A at low values of A, approaching a constant value at high values of A. The trend of her values may be gauged by some typical values given below

A	δ	$a\ (=\pi^2/6\delta)$	ν
40	0.25	6.58	0.165
100	0.1	16.45	0.164
200	0.09	18.3	0.091

(vi) El-Nadi and Wafik (1958): eq. (4), $\nu = 0.03$;

(vii) Allan ([27]) (1961): eq. (2), $\nu \sim 0.1$.

It will be observed that the ν values reported by different workers fall in a fairly wide range. The causes of such diverse values of ν are manyfold. While some of the discrepancies are certainly due to errors in the experimental data, nevertheless the serious discordance found in the a values obtained by different types of experiments points to the inadequacy of some of the assumptions in the statistical model.

It is interesting to see the magnitude of the odd-even effects as obtained from the present analysis. The results for the three equations are shown below:

(a) Bethe's equation

$$\frac{1}{D\ (\text{odd})} = \frac{2.13}{D\ (\text{odd-mass})} = \frac{7.23}{D\ (\text{even})}.$$

(b) Weisskopf's equation

$$\frac{1}{D\ (\text{odd})} = \frac{2.43}{D\ (\text{odd-mass})} = \frac{15.05}{D\ (\text{even})}.$$

(c) Lang-Le Couteur's equation

$$\frac{1}{D\ (\text{odd})} = \frac{1.83}{D\ (\text{odd-mass})} = \frac{10.17}{D\ (\text{even})}.$$

These may be compared with the values proposed by Weisskopf and Ewing ([21]):

$$\frac{1}{D\ (\text{odd})} = \frac{2}{D\ (\text{odd-mass})} = \frac{4}{D\ (\text{even})}.$$

([26]) A. A. Ross: *Phys. Rev.*, **108**, 720 (1957).
([27]) D. L. Allan: *Nucl. Phys.*, **24**, 274 (1961).

For odd-mass nuclei, the correction factor 2 is seen to be reasonably satisfactory, but for even nuclei the correction factor 4 is too low.

* * *

The author is highly grateful to Dr. TA-YOU WU for his kind interest in the work, and thanks the National Research Council for the award of a Postdoctorate Fellowship.

RIASSUNTO (*)

Le equazioni di Bethe, Weisskopf e di Lang e Le Couteur per gli intervalli fra i livelli nucleari sono state confrontate servendosi dei dati sperimentali per 40 nuclei. Gli errori medi ottenuti con le tre equazioni non sono molto differenti. Si è trovato che l'equazione di Bethe dà i migliori risultati. Si discutono gli effetti dispari-dispari sulle costanti che precedono gli esponenziali nelle tre equazioni.

(*) *Traduzione a cura della Redazione.*

On Reaction Cross-Sections with 14 MeV Neutrons.

N. B. Gove and R. Nakasima

Nuclear Data Project (*), *National Research Council - Washington, D. C.*

(ricevuto il 26 Luglio 1961)

Summary. — Cross-sections with 14 MeV neutrons for light- and medium-weight nuclei are analysed in terms of the compound nucleus model. The marked regularity in (n, p) cross-sections, pointed out by Gardner and by Levkovskii, can be reproduced fairly well. A systematic trend is found in the variation of σ(n, 2n) with the neutron number of the target nucleus. This is also analysed in terms of the compound nucleus model.

1. – Introduction.

Regularities in σ(n, p) with 14 MeV neutrons for isotopes of medium-weight nuclei have been noted by Gardner [1] and Levkovskii [2]. For a given value of Z, the cross-section decreases as neutrons are added to the target nucleus. There is no marked even-odd effect. Gardner fits this trend with an empirical formula,

$$(1) \qquad \begin{cases} \sigma_{Z,A}(\mathrm{n,\ p}) = 0.0222\,A\,\exp\left[0.0867\,A - 0.035(Z - 22\mathrm{P})\right], \\ \sigma_{Z,A+\Delta A}(\mathrm{n,\ p}) = \sigma_{Z,A}(\mathrm{n,\ p})\,2^{-\Delta A}. \qquad (A = 2Z + 4). \end{cases}$$

Levkovskii has measured cross-section ratios for isotopes of some elements

(*) Supported by the U. S. Atomic Energy Commission.

(1) D. Gardner: University of Arkansas, Progress Report, January 1, 1961; *Bull. Am. Phys. Soc.*, **6**, 66 (1961).

(2) V. N. Levkovskii: *Žurn. Eksp. Teor. Fiz.*, **33**, 1520 (1957); *Soviet Phys. JETP*, **6**, 1174 (1958).

and suggests an empirical relation,

$$\frac{\sigma_{Z,A+\Delta A}(\mathrm{n,\,p})}{\sigma_{Z,A}(\mathrm{n,\,p})} = \exp\left[\frac{-75Z\Delta A}{A^2}\right], \tag{2}$$

which suggests that $\sigma(\mathrm{n,\,p})$ is related to the relative number of interacting protons in the target nucleus. Although these formulas fit the experimental data fairly well, they do not clearly indicate which reaction mechanism is responsible.

Trends are also noticeable in cross-sections of the (n, 2n) reaction. For nuclei with $N \leqslant 30$, $\sigma(\mathrm{n,\,2n})$ is much less than σ_c, the expected value for compound nucleus formation, while for $N > 30$, $\sigma(\mathrm{n,\,2n})$ is usually more than $\sigma_c/5$.

For light nuclei, two groups can be distinguished; one contains the odd Z, $N = Z+1$ nuclei with $10 \leqslant N \leqslant 20$ and the other contains even Z, $N = Z+2$ nuclei with $24 \leqslant N \leqslant 28$. The (n, 2n) cross section for nuclei in each group decreases with increasing neutron number. This trend suggests a shell effect.

In this paper we show that these trends can be approximately reproduced by the statistical model of the compound nucleus. The model used here assumes a constant nuclear temperature. Angular momentum effects and γ emission, although probably important, are not included in the present calculation.

2. – Calculations.

According to the compound nucleus model ([3,4]), the cross section of the (n, ν) reaction is expressed by

$$\sigma(\mathrm{n,\,\nu}) = \frac{\sigma_c F_\nu}{\sum_i F_i}, \tag{3}$$

$$F_i = \mu_i g_i \int \varepsilon_i \sigma_c^*(\varepsilon_i)\, \varrho(E^*)\, \mathrm{d}\varepsilon_i\,, \tag{4}$$

where μ_i is the reduced mass, $g_i = 2s_i + 1$ is the spin factor of particle i. The relative probability of γ-emission, F_γ, is different from eq. (4), but it is not considered in our calculations because of our assumption that F_γ is very small when any other open channel exists.

It has been suggested ([4]) that the nuclear temperature T is roughly constant for the first few MeV of excitation energy. Accordingly, the level density of

([3]) J. M. Blatt and V. F. Weisskopf: *Theoretical Nuclear Physics* (New York, 1952).
([4]) T. Ericson: *Adv. in Phys.*, **9**, 425 (1960); *Nucl. Phys.*, **11**, 481 (1959).

the residual nucleus is chosen as

$$\varrho(E^*) = \varrho_0 \exp\left[\frac{Q_i + \delta_i - \varepsilon_i}{T}\right], \tag{5}$$

instead of that derived from the Fermi gas model. In eq. (5) Q_i is the Q-value for (n, i) reaction, δ_i is a parameter characterizing the odd-even effect in level density, and ε_i is the kinetic energy of the emitted particle i.

In eq. (4), the inverse cros-ssection is assumed to be

$$\sigma_c^*(\varepsilon_i) = \begin{cases} \pi R^2 \left(1 - \dfrac{B_i}{\varepsilon_i}\right), & (\varepsilon_i > B_i), \\ 0\,, & (\varepsilon_i < B_i), \end{cases} \tag{6}$$

where R is the interaction radius and B_i is the Coulomb barrier height. Limits of integration in eq. (4) are chosen for which the indicated reaction is energetically possible but subsequent particle emission is not possible.

The resulting cross sections are

$$\sigma(\mathrm{n}, \mathrm{p}) = f_1 \frac{\sigma_c}{\Sigma} \exp\left[\frac{\delta_\mathrm{p}}{T}\right], \tag{7}$$

$$\sigma(\mathrm{n}, 2\mathrm{n}) = f_2 \frac{\sigma_c}{\Sigma} \exp\left[\frac{\delta_\mathrm{n}}{T}\right], \tag{8}$$

where

$$f_1 = \begin{cases} 0 & (E < B_\mathrm{p} - Q_\mathrm{p}), \\ \exp\left[\dfrac{Q_\mathrm{p} - B_\mathrm{p}}{T}\right] - f_3\,, & (B_\mathrm{p} - Q_\mathrm{p} < E < B_\mathrm{p} + S_\mathrm{p}), \\ \dfrac{E + T - S_\mathrm{p} - B_\mathrm{p}}{T} \exp\left[\dfrac{S_\mathrm{p} + Q_\mathrm{p} - E}{T}\right] - f_3\,, & (E > B_\mathrm{p} + S_\mathrm{p}), \end{cases} \tag{9}$$

$$f_2 = \int_{S_n}^{E_n} \frac{E - x}{1 + f_4} \exp\left[\frac{x - E}{T}\right] \mathrm{d}x\,, \tag{10}$$

$$f_3 = \frac{E + Q_\mathrm{p} + T - B_\mathrm{p}}{T} \exp\left[\frac{-E}{T}\right], \tag{11}$$

$$f_4 = \frac{f_5}{f_6} \exp\left[\frac{\delta_\mathrm{np} - \delta_\mathrm{nn}}{T}\right], \tag{12}$$

$$(13)\quad f_5 = \begin{cases} 0\,, & (x < S_p + B_p), \\ T \exp\left[\dfrac{-S_p - B_p}{T}\right] + (S_p + B_p - x - T) \exp\left[\dfrac{-x}{T}\right], & (x > S_p + B_p), \end{cases}$$

$$(14)\quad f_6 = T \exp\left[\frac{-S_n}{T}\right] + (S_n - x - T) \exp\left[\frac{-x}{T}\right],$$

$$(15)\quad \Sigma = (1 - f_7) \exp\left[\frac{\delta_n}{T}\right] + f_8 \exp\left[\frac{\delta_p}{T}\right] + 2 f_9 \exp\left[\frac{\delta_\alpha}{T}\right],$$

$$(16)\quad f_7 = \frac{E + T}{T} \exp\left[\frac{-E}{T}\right],$$

$$(17)\quad f_8 = \begin{cases} 0\,, & (E < B_p - Q_p), \\ \exp\left[\dfrac{Q_p - B_p}{T}\right] - f_3\,, & (E > B_p - Q_p), \end{cases}$$

$$(18)\quad f_9 = \begin{cases} 0\,, & (E < B_\alpha - Q_\alpha), \\ \exp\left[\dfrac{Q_\alpha - B_\alpha}{T}\right] - \dfrac{E + Q_\alpha + T - B_\alpha}{T} \exp\left[\dfrac{-E}{T}\right], & (E > B_\alpha - Q_\alpha). \end{cases}$$

In these expressions S_p and S_n are the proton and neutron separation energies, respectively, and refer to the target nucleus. E is the incident neutron energy.

The formula for σ(n, p) can be used for emission of other charged particles if one multiplies by $\frac{1}{2}\mu_\nu g_\nu$. If any of these reactions becomes appreciable a correction term should be added to Σ in eq. (15) as is shown for the (n, α) reaction. The term f_4 can also be corrected for the (n, nα) and similar reactions if necessary.

3. – Results.

In the evaluations of eqs. (7) and (8), the following numerical values were used:

$$(19)\quad \sigma_c = 45.2(A^{\frac{1}{3}} + 1) \quad \text{mb}\,,$$

$$(20)\quad B_p = \frac{1.029\,(Z - 1)}{A^{\frac{1}{3}} + 1} \quad \text{MeV}\,,$$

$$(21)\quad B_\alpha = \frac{2.058\,(Z - 2)}{(A - 3)^{\frac{1}{3}} + 4^{\frac{1}{3}}} \quad \text{MeV}\,,$$

where Z and A refer to the target nucleus.

There is considerable evidence that the effective Coulomb barrier is lower than that given by (20) and (21) presumably due to diffuseness at the nuclear surface ([5]). In calculating σ(n, p) we have used an arbitrarily depressed barrier

$$B_{\text{eff}} = B_c \left(1 - \frac{1.13}{A^{\frac{1}{3}}}\right), \tag{22}$$

where B_c is the value given in (20) or (21).

For the even-odd effect we use $\delta = P(Z) + P(N)$ where Z and N refer to the residual nucleus and P is the pairing energy given by CAMERON ([6]).

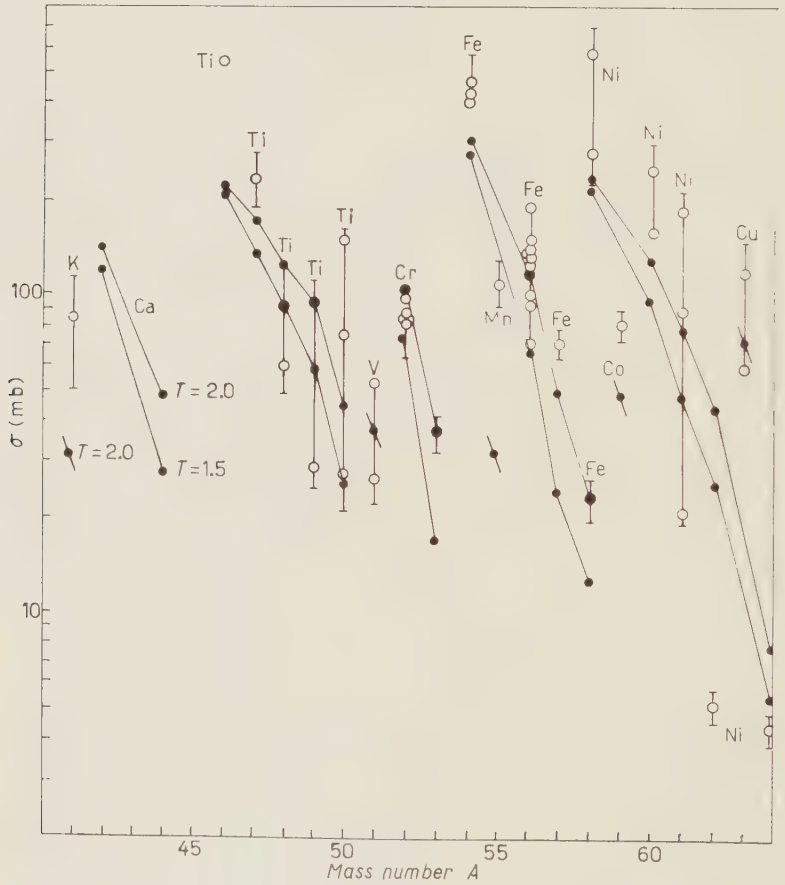

Fig. 1. – (n, p) cross-sections at 14 MeV. Open points (○): experimental values collected by Gardner. Closed points (●): theoretical values for $T = 2.0$ or 1.5 MeV. Where one value is shown it is for $T = 2.0$; where two values are shown the lower one is for $T = 1.5$. Points of constant Z are connected by slanting lines.

([5]) K. KIKUCHI: *Progr. Theor. Phys.*, **17**, 643 (1957).
([6]) A. G. W. CAMERON: *Can. Journ. Phys.*, **36**, 1040 (1958).

(i) σ(n, p). – The calculated values for $T = 2.0$ and $T = 1.5$ are shown in Fig. 1 along with experimental values as collected by GARDNER (1). Gardner's empirical curve is not shown but is similar to the $T = 2.0$ values. The trend in experimental cross sections is usually reproduced but there are some discrepancies, notably ^{55}Mn and ^{62}Ni.

TABLE I. – σ(n, p) *ratios at* 14 MeV.

	Present theory					LEVKOVSKII	
	$T=1.0$	$T=1.5$	$T=2.0$	$T=2.5$	$T=3.0$	experiment	exp[$75Z\,A^{-1.1-2}$]
^{66}Zn/^{64}Zn	.34	.52	.64	.70	.72	.36± .02	.33
^{67}Zn/^{64}Zn	.14	.32	.45	.55	.61	.23± .03	.19
^{71}Ga/^{69}Ga	.33	.48	.56	.60	.62	.50± .05	.38
^{72}Ge/^{70}Ge	.14	.29	.40	.48	.53	.39± .02	.38
^{73}Ge/^{70}Ge	.08	.23	.37	.47	.54	.24± .02	.22
^{74}Ge/^{70}Ge	.03	.09	.17	.24	.27	.13± .03	.14
^{8}Sr/^{86}Sr	.03	.10	.16	.20	.24	.46± .04	.46
^{91}Zr/^{90}Zr	.33	.48	.58	.65	.70	.74± .05	.70
^{92}Zr/^{90}Zr	.14	.30	.35	.41	.44	.46± .04	.48
^{94}Zr/^{90}Zr	.04	.13	.17	.21	.23	.20± .02	.23
^{106}Cd/^{111}Cd	21.	6.4	3.8	2.8	2.1	5 ±1	4.3
^{112}Cd/^{111}Cd	.65	.63	.62	.61	.58	.71± .03	.75
^{113}Cd/^{111}Cd	.41	.54	.67	.72	.78	.52± .02	.56
^{142}Ce/^{140}Ce	.43	.52	.57	.58	.60	.60± .15	.64

Ratios of cross-sections are somewhat less sensitive to assumptions about σ_r, B_c and δ while still sensitive to changes in T. Table I shows our calculated cross-section for various values of T along with Levkovskii's experimental values and those obtained from Levkovskii's empirical relation (2).

The trend can be generally reproduced but for some cases, especially that of $^{88}Sr/^{86}Sr$, satisfactory results cannot be obtained for any of these values of T.

(ii) $\sigma(n, 2n)$. – Calculated values of $\sigma(n, 2n)$ are shown in Fig. 2 together with available experimental values. The experimental trend is very roughly

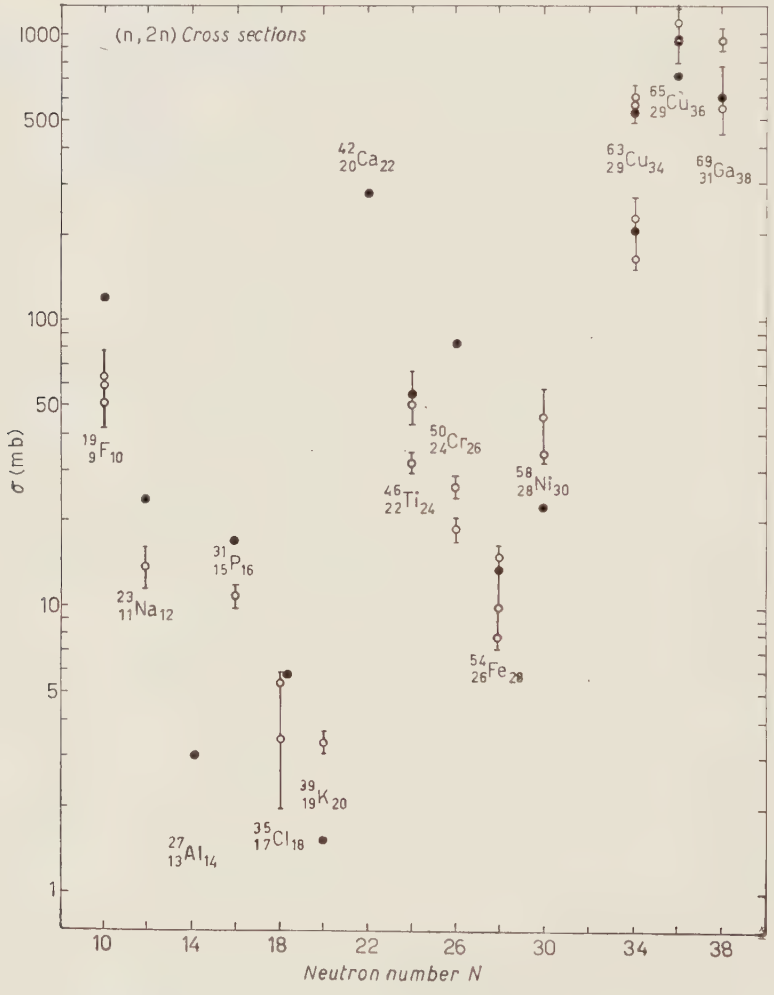

Fig. 2. – (n, 2n) cross-sections at 14 MeV. Open points (⊖): published experimental values. Closed points (●): theory for $T = 2.0$ MeV.

reproduced by eq. (8) with $T = 2$. Since the threshold energy of the (n, 2n) reaction is so close to the bombarding energy, the calculated values for $N \leqslant 30$ are very sensitive to slight changes in the parameters.

(iii) Excitation function of ^{56}Fe (n, p). By using eq. (7), the excitation function of ^{56}Fe (n, p) is calculated for $T = 2.2$ and its comparison with the experimental one (7) is illustrated in Fig. 3.

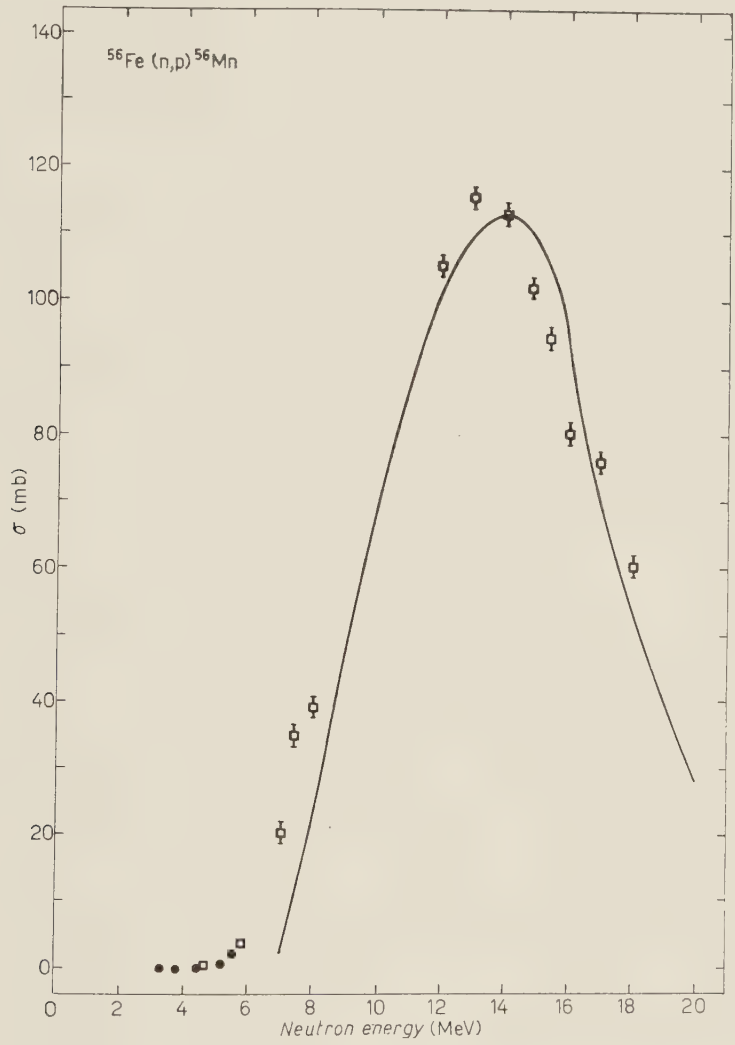

Fig. 3. – (n, p) cross-section of ^{56}Fe. Squares (⊟) and closed points (●): experimental values of Terrell and Holm. Curve: theory for $T = 2.2$ MeV.

The agreement is satisfactory. Similar results have been obtained by TERRELL and HOLM (7) using the Fermi gas model.

(7) J. TERRELL and D. M. HOLM: *Phys. Rev.*, **109**, 2031 (1958).

4. – Discussion.

(i) σ(n, p). – In these calculations we assume that, except for odd-even effects, the level density is roughly the same for the residual nucleus for the (n, p), (n, n) and (n, α) reactions. Discrepancies might be expected when one of these reactions leads to a magic number nucleus. If one assumes that the (n, α) reaction on Zn isotopes is retarded because the residual nucleus is magic, then the calculated σ(n, p) ratios for ^{66,67}Zn are reduced. The optimum value of T is then somewhat higher and the agreement with Rayburn's data ([8]) on σ(n, p) for ^{64}Zn is improved.

When the (n, n) reaction leads to a magic nucleus, similar assumptions will improve the agreement in some, but not all, of the above cases. The effect should be more pronounced when the residual nucleus has a closed proton shell plus a closed neutron subshell (*e.g.* ^{62}Ni (n, n)) or vice versa (*e.g.* ^{88}Sr (n, n) or ^{91}Zn (n, α)).

The values of T used here are somewhat higher than those found in evaporation spectrum studies (*). This may be due to direct interaction. If a roughly constant amount is subtracted from the experimental cross-sections the trend can still be obtained from the theory, but at lower values of T.

(ii) σ(n, 2n). – As is seen in Fig. 2, the experimental cross-section decreases with increasing neutron number in regions where $10 \lesssim N \lesssim 20$ and $24 \lesssim N \lesssim 28$. This seems to be an indication of a shell effect. However, the calculated values, including ^{27}Al for which experimental data are not available, show a strong subshell effect at $N = 14$. The overall tendency in σ(n, 2n) for such light nuclei seems to depend on that of the separation energies. The value $T = 2.0$ that is used here is in rough agreement with the magnetic spectrograph data of MacDonald and Douglas ([10]).

It is unusual to apply the statistical model for nucleon-induced reactions on such light nuclei. It is possible that a pick-up process or knock-on mechanism based on the cluster model may be more appropriate, but any such calculation should have considerable separation-energy dependence in order to explain the systematic trend in (n, 2n) cross sections.

([8]) L. A. Rayburn: *Bull. Am. Phys. Soc.*, Southeastern Section 13, F1 (1961).

(*) Recent work of Allan ([9]) indicates that $T = 1.2$ MeV. Eq. (7) gives for $T = 1.2$ cross-sections that are usually too low although the trends in Z and N are preserved. Allan finds better agreement for a Fermi gas type level density.

([9]) D. L. Allan: *Nucl. Phys.*, **24**, 274 (1961).

([10]) N. MacDonald and A. C. Douglas: *Nucl. Phys.*, **24**, 614 (1961).

* * *

Helpful conversations with K. WAY are gratefully acknowledged.

RIASSUNTO (*)

Analizziamo in base al modello del nucleo composto le sezioni d'urto fra i nuclei medi e leggeri e i neutroni di 14 MeV. La marcata regolarità delle sezioni d'urto (n, p), messa in luce da Gardner e da Levkovskii, può essere riprodotta abbastanza bene. Si nota un andamento sistematico nel variare di σ(n, 2n) con numero di neutroni dei nuclei del bersaglio. Anche questo fenomeno viene analizzato in base al modello del nucleo composto.

(*) *Traduzione a cura della Redazione.*

Interference Effects of Radiofrequency Fields in Resonance Radiation (*).

M. N. Hack

Argonne National Laboratory - Argonne, Ill.

(ricevuto il 26 Luglio 1961)

Summary. — The theory developed previously to investigate the splitting of Zeeman lines by r.f. magnetic fields leads directly to the Brossel-Bitter resonance obtained in experiments on double resonance. An extension of the theory accounts for the effects of the modulation of light recently observed in these experiments.

1. – Introduction.

In a previous paper (1), cited in the following as ERF, the splitting of spectral lines emitted in the decay of an excited atom from Zeeman levels between which an applied r.f. magnetic field is producing transitions, has been studied. While this splitting appears not yet to have been observed directly, it has for a consequence a phenomenon which has often been detected in combined magnetic resonance and optical experiments, namely, the double peaked Brossel-Bitter resonance found in experiments on double resonance (2).

In the present note we show that the split line amplitudes of the type obtained previously lead directly to the Brossel-Bitter resonance of the angular distribution of the emitted resonance radiation (as function of the magnetic field parameters). At the same time, this result contributes to the solution of a problem raised by P. Sagalyn (3). A direct extension of the theory leads

(*) Work performed under the auspices of the U. S. Atomic Energy Commission.

(1) M. N. Hack and M. Hamermesh: *Nuovo Cimento*, **19**, 546 (1961).

(2) J. Brossel and F. Bitter: *Phys. Rev.*, **86**, 308 (1952).

(3) P. Sagalyn: *Phys. Rev.*, **94**, 885 (1954).

to the quantum mechanical basis of the effects of the modulation of light, observed recently by DODD, SERIES and coworkers (4) and treated by them from the standpoint of semi-classical radiation theory.

2. – Brossel-Bitter resonance.

We make use of the expressions for the decay amplitudes in the Majorana case obtained in Sect. 3 of ERF. The general solution for the no-photon projection of the state vector is given by

$$\Psi = \sum_{\mu} \eta_{\mu} \Psi_{\mu} , \tag{1}$$

where the basic decay solutions have the form

$$\Psi_{\mu} = \sum_{m} b^{(j)}_{\mu m} \exp\left[-i\omega_m t\right] |m\rangle , \tag{2}$$

with

$$b^{(j)}_{\mu m} = d^{(j)}_{\mu m} \exp\left[-i[m(\omega-\omega_r) + \mu\sqrt{(\omega-\omega_r)^2 + 4H^2} - \tfrac{1}{2} i\Gamma]t\right] . \tag{3}$$

For excitation at $t_0 = 0$ to a single level m_0, the η_{μ} have the values

$$\eta_{\mu} = d^{(j)}_{\mu m_0} . \tag{4}$$

That eq. (1) with the η_{μ} given by eq. (4) reduces to $|m_0\rangle$ at time $t = 0$, follows from the orthogonality property of the rotation matrices $d^{(j)}_{\mu m}$.

The photon emission amplitudes for the decay transition $m \to f$ are given by

$$b_{m\to f}(\infty) = H_{f1_\lambda|m0} \sum_{\mu} \frac{d^{(j)}_{\mu m}\, d^{(j)}_{\mu m_0}}{\omega_\lambda - \left[\omega_{mf} + m(\omega-\omega_r) + \mu\sqrt{(\omega-\omega_r)^2 + 4H^2}\right] + \tfrac{1}{2} i\Gamma} , \tag{5}$$

as one obtains by superimposing the solutions (31) of ERF with the coefficients (4).

From eq. (5) we have for the angular distribution in the wave zone of the

(4) J. N. DODD, W. N. FOX, G. W. SERIES and M. J. TAYLOR: *Proc. Phys. Soc. (London)*, **74**, 789 (1959).

emitted radiation

$$(6)\ (^5) \qquad P_{fm}(\Omega_\lambda) = \int_0^\infty \mathrm{d}\omega_\lambda |H_{f1_\lambda|m0}|^2 \varrho(\omega_\lambda) \cdot$$

$$\cdot \sum_{\mu\mu'} \frac{d^{(j)}_{fm} d^{(j)}_{\mu m_0} d^{(j)}_{\mu' m} d^{(j)}_{\mu' m_0}}{\{\omega_\lambda - [\omega_{mf} + m(\omega - \omega_r) + \mu w_1] + \frac{1}{2} i\Gamma\}\{\omega_\lambda - [\omega_{mf} + m(\omega - \omega_r) + \mu' w_1] - \frac{1}{2} i\bar{\Gamma}\}},$$

where $w_1 = [(\omega - \omega_r)^2 + 4H^2]^{\frac{1}{2}}$, and Ω_λ denotes polarization and propagation directions. The integral in eq. (6) is readily evaluated if we neglect the weak ω_λ-dependence of $|H_{f1_\lambda m0}|^2 \varrho(\omega_\lambda)$, taking for this quantity its value say at $\omega_0 = \omega_{mf}$. In the case that $w_1, \Gamma \ll \omega_0$ (which is always well satisfied), we obtain

$$(7) \qquad P_{fm}(\Omega_\lambda) = \frac{2\pi}{\Gamma} |H_{f1_\lambda|m0}|^2 \varrho(\omega_0) \mathscr{F}^{(j)}_{mm_0},$$

where

$$(8) \qquad \mathscr{F}^{(j)}_{mm_0} = \sum_{\mu\mu'} d^{(j)}_{\mu m} d^{(j)}_{\mu m_0} d^{(j)}_{\mu' m} d^{(j)}_{\mu' m_0} \frac{\Gamma}{\Gamma + i(\mu - \mu')w_1}.$$

The matrix $\mathscr{F}^{(j)}_{mm_0}$ can be evaluated with the help of the expressions for the rotation matrices, of argument given by ERF, eq. (29). For the first two values of j:

$$(9a) \qquad \mathscr{F}^{(\frac{1}{2})} = \begin{pmatrix} 1-\delta & \delta \\ \delta & 1-\delta \end{pmatrix}, \qquad \mathscr{F}^{(1)} = \begin{pmatrix} 1-\varepsilon-\tau & \varepsilon & \tau \\ \varepsilon & 1-2\varepsilon & \varepsilon \\ \tau & \varepsilon & 1-\varepsilon-\tau \end{pmatrix},$$

$$(9b) \qquad \begin{cases} \delta = \dfrac{2H^2}{\Gamma^2 + (\omega - \omega_r)^2 + 4H^2}, \\ \varepsilon = \dfrac{4H^2[\Gamma^2 + 4(\omega - \omega_r)^2 + 4H^2]}{[\Gamma^2 + (\omega - \omega_r)^2 + 4H^2][\Gamma^2 + 4(\omega - \omega_r)^2 + 16H^2]}, \\ \tau = \dfrac{24H^4}{[\Gamma^2 + (\omega - \omega_r)^2 + 4H^2][\Gamma^2 + 4(\omega - \omega_r)^2 + 16H^2]}. \end{cases}$$

The second of eqs. (9*b*) gives the Brossel-Bitter resonance (2).

(5) We are supposing here for simplicity a unique association of final levels f to the decaying states m. When this restriction is removed (see the following sections), eqs. (6) and (7) remain valid on the time average, as long as only a single level m_0 is excited, or somewhat more generally as for example in the case of natural excitation in the sense of Condon and Shortley. General excitation is treated in Sect. 4 below.

3. – Modulation of light by r.f. fields.

The preceding results are independent of the excitation time t_0, which has been taken for simplicity at $t_0 = 0$. (We suppose « pulse » excitation of the decaying states, produced *e.g.* by radiation from atoms emitting broad spectral lines, in which case we can speak of a definite excitation time. A more general formulation is given in Sect. **4** below.)

This arises because in the preceding discussion we have supposed for simplicity that the final states f were connected in a one-to-one fashion to the decaying states m, by non-vanishing matrix elements of the radiation interaction. When, however, one takes into account that more than one state m can decay to the same final level f, cross terms appear in the decay amplitudes (ERF, ref. [9]), and it is precisely these interference terms which lead to the effect of the modulation of light emitted in the decay transitions, by the r.f. field which produces transitions between the decaying states.

In this case, the amplitudes b_{f1_λ} are subject to the equations

$$i\dot{b}_{f1_\lambda} = \sum_m H_{f1_\lambda|m0} \exp\left[i(\omega_\lambda - \omega_{mf})t\right] b_{m0} , \tag{10}$$

where the summation extends over all the states m connected to f by non-vanishing matrix elements of the radiation interaction.

The solutions for the amplitudes b_{m0}, on the other hand, have the same form as before, because the terms in the equation for b_{m0} of the form $\sum_\mu H_{m0|f1_\lambda} H_{f1_\lambda|m'0}$ vanish for $m' \neq m$ [6]. Hence for the Majorana case, eqs. (1)-(3) continue to hold.

We suppose the system excited at time t_0 to the single level m_0, *e.g.* by incident light of appropriate direction of propagation and polarization (the general case where several of the levels m may be initially excited is treated in the following section), so that η_μ is given by

$$\eta_\mu = d^{(j)}_{\mu m_0} \exp\left[i(\omega_{m_0} + m_0[\omega - \omega_r] + \mu w_1 - \tfrac{1}{2} i\Gamma)t_0\right] \equiv \equiv d^{(j)}_{\mu m_0} \exp\left[i(\varrho_\mu + m_0\omega)t_0\right] . \tag{11}$$

Superimposing the solutions (3) with these values of η_μ, we get

$$b^{(j)}_{m0} = \sum_\mu d^{(j)}_{\mu m} d^{(j)}_{\mu m_0} \exp\left[-i(m[\omega - \omega_r] + \mu w_1 - \tfrac{1}{2} i\Gamma)t\right] \cdot \exp\left[i(\varrho_\mu + m_0\omega)t_0\right] . \tag{12}$$

[6] V. WEISSKOPF: *Ann. d. Phys.*, **9**, 23 (1931), especially p. 50.

Inserting eq. (12) into (10) and integrating, subject to the initial condition that there are no photons in the radiation field at time $t = t_0$, we obtain

$$b_{f1_\lambda} = \sum_m H_{f1_\lambda | m_0} c_{m m_0, k_\lambda}, \tag{13}$$

where

$$c_{m m_0, k_\lambda} = -\sum_\mu d^{(f)}_{\mu m} d^{(f)}_{\mu m_0} \exp\left[i(\varrho_\mu + m_0\omega)t_0\right] \cdot$$

$$\cdot \exp\left[i(\omega_\lambda - (\bar{\omega}_0 + m\omega + \mu w_1) + \tfrac{1}{2}i\Gamma)\, t\right] - \exp\left[i(\omega_\lambda - (\bar{\omega}_0 + m\omega - \mu w_1) - \tfrac{1}{2}i\Gamma)\, t_0\right] \over \omega_\lambda - (\bar{\omega}_0 + m\omega + \mu w_1) + \tfrac{1}{2}i\Gamma, \tag{14}$$

and $\bar{\omega}_0 = \bar{\omega}_0(f) = \omega_{mf} - m\omega_r$.

The state vector

$$\Phi = \sum_m b^{(f)}_{m0} |m\rangle + \sum_{f,\lambda} b_{f1_\lambda} |\lambda, f\rangle \tag{15}$$

is formed with the help of the amplitudes (12) and (13), and if we make use of the commutation rules, the definition of the vacuum, and the orthogonality of the states f, we obtain the following expressions for the expectation values in the state (15) of the squares of the fields and their cross product:

$$\frac{1}{4\pi} \langle :E^2: \rangle = \sum_f \Big| \sum_\lambda \frac{\sqrt{\hbar\omega_\lambda}}{g} \boldsymbol{e}_\lambda \exp\left[i(\boldsymbol{k}_\lambda \cdot \boldsymbol{r} - \omega_\lambda t)\right] b_{f1_\lambda} \Big|^2, \tag{16a}$$

$$\frac{1}{4\pi} \langle :H^2: \rangle = \sum_f \Big| \sum_\lambda \frac{\sqrt{\hbar\omega_\lambda}}{g} \hat{\boldsymbol{k}}_\lambda \times \boldsymbol{e}_\lambda \exp\left[i(\boldsymbol{k}_\lambda \cdot \boldsymbol{r} - \omega_\lambda t)\right] b_{f1_\lambda} \Big|^2, \tag{16b}$$

$$\frac{1}{4\pi} \langle :\boldsymbol{E} \times \boldsymbol{H}: \rangle = \frac{1}{2} \sum_f \sum_\lambda \frac{\sqrt{\hbar\omega_\lambda}}{g} \boldsymbol{e}_\lambda \exp\left[-i(\boldsymbol{k}_\lambda \cdot \boldsymbol{r} - \omega_\lambda t)\right] b^*_{f1_\lambda} \times$$

$$\times \sum_\lambda \frac{\sqrt{\hbar\omega_\lambda}}{g} \hat{\boldsymbol{k}}_\lambda \times \boldsymbol{e}_\lambda \exp\left[i(\boldsymbol{k}_\lambda \cdot \boldsymbol{r} - \omega_\lambda t)\right] b_{f1_\lambda} + \text{complex conj.}, \tag{16c}$$

where :...: denotes normal ordering and g is a normalization factor.

For the evaluation of these expressions one writes out the sum over λ as an integral over all propagation vectors $\boldsymbol{k}$ and a sum over the two polarization vectors $\boldsymbol{e}_1$, $\boldsymbol{e}_2$ for each $\boldsymbol{k}$. The dependence of the polarization vectors on the direction of $\boldsymbol{k}$ is suppressed ($\boldsymbol{e}_i = \boldsymbol{e}_i(\hat{\boldsymbol{k}})$).

The integral over the direction of the propagation vector is carried out

by expanding

$$\sum_{i=1,2} \boldsymbol{e}_i H_{lm,\,\boldsymbol{k},\,i} = \sum_{lm} \boldsymbol{\alpha}_{lm} Y_l^m(\hat{\boldsymbol{k}}) \,, \tag{17}$$

and making use of the well-known relation

$$\exp\left[i\boldsymbol{k}\cdot\boldsymbol{r}\right] = \sum_{lm} 4\pi i^l j_l(kr)\, Y_l^{m*}(\hat{\boldsymbol{k}})\, Y_l^m(\hat{\boldsymbol{r}}) \,. \tag{18}$$

We now look for the expected value of the field intensity, according to the exponential decay approximation, at observation points in the wave zone ($\bar{k}_0 r \gg 1$). In this case, only the neighborhoods of the poles of the resonance denominators of $b_{f1\lambda}$ will contribute to the integral over the magnitude of $\boldsymbol{k}$, and we can make use of the asymptotic form $i^l j_l \sim (\exp[ikr] - (-1)^l \exp[-ikr])/2ikr$. Since (cf. below) the ingoing-wave term gives a vanishing contribution, and since the outgoing-wave term is independent of l, the integration over angles leads to

$$\frac{c}{4\pi} \langle : E^2(\boldsymbol{r}, t) : \rangle = \tag{19}\ (7)$$

$$= \sum_f c \left| \int_0^\infty k^2 \mathrm{d}k \sqrt{\hbar\omega_k}\, \frac{4\pi}{2ikr}\, \frac{\exp\left[ik(r - ct)\right]}{(2\pi)^{\frac{3}{2}}} \sum_m \boldsymbol{H}_{fm} c_{mm_0}(k) \right|^2 ,$$

for $\bar{k}_0 r \gg 1$, where

$$\boldsymbol{H}_{fm} = \sum_{i=1,2} \boldsymbol{e}_i(\hat{\boldsymbol{r}}) H_{fm,\,k\hat{\boldsymbol{r}},\,i} \,. \tag{20}$$

With the help of eq. (14), the integral over k is evaluated as follows (we neglect the slow variation (8) of the powers of k and of $\boldsymbol{H}_{fm}$ across the resonances and take them equal to their values at $\bar{k}_0$): for the first term of c_{mm_0}, the path

(7) Similarly, eq. (16*c*) gives

$$\frac{c}{4\pi} \langle : \boldsymbol{E} \times \boldsymbol{H} : \rangle = c \sum_f \sum_{i=1,2} \left| \int_0^\infty k^2 \mathrm{d}k \sqrt{\hbar\omega_k}\, \frac{4\pi}{2ikr}\, \frac{\exp\left[ik(r - ct)\right]}{(2\pi)^{\frac{3}{2}}}\, b_{f,k\hat{\boldsymbol{r}},\boldsymbol{e}_i} \right|^2 \hat{\boldsymbol{r}} \quad \text{for } \bar{k}_0 r \gg 1,$$

which apart from the unit vector is the same as eq. (19). Likewise eq. (16*b*) leads to the same result.

(8) The details of the behavior very early and very late in the decay (or, in the energy representation, in the « wings » of the line form) depend on this frequency variation (ERF, refs. (6,8)).

of integration is completed in the complex k-plane around the first quadrant, and for the second term, around the first or fourth quadrant, according as $r/c > t - t_0$ or $t - t_0 > r/c$.

We neglect the non-exponential contributions from the integrals along the imaginary axis (cf. ERF, ref. (6)) and are left with the contributions from the poles of c_{mm_0}. Since only the contour of integration around the fourth quadrant encloses the poles,

$$(21a)\quad \frac{c}{4\pi}\langle :E^2(\boldsymbol{r},t):\rangle = \sum_j \frac{2\pi\hbar\bar{\omega}_0^3}{c^3r^2}\Big|\sum_{m\mu}\boldsymbol{H}_{fm}d^{(j)}_{fm}d^{(j)}_{\mu m_0}\cdot$$

$$\cdot\exp\left[-i(\mu w_1 - \tfrac{1}{2}i\Gamma)(t-t_0-r/c)\right]\exp\left[-im\omega(t-r/c)\right]\Big|^2,$$

$$\text{for } r/c < t-t_0.$$

$$(21b)\ ^{(9,10)}\qquad = 0\ ; \qquad \text{for } t-t_0 < r/c\ ,$$

(wave zone).

This expression corresponds to a single (« pulse ») excitation of the source atom (located at the origin of coordinates). Actually, the radiation intensity observed at $\boldsymbol{r}$, t will be due to many such excitations. The incident beam is supposed sufficiently weak, which is scarcely a restriction in the double resonance experiments under consideration, that the source atom can complete its decay uninterruptedly before being struck again.

If the absorption rate is γ, the number of excitations during an interval $\mathrm{d}t_0$ is $\gamma\,\mathrm{d}t_0$, so that multiplying the preceding expression by γ and integrating

(9) S. KIKUCHI: *Zeits. Phys.*, **66**, 558 (1930). See also the well-known articles in the *Rev. of Mod. Phys.*: E. FERMI: *Rev. Mod. Phys.*, **4**, 87 (1932); G. BREIT: *Rev. Mod. Phys.*, **5**, 91 (1933).

(10) For the ingoing-wave terms one has to evaluate an integral similar to the one in (19), with $\exp[ikr]$ replaced by $\exp[-ikr]$. Combining the $\exp[-ik(r+ct)]$ with the ω_λ-exponential in (14), one has from the first term of c_{mm_0} a factor $\exp[-ikr]$ and from the second term $\exp[-ik[r+c(t-t_0)]]$, so that for both terms the path of integration may be completed around the fourth quadrant. The contributions from the poles then precisely cancel each other.

It must be remarked that we have consistently neglected the contributions (which are in general small compared to the exponential terms — except at the very beginning and end of the decay, cf. ERF, ref. (6)) from the compensating integrals along the imaginary axis, needed to complete the contours of integration around the first and fourth quadrants: *i.e.*, we have made the exponential decay approximation. Thus eq. (21*b*) has been obtained as the result of approximation; correspondingly, in refs. (9) the lower limit of integration over k is extended to $-\infty$. In the pulse limit the departures from exponential decay are independent of excitation conditions.

over t_0, we obtain for the radiation intensity at $\boldsymbol{r}, t$ due to repeated excitations

$$(22) \qquad \gamma \int_{-\infty}^{t-r/c} \frac{c}{4\pi} \langle :E^2: \rangle \, \mathrm{d}t_0 = \sum_f \frac{2\pi\hbar\bar{\omega}_0^3\gamma}{c^3 r^2 \bar{\Gamma}} \sum_{\substack{m\mu \\ m'\mu'}} \boldsymbol{H}_{fm} \cdot \boldsymbol{H}^*_{fm'} d^{(f)}_{\mu m} d^{(f)}_{\mu m_0} d^{(f)}_{\mu' m'} d^{(f)}_{\mu' m_0} \cdot$$

$$\cdot \exp\left[-i(m-m')\omega(t-r/c)\right] \frac{\bar{\Gamma}}{i(\mu-\mu')w_1 + \bar{\Gamma}} \qquad \text{(wave zone)}.$$

Eq. (22) (Dodd-Series resonance) exhibits explicitly the modulation of the light observed at the detector at harmonics of the frequency of the applied r.f. field ([11]).

4. – General excitation conditions.

Finally, we must remove the restriction which has been made in the preceding discussion, of excitation to a single level m_0. Moreover, we use for this purpose a procedure which is not restricted to pulse excitation, although it will suffice to confine the discussion to this case.

We wish to study the fluorescent dispersion of an incident photon by a system initially in the ground state 0, assumed nondegenerate for simplicity, which is capable of excitation by the incident light (*e.g.*, light of mixed polarization) to several of the group of levels m, between which the applied r.f. field causes transitions.

Instead of treating directly the resonance fluorescence of a one-photon incident packet, we proceed by a somewhat different method, which is a generalization to the time-dependent coupled case of one introduced by Weisskopf ([6]). That is, for the purpose of obtaining the form of the dispersion amplitude, the one-photon amplitudes are first replaced by many-photon amplitudes with occupation number distribution equivalent to the incident radiation intensity.

([11]) It should be noted that the procedure of Section 2 applied in the present case would not lead to eq. (22) but to a different result, which can also be obtained by integrating eq. (21) over t. The reason is that two different quantities are being calculated; in the first case the differential emission by the source atom per unit time at t_0, and in the present case, the flux received at the detector at time t. In the stationary case of Section 2, the two results are the same, and in general they agree on the time average (eq. (7), times $\hbar\omega_0 \cdot \gamma \cdot r^{-2}$ and summed over m, f, and polarizations).

The equations which govern the time development of the system then become

$$(23a) \qquad i\dot{b}_0 = \sum_{m\lambda} H_{0,m\lambda} \exp\left[i(\omega_\lambda - \omega_{m0})t\right] b_{m\lambda} ,$$

$$(23b) \qquad i\dot{b}_{m\lambda} = \sum_{m'} \gamma_j \mathscr{H}(j_x)_{mm'} \exp\left[i(\omega_{mm'} - (m-m')\omega)t\right] b_{m'\lambda} +$$

$$+ H_{m\lambda,0} \exp\left[i(\omega_{m0} - \omega_\lambda)t\right] b_0 + \sum_\sigma H_{m\lambda,\lambda\sigma} \exp\left[i(\omega_{m0} - \omega_\sigma)t\right] b_{\lambda\sigma}$$

$$(23c) \qquad i\dot{b}_{\lambda\sigma} = \sum_m H_{\lambda\sigma,m\lambda} \exp\left[i(\omega_\sigma - \omega_{m0})t\right] b_{m\lambda} .$$

By procedures which are similar to some which have been used in ERF, one obtains suitable approximation solutions of these equations given by

$$(24a) \qquad b_0 = \exp\left[-\tfrac{1}{2}\gamma(t-t_0)\right] ,$$

$$(24b) \qquad b_{m\lambda}(t) = \sum_{\mu m_0} C_{\mu m} C_{\mu m_0} K_{\mu m_0 \lambda} \Big(\exp\left\{ i[\omega_{m0} - (m-m_0)\omega - \omega_\lambda]t \right\} \cdot$$

$$\cdot \exp\left[-\tfrac{1}{2}\gamma(t-t_0)\right] - \exp\left[-im(\omega-\omega_r)t\right] \cdot$$

$$\cdot \exp\left[-i(\mu w_1 - \tfrac{1}{2} i\Gamma)(t-t_0)\right] \exp\left[i(\bar{\omega}_0 + m_0\omega - \omega_\lambda)t_0\right] \Big) ,$$

$$(24c) \qquad b_{\lambda\sigma}(t) = \sum_{m\mu m_0} H_{\lambda\sigma,m\lambda} C_{\mu m} C_{\mu m_0} K_{\mu m_0 \lambda} \cdot$$

$$\cdot \Bigg(\frac{\exp\left[i[\omega_\sigma - \omega_\lambda - (m-m_0)\omega]t\right] \exp\left[-\tfrac{1}{2}\gamma(t-t_0)\right] - \exp\left[i[\omega_\sigma - \omega_\lambda - (m-m_0)\omega]t_0\right]}{\omega_\lambda - \omega_\sigma + [m-m_0]\omega - \tfrac{1}{2} i\gamma} +$$

$$+ \frac{\exp\left[i(\omega_\sigma - m\omega)t\right] \exp\left[-i(\bar{\omega}_0 + \mu w_1 - \tfrac{1}{2} i\Gamma)(t-t_0)\right] \exp\left[-i(\omega_\lambda - m_0\omega)t_0\right]}{\omega_\sigma - (\bar{\omega}_0 + m\omega + \mu w_1) + \tfrac{1}{2} i\Gamma} -$$

$$- \frac{\exp\left[i[\omega_\sigma - \omega_\lambda - (m-m_0)\omega]t_0\right]}{\omega_\sigma - (\bar{\omega}_0 + m\omega + \mu w_1) + \tfrac{1}{2} i\Gamma} \Bigg) ,$$

where

$$(25) \qquad K_{\mu m_0 \lambda} = \frac{H_{m\lambda,0}}{\omega_\lambda - (\bar{\omega}_0 + m\omega + \mu w_1) - \tfrac{1}{2} i(\gamma - \Gamma)} ,$$

$C_{\mu m} = d^{(j)}_{\mu m}$, and the other quantities have the same significance as before. In particular the non-transient term of $b_{\lambda\sigma}$, which is all that contributes essentially to the final result [12], has the form

$$(26) \quad b_{\lambda\sigma}(\infty) = \sum_{m\mu m_0} \frac{H_{\lambda\sigma,m\lambda} d^{(j)}_{\mu m} d^{(j)}_{\mu m_0} H_{m_0\lambda,0} \exp\left[i[\omega_\sigma - \omega_\lambda - (m-m_0)\omega]t_0\right]}{[\omega_\sigma - (\bar{\omega}_0 + m\omega + \mu w_1) + \tfrac{1}{2} i\Gamma][\omega_\sigma - \omega_\lambda + (m_0 - m)\omega + \tfrac{1}{2} i\gamma]} .$$

We sum over the incident single-photon amplitudes

$$c_\lambda = \alpha_\lambda \frac{\exp\left[i\omega_\lambda t_0\right]}{\omega_\lambda - \omega_0' + \frac{1}{2} i\Gamma'}, \tag{27}$$

and specialize to the case of pulse excitations (broad width Γ') by photons incident in a given direction. The phase in (27) corresponds to a pulse which arrives at the source atom at time $t=t_0$. To find the dispersed radiation intensity corresponding to repeated excitations, one evaluates

$$\sum_\lambda c_\lambda b_{\lambda\sigma}(\infty) - \text{const} \cdot \sum_{m\mu m_0} H_{0\sigma,m} d^{(j)}_{\mu m} d^{(i)}_{\mu m_0} H_{m_0,0} \frac{\exp\left[i[\omega_\sigma - (m-m_0)\omega]t_0\right]}{\omega_\sigma - (\bar{\omega}_0 + m\omega + \mu w_1) + \frac{1}{2} i\Gamma}, \tag{28}$$

and obtains finally

$$\mathcal{N} \int_{-\infty}^{t-r/c} c \left| \sum_{\sigma,\lambda} \frac{\sqrt{\hbar\omega_\sigma}}{g} \boldsymbol{e}_\sigma \exp\left[i(\boldsymbol{k}_\sigma \times \boldsymbol{r} - \omega_\sigma t)\right] \cdot c_\lambda b_{\lambda\sigma} \right|^2 \mathrm{d}t_0 = \tag{29}$$

$$= \text{const}'\, r^{-2} \sum_{\substack{m\mu m_0 \\ m'\mu' m_0'}} (\boldsymbol{H}_{0,m} \cdot \boldsymbol{H}^*_{0,m'}) d^{(j)}_{\mu m} d^{(j)}_{\mu m_0} d^{(j)}_{\mu' m'} d^{(j)}_{\mu' m_0'} (H_{m_0,0} H^*_{m_0',0}) \cdot$$

$$\cdot \frac{\Gamma \exp\left[-i\omega[m - m' - m_0 + m_0'](t - r/c)\right]}{\Gamma + i[(\mu - \mu')w_1 + (m_0 - m_0')\omega]} \quad \text{(wave zone)},$$

where $\mathcal{N}$ = no. of photons incident per s, and const′ $= (32\pi^5\omega_0^2/c^4\Gamma) \times$ incident radiation intensity per unit frequency.

Eq. (29) (general Dodd-Series resonance) is the generalization to the case where several of the upper levels can be excited by the incident radiation. It may be noted that the total absorption rate is independent of the application of the r.f. field, as one can check by integrating eq. (29) over the sphere of radius r. All interference terms then drop out and one has the sum of the energy absorption rates for the individual levels m_0.

([12]) The transient term is of course essential for the cancellation in ref. ([10]).

RIASSUNTO (*)

La teoria precedentemente sviluppata per esaminare il frazionamento delle linee di Zeeman da parte di campi magnetici a r.f. porta direttamente alla risonanza di Brossel-Bitter ottenuta in esperimenti sulla doppia risonanza. Un'estensione della teoria dà ragione degli effetti di modulazione della luce recentemente osservati in tali esperimenti.

(*) *Traduzione a cura della Redazione.*

IL NUOVO CIMENTO Vol. XXII, N. 1 1° Ottobre 1961

Analytic Properties of n-Point Loops in Perturbation Theory (*).

L. M. Brown

Northwestern University - Evanston, Ill.

(ricevuto il 27 Luglio 1961)

Summary. — It is shown that simple perturbation graphs consisting of closed n-vertex loops have only the singularities possessed by reduced loops, obtained by «fusing» two or more of the vertices and omitting the internal lines which join them. The theorem holds providing $n \geqslant 6$.

1. – Introduction.

The study of the analytic structure of transition amplitudes represented by Feynman graphs may give essential insights into the complete scattering amplitude. This point has been emphasized by Landau [1], who has given simple rules for locating all possible singularities of arbitrary graphs. The difficult point in applying these rules is determining whether a possible singularity does or does not appear on the relevant Riemann sheet of the generalized scattering amplitude, namely the sheet determining the physical process under consideration. Studies to this end have been made by many authors [2-9],

(*) Supported in part by a grant from the National Science Foundation.

(1) L. D. Landau: *Nucl. Phys.*, **13**, 181 (1959); also *Sov. Fis. JEPT*, **10** (**37**), 45 (1960).

(2) J. C. Polkinghorne and G. R. Screaton: *Nuovo Cimento*, **15**, 289, 925 (1960).

(3) J. Tarski: *Journ. Math. Phys.*, **1**, 154 (1960).

(4) J. C. Taylor: *Phys. Rev.*, **117**, 261 (1960).

(5) M. Fowler, P. V. Landshoff and R. W. Lardner: *Nuovo Cimento*, **17**, 956 (1960).

(6) R. E. Cutkosky: *Journ. Math. Phys.*, **1**, 429 (1960).

(7) R. J. Eden, P. V. Landshoff, J. C. Polkinghorne and J. C. Taylor: *Phys. Rev.*, **122**, 307 (1961).

(8) S. Mandelstam: *Phys. Rev.*, **115**, 1741 (1959).

(9) R. J. Eden: *Phys. Rev.*, **119**, 1763 (1960).

who have particularly emphasized the important three- and four-point diagrams. Especially noteworthy are the studies of the lowest order three- and four-point loops in which the existence of singularities other than normal threshold singularities was discovered ([10]).

As applied to simple n-point loops, Landau's rules show that possible singularities correspond either to putting all the internal lines on their mass shells, or to the singularities of loops with fewer vertices (reduced diagrams) obtained by « fusing » two or more of the vertices by omitting the internal lines which connect them. Characteristic n-point singularities of the first type have been called ([2]) « leading » singularities, while those of the reduced diagrams have been called « lower-order » singularities. The object of the present work is to show that there are no leading singularities of simple n-point loop, if $n \geqslant 6$. This will be done by an explicit reduction of the n-point loop into a linear combination of reduced loops, the coefficients being non-singular functions of the external invariants. The reduction procedure has previously been given by FEYNMAN ([11]).

It is interesting to remark that the five-point function has been shown to have complex singularities when two of the invariants are considered as complex variables ([5]), and even when only one invariant is considered to be complex ([12]). Thus it is probably significant that our method fails for five-point loops ([13]).

It is also worth mentioning that, with the exception of the pioneering work of EDEN ([14]), all subsequent searching for singularities has been done using parametric forms of the amplitude ([15]), while our work is done with the original forms.

2. – Proof of the theorem.

The singularities of an n-point loop are those of the integral

$$I_n = \int \frac{\mathrm{d}^4 k}{[1][2] \dots [n]}, \tag{1}$$

([10]) R. KARPLUS, C. M. SOMMERFIELD and E. M. WICHMAN: *Phys. Rev.*, **114**, 376 (1959).

([11]) Private communication to the author in 1953.

([12]) P. V. LANDSHOFF and S. B. TREIMAN: *Nuovo Cimento*, **19**, 1249 (1961).

([13]) P. V. LANDSHOFF: *Nucl. Phys.*, **20**, 129 (1960) has observed that dual diagram construction for the six-point loop is overdetermined if all invariants but one are assigned definite values.

([14]) R. J. EDEN: *Proc. Roy. Soc.* (*London*), A **210**, 388 (1952).

([15]) See also Y. NAMBU: *Nuovo Cimento*, **6**, 1064 (1957).

with

$$[i] = k^2 - 2p_i \cdot k - \Delta_i; \qquad \Delta_i = m_i^2 - p_i^2 . \tag{2}$$

In general, the expression for the loop will have a numerator under the integral sign which will be a polynomial function of the loop variable k and the « internal variables » p_i, which are linear combinations of the momenta external to the loop. This numerator will not concern us as it cannot contribute to a singularity (though it may annul one). In any case, an algebraic method has been given ([16]) for expressing integrals containing k_σ, k_σ, k_τ, etc. in the numerator in terms of I_n and integrals containing at most $n-1$ factors in the denominator. We shall assume also that the n factors in I_n are distinct, though the case that two or more factors are the same presents no difficulty.

Assume *two* linear relations to hold among the p_i, so that we can write

$$\sum_1^n a_i p_i = 0 , \tag{3a}$$

and

$$\sum_1^n a_i = 0 , \tag{3b}$$

This is always true in a four-dimensional space, providing $n > 5$. It *may* also be true for $n \leqslant 5$.

Then,

$$\sum_1^n a_i [i] = \sum_1^n a_i \Delta_i \equiv \Delta . \tag{4}$$

In the case $\Delta \neq 0$, we have

$$I_n = \frac{1}{\Delta} \sum_1^n a_i \int \frac{\mathrm{d}^4 k [i]}{[1][2] \ldots [n]} . \tag{5}$$

The a_i may be found as follows: form the five-dimensional vectors $\boldsymbol{r}_i = (p_i, 1)$ where the fifth variable is Euclidean, *i.e.*, $\boldsymbol{r}_i^2 = p_i^2 + 1$.

Then conditions (3) read

$$\sum_1^n a_i \boldsymbol{r}_i = 0. \tag{6}$$

([16]) L. M. Brown and R. P. Feynman: *Phys. Rev.*, **85**, 231 (1952).

Let $n=6$, and form

$$\boldsymbol{D} = \mathrm{Det}\begin{vmatrix} \boldsymbol{r}_1 & \dots & \boldsymbol{r}_6 \\ p_{1x} & \dots & p_{6x} \\ \dots & & \dots \\ p_{1'} & \dots & p_{6'} \\ 1 & \dots & 1 \end{vmatrix}, \tag{7}$$

$\boldsymbol{D}$ is the 5-vector whose components D_j are obtained by substituting in (7) for each $\boldsymbol{r}_i$ its j^{th} component. Hence $\boldsymbol{D}$ is a zero vector. But then the expansion of $\boldsymbol{D}$ in minors of the first row gives just the conditions (6). Hence the minors of the $\boldsymbol{r}_i$ in $\boldsymbol{D}$ form a set of a_i satisfying (6).

For $n>6$ we can set $a_7=a_8=\dots=a_n=0$ and still satisfy (6), so it is sufficient to study the case $n=6$.

The a_i are in general non-rational functions of the invariants $p_k\cdot p_l$. However, the products a_ia_j are given by

$$a_ia_j = \mathrm{Det}\left(\|a_i\|^T\|a_j\|\right), \tag{8}$$

where $\|a_i\|$ is the matrix of the determinant which gives a_i, and $\|a_i\|^T\|a_j\|$ is by inspection a matrix whose kl element is

$$\boldsymbol{r}_k\cdot\boldsymbol{r}_l = p_k\cdot p_l + 1\,.$$

Thus the products a_ia_j are polynomials in the invariants $p_k\cdot p_l$ formed of the internal variables and they are therefore also polynomials formed of the external invariants.

It follows then that the quotients a_i/a_j are rational fractions formed of the external invariants, since

$$\frac{a_i}{a_j} = \frac{a_i^2}{a_ia_j}\,.$$

As this holds for *all* a_j, the expansion coefficients a_i/Δ are rational fractions and can give rise to no branch points in I_n. Obviously a_i is finite.

We have therefore, for $\Delta\neq 0$, the result: if all $a_i\neq 0$, the singularities of I_n are those of all the $I_n^{(i)}$, which are the loops obtained from I_n by omitting the i^{th} line.

If, let us say, a_k vanishes, all the singularities are still present as only the integral with $[k]$ omitted drops from the expansion. This corresponds to the invariance of the loop against translation ($k\to k+q$) by which we can *always* make one of the a_i vanish.

In the case $\Delta = 0$, the expansion (5) is not valid. However, certainly not all the a_i are zero; suppose $a_1 \neq 0$, then as we have in this case,

$$\sum_1^n a_i[i] = 0 \,, \tag{9}$$

we can write

$$a_1[1] = -\sum_2^n a_i[i] \,,$$

and

$$I_n = -\sum_2^n \frac{a_i}{a_1} \int \frac{\mathrm{d}k^4[i]}{[1]^2[2] \ldots [n]} \,. \tag{10}$$

We have shown that a_i/a_1 is rational and never infinite. Hence the above considerations can be applied as before, and the number and location of the singualrities of I_n are as described above. The appearance of second order poles in the integrand of (10) is probably spurious as it depended on the singling out of a_1, and they should cancel upon summation.

* * *

This article was written while the author was a Visiting Lecturer at the University of Colorado at Boulder, Colorado in summer, 1961, and he wishes to thank the Physics Department for its hospitality. He also wishes to thank Dr. G. Dell'Antonio for discussions on this subject.

RIASSUNTO (*)

Si dimostra che i grafici di perturbazione semplici formati da anse chiuse con n vertici hanno solo le singolarità proprie delle anse ridotte ottenute « fondendo » due o più vertici e omettendo le linee interne che li uniscono. Il teorema è valido purchè $n \geqslant 6$.

(*) *Traduzione a cura della Redazione.*

High-Energy Nucleon-Nucleon Collisions (*).

W. K. R. Watson

Jet Propulsion Laboratory, California Institute of Technology - Pasadena, Cal.

(ricevuto il 28 Luglio 1961)

Summary. — It is shown that single-vector meson exchange processes which may give rise to the repulsive core in nucleon-nucleon collisions, yield an elastic scattering cross section which approaches a constant value in the limit of infinitely large energy. Limits on the values of mass and coupling constant of this meson are inferred from high energy data, in particular a value for the strength of the ρ nucleon interaction is determined from the charge-exchange cross section data.

1. – Introduction.

Following the philosophy of Sakurai [1], and incorporating the later developments of Gell-Mann [2], we have assumed the existence of an octet of vector mesons which in the limit of unitary symmetry are coupled to conserved currents with equal coupling constants. Estimates of this effective coupling constant indicate that it lies in the neighborhood of $g^2/4\pi\hbar c \sim \frac{2}{3}$; in addition, some information concerning the variation of the appropriate form factors as a function of momentum transfer can be inferred from the work of Hofstadter, *et al.* [3]. At the present time, it is not clear whether these vector mesons are fundamental in the sense that each has its own independent coupling constant and mass, or whether they are dynamical resonances in which case the mass and coupling constant will be determined by

(*) Supported under contractual arrangment for the National Aeronautics and Space Administration NASA-6.

(1) J. J. Sakurai: *Ann. of Phys.*, **11**, 1 (1960).

(2) M. Gell-Mann: *The eightfold way: a theory of strong interaction symmetry*, California Institute of Technology Synchrotron Laboratory Report CTSL-20 (1961).

(3) R. Hofstadter and R. Herman: *Phys. Rev. Lett.*, **6**, 293 (1961).

already existing parameters. In any event, we shall treat them as elementary in the sense that they provide us with a « theory » which is easy to calculate with in this approximation. We shall not concern ourselves with the lack of renormalizability of these vector systems in the presence of other interactions and will use relativistic perturbation theory to draw some general conclusions about the nature of high energy nucleon-nucleon collisions. In addition, there is another singlet vector meson B_0 coupled to the baryon current which is renormalizable.

Provided that we are only dealing with lowest order vector meson exchange processes which are coupled to conserved currents, it can be shown that we are justified in using $(k^2 - m^2)^{-1}$ for the vector meson propagator [4]. The ω meson ($J = 1$, $T = 0$) couples to the hypercharge current which in the absence of weak interactions is conserved. The ρ meson ($J = 1$, $I = 1$) couples to the isotopic spin current which is conserved provided that we ignore electromagnetic and weak interactions, whereas the B_0 meson always couples to the totally conserved baryon current. Even at high energies the B_0 effective coupling constant and mass are as yet undetermined; however, an estimate of $g^2_{B_0}$ may in principle probably be obtained from the strength of the Yukawa potential required to form a pion consisting of a bound state nucleon-antinucleon system. (This point is currently being investigated by KAUS *et al.* [5].)

For high energy nucleon-nucleon scattering processes, there are two reasons why single pion effects can be ignored despite the inherently large coupling constant $(g^2_\pi/4\pi\hbar c) \approx 15$. One of these is exhibited in current work [6] in relatively low energy nucleon-nucleon collisions (100 to 300) MeV, which indicates that direct single pion exchange effects are substantially suppressed by the pseudoscalar vector interference effects which are negative. The other is due to the fact that in the limit of extremely high energies, the p.s. single pion exchange can be shown to give a vanishing contribution compared to a single vector meson exchange. Two-pion and three-pion exchange contributions are essentially « included » by using the ($I = 1$, $J = 1$, « two-pion » resonance) and ($I = 0$, $J = 1$, « three-pion » resonance) exchange in lowest order. It will be shown that the vector meson contributions yield a total elastic cross section which approaches a constant value in the high energy limit which is determined by two parameters (the coupling constant and the mass of the vector field). The masses of the ρ and ω mesons can be deduced from Hofstadter's experiments and show that $m_\rho \sim 5.5\mu_\pi$, $m_\omega \sim 5\mu_\pi$ [3].

[4] The author is indebted to Mr. S. COLEMAN for pointing this out.

[5] P. E. KAUS and W. K. R. WATSON: *Bull. Am. Phys. Soc.*, **6**, 377 (1961). The same problem is currently being attacked by a different method by Prof. F. ZACHARIASEN *et al.*

[6] W. K. R. WATSON: *Bull. Am. Phys. Soc.*, **6**, 372 (1961) and *Phys. Rev.*, to be published.

2. – Development.

The contribution to the differential cross section (C.M.) for identical nucleon-nucleon scattering arising from the exchange of a single neutral vector meson is given after considerable, but straightforward, algebra by the expression

$$(1)\qquad \left(\frac{\mathrm{d}\sigma}{\mathrm{d}\Omega}\right)_{v^2} = \left(\frac{g_v^2}{4\pi\hbar c}\right)^2\left(\frac{\hbar}{Mc}\right)^2\frac{1}{\gamma^2}\left\{\frac{2\gamma^4\beta^4\sin^4\theta/2 - 4\gamma^4\beta^2\cos^2\theta/2 + 1}{[2\beta^2\gamma^2(1-\cos\theta) + (m/M)^2]^2} + \right.$$

$$+ \frac{2\gamma^4\beta^4\cos^4\theta/2 + 4\gamma^4\beta^2\sin^2\theta/2 + 1}{[2\beta^2\gamma^2(1+\cos\theta) + (m/M)^2]^2} +$$

$$\left. + \frac{(2\gamma^2-1)(2\beta^2\gamma^2-1)}{[2\beta^2\gamma^2(1-\cos\theta) + (m/M)^2][2\beta^2\gamma^2(1+\cos\theta) + (m/M)^2]}\right\},$$

where:

m = mass of vector meson.

M = nucleon mass.

θ = center of mass angle.

g_v = coupling constant.

Notice that in the limit of $m \to 0$ and $\theta \to 0$ or π, $(\mathrm{d}\sigma/\mathrm{d}\Omega) \to \infty$ as required (photon case). Moreover, for the case $m \neq 0$ and $\theta = 0$ or π, we observe that $(\mathrm{d}\sigma/\mathrm{d}\Omega)$ increases as γ^2 (*i.e.*, as E^2) in the forward and backward directions. (This observation is in good agreement with the experiment results [7].)

The corresponding contribution to $(\mathrm{d}\sigma/\mathrm{d}\Omega)$ arising from single pion exchange can be shown to be

$$(2)\qquad \left(\frac{\mathrm{d}\sigma}{\mathrm{d}\Omega}\right)_{(\mathrm{p.s.})^2} = \left(\frac{g_\pi^2}{4\pi\hbar c}\right)^2\left(\frac{\hbar}{Mc}\right)^2\frac{1}{4\gamma^2}\left\{\frac{\gamma^4\beta^4(1-\cos\theta)^2}{[2\gamma^2\beta^2(1-\cos\theta) + (\mu/M)^2]^2} + \right.$$

$$+ \frac{\gamma^4\beta^4(1+\cos\theta)^2}{[2\gamma^2\beta^2(1+\cos\theta) + (\mu/M)^2]^2} +$$

$$\left. + \frac{\gamma^4\beta^4\sin^2\theta}{[2\gamma^2\beta^2(1+\cos\theta) + (\mu/M)^2][2\gamma^2\beta^2(1-\cos\theta) + (\mu/M)^2]}\right\},$$

μ = mass of pion.

g_π = pion nucleon coupling constant.

Integration of eq. (2) over all angles shows that this contribution to the elastic scattering cross section approaches zero as $\gamma \to \infty$. We are now left

(7) C. H. Tsao *et al.*: *Bull. Am. Phys. Soc.*, **6**, 343 (1961).

with the effects of (P.S.-V) interference contribution which is given by

$$(3)\qquad \left(\frac{\mathrm{d}\sigma}{\mathrm{d}\Omega}\right)_{(\mathrm{P.S.\text{-}V})} = -\left(\frac{g_\pi^2}{4\pi\hbar c}\right)\left(\frac{g_v^2}{4\pi\hbar c}\right)\left(\frac{\hbar}{Mc}\right)^2\frac{\gamma^2\beta^2}{2}\cdot$$
$$\cdot\left\{\frac{(1-\beta^2\cos\theta)(1-\cos\theta)}{[2\gamma^2\beta^2(1-\cos\theta)+(\mu/M)^2][2\gamma^2\beta^2(1+\cos\theta)+(m/M)^2}+\right.$$
$$\left.+\frac{(1+\beta^2\cos\theta)(1+\cos\theta)}{[2\gamma^2\beta^2(1-\cos\theta)+(m/M)^2][2\gamma^2\beta^2(1+\cos\theta)+(\mu/M)^2]}\right\}.$$

Integration of this expression over angles again yields a contribution to σ_{elastic} which vanishes in the limit of large γ. Thus, we are left with the contributions from eq. (1).

The only important terms arise from the following integrals:

$$(4)\qquad \operatorname*{Lt}_{\gamma\to\infty}\int_0^\pi \frac{4\gamma^2\cos^2\theta/2\,\mathrm{d}\Omega}{[2\gamma^2(1-\cos\theta)+(m/M)^2]^2} = \frac{4\pi M^2}{m^2},$$

and

$$(5)\qquad \operatorname*{Lt}_{\gamma\to\infty}\int_0^\pi \frac{4\gamma^2\sin^2\theta/2\,\mathrm{d}\Omega}{[2\gamma^2(1+\cos\theta)+(m/M)^2]^2} = \frac{4\pi M^2}{m^2},$$

so that in the limit of large γ, (with $\beta=1$) the elastic scattering cross section is finally given by

$$(6)\qquad \sigma_{\text{elastic}} \simeq 8\pi\left(\frac{g_v^2}{4\pi\hbar c}\right)^2\left(\frac{\hbar}{Mc}\right)^2\left(\frac{M}{m}\right)^2.$$

Experimental information concerning the behavior of σ_{elastic} at very high energies is somewhat vague, however reasonable estimates indicate that $\sigma_{\text{elastic}} \to (10 \text{ to } 20)$ m.b.s. Using this value and equating to (6), we see that

$$(7)\qquad \left(\frac{g^2}{4\pi\hbar c}\right)\left(\frac{M}{m}\right) \simeq 1 \text{ to } 1.4\,.$$

At estremely high energies the eightfold way makes no distinction between the various vector fields (*i.e.*, they become degenerate) so that the g^2/M values represent an effective g^2 and M; in particular, if we accept a $(g^2/4\pi\hbar c)$ in the neighborhood of unity, we see that the effective vector meson is required to have approximately one nucleon mass.

Another interesting experimental observation lies in the fact that the elastic charge exchange n-p scattering is very small at relatively high energies (7), *i.e.*, in the neighborhood of one millibarn. In lowest order only one meson (a charged ρ) can contribute, the mass of which is already known; this then allows us to determine the ρ-nucleon coupling constant within the framework of this approximation. Inserting the appropriate parameters into eq. (6) leads to a value for

$$\left(\frac{g^2_{\rho NN}}{4\pi\hbar c}\right) \sim 0.12 \,. \tag{8}$$

This number is considerably smaller than that predicted by the eightfold way, but appears to be the only way of explaining the small charge exchange elastic scattering cross section data.

3. – Conclusion.

In addition, it should be pointed out that vector interactions of this type produce an effective repulsion between two nucleon systems and thus gives automatically credence to the two-fireball model of N-N collisions used for the computation of ultra-relativistic processes (8). This model is in fairly good agreement with experiments at very high energies and is probably qualitatively correct for energies sufficient for the fireballs to achieve thermodynamic equilibrium. Experimentally, the inelasticity appears to fall off as $1/E_{\text{C.M.}}$, *i.e.*, as $1/\gamma$ implying, therefore, that the inelastic cross section also approaches a constant value. Best estimates indicate that $\sigma_{\text{inelastic}} = 20$ mbs (9). Hence, we might expect an upper limit for $\sigma_{\text{total}} = 40$ mbs. Finally, it is hoped that a determination of $g^2_{\rho NN}$ can be obtained from the experimental forward direction pion-nucleon scattering data, and by making use of the ϱ pole contribution. The $g^2_{\rho\pi\pi}$ coupling constant is essentially determined by the width of the pion resonance, thus allowing $g_{\rho NN}$ to be found. Preliminasy estimates indicate $g^2_{\rho NN}$ to be approximately 0.2. in fairly good agreement with equation (8).

(8) W. K. R. Watson and D. Hankins: *Pion production in* 300 GeV *nucleon-nucleon Collisions*, Calif. Inst. of Technology Synchrotron Laboratory Report CTSL-29 (1961).

(9) D. H. Perkins: *Elementary Particle and Cosmic Ray Physics*, vol. 5 (Amsterdam, 1960), pp. 259-360.

* * *

Finally, the author would like to take this opportunity to thank Professors GELL-MANN, KAUS and ZACHARIASEN for several enlightening discussions, and is particularly grateful to Mr. DENIS HANKINS for checking some of the integrals involved in this work.

RIASSUNTO (*)

Mostro che i processi di scambio di mesoni univettoriali, che possono dar luogo al centro repulsivo nelle collisioni nucleone-nucleone, generano una sezione d'urto di scattering elastico che si approssima ad un valore costante al limite di energia infinitamente grande. Dai dati alle alte energie si deducono i limiti per i valori della massa e della costante di accoppiamento di questo mesone, ed in particolare dai dati della sezione d'urto per lo scambio di carica si determina un valore per la forza della interazione ρ-nucleone.

(*) *Traduzione a cura della Redazione.*

LETTERE ALLA REDAZIONE

(La responsabilità scientifica degli scritti inseriti in questa rubrica è completamente lasciata dalla Direzione del periodico ai singoli autori)

Über die Berechnung der Schallgeschwindigkeit in Gasmischungen

II. Mitteilung.

V. S. Vrkljan

Zagreb

(ricevuto il 27 Marzo 1961)

In einer Mitteilung [1], welche in dieser Zeitschrift veröffentlicht wurde, wurde gezeigt, wie man das Verhältnis der spezifischen Wärmen mittels einer geeigneten Definition der mittleren Zahl der Freiheitsgrade einer Gasmischung idealer Gase und damit zuletzt die Schallgeschwindigkeit dieser Gasmischung ableiten kann. Bei der Ableitung wurde die Formel [2]

$$(1) \qquad c_j^2 = 3\frac{R}{m_j}T_j\,, \qquad (j = 1, 2, \ldots, n),$$

verwendet, wo $\overline{c_j^2}$ den Mittelwert des Quadrates der fortschreitenden Geschwindigkeiten der Molekeln bedeutet, m_j die (relative) Molekularmasse und T_j die Temperatur der einzelnen Gase der Gasmischung (welche selbstverständlich gleich der Temperatur T der Gasmischung wird, wenn sich die Gasmischung im Gleichgewicht befinden sollte). Daß diese Formel für die Ableitung nicht notwendig ist, ist der Gegenstand dieser Mitteilung. Dies zu zeigen scheint deswegen eingermaßen wichtig zu sein, weil die Anwendung der Formel (1) eventuell zu der irrtümlichen Auffassung führen könnte, als ob sich die vorhergehende Ableitung trotz anfänglicher Voraussetzung einer beliebigen Zahl der Freiheitsgrade nur auf solche Gase erstrecken sollte, bei welchen die ganze innere Energie in der fortschreitenden Bewegung der Molekeln bestände (abgesehen von einer Konstanten, die von der Temperatur unabhängig ist [2]). Damit wird aber zugleich die Ableitung vereinfacht und verkürzt.

Die Voraussetzung dieser Ableitung ist weiter, daß keine Dispersion der Schallwellen auftritt.

Wir definieren als die mittlere Zahl der Freiheitsgrade einer Gasmischung im thermischen Gleichgewicht einfach den arithmetischen Mittelwert der Zahl der Freiheitsgrade, welche zu den einzelnen Molekeln gehören, d. h.

$$(2) \qquad f = \frac{\sum_{j=1}^{n} N_j f_j}{N}\,. \qquad \left(N = \sum_{j=1}^{n} N_j\right).$$

(1) V. S. Vrkljan: *Nuovo Cimento*, **17**, 845 (1960).

(2) C. Sthaefer: *Theor. Phys.*, **2**, 330 (1921).

Es bedeutet hier N_j die Zahl der Molekeln der einzelnen homogenen Gase im Einheitsvolumen der Gasmischung und f_j die Zahl der Freiheitsgrade der Molekeln des j-ten Gases.

Führt man diesen Ausdruck in die bekannte Formel für das Verhältnis der spezifischen Wärmen idealer Gase

$$k = 1 + \frac{2}{f} \tag{3}$$

ein und beachtet man dabei, daß

$$N_j = \frac{\varrho_j}{m_j} \qquad (j = 1, 2, \ldots, n), \tag{4}$$

ist, falls mit m_j die absoluten Werte der Molekularmassen und mit ϱ_j die Dichten der einzelnen homogenen Gase in der Gasmischung bezeichnet werden, so erhält man

$$k = 1 + 2 \frac{\sum_{j=1}^{n} \varrho_j/m_j}{\sum_{j=1}^{n} (\varrho_j/m_j) f_j} . \tag{5}$$

Mittels der Anwendung des Ausdrucks für f aus der Gleichung (3) im Nenner auf der rechten Seite der Gleichung (5), diesmal aber selbstverständlich auf die einzelnen homogenen Gase, die Bestandteile der Gasmischung (also $f_j = 2/(k_j - 1)$) kommt man gleich zu der Formel für das Verhältnis der spezifischen Wärmen der Gasmischung

$$k = 1 + \frac{\sum_{j=1}^{n} \varrho_j/m_j}{\sum_{j=1}^{n} (\varrho_j/m_j) \cdot 1/(k_j - 1)} , \tag{6}$$

welche uns schon aus der vorhergehenden Mitteilung bekannt ist. Wie in dieser Mitteilung gezeigt wurde, führt die Anwendung dieses Ausdruckes für k in der Gleichung

$$\frac{v^2 \varrho}{k} = \sum_{j=1}^{n} \frac{v_j^2 \varrho_j}{k_j} , \tag{7}$$

gleich zu der Formel für die Schallgeschwindigkeit in den Gasmischungen, welche gerade in der schon erwähnten vorhergehenden Mitteilung abgeleitet wurde.

Und zuletzt noch eine Bemerkung. In der Gleichung (4) bedeutet m_j, wie schon dort erwähnt wurde, den absoluten Wert der Molekularmasse der einzelnen homogenen Gase; trotzdem kann man in den Gleichungen (5) und (6) für m_j die relativen Molekularmassen, wie sie aus der Chemie bekannt sind, anwenden, weil sich in diesen Gleichungen um einen Quotienten handelt, wo sowohl im Zähler als auch im Nenner die Molekularmassen m_j in den entsprechenden Ausdrücken ϱ_j/m_j vorkommen und weil die relativen Molekularmassen den wirklichen Molekularmassen proportional sind. Im letzten Fall bedeuten aber die Ausdrücke ϱ_j/m_j nicht mehr die Zahlen der Molekeln im Einheitsvolumen.

Elimination of the Inelastic Cut in the N/D Method (*).

M. Froissart (**)

Department of Physics, University of California - Berkeley, Cal.

(ricevuto il 3 Luglio 1961)

We want to propose here a method to handle the contributions from the inelastic region, in a problem to be solved by the N/D method [1,2] in order to reduce it to a problem without inelastic parts. Let us put the problem this way: we seek a function $A(\nu)$ satisfying:

a) $A(\nu)$ is analytic in ν in a plane cut from 0 to $+\infty$ and from $-\infty$ to -1.

b) $A(\nu)$ has a given discontinuity $\Delta A(\nu)$ across the left-hand cut;

c) $A(\nu)$ on the right-hand cut is of the form:

$$A(\nu) = f(\nu)\frac{\eta(\nu)\exp[2i\delta]-1}{2i},$$

where $f(\nu)$ is a given kinematical factor, δ a real phase, and $\eta(\nu)$ is a given elasticity coefficient: $\eta=1$ for elastic scattering: $\eta=0$ for total absorption. We know [2,3] the solution of the problem for $\eta\equiv 1$. Our aim is to come back to this case.

Let us introduce the following function:

$$R(\nu) = \exp\frac{-iq}{\pi}\int_0^\infty \frac{\ln\eta(\nu')\,d\nu'}{q'(\nu'-\nu)}.$$

(*) This research was supported by the U. S. Air Force under Contract No. AF 49(638)-327 monitored by the A. F. Office of Scientific Research of the Air Research and Development Command.

(**) On leave from C.E.N. Saclay, B. P. 2 Gif s/Yvette, (Seine et Oise).

(1) G. F. Chew and F. E. Low; *Phys. Rev.* **101**. 1570 (1956).

(2) G. F. Chew and S. Mandelstam; *Phys. Rev.*, **119**, 467 (1960).

(3) R. Omnès: *On a Mathematical Problem Encountered in Quantum Field Theory* (preprint, C.E.N. Saclay).

This function exists as long as $\eta(\nu')$ does not decrease too fast. It has a cut from zero to infinity, and $|R(\nu)| = \eta$ on both sides of the cut. Condition *c*) implies now that

$$A(\nu) = f(\nu) \frac{R(\nu)}{} \frac{\exp[2i\alpha] - 1}{2i}, \qquad \text{where} \quad \alpha = \delta - \tfrac{1}{2} \arg R(\nu),$$

$$\alpha = \delta + \frac{q}{2\pi} P \int_0^\infty \frac{\ln \eta(\nu') \, d\nu'}{q'(\nu' - \nu)}, \qquad \text{for positive real } \nu.$$

Furthermore R is non-vanishing in the cut plane. If we introduce the function

$$A'(\nu) = \frac{A(\nu)}{R(\nu)} + f(\nu) \frac{1 - R(\nu)}{2iR(\nu)},$$

we see that is satisfies condition *a*), as the commonly used f factors do; it has a jump across the left-hand cut which is

$$\frac{\Delta A(\nu)}{R(\nu)} + \Delta f(\nu) \frac{1 - R(\nu)}{2iR(\nu)}.$$

This is a known quantity.

Finally, on the right-hand cut, it is simply equal to $f(\nu)(\exp[2i\alpha] - 1)/2i$, and we are thus led back to the usual elastic problem, which one can solve by either the method of Chew and Mandelstam [2] or the method recently proposed by Omnès [3].

The advantage of this method over that of Frazer and Ball [4] is that it does not lead to an equation involving principal value integrals. However, the final equations that we obtain will in general be singular, owing to the fact that if η goes to zero at infinity, $R(\nu)$ will also go to zero at infinity along the negative axis, thus making the left-hand cut of $A'(\nu)$ behave badly, unless it happens that some cancellation arises between $\Delta A(\nu)$ and $\Delta f(\nu)$.

[4] W. Frazer and J. Ball: *Phys. Rev. Lett.*, **7**, 204 (1961).

IL NUOVO CIMENTO Vol. XXII, N. 1 1° Ottobre 1961

π^--Proton Scattering at 516, 616, 710, 887, and 1085 MeV.

F. Grard (*), G. Macleod and L. Montanet
(*CERN - Geneva*)

M. Cresti
(*Istituto di Fisica dell'Università - Padova*)

R. Barloutaud, C. Choquet, J.-M. Gaillard, J. Heughebaert (*), A. Leveque, P. Lehmann, J. Meyer and D. Revel
(*CEN - Saclay*)

(ricevuto il 15 Luglio 1961)

We present results on π^--p scattering at kinetic energies in the laboratory of 516, 616, 710, 887 and 1 085 MeV. The data were obtained by exposing a liquid hydrogen bubble chamber to a pion beam from the Saclay proton synchrotron Saturne. The chamber had a diameter of 20 cm and a depth of 10 cm. There was no magnetic field. Two cameras, 15 cm apart, were situated at 84 cm from the center of the chamber.

A triple quadrupole lens looking at an internal target, and a bending magnet, defined the beam, whose momentum spread was less than 2%. The value of the momentum was measured by the wire-orbit method and by time of flight technique, and the computed momentum spread was checked by means of a Čerenkov counter.

The pictures were scanned twice for all pion interactions. Only those events with primaries at most 3° off from the mean beam direction and with vertices inside a well defined fiducial volume were considered. All not obviously inelastic events were measured and computed by means of a Mercury Ferranti computer. The elasticity of the event was established by coplanarity and angular correlation of the outgoing tracks.

We checked that no bias was introduced for elastic events with dip angles for the scattering plane of less than 80° and with cosines of the scattering angles in the C.M.S. of less than 0.95.

Figs. 1 to 5 show the angular distributions for elastic scattering, for all events with dip angles for the scattering plane less than 80°. The solid curves represent a best fit to the differential cross section. The ratio of charged inelastic to elastic events, was obtained by comparing the number of inelastic scatterings to the areas under the solid curves which give the number of elastic scatterings.

(*) Chercheur I.I.S.N., Laboratoire des Hautes Energies (Bruxelles).

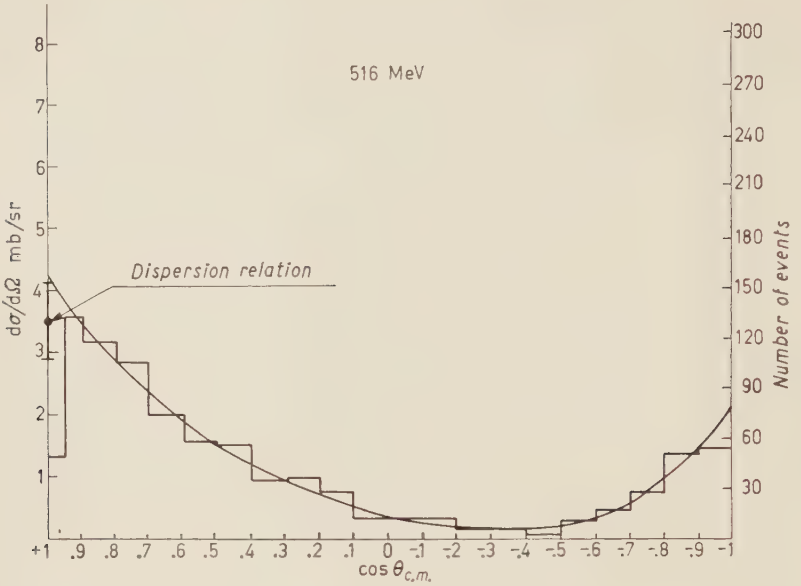

Fig. 1.

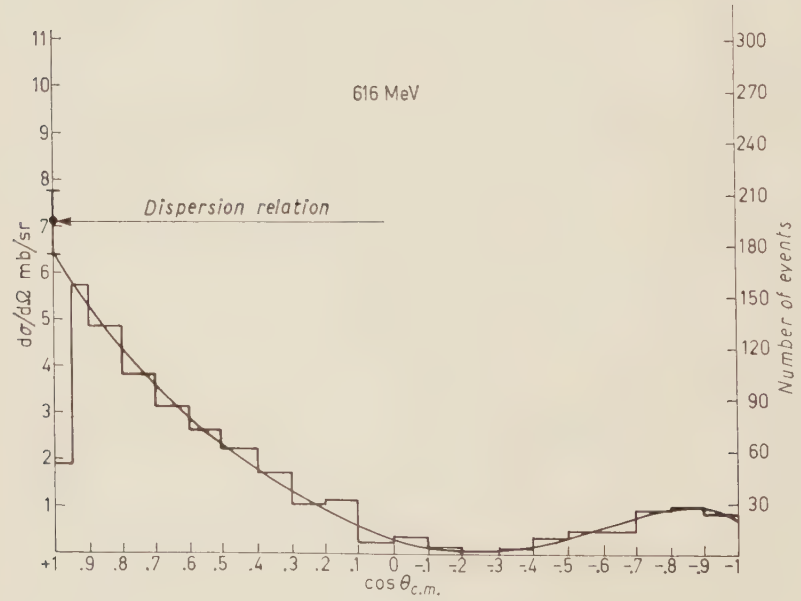

Fig. 2.

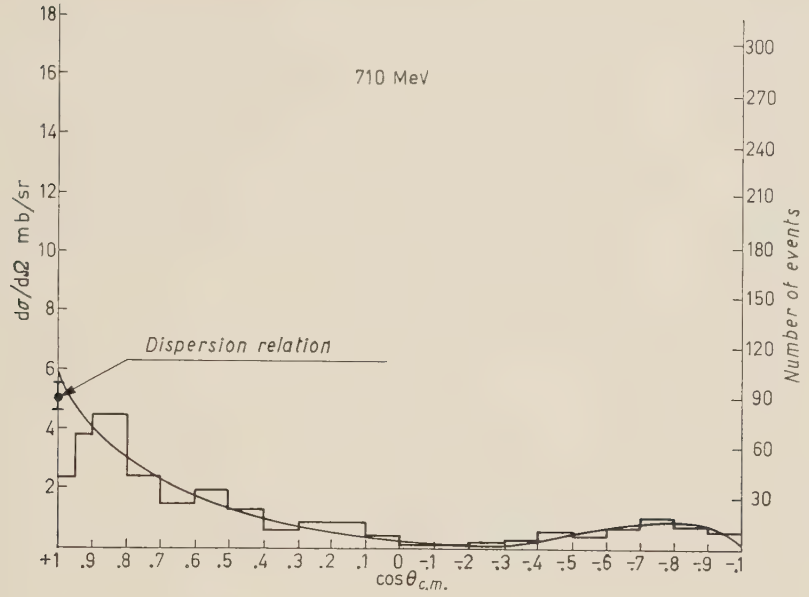
710 MeV
Dispersion relation
dσ/dΩ mb/sr
Number of events
cos θc.m.

Fig. 3.

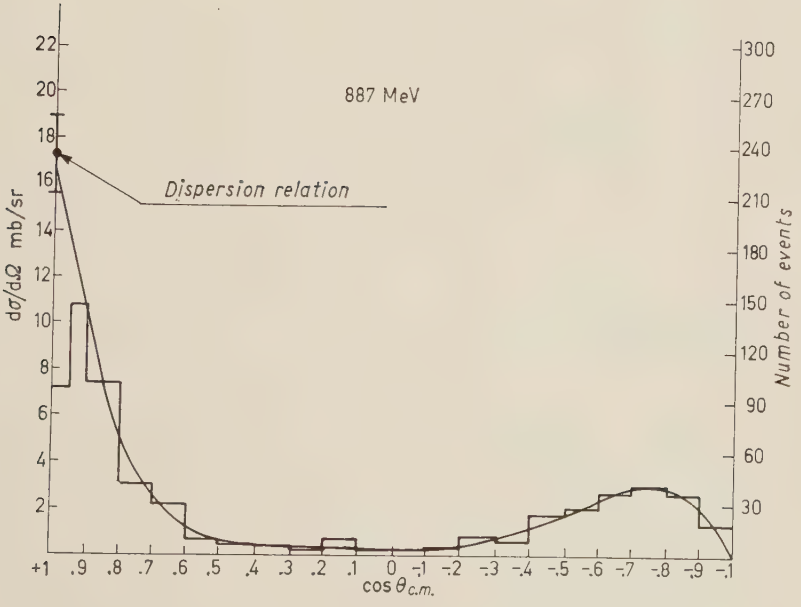
887 MeV
Dispersion relation
dσ/dΩ mb/sr
Number of events
cos θc.m.

Fig. 4.

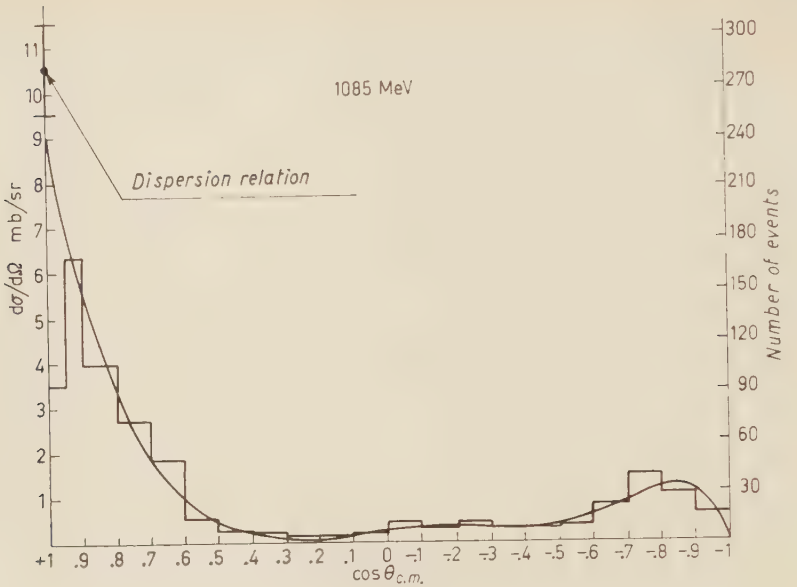

Fig. 5.

Absolute values of cross sections for elastic, charged inelastic and total inelastic cross sections were obtained by normalizing our data to the measurements of BRISSON *et al.* ([1,2]) for total, charge exchange and $2\pi^0$ production cross sections. Our results are shown in Table I. They should be compared to those of other workers ([3-6]).

([1]) J. C. BRISSON, J. F. DETOEUF, P. FALK-VAIRANT, L. VAN ROSSUM and G. VALLADAS: *Nuovo Cimento*, **19**, 210 (1961).

([2]) J. C. BRISSON, P. FALK-VAIRANT, J. P. MERLO, P. SONDEREGGER, R. TURLAY and G. VALLADAS: *Proc. of the Annual Intern. Conf. at Rochester* (1960), p. 191; and private communication.

([3]) R. R. CRITTENDEN, J. H. SCANDRETT, W. D. SHEPHARD, W. D. WALKER and J. BALLAM: *Phys. Rev. Lett.*, **2**, 121 (1959).

([4]) I. SHONLE: *Phys. Rev. Lett.*, **5**, 156 (1960).

([5]) C. D. WOOD, T. J. DEVLIN, J. A. HELLAND, M. J. LONGO, B. J. MOYER and V. PEREZ-MENDEZ: *Phys. Rev. Lett.*, **6**, 481 (1961).

([6]) S. BERGIA, L. BERTOCCHI, V. BORELLI, G. BRAUTTI, L. CHERSOVANI, I. LAVATELLI, A. MINGUZZI-RANZI, R. TOSI, P. WALOSCHEK and V. ZOBOLI: *Nuovo Cimento*, **15**, 551 (1960).

The angular distributions may be written:

$$\left(\frac{\mathrm{d}\sigma}{\mathrm{d}\omega}\right)_{\mathrm{CM}} = \sum_{l=0}^{k} a_l \cos^l \theta_{\mathrm{CM}} .$$

Table II shows the values of the coefficients a_l obtained by a least-squares fit. The value of the maximum power k of the series was obtained when the χ^2 parameter did not improve, when a fit with a larger k was attempted. It was found that at 516 MeV, k was equal to 4, at 616, 710 and 887 MeV it was 5, while at 1 085 MeV terms up to $\cos^7 \theta_{\mathrm{CM}}$ had to be taken into account. At each energy the power series was extrapolated to 0° scattering, and very good agreement with forward scattering as given by the optical theorem and dispersion relations ([8]) was found, as can be seen in Fig. 1 to 5. This is considered a check of our normalization procedure.

The values of the coefficients given in Table II complete the results of other

TABLE I.

	516	616	710	887	1 085
$\sigma_{el}(\pi^-\text{-p})$	14.8±1.3	19.4±1.4	14.9±1.3	27.3±1.7	14.1 ±1.0
$\sigma_{ch\ in}(\pi^-\text{-p})$	7.9±1.1	12.5±1.0	10.4±1.0	17.9±1.5	15.85±1.3
$\sigma_{tot\ in}(\pi^-\text{-p})$	12.0±1.3	16 ±1.2	14.1±1.1	21.5±1.7	20.4 ±1.4
$\sigma_{tot}(T=\frac{1}{2})$	42 ±2	60.1±2.7	44.2±3.0	74.6±3.3	38.5 ±2.1
$\sigma_{el}\ (T=\frac{1}{2})$	29.0±2.8	37.8±2.7	25.4±2.6	48.6±2.9	20 ±2
$\sigma_{in}\ (T=\frac{1}{2})$	13.0±1.8	22.3±2.1	18.3±2.0	26.0±2.5	18.5 ±1.5

TABLE II.

Energy (MeV)	516	616	710	887	1 085
a_0	0.40±0.04	0.33±0.06	0.27±0.08	0.28±0.08	0.26±0.04
a_1	1.45±0.16	2.3 ±0.3	1.2 ±0.4	0.1 ±0.3	0.87 ±0.26
a_2	1.47±0.39	4.3 ±0.6	2.4 ±0.8	2.1 ±0.7	−1.36±0.79
a_3	−0.35±0.35	−1.6 ±1.2	−2.5 ±1.9	−9.1 ±1.9	6.1 ±2.6
a_4	1.31±0.36	−3.6 ±0.8	0.3 ±1.1	5.8 ±1.1	9.5 ±3.1
a_5	—	2.3 ±1.3	4.1 ±2.1	17 ±2	−11.1±6.8
a_6	—	—	—	—	−3.9±2.9
a_7	—	—	—	—	10.5±5.1

authors ([5,7]). The prominence of a_5 at 887 MeV is confirmed. If we admit that in the angular distribution, powers larger than fifth are negligible, then the conclusion is that the term in $\cos^5\theta_{CM}$ is due to a $D_{\frac{5}{2}}$-$F_{\frac{5}{2}}$ interference. At 1 085 MeV we obtain, within the rather large statistical errors a negative value for a_5. Furthermore, at this energy, the fast decrease of a_5 is accompanied by the appearence of terms of the sixth and expecially of the seventh power of $\cos\theta_{CM}$. However, we did not have to consider, even at 1 085 MeV, higher powers, although they are already required at 1 200 MeV ([7]).

Table II also shows that a_3 increases rapidly to a positive value after the minimum at 900 MeV. The general behaviour of the other coefficients as a function of energy, agrees well with the curves given by WOOD *et al.* ([5]). One may notice however that a_4 is definitely positive at 516 MeV.

Our data confirm the evolution of the backward bump in the angular distribution. It increases from 710 MeV onwards, comes to a maximum at 887 MeV, and then decreases. At 887 and 1 085 MeV $(d\sigma/d\omega)_{CM}\ (180°)$ is zero, within our experimental errors, while at 1 200 MeV and 1 300 MeV it has increased again to a finite value ([7-12]).

([7]) L. BERTANZA, R. CARRARA, A. DRAGO, P. FRANZINI, I. MANNELLI, G. V. SILVESTRINI and P. H. STOKER: *Nuovo Cimento*, **19**, 467 (1961).

([8]) J. W. CRONIN: *Phys. Rev.*, **118**, 824 (1960).

([9]) P. FALK-VAIRANT and G. VALLADAS: *Rev. Mod. Phys.*, **33**, 362 (1961).

([10]) D. STONEHILL, C. BALTAY, H. COURANT, W. FICKINGER, E. FOWLER, H. KRAYBILL, J. SANDWEISS, J. SANFORD and H. TAFT: *Phys. Rev. Lett.*, **6**, 623 (1961).

([11]) W. J. WILLIS: *Phys. Rev.*, **116**, 753 (1959).

([12]) M. CHRETIEN, J. LEITNER, N. P. SAMIOS, M. SCHWARTZ and J. STEINBERGER: *Phys. Rev.*, **108**, 383 (1957).

At the highest energies under consideration, a peak appears in the forward direction. If one tries to interpret this peak as due only to shadow scattering, one obtains reasonable agreement with our angular distribution at 1 085 MeV by taking for the optical radius a value of $1.08 \cdot 10^{-13}$ cm, consistent with results at 1 200 an 1 300 MeV ([7,12]).

Although few results on π^+-p inelastic scattering are available ([9-11]) we computed the cross sections for total, elastic and inelastic scattering in the isotopic spin $T=\frac{1}{2}$ state. These are shown in the last rows of Table I. It is seen that the inelastic cross section for $T=\frac{1}{2}$ state does not show a very marked variation as the pion energy changes from 616 to 887 MeV.

* * *

We wish to thank Dr. G. MOORHEAD for helping with the programs for the computer, Dr. R. OMNÈS for many helpful discussions, Professors A. BERTHELOT and Y. GOLDSCHMIDT-CLERMONT for their kind interest.

Quenching of Muon Depolarization by Weak Magnetic Fields (*).

G. Charpak (**), F. J. M. Farley, R. L. Garwin (***), T. Muller (***),
J. C. Sens, V. L. Telegdi (***), C. M. York (***) and A. Zichichi

CERN - Geneva

(ricevuto il 18 Luglio 1961)

Polarized positive muons when coming to rest inside various materials, are known to lose part of their initial polarization, the remaining fraction being critically dependent on the medium in which they are stopped. This effect anticipated by Landau [1], has been observed in a large number of elements and compounds [2]. The mechanism by which polarized positive muons are depolarized when stopped in matter is still not clearly understood. The experimental results obtained so far may be summarized as follows. If muons are stopped in an electrically conducting material they suffer very little depolarization. In insulators, on the other hand, the results are very variable, some materials giving no depolarization (bromoform, methylene iodide), while in others (sulphur, NaCl) the depolarization is almost complete. It should be noted that these measurements are carried out in transverse fields ~ 50 G. The application of a magnetic field of $\sim 10^4$ G along the axis of the polarization prevents the depolarization to a large extent [3].

In argon gas the observed depolari-

(*) Presented by A. Zichichi at the Annual Meeting of the Italian Physical Society, Naples, September 1960.

(**) On leave from Centre National de la Recherche Scientifique (France).

(***) Ford Foundation Fellow, from IBM Watson Laboratory, Columbia University, New York.

(***) On leave from Centre National de la Recherche Scientifique and Institut de Recherches Nucléaires, Strasbourg (France).

(***) NSF Senior Fellow, on leave from University of Chicago.

(***) Ford Foundation Fellow, now at Physics Dept., UCLA, Los Angeles, California.

(1) L. Landau: *Nucl. Phys.*, **3**, 127 (1957).

(2) S. C. Wright: *Proc. of the Seventh Annual Rochester Conference* (New York, 1957), chap. VII, p. 31; J. M. Cassels, T. W. O'Keefe, M. Rigby, A. M. Wetherell and J. R. Wormald: *Proc. Phys. Soc.*, A **70**, 543 (1957); R. A. Swanson: *Phys. Rev.*, **112**, 580 (1958).

(3) *Experimental*: S. C. Wright: loc. cit.; J. C. Sens, R. A. Swanson, V. L. Telegdi and D. D. Yovanovitch: *Phys. Rev.*, **107**, 1465 (1957); B. A. Nikolsky and S. A. Alizade: *Proc. of the 1960 Annual International Conference on High Energy Physics at Rochester* (New York), p. 614 (this paper contains a summary of earlier emulsion work).

Theoretical: G. Breit and V. W. Hughes: *Phys. Rev.*, **106**, 1293 (1957); R. A. Ferrell and F. Chaos: *Phys. Rev.*, **107**, 1322 (1957); R. A. Ferrell, Y. C. Lee and M. K. Pal: *Phys. Rev.*, **118**, 317 (1960).

zation has been shown to be associated with the formation of muonium. The restoration of the polarization by strong fields is in this case explained within the rather large experimental error by considering the gradual decoupling of the electron and muon spins in muonium ([4]).

In solids the analogy between muons and positrons suggests that muonium, as well as positronium, may be formed. Attempts to detect its precession in a 0.4 G field have, however, led to negative results ([5]). But this does not permit the conclusion that muonium is not formed in solids: small ((1÷10) G) local fields or the presence of a quenching mechanism allowing triplet-singlet transitions in times less than ~100 ns could make the process unobservable.

The measurements on the re-establishment of polarization in large magnetic fields are not well explained by the theory of muonium formation ([6]), showing that the mechanism of depolarization is more complicated: but it has, nevertheless, been thought to be associated with muon-electron interactions involving fields of several kilogauss. We report here a measurement which indicates that much weaker fields of order 100 G can influence the depolarization in the case of a plastic scintillator target. This suggests that, in this medium muon depolarization is associated at least partly with internal fields of order (10÷100) G in the solid.

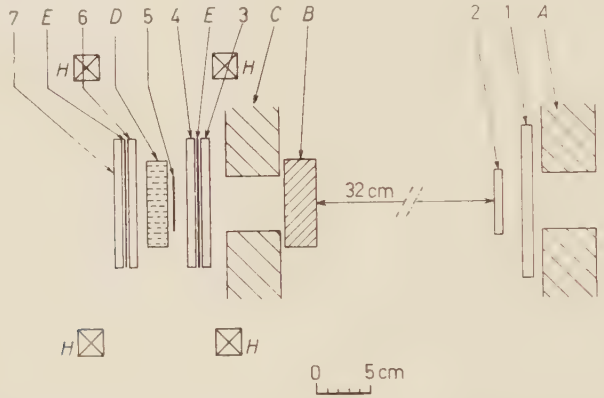

Fig. 1. – Experimental set-up. *A*) brass collimator 5×5 cm; *B*) copper absorber 3.1 cm; *C*) brass collimator 5 cm high×3.5 cm wide; 1, 2, 3, 4, 6, 7 plastic scintillator 0.8 cm thick; 5 plastic scintillator 0.1 cm thick; *D*) plastic scintillator target; *E*) 0.1 cm copper sheets; *H*) the Helmoltz coils that provide the variable longitudinal field.

In our apparatus (shown in Fig. 1) a coincidence 123456̄ indicates a muon stopping in the target material (plastic scintillator type NE 102, Nuclear Enterprises, Ltd., Edinburgh). This signal, after a delay of 1.1 μs, opens a gate 5 μs long through which decay positrons may be counted. Decays forward (F) are indicated by a coincidence 2̄67, and backward (B) by a coincidence 2̄34. The stray field of the cyclotron is com-

([4]) V. W. HUGHES, D. W. MCCOLIN, R. PREPOST and K. ZIOCK: *Phys. Rev. Lett.*, **5**, 63 (1960); R. PREPOST, V. W. HUGHES and K. ZIOCK: *Phys. Rev. Lett.*, **6**, 19 (1961).

([5]) N. P. CAMPBELL, E. L. GARWIN, J. C. SENS, R. A. SWANSON, V. L. TELEGDI and D. D. YOVANOVITCH: *Bull. Am. Phys. Soc.*, **2**, 205 (1957).

([6]) B. A. NIKOLSKY and S. A. ALI-ZADE: loc. cit.

pensated by a large pair of horizontal Helmholtz coils (not shown), and a longitudinal field (*i.e.* parallel to the incident beam) of up to 150 G is produced at the target (D) by a smaller pair of Helmholtz coils (H). It has been

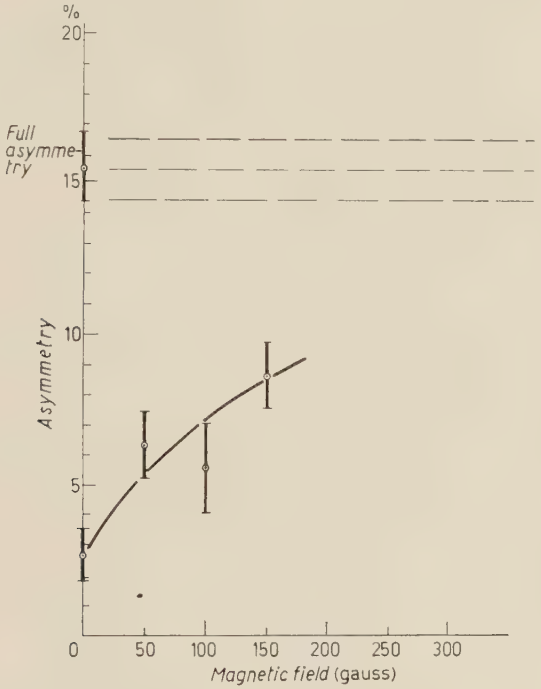

Fig. 2. — Asymmetry *vs.* magnetic field. The experimental results with their statistical errors are best-fitted by eye with the field-curve. The point at (15.5 %) represents the value of the full asymmetry and is obtained by stopping the beam in a non-depolarizing material (methylene iodide) and by using the same counter arrangement for measurement of the variation of asymmetry *vs.* applied magnetic field.

checked that the applied field does not influence the photomultipliers. If N_F and N_B are the number of decay positrons counted in the two telescopes the asymmetry $A=(N_F-N_B)/(N_F+N_B)$ will include some instrumental asymmetry because the counters do not see the target D with the same solid angle, and because their electronic efficiencies and backgrounds are not equal. One can, however, determine the change of A as a function of the applied field. To normalize the scale, we measure the absolute value of the asymmetry at zero field by removing the instrumental effects with the spin flipping technique (7). In this measurement the counter to target geometry is unchanged, but the muon spin is flipped through 180°, by means of a pulsed vertical magnetic field in the 1.1 μs interval before the opening of the electron gate. This field was produced by applying a current pulse to an aluminium tape coil wound directly on the target.

The same flipping technique was used to find the asymmetry for a thin (5 mm) methylene iodide target to indi-

(7) T. Coffin, R. L. Garwin, S. Penman, L. M. Lederman and A. M. Sachs: *Phys. Rev.*, **109**, 973 (1958).

cate the asymmetry available with this beam and counter geometry when there is no depolarization. The methylene iodide was thin enough to give negligible increase in asymmetry due to the hardening of the electron spectrum by absorption.

The results which are plotted in Fig. 2 show clearly the re-establishment of polarization at low fields. It is interesting to note that already at ~ 150 G the asymmetry reaches about 50% of its full value. We note that the asymmetry in zero field ($\sim 2.5\%$) is well below the value ($(6 \div 7)\%$) measured with the « precession » method ([8]). This is partly due to the lower maximum asymmetry in our apparatus, 16% instead of 24%, but a lower value would not be surprising because in the precession method a transverse field of 100 G is applied in order to make the muon magnetic moment rotate at a convenient frequency; although one would not expect identical effects for longitudinal and transverse fields, we see from our results that in plastic scintillator a field of this order substantially increases the polarization.

It is now clear that measurements of depolarization by the precession method may give an incorrect indication of the properties of the material in zero field, so that some care is needed in interpreting the results of such measurements in this respect.

Whether or not muonium is formed, the change of polarization at low fields indicates that some other mechanism is probably at least as important in the depolarization process. One possibility is that the external field swamps a random internal field of order 100 G which is responsible for the depolarization.

If this is so then in zero field a decay of the longitudinal component of polarization should be observable in the first few microseconds.

([8]) J. M. CASSELS *et al.*: loc. cit.; R. A. SWANSON: loc. cit.

Relations between Polarizations Due to Charge Independence (*)

L. Michel

Physique Théorique et Hautes Energies - Orsay

(ricevuto il 22 Agosto 1961)

We want to study the relation that exists between the polarizations of corresponding particles in reactions identical from the point of view of charge independence.

When the total isospin has only one possible value, the polarizations are identical for the same values of the particles energies and momenta; this is the case for example of the polarizations of the recoiling nucleons in $\pi^- + p^+ \to \pi^- + p^+$ and $\pi^- + p^+ \to \pi^0 + n$ at the $T = \frac{3}{2}$, $J = \frac{3}{2}$ resonance.

We shall study the simplest non-trivial case and the most useful for practical applications, when there are *two* possible values T' and T'' for the total isospin of the considered reactions. Let $f'(x)$ and $f''(x)$ be the corresponding transition amplitudes for a given kinematics (*i.e.* known energy, momentum and total polarization for each particle) represented by the general variable x; if the index α labels the different reactions corresponding by charge independence, the transition amplitudes $f_\alpha(x)$ are linear combinations of $f'(x)$ and $f''(x)$. Hence there is a linear relation $\sum \lambda_\alpha f_\alpha(x) = 0$ for any three values of α; the three complex numbers $\lambda_\alpha f_\alpha(x)$ form a triangle whose sides have length $|\lambda_\alpha|\,|f_\alpha(x)| = |\lambda_\alpha| \sqrt{\sigma_\alpha(x)}$ where $\sqrt{\sigma_\alpha(x)}$ is the positive square root of the cross-section $\sigma_\alpha(x)$ for the reaction α. Usually one says the three $|\lambda_\alpha| \sqrt{\sigma_\alpha(x)}$ satisfy a triangular relation.

Three positive numbers a, b, c satisfy a triangular relation if:

$$(1) \qquad |a - b| \leqslant c \leqslant a + b\,, \quad |a - c| \leqslant b \leqslant a + c\,, \quad |b - c| \leqslant a \leqslant b + c\,.$$

We leave to the reader to prove that equivalents relations are:

$$(2) \qquad -2ab < a^2 + b^2 - c^2 \leqslant 2ab\,,$$

or

$$(3) \qquad \Delta(a, b, c) = (a + b - c)(a - b + c)(-a + b + c) \geqslant 0\,.$$

(*) This research has been sponsored in part by the Air Force Research Division of the Air Research and Development Command, United States Air Force, under contract no. AF 61(052)-474.

We shall need the following theorem: let a, b, c, three positive functions of x defined on a domain D; let $\mathrm{d}\mu$ be a positive measure on D and let

$$\alpha^2 = \int_D a^2 \,\mathrm{d}\mu\,, \qquad \beta^2 = \int_D b^2 \,\mathrm{d}\mu\,, \qquad \gamma^2 = \int_D c^2 \,\mathrm{d}\mu\,,$$

be finite; if $\Delta(a, b, c) \geqslant 0$ everywhere on D, then $\Delta(|\alpha|, |\beta|, |\gamma|) \geqslant 0$.

Proof: the relation (2) is also satisfied when integrated with $\mathrm{d}\mu$:

$$-2\int_D ab \,\mathrm{d}\mu \leqslant \alpha^2 + \beta^2 - \gamma^2 \leqslant 2\int_D ab \,\mathrm{d}\mu$$

On the other hand, Schwartz's inequality (that is the condition which expresses that $\int_D (a\lambda + b)^2 \,\mathrm{d}\mu \geqslant 0$ whatever λ real) yields $\int_D ab \,\mathrm{d}\mu \leqslant |\alpha|\,|\beta|$; hence:

$$-2|\alpha|\,|\beta| \leqslant -2\int_D ab \,\mathrm{d}\mu \leqslant \alpha^2 + \beta^2 - \gamma^2 \leqslant 2\int_D ab \,\mathrm{d}\mu \leqslant 2|\alpha|\,|\beta|\,,$$

i.e.

$$\Delta(|\alpha|, |\beta|, |\gamma|) \geqslant 0 \quad \text{(relation (2) for } |\alpha|, |\beta|, |\gamma|).$$

This theorem is relevant to our problem as follows. The quantities $|f_\alpha(x)|^2$ are differential cross-sections for given energy-momenta and for totally polarized particles: however they are not the quantities directly measured in experiments. The recording apparati (*e.g.* counters) integrate cross-sections over some solid angle Ω and some energy band ΔE with a positive weight function $\varrho(E, \Omega, \ldots)$ that we call the « efficacity function » of the detection device; furthermore the polarizations might or might not have been measured. So, an experimental setting measures the cross-sections:

$$\sigma_\alpha = \int |f_\alpha|^2 \,\mathrm{d}\mu \equiv \sum_i \int |f_\alpha(E, \Omega, i)|^2 \,\varrho(E, \Omega, i) \,\mathrm{d}E \,\mathrm{d}\Omega\,, \tag{4}$$

where the discrete variable i represents the spin variables and $\varrho \geqslant 0$.

By application of the theorem, we obtain a triangular relation, for three values of α, between $|\lambda_\alpha| \sqrt{\sigma_\alpha} = \alpha_\alpha$. We shall call ω_α the angles of the triangle; *i.e.*:

$$\cos \omega_\gamma = (a_\alpha^2 + a_\beta^2 - a_\gamma^2)/2a_\alpha a_\beta\,. \tag{5}$$

To be more concrete, we shall show on an example what we want to prove about polarizations. Let us consider the reactions of associated production:

$$\pi^+ + \mathrm{p}^+ \to \Sigma^+ + \mathrm{K}^+\,, \tag{6}$$

or the charge symmetric

$$\pi^- + n \to \Sigma^- + K^0 ,$$

(7) $$\pi^- + p^+ \to \Sigma^0 + K^0 \qquad \text{or} \qquad \pi^+ + n \to \Sigma^0 + K^+ ,$$

(8) $$\pi^- + p^+ \to \Sigma^- + K^+ \qquad \text{or} \qquad \pi^+ + n \to \Sigma^+ + K^0 .$$

For given states of energy momentum and polarization of the involved particles, let us call $f_+(x)$, $f_0(x)$, $f_-(x)$ the final state amplitudes for reactions 1, 2, 3 (or 1', 2', 3') and $f_{\frac{3}{2}}(x)$, $f_{\frac{1}{2}}(x)$ the corresponding amplitudes for total isobaric spins $\frac{3}{2}$, $\frac{1}{2}$:

The f's satisfy the following relations:

(9) $$f_+ = f_{\frac{3}{2}} , \qquad f_0 = \frac{\sqrt{2}}{3} f_{\frac{3}{2}} - \frac{\sqrt{2}}{3} f_{\frac{1}{2}} , \qquad f_- = \frac{1}{3} f_{\frac{3}{2}} + \frac{2}{3} f_{\frac{1}{2}} ,$$

and by elimination of $f_{\frac{3}{2}}$ and $f_{\frac{1}{2}}$:

(10) $$- f_+ + \sqrt{2} f_0 + f_- = 0 ,$$

that is

(10') $$\lambda_+ = -1 , \qquad \lambda_0 = \sqrt{2} , \qquad \lambda_- = 1 .$$

Hence the triangular relation between cross-sections:

(11) $$\Delta(\sqrt{\sigma_+}, \sqrt{2\sigma_0}, \sqrt{\sigma_-}) \geqslant 0 .$$

From now on we shall assume that the target p^+'s are unpolarized and that Σ's have spin $\frac{1}{2}$. *We are interested in the Σ polarization.* For given momenta of the particles, for instance, in the laboratory: $\boldsymbol{p}_\pi$, $\boldsymbol{p}_p = 0$, $\boldsymbol{p}_\Sigma$, space and time reversal invariance require that polarization is transverse and represented by the pseudo-vector

$$\eta \boldsymbol{n} = \eta \boldsymbol{p}_\pi \times \boldsymbol{p}_\Sigma / |\boldsymbol{p}_p \times \boldsymbol{p}_\Sigma| ,$$

(there is no polarization if $\boldsymbol{p}_\pi \times \boldsymbol{p}_\Sigma = 0$), where $-1 \leqslant \eta \leqslant 1$, *i.e.* η is the sign and the the degree of the Σ polarization. More generally, for a given beam $\boldsymbol{p}_\pi$, if φ is azimuth around p_π of $\boldsymbol{n}(\varphi) = \boldsymbol{p}_\pi \times \boldsymbol{p}_\Sigma / |\boldsymbol{p}_\pi \times \boldsymbol{p}_\Sigma|$, the Σ polarization is

$$\eta \boldsymbol{n} = \eta \int_0^{2\pi} \boldsymbol{n}(\varphi)\, \varrho(E, \theta, \varphi)\, \mathrm{d}\varphi$$

since rotational invariance requires η to be independent of φ.

Let σ_α be the production cross-sections for unpolarized target p^+ and some experimental conditions (beam energy, solid angles, etc.) and η_α the Σ^α polarization. *Our problem is: given the three σ_α, which relations satisfy the three η_α?* These relations depend only on $|\lambda_\alpha| \sqrt{\sigma_\alpha} = a_\alpha$.

Let $\sigma_\alpha^{(\pm)}$ be the corresponding cross-sections for $\eta_\alpha = \pm 1$, *i.e.* if the Σ^α were observed totally polarized.

With the assumption that the recording of events is independent of the Σ polarization, the observed cross-section is

$$\sigma_\alpha = \sigma_\alpha^{(+)} + \sigma_\alpha^{(-)}, \tag{12}$$

and the polarization of the observed Σ is:

$$\eta_\alpha = (\sigma_\alpha^{(+)} - \sigma_\alpha^{(-)})/\sigma_\alpha . \tag{13}$$

Hence the relation:

$$\sigma_\alpha^{(\pm)} = \tfrac{1}{2}\sigma_\alpha(1 \pm \eta_\alpha) . \tag{14}$$

The corresponding triangular relations (in the form (2)) for $\sigma^{(\pm)}$ are

$$-2a_\alpha a_\beta \sqrt{1 \pm \eta_\alpha}\sqrt{1 \pm \eta_\beta} \leqslant a_\alpha^2(1 \pm \eta_\alpha) + a_\beta^2(1 \pm \eta_\beta) - a_\gamma^2(1 \pm \eta_\gamma) \leqslant \leqslant 2a_\alpha a_\beta \sqrt{1 \pm \eta_\alpha}\sqrt{1 \pm \eta_\beta}, \tag{15}$$

and by addition of these inequalities with + and with — sign in front of the η_α (using (5)):

$$-\sqrt{(1+\eta_\alpha)(1+\eta_\beta)} - \sqrt{(1-\eta_\alpha)(1-\eta_\beta)} - 2\cos\omega_\gamma \leqslant \leqslant \sqrt{(1+\eta_\alpha)(1+\eta_\beta)} + \sqrt{(1-\eta_\alpha)(1-\eta_\beta)} . \tag{16}$$

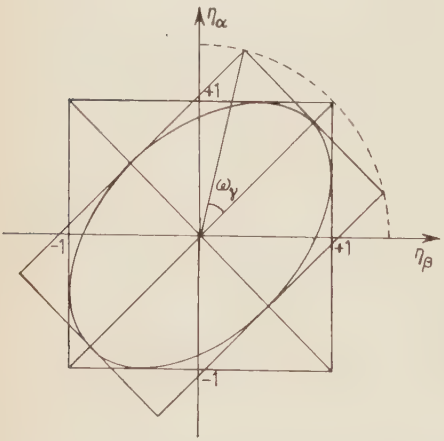

Fig. 1. — For the three reactions of cross-section σ_α and polarization η_α of one spin-$\frac{1}{2}$ particle ($-1 \leqslant \eta_\alpha \leqslant 1$), charge independence requires, when there are two possible values of the total isospin that $|\lambda_\alpha|\sqrt{\sigma_\alpha} = a_\alpha$ satisfy a triangular relation and any two of the η lie inside the above elipse.

Taking the square yields:

$$2\cos^2\omega_\gamma - 1 - \eta_\alpha\eta_\beta \leqslant \leqslant (1-\eta_\alpha^2)^{\frac{1}{2}}(1-\eta_\beta^2)^{\frac{1}{2}}, \tag{17}$$

and taking the square again:

$$\eta_\alpha^2 + \eta_\beta^2 - 2\eta_\alpha\eta_\beta\cos 2\omega_\gamma - \sin^2 2\omega_\gamma \leqslant 0 . \tag{18}$$

This means that the point of coordinates η_α, η_β is inside an ellipse whose properties are (see Fig. 1):

Its axes are bissectors of the axes $\eta_\alpha = 0$, $\eta_\beta = 0$.

The sum of the square of the axes' lengths is 2.

It is inscribed in the square $-1 \leqslant \eta_\alpha \leqslant 1$; $-1 \leqslant \eta_\beta \leqslant 1$.

Its excentricity is given by the angle ω_γ.

In the particular case where the triangle a_α, a_β, a_γ is flat, then $2\omega_\alpha = 0$ or 2π and $\eta_\alpha = \eta_\beta = \eta_\gamma$; indeed there is only one channel for the total isotopic spin. Another case where the knowledge of η_α gives η_β is for $\omega_\gamma = \pi/2$, then $\eta_\beta = -\eta_\alpha$.

In the example of associated production, some lower limit is known for $|\eta_+|$ from the asymmetry in the decay $\Sigma^+ \to n + \pi^+$. However the experimental data (1) do not yet allow to draw very strong conclusions for produced Σ^0 and Σ^+. Some tentative conclusions were made in ref. (2), p. 250.

(1) J. L. Brown, D. A. Glaser, D. I. Meyer, M. C. Perl and J. Vander Velde: *Phys. Rev.*, **107**, 906 (1957); A. R. Envin, J. K. Kopp and A. M. Shapiro: *Phys. Rev.*, **115**, 669 (1959); F. S. Crawford jr., R. L. Douglass, M. L. Good, G. R. Kalbfleisch, M. L. Stevenson and H. K. Ticho: *Phys. Rev. Lett.*, **3**, 394 (1959); W. H. Hannum, H. Courant, E. C. Fowler, H. L. Kraybill, J. Sandweiss and J. Sanford: *Phys. Rev.*, **118**, 577 (1960); B. Cork, L. Kerth, J. Cronin and R. Cool: *Phys. Rev.*, **120**, 1000 (1960); A. Berthelot, A. Daudin, O. Goussu, F. Grard, M. Jubiol, F. Lévy, C. Lewin, A. Rogozinski, J. Laberrigue-Frolow, C. Ouannes and L. Vigneron: preprint from Centre d'Etudes Nucléaires (Saclay) France; C. Baltay, H. Courant, W. J. Fichinger, E. C. Fowler, H. L. Kraybill, J. Sandweiss, J. R. Sanford, D. L. Stonehill and H. D. Taft: preprint from Sloane Physics Laboratory, Yale University, Conn.

(2) L. Michel and H. Rouhaninejad: *Phys. Rev.*, **122**, 242 (1961).

IL NUOVO CIMENTO Vol. XXII, N. 1 1° Ottobre 1961

Kaon-Nucleon Dispersion Relation and the Hyperon Excited States.

K. Igi (*) and H. Shimoida

Department of Physics, Tokyo University of Education - Tokyo

(ricevuto il 2 Settembre 1961)

1. – A recent experimental evidence (1) seems to suggest the possible existence of the $I=0$ excited state Y_0^* which strongly decays into $\pi+\Sigma$, in addition to the $I=1$ excited state which was found last year. A remarkable fact is that the half-widths of these states are very narrow; according to the latest report they are (1) less than 20 MeV. As was first pointed out by Dalitz and Tuan (2) and discussed by Fujii (3) and Miyamoto (4), Y_1^* may be induced by the S-wave interaction of the $\bar{K}$-nucleon system.

Another interesting possibility has also been suggested by Amati *et al.* (5)and by Lee and Yang (6), who showed that the global symmetry model leads to the occurrence of an $I=1$, $j=\frac{3}{2}$ P-state π-Λ resonance, the calculated resonance energy half-width and Σ/Λ decay ratio being all compatible with the Y_1^* observations.

Anyhow the parity and angular momentum of the resonant systems are not well confirmed at present (7). In this short note, we would like to discuss the following two points:

i) Analysis to determine the type of the K-coupling by making use of dispersion relations must be re-examined in view of the new situation.

ii) It is interesting to note that the $(a\,-)$ solution predicts the binding energy for Y_1^* to be ~ 47 MeV and the half width $\Gamma/2 \sim 15$ MeV on the basis of the zero range theory, values which are consistent with experimental data. This solution also suggests, however, the binding energy for the Y_1^* to be ~ 0.5 MeV and a wider width

(*) Present address: Department of Physics, University of California, Berkeley, Calif., U.S.A.

(1) M. H. Alston, L. W. Alvarez, P. Eberhand and M. L. Good: preprint.

(2) R. H. Dalitz and S. F. Tuan: *Phys. Rev. Lett.*, **2**, 425 (1959); *Ann. Phys.*, **10**, 307 (1960). R. H. Dalitz: *Phys. Rev. Lett.*, **6**, 239 (1961). S. F. Tuan: *Nuovo Cimento*, **18**, 1301 (1960). J. Franklin and S. F. Tuan: preprint.

(3) Y. Fujii: preprint.

(4) Y. Miyamoto: preprint.

(5) D. Amati, B. Vitale and A. Stanghellini: *Phys. Rev. Lett.*, **5**, 524 (1960).

(6) T. D. Lee and C. N. Yang: preprint.

(7) H. J. Martin, L. B. Leipuner, W. Chinowsky, F. T. Shively and R. K. Adair: *Phys. Rev. Lett.*, **6**, 283 (1961). J. P. Berge, P. Bastien, O. Dahl, M. Ferro-Luzzi, J. Kirg, D. H. Miller, J. J. Muvay, A. H. Rosenfeld, R. D. Tripp and M. B. Watson: *Phys. Rev. Lett.*, **6**, 557 (1961).

27 MeV which do not seem to be consistent with the present data, namely, $m_{Y_0^*} \sim 1405$ MeV corresponding to the binding energy of ~ 29 MeV, and $\Gamma/2 \leqslant 20$ MeV([1]). It is interesting, therefore, to check the consistency of this $(a-)$ solution by making use of an appropriate form of the dispersion relation.

2. – We shall first discuss the K-coupling type. The analysis to determine the coupling type of dispersion relations must be re-examined since the contribution from Y_1^* and Y_0^* in the unphysical region might be large. The Pomerančuk theorem allows us to use the relation ([8])

$$(1)\quad \frac{D^+(\omega)-D^+(K)}{\omega - K} = B_\Lambda^+(\omega) + B_\Sigma^+(\omega) + \frac{1}{4\pi^2} P \int_K^\infty \frac{k'\sigma^+(\omega')\,\mathrm{d}\omega'}{(\omega'-\omega)(\omega'-K)} - \frac{1}{4\pi^2}\int_K^\infty \frac{k'\sigma^-(\omega')\,\mathrm{d}\omega'}{(\omega'+\omega)(\omega'+K)} - \frac{1}{\pi}\int_{\omega_{\Lambda\pi}}^K \frac{A^-(\omega')\,\mathrm{d}\omega'}{(\omega'+\omega)(\omega'+K)},$$

which turns out to be convenient for the present purpose on account of the following reasons:

1) the integral over the unphysical region, where we have no definite information on the parity of the resonant states, will be well suppressed owing to the large denominator;

2) the sign of D^- which has not yet been confirmed does not appear in the above relation;

3) the low-energy behavior of K^+-p scattering gives us a clear-cut indication of the parities.

In eq. (1), $B_\Lambda^+(\omega)$ and $B_\Sigma^+(\omega)$ are Born terms which have different signs depending upon the relative parities.

The calculations have been carried out at two energies $\omega = 1.25K$ and $1.5K$ using the following data:

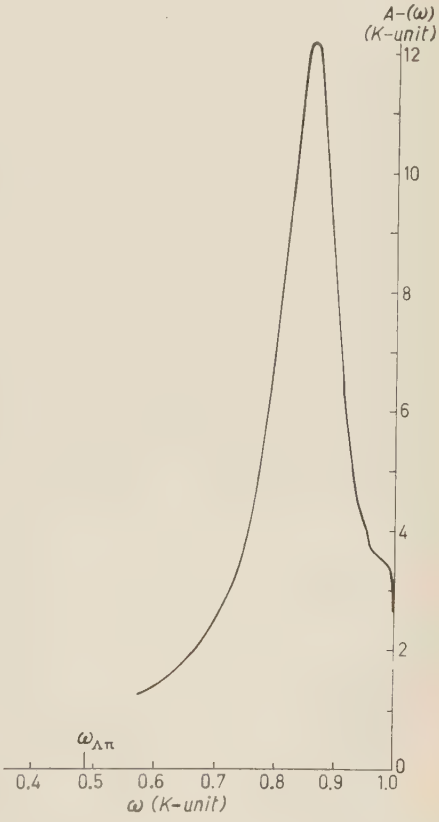

Fig. 1. – $A^-(\omega)$ analytically continuated for the region of unphysical K-p energies for solution $(a-)$.

([8]) D. Amati: *Phys. Rev.*, **113**, 1692 (1959).

i) the quantity $D^+(\omega)$ was obtained in terms of the S-wave effective range relation obtained by RODBERG and THALER [9];

ii) the contribution from resonant states in the unphysical region was tentatively estimated in terms of the analytic continuation of the $\bar{K}$-$\mathcal{N}$ scattering amplitude for the $(a\ -)$ solution which was recently re-determined (Fig. 1) [10]

$$\begin{cases} A_0 = -0.25 + 1.65\,i = a_0 + ib_0\,, \\ A_1 = -1.09 + 0.20\,i = a_1 + ib_1; \end{cases} \tag{2}$$

iii) the curve of $k\sigma^-(\omega)$ was evaluated up to 200 MeV/c by making use of the $(a\,-)$ solution and by taking into account the $K^- - \widetilde{K}^0$ mass difference, and was smoothly extrapolated to fit the experimental data $k\sigma^-(\omega)$ at higher energies. The latest experimental data for the K^+-p total cross sections were used in $k\sigma^-(\omega)$ [11,12].

We shall write down the results of calculation for two energies.
At $\omega = 1.25K$,

$$0.032\,\frac{1}{K^2} = \frac{1}{K^2}\begin{bmatrix} -0.58 g_\Lambda^2 \\ 0.032 g_\Lambda^2 \end{bmatrix} + \frac{1}{K^2}\begin{bmatrix} -0.46 g_\Sigma^2 \\ 0.020 g_\Sigma^2 \end{bmatrix} + \frac{0.081}{K^2} - \frac{0.37}{K^2} - \frac{0.20}{K^2}\,. \tag{3}$$

and at $\omega = 1.5K$,

$$0.09\,\frac{1}{K^2} = \frac{1}{K^2}\begin{bmatrix} -0.049 g_\Lambda^2 \\ 0.027 g_\Lambda^2 \end{bmatrix} + \frac{1}{K^2}\begin{bmatrix} -0.40 g_\Sigma^2 \\ 0.017 g_\Sigma^2 \end{bmatrix} + \frac{0.32}{K^2} - \frac{0.34}{K^2} - \frac{0.17}{K^2}\,, \tag{4}$$

where g_Σ^2 and g_Λ^2 are the unrationalized, renormalized coupling constants and in the above bracket the upper (lower) value corresponds to the scalar (pseudoscalar) case. In writing (3) and (4) we have neglected the contributions from high energies $(\omega' > 4K)$, but fortunately the third and forth term on the right-hand side of (1) have tendency to cancel out each other. Eq. (3) and (4) indicate that the K-meson is pseudoscalar with respect to at least one of the two hyperons, Λ and Σ, which is not contradictory with the previous analysis [13].

Assuming that the relative parity of Λ and Σ is the same it turns out that

$$\frac{g_\Lambda^2 + g_\Sigma^2}{2} \sim 9.9\,, \quad \text{from (3)}, \tag{5}$$

and

$$\frac{g_\Lambda^2 + g_\Sigma^2}{2} \sim 6.5\,, \quad \text{from (4)}. \tag{6}$$

[9] L. S. RODBERG and R. M. THALER: *Phys. Rev. Lett.*, **4**, 372 (1960).
[10] R. H. DALITZ: *Rev. Mod. Phys.*, to be published (1961).
[11] *Report at* 1960 *Annual International Conference on High Energy Physics at Rochester.*
[12] *Report at* 1959 *Annual International Conference on High Energy Physics at Kiev.*
[13] P. T. MATTHEWS and A. SALAM: *Phys. Rev.*, **110**, 569 (1958). C. GOEBEL: *Phys. Rev.*, **110**, 572 (1958). K. IGI: *Progr. Theor. Phys.*, **20**, 403 (1958).

Though these values for the coupling constants should not be taken seriously, they will become useful in the following analysis. Furthermore it should be remarked that so long as one uses the above dispersion relation, one will get more or less the same conclusion irrespective of the parity states of Y_1^*, Y_0^* since the contribution from the unphysical region will be well suppressed.

3. – Next we would like to discuss the second problem.

As was previously described, the $(a-)$ solution predicts the binding energy for the $I=1$ state resonance to be ~ 47 MeV and the half width $\Gamma/2 \sim 15$ MeV. It is attractive to identify this S-state resonance as Y_1^* [2]. It also predicts the binding energy for the $I=0$ state resonance to be ~ 0.5 MeV and a wider half width, but this S-state resonance might not be identified as the recently discovered Y_0^*.

Fig. 2. – The location and width of the resonance.

	$(a-)$ solution	
$I=1$ state	$E_1 = 47$ MeV	$\Gamma/2 = 15$ MeV
$I=0$ state	$E_0 = 0.5$ MeV	$\Gamma/2 = 27$ MeV
	Experimental value	
$I=1$ state	$E_1 = 49$ MeV	$\Gamma/2 \sim 17$ MeV
$I=0$ state	$E_0 = 29$ MeV	$\Gamma/2 \sim 20$ MeV

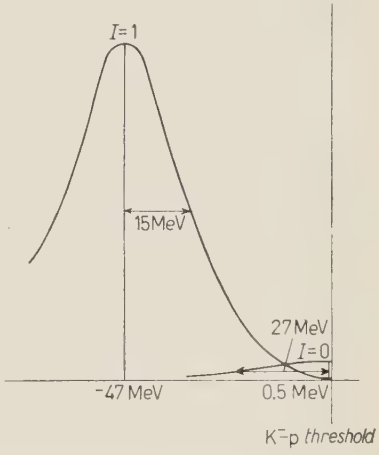

This stimulates us to investigate the validity of the $(a-)$ solution which predicts the S-state Y_1^* and Y_0^* resonances. The Pomerančuk theorem enables us to use the relations for $D^-(\omega) - D^+(\omega)$, but the contribution from high energy cross sections might be large because of the slow convergence of the dispersion integral even though the above theorem is assured. Following Haber-Schaim [14] let us rewrite the dispersion relation into a form more convenient for the present purpose.

Making use of the following identity,

$$\frac{1}{\omega'^2 - \omega^2} = \frac{1}{\omega'^2} + \frac{\omega^2}{\omega'^2(\omega'^2 - \omega^2)}, \tag{7}$$

we get a modified expression as

$$\frac{1}{2}\omega[D^-(\omega) - D^+(\omega)] - \frac{\omega^4}{\pi}\int_{\omega_{\Lambda\pi}}^{K} \frac{d\omega' A^-(\omega')}{\omega'^2(\omega'^2 - \omega^2)} - \frac{\omega^4}{4\pi^2}\int_{K}^{\infty} \frac{d\omega' k'}{\omega'^2 - \omega^2}\left(\frac{\sigma^-(\omega') - \sigma^+(\omega')}{\omega'^2}\right) - \tag{8}$$

$$= -[P_\Lambda X(\Lambda) + P_\Sigma X(\Sigma)] + \omega^2\left[\frac{1}{\pi}\int_{\omega_{\Lambda\pi}}^{K} \frac{d\omega' A^-(\omega')}{\omega'^2} + \frac{1}{4\pi^2}\int_{K}^{\infty} \frac{d\omega' k'}{\omega'^2}(\sigma^-(\omega') - \sigma^+(\omega'))\right],$$

(14) V. Haber-Schaim: *Phys. Rev.*, **104**, 1113 (1956).

where $P_\Lambda(P_\Sigma)$ represents the relative K-Λ(K-Σ) parity, and

$$(9)\qquad \begin{cases} X(Y) = g_{KY}^2 \dfrac{(Y+N)^2 - K^2}{4NY}, & \text{for } P_Y = 1, \\ = g_{KY}^2 \dfrac{K^2 - (Y-N)^2}{4NY}. & \text{for } P_Y = -1. \end{cases}$$

Then the apparently complicated ω-dependence of the left-hand side of (8) boils down to a linear function of ω^2, and its value at $\omega=0$ determines the coupling constants.

It is expected, therefore, that the experimental plot of the left-hand side of (8) *vs.* ω^2 will give a straight line, provided that the correct experimental values are used. This point is essential for investigating the validity of the $(a-)$ solution which predicts the S-state Y_1^* and Y_0^* resonances. The estimates of the left-hand side of (8) have been carried out at $\omega^2=1.07K^2$, $1.14K^2$, $1.21K^2$ and $1.66K^2$ by using the same data as in the first problem: namely, 2i) was used for $D^+(\omega)$; 2ii) for the contributions from resonant states in the unphysical region and 2iii) for $k\sigma^\pm(\omega)$. $D^-(\omega)$ was calculated in terms of the $(a-)$ solution. Especially, at $\omega^2=1.66K^2$ which corresponds to 400 MeV c in the lab. system, the K-p angular distribution [11] was used in order to get D^-, which can be calculated with ambiguity of its sign. The experimental plot of the left-hand side of (8) *vs.* ω^2 is shown in Fig. 3.

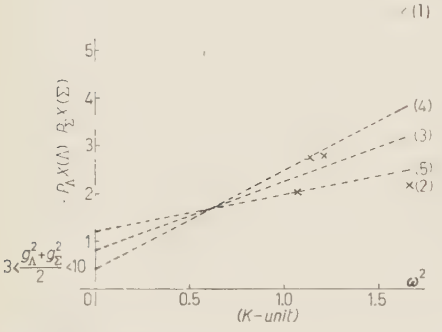

Fig. 3. The left-hand side of (8) plotted *vs.* ω^2. Point 1: when K-p force is attractive; point 2: when K-p force is repulsive. The points at $\omega^2=0$ were varied corresponding to $3<[g_\Lambda^2(ps)+g^2{}_\Sigma(ps)]/2<10$. Line 3: an average gradient; line 4: the steepest gradient; line 5: the easiest gradient.

What can we say about the $(a-)$ solution from this graph? The point at $\omega^2=1.66K^2$ does not seem to lie in the allowed area between (4) and (5), although future improved experiments might change the situation.

Though not definite, one may say that the $(a-)$ solution, which predicts the S-state both for Y_1^* and Y_0^*, is not adequate. This would suggest that at least one of the two resonant states may be the P-state.

If we assume that the experimental indications of Y_1^* and Y_0^* are true, then the following four possibilities can be considered with respect to their parities. For simplicity, let us introduce $Y_{1,0}^*$ as new elementary particles similar to Λ and Σ. If Y^* is in the S-state (P-state), the effective KY^*N coupling is scalar (pseudoscalar). The Y^*-state contributes therefore to $A^-(\omega)$ with different signs according to the coupling type, and the dispersion relation becomes quite sensitive to the Y^* parity. The dispersion-theoretic determination of parities of Y_1^* and Y_0^* will be explained as follows. Consider the dispersion relation

$$(10)\quad D^-(\omega) - D^+(\omega) = \frac{g_\Lambda^3}{\omega-\omega_\Lambda} + \frac{g_\Sigma^2}{\omega-\omega_\Sigma} + \frac{\pm g_{Y_1^*}^2}{\omega-\omega_{Y_1^*}} + \frac{\pm g_{Y_0^*}^2}{\omega-\omega_{Y_0^*}} + \int \frac{\sigma^- - \sigma^+}{\omega'-\omega}\,d\omega',$$

assuming that the locations of the Y^* pole are given. Then the comparison of the left and right-hand side of (10) for various values of ω allows us to determine in principle the possible parities of Y_1^* and Y_0^*.

TABLE I.

Case	Y_1^*	Y_0^*
a	s	s
b	s	p
c	p	s
d	p	p

Again let us see, Fig. 3. Introduction of the $I=0$ P-state pole has tendency to lower the points ($\omega^2=1.07K^2$, $1.14K^2$ and $1.21K^2$) downwards and the allowed area, between point (4) and (5), will go down simultaneously (it is possible that (2) will fall into this regions). If we choose the point (2) the dispersion analysis will be consistent and the possibility of (1) will be ruled out.

Thus the above analysis favors (case b) rather than (case a). Quite similarly, (case c) has a good tendency. As for the possibility of (case d), nothing can be said within the present accuracy of experiment.

* * *

The authors would like to express their sincere gratitude to Professor N. FUKUDA for his kind interest and encouragement. Thanks are also due to Professors H. MIYAZAWA and Y. MIYAMOTO for helpful discussions. They are also indebted to Professor T. UNO and Mrs. H. KONO of the Department of Mathematics, Nihon University, for helping them in calculating the numerical integrations by the use of FACOM 128B.

IL NUOVO CIMENTO Vol. XXII, N. 1 1° Ottobre 1961

Pology and ND^{-1} Solutions in the Multiple-Channel Problems.

G. Costa

Istituto di Fisica dell'Università - Padova
Istituto Nazionale di Fisica Nucleare - Sezione di Padova

F. Ferrari

Istituto di Fisica dell'Università - Bari

(ricevuto il 4 Settembre 1961)

The ND^{-1} technique has been successfully extended to the multiple-channel problems [1], providing also in this case a receipe for constructing partial wave amplitudes satisfying the requirements of unitarity and analyticity. In such problems, however, the complexity deriving from the matrix nature of the amplitude $G=ND^{-1}$ greatly limits the possibility of practical application to the cases in which the unphysical singularities are approximated by a certain — usually very small — number of poles [2]. In fact, if one considers the residues of some of these poles as parameters, the complexity of the dependence of the different amplitudes on these parameters renders extremely difficult their determination from an experimental fit. Moreover, it is also very difficult to check the symmetry of the G-matrix, which is required by time-reversal invariance.

A possible way of avoiding such difficulties would be to write down dispersion relations for an inverse amplitude f^{-1}. In this case the symmetry is authomatically controlled, and one can obtain expressions for the different amplitudes which contain in a simple way the input parameters [3]. Unfortunately, such f^{-1} technique reveals an uncorrect feature, if one examines the problem of the bound or resonant states. In fact, if one puts a certain number of poles into f, such poles generate other poles which do not correspond to physical states.

From this point of view, the ND^{-1} technique seems to be the correct one. In fact, for the one-channel case, it has been shown by Jost and Bargman that the poles generated in the amplitudes G by the zeros of D give the correct bound states [4].

[1] J. Bjorken: *Phys. Rev. Lett.*, **4**, 473 (1960); F. Ferrari, M. Nauenberg and M. Pusterla: *Partial waves amplitudes for $\overline{K}$-nucleon scattering*, Lawrence Radiation Laboratory Report UCRL-8985.

[2] F. Ferrari, G. Frye and M. Pusterla: *Phys. Rev.*, **123**, 315 (1961).

[3] P. T. Matthews and A. Salam: *Nuovo Cimento*, **13**, 381 (1959); O. Feldman, P. T. Matthews and A. Salam: *Nuovo Cimento*, **16**, 549 (1960).

[4] Lectures given by Goldberger (Princeton University, 1959).

These results are generalized to the multiple-channel case as follows (5): the locations of all the bound and resonant states are given by the real roots s_i of the equation $\det(\mathrm{Re}\, D(s))=0$; the bound states are given by those roots s_i which lie below all the physical thresholds of the different channels; the resonances by those roots s_i which lie between two or above all physical thresholds.

For this reason it is important to try to simplify the machinery involved in the use of the ND^{-1} technique. We shall examine here the problem of the symmetry of the G-matrix. BJORKEN and NAUENBERG proved that the matrix $G=ND^{-1}$ is symmetric provided that its discontinuity across the unphysical cuts is a symmetric matrix (6). The theorem is based on the proof that the expression

$$\mathrm{Im}\,(D^T(G-G^T)D)\,,$$

is zero, without examining the structure of the matrices N and D. It is not immediately evident that it holds also in the case in which all the unphysical cuts are approximated by poles. We think it worth-while to give a direct proof of the symmetry of the G-matrix in the case of an arbitrary number of poles, by using explicitly the actual expressions of the matrices N and D. The sketch of the proof we give below gives the opportunity of reporting some formulae which may turn out useful for practical calculations.

We start from the usual dispersion relations for the matrices N and D:

$$N(s)=\frac{1}{\pi}\int_L \frac{\mathrm{Abs}\, G(s')\,D(s')}{(s'-s)}\,\mathrm{d}s', \tag{1}$$

$$D(s)=1-\frac{s-s_0}{\pi}\int_{S_D}^{\infty}\frac{\mathrm{Im}\, G^{-1}(s')\,N(s')}{(s'-s)(s'-s_0)}\,\mathrm{d}s'. \tag{2}$$

The integral on the right hand side of (1) is extended along all the unphysical cuts, which generally are situated only in part on the real axis; $\mathrm{Abs}\, G(s')$ is the discontinuity of $G(s')$ across the cuts. We have made a subtraction in D at an arbitrary point s_0, for the sake of generality.

We assume now that we can write on the unphysical cuts:

$$\mathrm{Abs}\, G(s)=-\pi\sum_{i=1}^{n}R_i\,\delta(s-a_i)\,, \tag{3}$$

where the R_i's are symmetric matrices in channel space, and the a_i's are points conveniently chosen in the s-plane. We get then for $N(s)$:

$$N(s)=\sum_i N_i=\sum_i\frac{R_i}{s-a_i}\,D(a_i)\,, \tag{4}$$

(5) R. H. DALITZ: *Rev. Mod. Phys.*, **33**, 471 (1961).
(6) J. BJORKEN and M. NAUENBERG: *Phys. Rev.*, **121**, 1250 (1961).

and, by inserting (4) into (2):

$$D(s) = 1 - \lambda(s)\, N(s) + \sum_i \Lambda_i N_i \,, \tag{5}$$

where

$$\lambda(s) = \frac{s - s_0}{\pi} \mathscr{P} \int_{s_D}^{\infty} \frac{\varrho(s')}{(s' - s)(s' - s_0)}\, \mathrm{d}s' - i\varrho(s) \,, \tag{6}$$

$$\Lambda_i = \frac{s - s_0}{\pi} \int_{s_D}^{\infty} \frac{\varrho(s')}{(s' - a_i)(s' - s_0)}\, \mathrm{d}s', \tag{7}$$

and

$$\varrho(s) = \mathrm{Im}\, G^{-1}(s) \,. \tag{8}$$

The problem of determining the G-matrix is then solved in principle. In practice, it is necessary to determine the elements of the matrices $D(a_i)$, which are given by the solution of a system of $m \cdot n$ linear equations, m being the number of channels and n the number of poles. The solution, however, can be written in a formally simple way, by looking directly at the structure of the system of equations. In fact, the matrix $D(a_i)$ can be written as:

$$D(a_i) = \mathrm{Tr}\, (1 - \beta K R)^{-1}\, U_i \,, \tag{9}$$

from which follows:

$$N(s) = \mathrm{Tr}\, U \alpha R (1 - \beta K R)^{-1} \,, \tag{10}$$

$$D(s) = 1 - \lambda(s) N(s) + \mathrm{Tr}\, U \Lambda \alpha R (1 - \beta K R)^{-1} \,. \tag{11}$$

The expressions (10), (11) can be obtained also directly by an iteration procedure applied to the coupled integral eq. (1), (2). In the above formulae we have introduced a certain number of $n \times n$ supermatrices: R is a diagonal matrix, whose elements are the symmetric $m \times m$ matrices R_i in the channel space; K is a symmetric matrix with elements

$$K_{ij} = \frac{1}{\pi} \int_{s_D}^{\infty} \frac{\varrho(s')}{(s' - s_0)(s' - a_i)(s' - a_j)}\, \mathrm{d}s', \tag{12}$$

Λ is a diagonal matrix whose elements Λ_i are given in (7); α and β are diagonal matrices with elements

$$\alpha_i = \frac{1}{s \quad a_i} \,, \tag{13}$$

$$\beta_i = s_0 \quad a_i \,, \tag{14}$$

U_i is an $n \times n$ matrix whose elements are zero except for those in the i-th column which are all unity; and U is an $n \times n$ matrix with all elements equal to unity. The trace stands for a sum over the diagonal elements of the supermatrices only.

We are now in a position of expressing in a simple way the proof of the symmetry of the G-matrix.

From the relations (4), (5) it follows immediately (the superscript T specifies a transposed matrix):

$$D^T N - N^T D = N - N^T + X \,, \tag{15}$$

where X is a skew-symmetric matrix:

$$X = \sum_{i,j} N_i^T (\Lambda_i - \Lambda_j) N_j \,. \tag{16}$$

By means of the relation:

$$\Lambda_i - \Lambda_j = (s - s_0)(a_j - a_i) K_{ij} \,, \tag{17}$$

it can also be written:

$$X = (s - s_0) \sum_{i,j} a_{ij} N_i^T K_{ij} N_j \,, \tag{18}$$

with

$$a_{ij} = \frac{a_i - a_j}{(s - a_i)(s - a_j)} \,. \tag{19}$$

By using the expansion (7)

$$(1 - \beta KR)^{-1} = 1 + \beta KR + \beta KR \beta KR + \dots \,, \tag{20}$$

and the following algebric relations

$$\frac{\beta_i}{s - a_i} - \frac{\beta_j}{s - a_j} = (s - s_0)\, a_{ij} \,, \tag{21}$$

$$a_{ij} + a_{jk} + a_{ki} = 0 \,, \tag{22}$$

one can easily prove that the following identity holds:

$$X = N^T - N \,. \tag{23}$$

According to (15), this identity assures that

$$D^T N - N^T D = 0 \,, \tag{24}$$

that is, it proves the symmetry of the matrix $G = ND^{-1}$.

(7) The expansion is justified by the iterated solution of the coupled eq. (1), (2).

π-Y Resonances and K^- Absorption Reactions.

J. S. Dowker

Department of Mathematical Physics, University of Birmingham - Birmingham

(ricevuto il 14 Settembre 1961)

In this note we should like to consider, with π-Y resonances in mind, the capture reactions

$$K^- + {}^4\mathrm{He} \to \Lambda + \pi^- + {}^3\mathrm{He}\,, \tag{1}$$

$$K^- + {}^4\mathrm{He} \to \Sigma^{\pm} + \pi^{\mp} + {}^3\mathrm{H}\,, \tag{2}$$

data on which have recently been reported [1]. Block [2] has calculated the I^3 ($=^3$H or ^{3}He) spectrum for these reactions assuming an impulse approximation. The agreement with experiment is not too good and in the following we shall try to better the fits by invoking an isospin 1 resonance, the Y_1^*, and isospin 0 resonance, the Y_0^*, in the π-Y system. The first is fairly definite [6] while the second is less so. Some data on the Y_0^* have recently appeared [5].

The transition rate spectrum has a pole at the unphysical point $p^2 = -\alpha^2$ [3,4], where p is the I^3 momentum and $\alpha^2 = 3M(\mathrm{B.E.}^4\mathrm{He} - \mathrm{B.E.}I^3)/2$. At the pole we have for this spectrum

$$\frac{\mathrm{d}R}{\mathrm{d}p} = \frac{8|\Gamma_0|^2 p |t_i|^2}{(p^2+\alpha^2)^2}\,. \tag{3}$$

Γ_0 will be related to the asymptotic normalization of the I^3-$\mathcal{N}$ bound system which makes up the ^{4}He.

t_i is connected to the total $K^- + \mathcal{N} \to Y_i + \pi$ cross section by

$$p\sigma_{\mathrm{tot}} = 4\pi |t_i|^2\,.$$

(1) Helium Bubble Chamber Collaboration Group: *Nuovo Cimento*, **20**, 724 (1961).
(2) M. M. Block: *Nuovo Cimento*, **20**, 715 (1961).
(3) J. S. Dowker: *Nuovo Cimento*, **20**, 182 (1961).
(4) G. F. Chew and F. E. Low: *Phys. Rev.*, **113**, 1640 (1959).
(5) M. H. Alston, L. W. Alvarez, Ph. Eberard, M. L. Good, W. Graziano, H. K. Ticho and S. G. Wojcicki: *Phys. Rev. Lett.*, **6**, 698 (1961).
(6) M. H. Alston and M. Ferro-Luzzi: UCRL-9587.

Away from the pole t_i is off the energy shell and can no longer be related to a physical cross-section. We shall take formula (3) to give the spectator spectrum away from the pole and shall approximate t_i by its form on the energy shell. Γ_0 will also be replaced by a function of p. We shall discuss t_i first.

It is known that there exists a resonance in the π-Λ system at a mass of about 1380 MeV and with a half width of about 20 MeV. It is also well known that the $(a -)$ scattering length set of DALITZ and TUAN (7) predicts an isotopic spin 1 resonance at about the experimental position with about the experimental width. To achieve the small isotopic spin 1 ratio $(\Sigma/\Lambda)_1$ observed at resonance the relative parity of the Σ and Λ must be odd if the $(a -)$ set is correct (11). In the following we shall take this to be the case. Then we may interpret the Y_1^* as a pseudoscalar particle (with respect to the $\mathcal{N}$-Λ system) with spin $\frac{1}{2}$ and a complex mass.

Regarding the Y_0^*, we shall assume that this too has spin $\frac{1}{2}$ and that it can be regarded as a scalar particle with a complex mass. For the preceding parities, the Y_0^* will show up as an s-wave resonance in π-Σ elastic scattering. Other quantum numbers are possible and give similar, but slightly worse, fits.

Assuming the Y_0^* to be a narrow resonance we find for the relevant $|t_i|^2$ below the $K^-\mathcal{N}$ threshold the following forms

$$|t(\Lambda\pi^-)|^2 = \frac{G_\Lambda q_\Lambda}{(M_1 - \sqrt{s})^2 + \Delta_1^2}, \tag{4}$$

$$|t(\Sigma^-\pi^+)|^2 + |t(\Sigma^+\pi^-)|^2 = \frac{G_\Sigma^0 q_\Sigma \varkappa^3}{(M_0 - \sqrt{s})^2 + \Delta_0^2} + \frac{G_\Sigma^1 q_\Sigma^3}{(M_1 - \sqrt{s})^2 + \Delta_1^2}, \tag{5}$$

where G_Λ, G_Σ^0 and G_Σ^1 are constants, $\sqrt{s}$ and q_Y are the π-Y c.m. energy and momentum, respectively; $M_1 - i\,\Delta_1$ and $M_0 - i\,\Delta_0$ are the masses of the Y_1^* and Y_0^*. These are to be treated as parameters. $\varkappa$ is related to s by

$$\varkappa^2 = \frac{[s - (M - m)^2][s - (M - m)^2]}{4s},$$

m is the mass of the kaon.

We have added the $\Sigma^-\pi^+$ ^{3}H and $\Sigma^+\pi^-$ ^{3}H rates to avoid interference effects between the isotopic spin channels. In what follows we shall ignore the isotopic spin 1 contribution. This is certainly a reasonable approximation near threshold.

As we have previously mentioned Γ_0 in (3) is to be replaced by $\Gamma(p^2)$ which can be interpreted as the $^4\text{He} \to \text{I}^3 + \mathcal{N}$ vertex function and may be related (8) to the momentum space wave function, φ, of the bound s-wave I^3-$\mathcal{N}$ system by

$$\Gamma(p^2) \approx (p^2 + \alpha^2)\varphi(p), \tag{6}$$

$\varphi(p)$ will be the Fourier transform of the overlap of the ^{4}He and I^3 coordinate space wave functions. For example using Gaussian wave functions for the I^3 and ^{4}He

(7) R. H. DALITZ and S. F. TUAN: *Ann. Phys.*, **3**, 307 (1960).

(8) R. BLANKENBECLER, M. L. GOLDBERGER and F. R. HALPERN: *Nucl. Phys.*, **12**, 629 (1959).

we find

$$\Gamma(p^2) \approx (p^2 + \alpha^2) \exp\left[-\frac{p^2}{6\beta}\right], \tag{7}$$

where β is related to the ^{4}He radius, R_4, by $\beta = 9/32R_4^2$. The first thing to notice about (7) is that $\Gamma(-\alpha^2) = 0$, *i.e.* $\Gamma_0 = 0$; there is no pole. This is a consequence of the fact that the Gaussian functions possess the wrong asymptotic behaviour. We do not dwell on this point but pass on to a more important deficiency connected with the straightforward application of (6).

Substituting (7) into (3) and taking t_l constant gives essentially the result of Block [2] and corresponds to the assumption of the « complete » Born approximation. This, however, does not take into account the fact that the K^- is unlikely to interact with only one nucleon while this is within the nuclear volume of the others. In this region of configuration space we would expect that other processes, such as many body effects, would occur. Thus to be consistent with our « direct interaction » model we should exclude the inner region from the Fourier transformation defining $\varphi(p)$. This constitutes, in effect, a redefinition of the vertex $\Gamma(p^2)$.

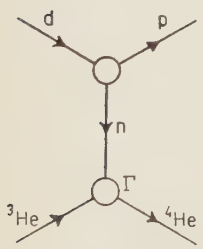

Fig. 1. – Pseudo Feynman graph of the stripping reaction $d + {}^3He \to p + {}^4He$.

The situation is exactly that encountered in Butler [9] stripping theory and we may in fact find an approximate form for Γ by using a cut-off shape for the I^3-N^3 coordinate space wave function.

We used the vertex form that appears in the Butler theory expression for the angular distribution of the reaction $d + {}^3He \to p + {}^4He$ which, as Amado [10] has pointed out, can be looked upon Feynman-diagramwise (Fig. 1) and which contains the vertex $^4He \to {}^3He + n$.

For the case of s-wave neutron capture that interests us here, we have

$$\Gamma(p^2) \approx \frac{\sin pR}{p} + \frac{\cos pR}{\alpha}, \tag{8}$$

where R is the fitting radius. The angular distribution [12] of the reaction $d + {}^3He \to p + {}^4He$ was fitted using the form (8) and it was found that the first minimum could be reproduced with $R \approx 5.5$ fermi. This value is larger than the one of 4.2 fermi quoted by Benveniste and Cork [13] who, apparently, use the Butler theory without allowing for the recoil of the nuclei.

The results for the spectator spectrum calculated from (3), (4), (5), (7) and (8) are shown in Figs. 2 and 3.

It will be seen that in the $\Lambda\pi^- {}^3He$ spectrum, the Butler form (8), provides the best fit all round, reproducing the rather broad nature of the hump. The zeros

[9] S. T. Butler: *Nuclear Stripping Reactions* (New York, 1960).
[10] R. D. Amado: *Phys. Rev. Lett.*, **2**, 399 (1959).
[11] R. H. Dalitz: *Phys. Rev. Lett.*, **6**, 239 (1961).
[12] L. Stewart, J. E. Brolley and L. Rosen: *Phys. Rev.*, **119**, 1649 (1960).
[13] J. Benveniste and B. Cork: *Phys. Rev.*, **89**, 422 (1953).

should not be taken seriously. They are a consequence of the Butler approximation and we would expect them to be filled in somewhat in a more realistic calculation. The Butler form predicts an unsubstantiated peak around 50 MeV/c. This is probably a symptom of the well known feature of the Butler theory that it exaggerates the size of the forward peak relative to the other peaks in the angular distribution of stripping reactions. The worst

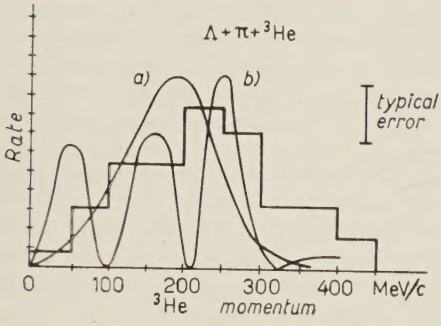

Fig. 2. – ^{3}He recoil spectrum with $M_1 \approx 1380$ MeV, $\Delta^0 \approx 15$ MeV, calculated with (*a*) the Gaussian vertex and (*b*) the Butler vertex.

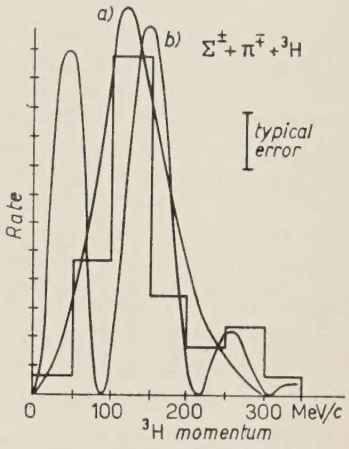

Fig. 3. – ^{3}H recoil spectrum with $M_0 \approx$ ≈ 1410 MeV, $\Delta_0 \approx 15$ MeV for (*a*) the Gaussian vertex, (*b*) the Butler vertex.

part of the fit is at large p but in view of the poor statistics it is difficult to say whether this is due to the approximations made within the above model or to the inadequacy of the latter. Turning to the $(\Sigma^-\pi^+\,{}^3\mathrm{H}) + (\Sigma^+\pi^-\,{}^3\mathrm{H})$, spectrum a passable fit can be achieved by taking $M_0 \approx 1410$ MeV and $\Delta_0 \approx 15$ MeV although statistics do not allow for an accurate determination of these parameters; any value around 1400 MeV for M_0 produced a reasonable fit. There is evidence of a peak around $p \approx 280$ MeV/c which does seem to be reproduced by the Butler vertex. The Butler vertex also predicts the peak around 50 MeV/c which was discussed above.

Conclusions are that, as far as the data allow, there seems to be evidence for a π-Σ isospin 0 resonance with mass around 1400 MeV and width ~ 15 MeV. Further our analysis shows the importance of the $^4\mathrm{He} \to \mathrm{I}^3 + \mathcal{N}$ vertex the variation of which introduces structure into the spectator spectrum ([3]). This structure is likely to be a general feature of capture by nuclei, other than the deuteron, and is not due to the assumption of the Butler form of the vertex. We might say that the structure is related to the assumption of the impulse approximation.

A more realistic calculation of the vertex is obviously desirable. We might mention in this connection that the variation of the vertex could be found from the angular distributions of the reactions $\mathrm{d} + {}^3\mathrm{He} \to {}^4\mathrm{He} + \mathrm{p}$ and $^3\mathrm{He} + {}^4\mathrm{He} \to {}^4\mathrm{He} + {}^3\mathrm{He}$ although in the first reaction heavy particle stripping (« crossed deuteron pole ») introduces complications.

* * *

I am very grateful to Mr. L. Castillejo and Professor R. E. Peierls for useful discussions. A Maintenance Grant from the Department of Scientific and Industrial Research is also gratefully acknowledged.

LIBRI RICEVUTI E RECENSIONI

Progress in Cryogenics edited by K. Mendelssohn, Heywood & Co. Ltd., London; III Vol., pp. VII-173, prezzo 45 s.

Questo terzo volume della serie dedicata ai problemi delle basse temperature, da un punto di vista prevalentemente sperimentale, è di minor mole dei precedenti e contiene solo sei articoli; i problemi trattati però sono di grande interesse pratico e tra loro armonizzati con cura particolare in modo da formare un insieme coerente e collegato coi precedenti volumi. Se una critica si può fare a questi lavori è quella di essere nella maggior parte troppo stringati, in modo che le notizie di dettaglio non risultano sempre messe sufficientemente in luce.

I lavori si possono dividere in due gruppi: i primi quattro trattano di liquefattori, impianti criogenici e applicazioni, gli altri due sviluppano argomenti relativi alla orientazione nucleare, ricollegandosi alla rassegna apparsa nel secondo volume di questa collezione ad opera di E. AMBLER.

I liquefattori di elio si vanno diffondendo rapidamente in molti laboratori: perciò l'articolo di A. J. CROFT interesserà un largo pubblico di specialisti. Dopo brevi cenni storici vi sono descritti i principi di funzionamento, i più noti liquefattori in commercio o in uso presso grandi Istituti ed anche alcuni piccoli modelli che possono, sia pure con notevole impegno, essere costruiti in laboratorio. L'articolo può essere utile a chi voglia acquistare un liquefattore o cerchi un primo orientamento per scegliere un impianto.

Il secondo scritto ad opera di A. G. LENFESTEY concentra l'attenzione sugli scambi di calore per basse temperature, uno dei costituenti essenziali dei circuiti di refrigerazione e quello, forse, che presenta le maggiori difficoltà di progetto e costruttive. Anche questo articolo è piuttosto breve e non ci sembra che esaurisca l'argomento se non nelle sue linee essenziali.

W. E. GIFFORD, dell'ufficio ricerche di una dell più importanti industrie nel campo delle basse temperature, presenta alcuni progressi recenti della tecnica del freddo. Si tratta più precisamente di due nuovi cicli di refrigerazione adatti per la costruzione di piccoli apparecchi. Vengono anche illustrate alcune applicazioni tra cui un refrigeratore di dimensioni tascabili, capace di raggiungere 60 °K.

L'ultimo articolo del primo gruppo ad opera di I. E. SMITH tratta dell'impiego dei gas liquefatti nella propulsione dei razzi: è strettamente applicativo e piuttosto generico, ma serva a dare idee generali sull'argomento.

Delle proprietà delle sostanze paramagnetiche adatte per l'orientazione nucleare discute R. P. HUDSON par-

tendo da fondamenti teorici, brevemente esposti, per arrivare ad un elenco critico dei singoli gruppi di sostanze.

L'argomento dell'ultimo lavoro scritto da C. D. Jeffries è quello dei metodi dinamici di orientazione nucleare, sviluppato con qualche dettaglio in forma di concisa rassegna. Tutti gli aspetti principali del problema sono presi in considerazione; principi fondamentali, tecniche sperimentali, risultati e applicazioni.

Questo lavoro, appoggiato su una bibliografia aggiornata di oltre settanta voci potrà certo servire come punto di partenza per una più vasta ricerca bibliografica.

F. A. Levi

R. L. Chase – *Nuclear Pulse Spectrometry*. Mc Graw-Hill Book Co. Inc., New Yok and London, 1961; pp. VIII-221, 66 s.

Nella breve prefazione di questo volumetto, l'autore, definendo gli scopi ed i confini della sua trattazione, si propone di raggiungere sostanzialmente tre obiettivi.

Il primo consiste nel familiarizzare i fisici nucleari con i problemi sperimentali connessi a quegli importanti strumenti di misura che sono i vari tipi di contatori (Geiger, scintillatori, ecc.). Come secondo obiettivo, l'A. si propone di introdurre ed informare gli elettronici sui particolari aspetti dei circuiti indispensabili per l'elaborazione e l'utilizzazione delle informazioni fornite dai predetti rivelatori. Infine, come terzo obiettivo, il Chase intende dare una rassegna degli spettrometri per fisica nucleare usati per studiare le distribuzioni in ampiezza e in tempo dei transienti forniti da rivelatori nucleari.

Questo libro si propone perciò di trattare varie nozioni scientifiche e tecniche dal punto di vista unitario della loro utilizzazione nell'ambito della strumentazione nucleare.

Libri come questo sono oggi quanto mai utili poichè facilitano il superamento di quella eccessiva e dannosa specializzazione scientifica che viene incrementata non solo dalla crescente complessità della fisica, ma pure, talvolta, dalla pigrizia mentale di taluni ricercatori.

Frequentemente libri di questo tipo sono o troppo divulgativi o troppo tecnicamente specializzati; R. L. Chase, giova subito riconoscerlo, ha saputo assai bene evitare entrambe queste possibilità, mantenendo sul giusto tono l'intero volume.

La trattazione è ovunque semplice ma densa dei concetti essenziali e ricca di informazioni che il lettore si trova facilitato ad allargare attraverso una bibliografia ben selezionata. Sotto quest'ultimo profilo gioverebbe aggiungere al volume un indice dei nomi.

Il volume è suddiviso in nove capitoli che ora elenchiamo per dare al lettore un'idea dettagliata, anche se estremamente concisa, della materia trattata: 1) Rivelatori di radiazioni nucleari e loro caratteristiche; 2) Amplificatori lineari; 3) Analizzatori d'ampiezze d'impulsi monocanali; 4), 5) Analizzatori d'ampiezze d'impulsi multicanali; 6) Analizzatori fotografici d'ampiezze d'impulsi; 7) Analizzatori temporali; 8) Analisi multidimensionali; 9) Perdita di conteggio.

A. Alberigi Quaranta

E. H. Putley: *The Hall Effect and Related Phenomena*. Butterworths, London, 1960; pp. 263; 50 s.

Si tratta di una monografia di carattere specifico nel campo dei semiconduttori, scritta con passione da un cultore riconosciuto della materia. Il libro è essenzialmente diviso in due parti di rilievo, una prima di carattere generale

sulle proprietà di trasporto e gli effetti termo-galvano-magnetici, ed una seconda sul comportamento di alcuni tipici semiconduttori. Il livello è piuttosto elementare nella prima parte, e un po' da articolo di rivista nella seconda; ed in entrambe non abbiamo trovato un approfondimento originale del problema. Riteniamo però che l'opera sia utile ai fisici dello stato solido appena iniziati nel campo dei semiconduttori.

G. Careri

H. C. Corben and P. Stehle – *Classical Mechanics*, 2nd edition; John Wiley and Sons Inc., New York and London; pp. xi-389.

È questa la seconda edizione di un libro ormai ben noto e che ha già incontrato unanime favore. Ci limiteremo pertanto ad accennare alle principali differenze rispetto alla prima edizione.

Lo sforzo principale è stato inteso ad includere nuove applicazioni suggerite da recenti sviluppi. Una parte di queste applicazioni riguardano il nuovo importante campo di studio sul moto dei missili. Gli autori discutono l'uso di metodi variazionali allo scopo di determinare le traiettorie. Inoltre vengono presentati applicazioni a problemi di trascinamento atmosferico, di moto di polveri meteoriche, di limitazioni dovute a cariche spaziali ecc. Notevole l'inclusione di una discussione degli spin e dei sistemi rotanti di coordinate, della precessione di Thomas, e dell'equazione di Boltzmann. Infine un cenno a parte merita il capitolo sugli acceleratori di particelle, reso aggiornato e particolarmente chiaro nella esposizione dei metodi.

Si tratta di un libro di grande valore, e per la chiarezza e per la completezza dell'esposizione, e lo raccomandiamo vivamente, soprattutto agli studenti del secondo biennio.

R. Gatto

J. Wilks: *The Third Law of Thermodynamics*. Oxford University Press, 1961; pp. 142; 15 s.

Questo libretto è destinato ad esporre la terza legge della termodinamica e soprattutto le sue applicazioni a studenti di un livello confrontabile con il nostro terzo anno di fisica. In questo senso limitato l'autore raggiunge certo il suo scopo, benchè si sarebbe desiderato una discussione più approfondita delle diverse formulazioni della terza legge e della storia stessa di queste diverse formulazioni.

G. Careri

Direttore responsabile: G. POLVANI Tipografia Compositori - Bologna

Questo fascicolo è stato licenziato dai torchi il 10 -X- 1961

3924